INTERACTIONS OF XENON(II) FLUORIDE WITH SOME METAL TETRAFLUORIDES

Kristian Radan

Doctoral Dissertation
Jožef Stefan International Postgraduate School
Ljubljana, Slovenia

Supervisor: Prof. Dr. Boris Žemva, Jožef Stefan International Postgraduate School (IPS) and Jožef Stefan Institute (JSI), Jamova cesta 39, SI-1000 Ljubljana, Slovenia

Evaluation Board:
Prof. Dr. Venčeslav Kaučič, Chair, National Institute of Chemistry (NIC), Hajdrihova 19, SI-1001 Ljubljana, Slovenia
Prof. Dr. Mihael Drofenik, Member, Faculty of Chemistry and Chemical Engineering (UM FKKT), University of Maribor, Smetanova ulica 17, 2000 Maribor, Slovenia
Asst. Prof. Gašper Tavčar, Member, Jožef Stefan International Postgraduate School (IPS) and Jožef Stefan Institute (JSI), Jamova cesta 39, SI-1000 Ljubljana, Slovenia
Prof. Dr. Hermann-Josef Frohn, Member, Faculty of Chemistry, University of Duisburg-Essen (UDE), Forsthausweg 2, 47057 Duisburg, Germany

MEDNARODNA PODIPLOMSKA ŠOLA JOŽEFA STEFANA
JOŽEF STEFAN INTERNATIONAL POSTGRADUATE SCHOOL



Kristian Radan

INTERACTIONS OF XENON(II) FLUORIDE WITH SOME METAL TETRAFLUORIDES

Doctoral Dissertation

INTERAKCIJE KSENONOVEGA(II) FLUORIDA Z NEKATERIMI KOVINSKIMI TETRAFLUORIDI

Doktorska disertacija

Supervisor: Prof. Dr. Boris Žemva

Ljubljana, Slovenia, March 2017

To my family

Acknowledgments

I wish to acknowledge Prof. Dr. Boris Žemva for sharing with me his vast experience in the field of noble gas-chemistry and for giving me the opportunity to work on such a challenging and exciting research project. I am deeply grateful for his continuous support and his confidence in me over the past years.
Special thanks are directed to my colleagues, Dr. Matic Lozinšek and Aleš Štefančič. More than ten years of science fairs, chemical demonstrations, unforgettable experiences and countless discussions developed in a longstanding friendship and mutual trust. Their multifaceted assistance towards this work is gratefully acknowledged.
I wish to thank Prof. Dr. Gary J. Schrobilgen, Dr. Hélène P.A. Mercier and their research group at McMaster University (Canada) for the time dedicated in extending my knowledge and experimental skills to krypton chemistry and low-temperature techniques.
I am also thankful to many former co-workers, who contributed significantly to the present research. I would like to thank Asst. Prof. Dr. Gašper Tavčar, head of the Department of Inorganic Chemistry and Technology at the Jožef Stefan Institute for several fruitful suggestions, support and constant stimulation. I thank Asst. Prof. Dr. Evgeny Goreshnik for the crystal structure determinations and Dr. Melita Tramšek for her help with Raman spectroscopy. I wish to thank Asst. Prof. Dr. Maja Ponikvar Svet and Mira Zupančič for chemical analyses and help with precision weighing. I learnt several experimental techniques from Robert Moravec through his efficient hands-on teaching approach. His skilful assistance was crucial for the practical part of this work. I am also very thankful to the workshop master Roman Bevc and to the glassblower Pero Kolobarić for their help in the maintenance of the vacuum line.
I want to thank Dr. Igor Shlyapnikov, who shared his knowledge and numerous experiences with fluoridotitanates(IV). I will never forget our excellent collaboration and memorable evenings at work, as well as the time we spent together with Blaž Alič, who upgraded our long discussions with his company, deep views and tasteful coffee.
I also wish to thank the other members of my evaluation board, Prof. Dr. Hermann-Josef Frohn, Prof. Dr. Venčeslav Kaučič and Prof. Dr. Mihael Drofenik, for their insights and interest in my research work.
I would like to extend my gratitude to my parents and my brother, for their patience, immeasurable and unconditional support and for holding together as a family through many difficult times during the last years.
Finally, the Slovenian Research Agency (ARRS) and the Slovene Human Resources Development and Scholarship Fund are acknowledged for their financial support.

Abstract

The unexplained nature of the first noble gas compound and the rich structural diversity exhibited by four previously determined xenon(II) fluoridometalates(IV) prompted to a more comprehensive investigation of XeF_2 – MF_4 systems. The present work covers the results obtained during the systematic investigation of reactions between XeF_2 and particularly two metal(IV) fluorides, TiF_4 and SnF_4.

In the XeF_2 – TiF_4 system, where three novel compounds were isolated and characterized by Raman spectroscopy and low-temperature single-crystal X-ray diffraction: $[XeF_2{\cdot}TiF_4]_2{\cdot}XeF_2$, $[Xe_2F_3][Ti_8F_{33}]$ and $[XeF]_2[Ti_9F_{38}]$. $[XeF_2{\cdot}TiF_4]_2{\cdot}XeF_2$ crystallized from a solution of TiF_4 and an excess of XeF_2 in anhydrous hydrofluoric acid (aHF) and turned out to be isostructural with the previously reported manganese analogue. The compounds $[Xe_2F_3][Ti_8F_{33}]$ and $[XeF]_2[Ti_9F_{38}]$ were obtained from a reaction mixture of XeF_2 and excessive TiF_4 in a thermal (135 °C) one-step of synthesis and crystallization. The formation of both noble gas compounds under thermal reaction conditions and their remarkable thermal stability was fairly unexpected. Both products represent the first examples of $Xe_2F_3^+$ and XeF^+ salts with anions of higher dimensionality. The reaction path to the new layered structural type of $[Ti_8F_{33}]^-$ and to the novel columnar type of $[Ti_9F_{38}]^{2-}$ polyanions are discussed. TiF_4 was also reacted at low temperature with an excess of the weak fluoride ion donor KrF_2 in aHF at low temperature, where an undefined product was formed and characterized by Raman spectroscopy.

The system XeF_2 – SnF_4 was thoroughly investigated using different types of inorganic solvents, like aHF and Xe^0. The compound $[Xe_2F_3][Sn_4F_{17}]{\cdot}XeF_2{\cdot}HF$ was synthetized from SnF_4 and multifold molar excesses of XeF_2 in aHF at low temperature (−20 °C). Its crystal structure revealed the presence of XeF_2 – $Xe_2F_3^+$ cationic networks situated between the wave-like anionic layers. The new 2-D $[Sn_4F_{17}]^-$ polyanion of this product consists of octahedral SnF_6 and firstly observed pentagonal-bipyramidal SnF_7 units. Moreover, the reaction between XeF_2 and SnF_4 in liquid xenon led to the formation of a new phase with unknown composition, which was detected and partially characterized by Raman spectroscopy immediately after its isolation.

In addition, a series of by-products were obtained within the experimental work. A new polymorphic modification of $[H_3O][Ti_2F_9]$ and novel compounds $[H_3O]_2[SnF_6]$, $[H_3O][SnF_5]$, $Na[SnF_5]$, $Na[H_3O][SnF_5]_2$ and $Na[Sn_2F_9]{\cdot}HF$ were isolated and structurally characterized. In order to explore the factors affecting the preferential formation of anionic species in aHF, targeted syntheses and re-determinations of the aforementioned oxonium and sodium fluoridostannate(IV) salts were carried out. The structural knowledge of inorganic fluoridostannates(IV), which had been previously limited to the monomeric $[SnF_6]^{2-}$ anion, was considerably extended, especially with the first structural characterization of the 2-D layered wave-like structure of $[Sn_4F_{17}]^-$, the chain-type $[SnF_5]^-$ and the ladder-type $[Sn_2F_9]^-$ polyanion assembly.

Povzetek

Spodbuda k celovitejši preiskavi sistemov XeF_2 – TiF_4 izhaja iz še vedno nepojasnjene narave prve spojine z žlahtnim plinom in bogate strukturne raznolikosti štirih predhodno določenih xenonovih(II) fluoridometalatov(IV). V pričujoči doktorski disertaciji so zbrani rezultati sistematske študije interakcij med XeF_2 in predvsem dvema kovinskima(IV) fluoridoma, TiF_4 in SnF_4.

Prvi del raziskav se je osredotočal na sistem XeF_2 – TiF_4, v okviru katerega so bile izolirane in karakterizirane z ramansko spektroskopijo in nizko-temperaturno rentgensko strukturno analizo na monokristalih tri nove spojine: $(XeF_2{\cdot}TiF_4)_2{\cdot}XeF_2$, $[Xe_2F_3][Ti_8F_{33}]$ in $[XeF]_2[Ti_9F_{38}]$. Prvi produkt je izkristaliziral iz raztopine TiF_4 in presežka XeF_2 v brezvodnem vodikovem fluoridu (aHF). Izkazalo se je, da je izostrukturen s predhodno določeno analogno manganovo spojino. Spojini $[Xe_2F_3][Ti_8F_{33}]$ in $[XeF]_2[Ti_9F_{38}]$ sta bili dobljeni iz reakcijske zmesi XeF_2 in presežka TiF_4 v termičnem (135 °C) eno-stopenjskem sintezno-kristalizacijskem procesu. Nastanek takšnih spojin z žlahtnimi plini z izjemno termično obstojnostjo je bil pod danimi pogoji povsem nepričakovan, spojini pa predstavljata prva primera $[Xe_2F_3]^+$ in $[XeF]^+$ soli z anioni višjih dimenzionalnosti. Podana je razprava glede vloge združevanja pri povečanju Lewisove kislosti in sinteznih poti, ki bi vodile do nastanka opaženega novega plastovitega strukturnega tipa $[Ti_8F_{33}]^-$ in novega stebričastega $[Ti_9F_{38}]^{2-}$ polimernega aniona. Z ramansko spektroskopijo je bil potrjen tudi nastanek nedefiniranega produkta po reakciji med TiF_4 in KrF_2 v aHF pri nizki temperaturi.

Drugi sklop raziskav je zajemal študijo sistema XeF_2 – SnF_4 v različnih anorganskih topilih. Spojina $[Xe_2F_3][Sn_4F_{17}]{\cdot}XeF_2{\cdot}HF$ je bila sintetizirana pri nizki temperaturi (−20 °C) iz SnF_4 in mnogokratnega molarnega presežka XeF_2 v aHF. Rešena kristalna struktura te spojine razkriva tvorbo kationskih XeF_2 – $Xe_2F_3^+$ mrež, ki se nahajajo med valovitimi anionskimi plastmi. Slednje so sestavljene iz oktaedričnih SnF_6 in prvič opaženih pantagonalno-bipiramidalnih SnF_7 enot. Reakcija med XeF_2 in SnF_4 v tekočem ksenonu je vodila do nastanka nove faze z neznano sestavo, ki je bila takoj po izolaciji deloma karakterizirana z ramansko spektroskopijo.

Tekom eksperimentalnega dela je bilo v okviru predstavljenih raziskav dobljenih tudi več stranskih produktov. Izolirane in strukturno okarakterizirane so bile nove spojine $[H_3O]_2[SnF_6]$, $[H_3O][SnF_5]$, $Na[SnF_5]$, $Na[H_3O][SnF_5]_2$ in $Na[Sn_2F_9]{\cdot}HF$ ter nova polimorfna modifikacija spojine $[H_3O][Ti_2F_9]$. Z namenom študije prisotnih kemijskih ravnotežij in dejavnikov, ki bi lahko vplivali na preferenčni nastanek določenih anionskih zvrsti v aHF, so bili zgoraj omenjeni oksonijevi in natrijevi fluoridostanati(IV) ciljno sintetizirani in njihove strukture ponovno določene. S prvim vpogledom v valovito 2-D strukturo $[Sn_4F_{17}]^-$, verižni $[SnF_5]^-$ anion in v polimerno $[Sn_2F_9]^-$ anionsko lestev se je nabor znanja o strukturah anorganskih fluoridostanatov(IV), ki je bil pred tem omejen zgolj na strukturo monomernega $[SnF_6]^{2-}$ aniona, znatno razširil.

Contents

List of Figures **xv**

List of Tables **xix**

Abbreviations **xxi**

1 Introduction **1**
1.1 Historical Introduction into Nobel-Gas Reactivity ... 1
1.2 Estimating Lewis Acidity ... 3
1.3 The Chemistry of XeF_2 ... 5
1.3.1 XeF_2 ... 5
1.3.2 XeF^+ and $Xe_2F_3^+$ Compounds ... 7
1.4 Metal Tetrafluorides and Fluoridometalates(IV) ... 7
1.4.1 TiF_4 and Fluoridotitanates(IV) ... 8
1.4.2 SnF_4 and Fluoridostannates(IV) ... 10
1.5 $XeF_2 – MF_4$ Systems ... 10
1.5.1 $XeF_2 – PtF_4$ System ... 10
1.5.2 $XeF_2 – PdF_4$ System ... 13
1.5.3 $XeF_2 – CrF_4$ System ... 13
1.5.3.1 $XeF_2 \cdot CrF_4$ ... 13
1.5.3.2 $XeF_2 \cdot 2CrF_4$ ... 14
1.5.4 $XeF_2 – MnF_4$ System ... 15
1.5.4.1 $XeF_2 \cdot MnF_4$ ... 15
1.5.4.2 $XeF_2 \cdot 2MnF_4$ ... 16
1.5.4.3 $3XeF_2 \cdot 2MnF_4$ ... 16
1.5.5 Other $XeF_2 – MF_4$ Systems ... 17
1.6 $XeF_6 – MF_4$ Systems ... 17

2 Aims and Hypothesis **21**
2.1 Aims 21
2.2 Hypothesis ... 21

3 Materials and Methods **23**
3.1 Materials ... 23
3.2 Synthetic Procedures ... 24
3.3 Characterization ... 26
3.3.1 X-ray Crystal Structure Determinations ... 26
3.3.2 Raman Spectroscopy ... 26

4 Results and Discussion **29**
4.1 XeF_2 - TiF_4 System ... 29
4.1.1 Background ... 29
4.1.2 $(XeF_2 \cdot TiF_4)_2 \cdot XeF_2$ ... 30
4.1.3 $[Xe_2F_3][Ti_8F_{33}]$ ... 41
4.1.4 $[XeF]_2[Ti_9F_{38}]$ ... 55
4.1.5 Other Fluoridotitanate(IV) Salts and By-Products ... 77
4.1.5.1 $KrF_2 – TiF_4$ System ... 77
4.1.5.2 β-$[H_3O][Ti_2F_9]$ ... 78

4.2 XeF_2 – SnF_4 System 82
4.2.1 Background 82
4.2.2 $[Xe_2F_3][Sn_4F_{17}]\cdot XeF_2\cdot HF$ 83
4.2.3 $XeF_2\cdot 2SnF_4$ 98
4.2.3.1 Reactions in Anhydrous HF 98
4.2.3.2 Reactions in Liquid Xenon 101
4.2.4 Other Fluoridostannate(IV) Salts and By-Products 105
4.2.4.1 $[H_3O]_2[SnF_6]$ 106
4.2.4.2 $[H_3O][SnF_5]$ 110
4.2.4.3 $Na[SnF_5]$ 114
4.2.4.4 $Na[H_3O][SnF_5]_2$ 118
4.2.4.5 $Na[Sn_2F_9]\cdot HF$ 122

5 Conclusions **129**

Appendix A Xenon(II) Fluoridometalates(IV) – General Supporting Information **131**
A.1 $XeF_2\cdot 2CrF_4$ 131

Appendix B XeF_2 – TiF_4 System **133**
B.1 $(XeF_2\cdot TiF_4)_2\cdot XeF_2$ 133
B.2 $[Xe_2F_3][Ti_8F_{33}]$ 135
B.3 $[XeF]_2[Ti_9F_{38}]$ 137
B.4 β-$[H_3O][Ti_2F_9]$ 140

Appendix C XeF_2 – SnF_4 System **141**
C.1 $[Xe_2F_3][Sn_4F_{17}]\cdot XeF_2\cdot HF$ 141
C.1.1 Supplementary Data 141
C.1.2 Anionic $[Sn_4F_{17}]^-$ Layers – Sinusoidal Approximation 143
C.2 Experiments in Liquid Xenon 145
C.3 $[H_3O]_2[SnF_6]$ 146
C.4 $[H_3O][SnF_5]$ 146
C.5 $Na[SnF_5]$ 147
C.6 $Na[H_3O][SnF_5]_2$ 147
C.7 $Na[Sn_2F_9]\cdot HF$ 148

Bibliography **151**

Biography **153**

References **155**

List of Figures

Figure 1.1: The structure of a Xenon Hydrate, $Xe_{3.27}[H_2O]_{23}$ (hydrogen atoms have been omitted for clarity). 2
Figure 1.2: Unit cell of XeF_2 viewed along the a-axis, showing eight intermolecular Xe---F contacts (dashed lines). 6
Figure 1.3: Three structural types of ion pairs demonstrated by the interactions of XeF_2 with SbF_5 (left to right): of $[XeF][SbF_6]$,[74] $[XeF][Sb_2F_{11}]$,[74] $[Xe_2F_3][SbF_6]$.[122] 7
Figure 1.4: Ti_3F_{15} rings in the crystal structure of TiF_4.[135] 8
Figure 1.5: Octahedral SnF_6 units forming a layered structure in SnF_4. 10
Figure 1.6: The historic experiment producing the first noble-gas compound as it was recreated at the Lawrence Berkeley National Laboratory. 11
Figure 1.7: A sealed sample of a compound closest to the formulation "$XePtF_6$" prepared by Graham in 1976. 12
Figure 1.8: Crystal structure of $XeF_2{\cdot}CrF_4$.[182] 14
Figure 1.9: XeF_2 bonding and centrosymmetric rings found in the structure of $XeF_2{\cdot}2CrF_4$.[183] .. 15
Figure 1.10: Four-membered ring with XeF_2 units in the crystal structure of $XeF_2{\cdot}MnF_4$. 16
Figure 1.11: $3XeF_2{\cdot}2MnF_4$ is $XeF_2{\cdot}MnF_4$ co-crystalized with XeF_2 molecules. 17
Figure 1.12: *Left* - $[XeF_5]^+$ coordination environment in $[XeF_5]_2[PdF_6]$. *Right* – basic structural unit in $[Xe_2F_{11}]_2[NiF_6]$. 18
Figure 1.13: The polymeric CrF_5 anion found in the crystal structure of $[XeF_5][CrF_5]$ consists of highly distorted CrF_6 octahedra joined via cis vertexes. 19
Figure 1.14: Ten TiF_6 units in a double star-like structural arrangement represent $[Ti_{10}F_{45}]^{5-}$, the largest observed discrete perfluoridometallate anion present in the recently isolated β-$[XeF_5]_5[Ti_{10}F_{45}]$. 19
Figure 3.1: *Left* – a typical T-shaped crystallization vessel was comprised of two FEP (*Right* – All PTFE parts have been encased in full-metal housings. 25
Figure 3.2: *Left* – a small T-shaped crystallization vessel allowed a better control over the 25
Figure 3.3: Agilent Gemini A diffractometer with a 4-circle kappa goniometer, Atlas S2 CCD detector and Cryojet5 (Oxford Instruments) cryogenic device. 26
Figure 3.4: Raman spectra were recorded at room temperature on a Horiba Jobin Yvon Labram-HR spectrometer coupled with an Olympus BXFM-ILHS microscope. Samples were excited by the red 633-nm emission line of a 24.3-mW He−Ne laser with a power output of 14 mW on the sample. 27
Figure 4.1: The asymmetric unit (labeled atoms) in the compound $(XeFTiF_5)_2{\cdot}XeF_2$. Thermal ellipsoids are drawn at the 50 % probability level. 31
Figure 4.2: Selected part of the polymeric chain showing the connectivity of the $FXeFTiF_3F_{2/2}$ units (*left*) and torsion of neighboring TiF_6 octahedra (*right*) observed in the compound $(XeF_2{\cdot}TiF_4)_2{\cdot}XeF_2$. 32
Figure 4.3: The unit cell of compound $(XeF_2{\cdot}TiF_4)_2{\cdot}XeF_2$ viewed along the *b*-axis. 33
Figure 4.4: Isoformulaic $[TiF_5]$-type architectures found in compounds $(XeF_2{\cdot}TiF_4)_2{\cdot}XeF_2$, $[NH_4][TiF_5]$ and $[H_3O][TiF_5]$.. 34
Figure 4.5: Selected part of the crystal structure of $(XeF_2{\cdot}TiF_4)_2{\cdot}XeF_2$, illustrating the $([FXeFTiF_4])_\infty$ chain. 35
Figure 4.6: Packing of $([FXeFTiF_4])_\infty$ chains and XeF_2 molecules in the crystal structure of $(XeF_2{\cdot}TiF_4)_2{\cdot}XeF_2$. 36
Figure 4.7: Xe1 coordination sphere in the compound $(XeF_2{\cdot}TiF_4)_2{\cdot}XeF_2$. Thin bonds d..... 37

Figure 4.8: Xe2 coordination sphere in the compound $(XeF_2{\cdot}TiF_4)_2{\cdot}XeF_2$. Thin bonds denote long contacts. Symmetry codes: (iii) −*x*+2.5, *y*+0.5, −*z*+1.5 (vi) −*x*+1.5, *y*−0.5, −*z*+1.5; (x) *x*, *y*+1, *z*; (xi) −*x*+2, −*y*, −*z*+1; (xii) −*x*+2, −*y*+1, −*z*+1; (xiii) −*x*+1.5, *y*+0.5, −*z*+1.5..... 38
Figure 4.9: Raman spectrum of $(XeF_2{\cdot}TiF_4)_2{\cdot}XeF_2$ recorded at room temperature on randomly oriented crystals..... 39
Figure 4.10: Crystals of $[Xe_2F_3][Ti_8F_{33}]$ growing on the inner wall of the FEP reactor..... 42
Figure 4.11: The assymetric unit of the compound $[Xe_2F_3][Ti_8F_{33}]$ consist of two separate..... 43
Figure 4.12: Representative structural part of the compound $[Xe_2F_3][Ti_8F_{33}]$. Ellipsoids are drawn at the 50% probability..... 44
Figure 4.13: Labeling scheme and connectivity of two crystallographically independent cubic assemblies found in $[Xe_2F_3][Ti_8F_{33}]$. The notation (‘) indicates a symmetrically generated atom. 45
Figure 4.14: Cube-like architectures found in different fluoridotitanates(IV). The terminal..... 49
Figure 4.15: Layered structure, cubic assemblies and different cation orientations found in $[Xe_2F_3][Ti_8F_{33}]$. All fluorine atoms, except the bridging ones of the $Xe_2F_3^+$ cations, have 50
Figure 4.16: The layered structure of $[(Ti_8F_{33})^-]$ anion. 51
Figure 4.17: Packing diagram and the unit cell of $[Xe_2F_3][Ti_8F_{33}]$; view along the *a*-axis. 51
Figure 4.18: Unit cell edges and packing diagram of $[Xe_2F_3][Ti_8F_{33}]$; view along the *b*-axis..... 52
Figure 4.19: Xe1 and Xe2 coordination environment in $[Xe_2F_3][Ti_8F_{33}]$. The Xe2F3 moieties are graphically depicted with thick bonds, while thin lines are used for long contacts within the Van der Waals sphere..... 53
Figure 4.20: Raman spectrum of $[Xe_2F_3][Ti_8F_{33}]$ recorded at room temperature on a powdered sample. 54
Figure 4.21: A magnified view on different crystal morphologies of $[Xe_2F_3][Ti_8F_{33}]$ and $[XeF]_2[Ti_9F_{38}]$ inside a sealed quartz capillary. The pale-white shade on some crystals is related to a partial decomposition on their surface..... 55
Figure 4.22: The assymetric unit of the compound $[XeF]_2[Ti_9F_{38}]$ (ellipsoids are drawn at the 50% probability level)..... 56
Figure 4.23: Construction of $[(XeF)_2(Ti_9F_{36}F_{2/2})]$ units found in $[XeF]_2[Ti_9F_{38}]$. The trigonal prismatic 57
Figure 4.24: Columns found in crystal structures of TiF_4 (*left*) and $[XeF]_2[Ti_9F_{38}]$ (*middle*). On the *right*, the trigonal prismatic anion $[Ti_6F_{27}]^{3-}$ determined in $[GuH]_3[Ti_6F_{27}] \cdot SO_2$..... 59
Figure 4.25: The trimeric $[Ti_3F_9F_{6/2}]$-rings in $[XeF]_2[Ti_9F_{38}]$ are connected through μ-F bridges into a prismatic skeleton, which is further linked to neighboring $[Ti_9F_{36}F_{2/2}]$ units by single-vertex sharing. Some transversally bridging and terminal fluorine atoms have been removed for clarity. 60
Figure 4.26: Correlation between measured Xe−F_b (F_b-bridging fluorine) bond lengths of some XeF^+ compounds and calculated FIA (fluoride ion activity) values of their parent MF_5 and M_2F_{10} Lewis acids (see references in Table 1.1). The missing FIAs of fluoride ion acceptors relevant to this work are estimated by extrapolation assuming a linear relationship (source data for linear regression supplied in table within the diagram). 62
Figure 4.27: Columnar structures of $[XeF]_2[Ti_9F_{38}]$ (*left*) and TiF_4 (*right*)..... 67
Figure 4.28: Columns in $[XeF]_2[Ti_9F_{38}]$ are comprised of chiral prismatic $[Ti_9F_{36}F_{2/2}]$-units multiplied and stacked by axial glide planes perpendicular to the *b*-axis. 67
Figure 4.29: Xe1 coordination environment with long intra- and intermolecular contacts (*thin* bonds) in $[XeF]_2[Ti_9F_{38}]$. 69
Figure 4.30: Xe2 coordination environment including long intermolecular contacts (*thin* bonds) in $[XeF]_2[Ti_9F_{38}]$. 70
Figure 4.31: : Raman spectrum of $[XeF]_2[Ti_9F_{38}]$ recorded at room temperature on a powdered sample. 71
Figure 4.32: Scatter plot showing the corelation between observed Ti – F_t stretching f 72
Figure 4.33: T..... 73
Figure 4.34: Formation of compound $[Xe_2F_3][Ti_8F_{33}]$ followed by Raman spectroscopy. The spectra (*a*-*c*) were recorded on the glassy material of unknown composition using a st matrix. 74
Figure 4.35: Crystalogenesis of product $[Xe_2F_3][Ti_8F_{33}]$ from the gel-like matrix observed t..... 75
Figure 4.36: The Raman spectrum is dominated by unreacted KrF_2 (464 cm^{-1}) and TiF_4 (804 and 829 cm^{-1}).. 78

Figure 4.37: Construction of the double-chained $[Ti_2F_9]^{-1}$ anion found in β-$[H_3O][Ti_2F_9]$. The corresponding geometric parameters are given in Table 4.13. 79
Figure 4.38: Selected part of the crystal structure of β-$[H_3O][Ti_2F_9]$. Several H_3O^+ cations were omitted for clarity. 81
Figure 4.39: The atoms in the asymmetric unit (black labels) of $[Xe_2F_3][Sn_4F_{17}]\cdot XeF_2\cdot HF$ with completed coordination of symmetrically generated atoms (grey labels). Thermal ellipsoids are drawn at the 50 % probability level. A standard representation model is used for hydrogen. . 85
Figure 4.40: Pentagonal bipyramidal geometry of the Sn(3) atom found in $[Xe_2F_3][Sn_4F_{17}]\cdot XeF_2\cdot HF$ with Sn–F bond lengths (Å) of axial (*left*) and equatorial (*right*) fluorine atoms. Thermal ellipsoids are shown at the 50% probability level, Further bridging connections to neighboring Sn atoms are drawn with broken-off bonds. 86
Figure 4.41: Extended coordination environment of the $(Sn3)F_2F_{5/2}$ –unit. HF molecules are omitted for clarity; the probability of the thermal ellipsoids is 50 %. Broken-off bonds denote further connections..... 87
Figure 4.42: The $[(Sn_4F_{17})^-]$ anion found in $[Xe_2F_3][Sn_4F_{17}]\cdot XeF_2\cdot HF$ exhibits a layered structure of vertex-sharing octahedral and pentagonal bipyramidal units. 88
Figure 4.43: The derived model function is based on narrow 1-D selection - a backbone. 90
Figure 4.44: The wave-like 2-D structure of the polymeric $[Sn_4F_{17}]^-$ anion found in $[Xe_2F_3][Sn_4F_{17}]\cdot XeF_2\cdot HF$. Terminal F atoms are omitted for clarity. 91
Figure 4.45: Layered structure of $[Xe_2F_3][Sn_4F_{17}]\cdot XeF_2\cdot HF$. 91
Figure 4.46: Coordination environment of the $Xe_2F_3^+$ cation in $[Xe_2F_3][Sn_4F_{17}]\cdot XeF_2\cdot HF$. Long contacts lying within the sum of the F and Xe Van Der Waals radii (3.63 Å) are drawn as thin bonds..... 93
Figure 4.47: Coordination sphere of the non-bonded XeF_2 molecule in the crystal structure of $[Xe_2F_3][Sn_4F_{17}]\cdot XeF_2\cdot HF$. Thin bonds denote long intermolecular contacts..... 94
Figure 4.48: Cationic $\{Xe_2F_3^+—XeF_2\}$ networks follow the wave-like pattern between anionic layers in compound $[Xe_2F_3][Sn_4F_{17}]\cdot XeF_2\cdot HF$. Long interactions are depicted with thin bonds. . 94
Figure 4.49: Comparison of $Ng_2F_3^+\cdots NgF_2$ contacts (only NgF_2 secondary spheres are shown) found in analogous compounds $[Kr_2F_3][SbF_6]\cdot KrF_2$ (*left*), $[Kr_2F_3]_2[SbF_6]_2\cdot KrF_2$ (*middle*) and $[Xe_2F_3][RuF_6]\cdot XeF_2$ (*right*)..... 95
Figure 4.50: Raman spectrum of $[Xe_2F_3][Sn_4F_{17}]\cdot XeF_2\cdot HF$ recorded on a single crystal under a thin protective layer of perfluorinated oil (peak denoted by asterisk(*)) at room temperature. 96
Figure 4.51: The Raman spectrum of thermally obtained XeF_2-rich product corresponds to the $3XeF_2\cdot 4SnF_4$ phase reported previously. 97
Figure 4.52: Raman spectroscopy analysis of a synthetic attempt (middle spectrum) in the system XeF_2-PbF_4. Peaks arising from FEP sample tube are denoted by asterisks (*). 98
Figure 4.53: The Raman spectrum of the white product, which precipitates first from XeF_2-SnF_4 systems of diluted aHF solutions, indicates the previously reported 1:2 phase and the presence of initial SnF_4 (lines 228 cm^{-1} and 620 cm^{-1}, Figure C. 2, Appendix C.1.1)..... 99
Figure 4.54: X-ray powder diffractograms of the reactants, powdered sample of $XeF_2\cdot 2SnF_4$ and simulated diffraction pattern of $[Xe_2F_3][Sn_4F_{17}]\cdot XeF_2\cdot HF$. 100
Figure 4.55: Xenon phase diagram. Adapted from Solid Xenon R&D Project by J. Yoo (FERMILAB, LBNL). 102
Figure 4.56: : a – Nickel vessel for experiments in supercritical xenon. b – Thick walled FEP reaction vessel for studies in liquid xenon. c – Synthesis and sedimentation in liquid xenon viewed through a transparent Dewar flask filed with cold ethanol. 103
Figure 4.57: Isolated crystals (sealed in quartz capillary, magnified view) of undefined composition grown upon reaction of XeF_2 and SnF_4 in liquid xenon. 104
Figure 4.58: Raman spectrum of undefined crystalline product obtained by reaction of XeF_2 with SnF_4 in liquid xenon. 104
Figure 4.59: Coordination environment of H_3O^+ and SnF_6^- ions in $[H_3O]_2[SnF_6]$. Through strong hydrogen bonds, each H_3O^+ cation is coordinated by three adjacent anions and each SnF_6-unit is connected to six H_3O^+ cations. Symmetry code: (i) $-x+1, -y+1, -z+1$. 108
Figure 4.60: Unit cell, hydrogen bonding and packing arrangement of cations and anions in compound $[H_3O]_2[SnF_6]$..... 109
Figure 4.61: Raman spectrum of $[H_3O]_2[SnF_6]$ recorded on a bulk sample is consistent with spectra obtained on randomly oriented single crystals with verified unit cell parameters. 110

Figure 4.62: The polymeric $[SnF_5]^-$ anion determined in the crystal structure of $[H_3O][SnF_5]$ consists of *cis*-μ-F bridged SnF_6-octahedra. 111
Figure 4.63: Coordination environment of SnF_6-octahedra (*left*) and oxonium cations (*right*) found in the crystal structure of $[H_3O][SnF_5]$. 112
Figure 4.64: Raman spectrum of $[H_3O][SnF_5]$ obtained on a randomly oriented crystal. 114
Figure 4.65: Packing diagram showing the unit cell and hydrogen interactions between the $[SnF_5]^-$ chains and H_3O^+ cations. ..... **Error! Bookmark not defined.**
Figure 4.66: Linkage of SnF_6-octahedra in the polymeric $[SnF_5]^-$ anion found in the structure of $Na[SnF_5]$. 115
Figure 4.67: Coordination environment of Sn (left) and Na (right) atoms in $Na[SnF_5]$. 116
Figure 4.68: Raman spectrum of compound $Na[SnF_5]$ obtained on a randomly oriented single crystal with certified unit cell parameters. 117
Figure 4.69: Packing diagram of compound $Na[SnF_5]$. View along the *b*-axis 118
Figure 4.70: Chain-like structure of the polymeric $[SnF_5]$ anion and hydrogen bonding found in the double-salt $Na[H_3O][SnF_5]_2$. 121
Figure 4.71: Coordination environment of $Sn(1)F_6$ and $Sn(2)F_6$ octahedra in $Na[H_3O][SnF_5]_2$. 121
Figure 4.72: Coordination environment of Na^+ (*left*) and H_3O^+ (*right*) cations in $Na[H_3O][SnF_5]_2$. 122
Figure 4.73: Packing of Na^+, $[H_3O]^+$ and $[SnF_5]^-$ ions in the crystal structure of $Na[H_3O][SnF_5]_2$. 122
Figure 4.74: Ladder-like structure of the $([Sn_2F_9]^-)_\infty$ anion determined in the compound $Na[Sn_2F_9]\cdot HF$. Broken-off bonds denote further connections. 124
Figure 4.75: The $([Sn_2F_9]^-)_\infty$ anion found in $Na[Sn_2F_9]\cdot HF$ viewed along the crystallographic *c*-axis. The SnF_6 octahedra belonging to separate chains are in eclipsed conformation. 124
Figure 4.76: Interactions between Na^+ cations, HF molecules and $([Sn_2F_9]^-)_\infty$ anions in the crystal structure of $Na[Sn_2F_9]\cdot HF$. 127
Figure 4.77: Selected structural features of compound $Na[Sn_2F_9]\cdot HF$. *Left* - coordination environment of sodium cations. *Right* - $Sn(1)F_6$ and $Sn(2)F_6$ environment. 128

Figure A. 1: Extended structure of the adduct $XeF_2\cdot 2CrF_4$. 131
Figure A. 2: A wave-like ribbon was selected from the anionic layer found in the s ..... **Error! Bookmark not defined.**

Figure B. 1: Crystal structure (*left*) and tiny crystals of $(XeF_2\cdot TiF_4)_2\cdot XeF_2$ (*right*) produced with a high-yield preparative method. 134
Figure B. 2: Low temperature (−150 °C) Raman spectrum (with applied baseline c (**). 134
Figure B. 3: Low temperature (−150 °C) Raman spectrum (with applied baseline c. 135
Figure B. 4: X-ray diffraction pattern of a powdered sample of the glassy material found in thermal reactions between XeF_2 and TiF_4. 139

Figure C. 1: Raman spectrum recorded on a single-crystal of $[Xe_2F_3][Sn_4F_{17}]\cdot XeF_2\cdot HF$. The background is dominated by peaks (*) arising from a protective layer of perfluorinated oil (perfluordecalin). 142
Figure C. 2: Raman spectrum of SnF_4 recorded on a powdered sample. 142
Figure C. 3: A wave-like ribbon was selected from the anionic layer found in the s 145
Figure C. 4: Raman spectrum of a sample at RT obtained after aHF-solvolysis of the product formed in a reaction of XeF_2 and SnF_4 in liquid xenon. 146

List of Tables

Table 1.1: Abbreviated pF^- scale and corresponding fluoride ion affinities for selected species. 4
Table 1.2: Overview of structurally determined oligomeric and polymeric fluoridotitanates. 9
Table 3.1: Overview of chemicals used in this work and their synthetic role. 23
Table 4.1: Characterization results obtained from the previous studies of the system XeF_2 -TiF_4. 29
Table 4.2: Crystal structure determination and refinement details for compound $(XeFTiF_5)_2{\cdot}XeF_2$. 30
Table 4.3: Selected geometric parameters for the compound $(XeF_2{\cdot}TiF_4)_2{\cdot}XeF_2$. 33
Table 4.4: Xe1 and Xe2 coordination environment in the compound $(XeF_2{\cdot}TiF_4)_2{\cdot}XeF_2$. 36
Table 4.5: Crystal structure determination and refinement details for compound $[Xe_2F_3][Ti_8F_{33}]$. 42
Table 4.6: Selected geometric parameters for the compound $[Xe_2F_3][Ti_8F_{33}]$. 45
Table 4.7: Xe1 and Xe2 coordination environment in the compound $[Xe_2F_3][Ti_8F_{33}]$. 52
Table 4.8: Crystal structure determination and refinement details for compound $[XeF]_2[Ti_9F_{38}]$. 55
Table 4.9: An overview of reported Xe−F_t (F_t, terminal fluorine) and Xe−F_b (F_b, bridging fluorine) bond lengths and Xe−F_t vibrational assignments among selected XeF^+ compounds and $[XeF]_2[Ti_9F_{38}]$. 61
Table 4.10: Selected geometric parameters for the compound $[XeF]_2[Ti_9F_{38}]$. 62
Table 4.11: Xe1 and Xe2 coordination environment in the compound $[XeF]_2[Ti_9F_{38}]$. 67
Table 4.12: Crystal structure determination and refinement details for compound β-$[H_3O][Ti_2F_9]$. 79
Table 4.13: Selected geometric parameters for the compound β-$[H_3O][Ti_2F_9]$. 79
Table 4.14: Characterization results obtained from previous studies of the system XeF_2 -SnF_4. 82
Table 4.15: Crystal structure determination and refinement details for compound $[Xe_2F_3][Sn_4F_{17}]{\cdot}XeF_2{\cdot}HF$. 84
Table 4.16: Selected geometric parameters for the compound $[Xe_2F_3][Sn_4F_{17}]{\cdot}XeF_2{\cdot}HF$. 88
Table 4.17: Xe1 and Xe2 coordination environment in the compound $[Xe_2F_3][Sn_4F_{17}]{\cdot}XeF_2{\cdot}HF$. 92
Table 4.18: Crystal structure determination and refinement details for compound $[H_3O]_2[SnF_6]$. 106
Table 4.19: Selected geometric parameters for the compound $[H_3O]_2[SnF_6]$. 107
Table 4.20: Geometric parameters associated with hydrogen bonding in $[H_3O]_2[SnF_6]$. 109
Table 4.21: Crystal structure determination and refinement details for compound $[H_3O][SnF_5]$. 110
Table 4.22: Selected geometric parameters for the compound $[H_3O][SnF_5]$. 112
Table 4.23: Geometric parameters associated with hydrogen bonding in $[H_3O][SnF_5]$. 112
Table 4.24: Crystal structure determination and refinement details for compound $Na[SnF_5]$. 114
Table 4.25: Selected geometric parameters for the compound $Na[SnF_5]$. 116
Table 4.26: Crystal structure determination and refinement details for compound $Na[H_3O][SnF_5]_2$. 118
Table 4.27: Selected geometric parameters for the compound $Na[H_3O][SnF_5]_2$. 119
Table 4.28: Geometric parameters associated with hydrogen bonding in $Na[H_3O][SnF_5]_2$ 121
Table 4.29: Crystal structure determination and refinement details for $Na[Sn_2F_9]{\cdot}HF$. 123
Table 4.30: Selected geometric parameters for the compound $Na[Sn_2F_9]{\cdot}HF$. 124

Abbreviations

aHF . . . Anhydrous hydrogen fluoride
BV . . . Bond valence
CN . . . Coordination number
DFT . . . Density functional theory (method)
En . . . Ethylenediamine (ligand)
F_b . . . Bridging fluorine atoms
FEP . . . Fluorinated ethylene propylene
F_t . . . Terminal fluorine atoms
GOF . . . Goodness of fit
Gu . . . Guanidine
HSAB . . . Hard and soft acids and bases (concept)
i.d. . . . Inner diameter
Im . . . Imidazole
Kel-F . . . Polychlorotrifluoroethylene
LS . . . Least Squares (method)
MO . . . Molecular orbital (theory)
MP2 . . . Second-order Møller-Plesset Perturbation Theory
o.d. . . . Outer diameter
PTFE . . . Polytetrafluoroethylene
Py . . . Pyridine
VBT . . . Volume-based thermodynamics
VSEPR . . . Valence shell electron pair repulsion (model)
WCA . . . Weakly coordinating anion

Chapter 1

Introduction

1.1 Historical Introduction into Nobel-Gas Reactivity

In 1894, J. W. Strutt (Lord Rayleigh) and his collaborator Sir William Ramsay announced the isolation of a new element – argon, the most plentiful of the group 18 – the noble gases. Although Cavendish had obtained an inert residue from atmospheric nitrogen more than 100 years earlier and the presence of helium in the sun had been spectroscopically observed in 1868, the discovery of argon (from the Greek argos – meaning "lazy") was unexpected and received with skepticism. Then, within a period of only five years, the isolation of the rest of the noble gases was reported: krypton (from the Greek kryptos, meaning "hidden"), neon (neos –"new"), xenon (xenos – "strange") and finally, in 1900, radon (radioactive emanation). It was clear that the new group completed well the Mendeléev table, fitting perfectly between the electro-negative elements (the halogens) and the electro-positive elements (the alkali metals) [1]. However, their chemical non-reactivity was found anomalous and not predicted by Mendeléev's periodic laws.

Stimulated by the suggestion of Professor Giuseppe Oddo, who in 1902 predicted and later reported[2] that at least krypton and xenon ought to show a certain tendency towards chemical combination due to the general increase in valence down a row of the periodic table, Ramsay sent a sample of argon to the French chemist Henri Moissan, the discoverer of elemental fluorine. Moissan's attempt to synthesize a fluoride failed and Ramsay considered his friend's report the ultimate proof for the inertness of argon. Among other events that fed the need for such attempts is definitely Walther Kossel's 1916 prediction about the existence of krypton and xenon fluorides, which was based on the ionization potentials for these atoms. Similarly, another simple consideration of ionic radii led the Nobel-prize winning chemist Linus Pauling to predict oxygen coordination numbers of four and six for krypton and xenon, respectively. In 1933, he published a paper[3] dealing mainly with the formula of antimonic acid, and he used the same sphere-packing reasoning to conjecture structures and formulas as H_4XeO_6 for xenic acid and its salts Ag_4XeO_6, AgH_3XeO_6. Additionally, he predicted KrF_6 and XeF_6, with XeF_8 as an unstable compound which might be capable of existence. His colleagues Don Yost and Albert Kaye came close[4] to preparing xenon fluorides using electric discharges of xenon-fluorine mixtures, and their efforts were later often described as a "near-miss".[5] Ironically, 32 years later, a similar experiment[6,7] using sunlight instead of electric discharge provided a convenient method for the synthesis of XeF_2.

In order to verify the aforementioned predictions, more famous experimentalists of the time joined the challenge – among others, Andreas von Antropoff, Walter Menzel and Otto Ruff, who was considered as one of the greatest inorganic fluorine chemists of all time (unfortunately, his research work focused on krypton and argon fluorides). The result were only reports[8,9,10] of unsuccessful experiments, which were taken generally as the ultimate proof that the noble gases are indeed inert, a principle that found its way into practically all chemistry textbooks.

The Bohr model of the atom, formulated by Niels Bohr in 1913, sees the group 18 of the periodic table on a confirming position in the electronic theory of valence. The widely held belief in the intrinsic lack of reactivity of the noble gases was firmly supported by their electronic structure: s^2p^6 (and s^2 for helium) – the configuration that became known as "the stable octet" leaves the noble gases without a tendency to gain or lose electrons, which is basically the valence electron arrangement to which other elements tend in their chemical bonding.

For many years, conventional scientific wisdom held that the only compounds “inert” gases could form were clathrates (Figure 1.1). These solids are composed of a guest (usually a gas or a volatile substance), trapped in the holes of a crystal skeleton formed by the host substance. The forming process of a clathrate does not involve the formation of true chemical bonds between the two components, thus the guest molecules are easily released upon heating or dissolution of a clathrate. Since their discovery, due to their unique physical and chemical properties, from which their role in the geosphere[11] and Solar System,[12] applications in medicine,[13] material science[14] and more are derived, the wide interest in the clathrate compounds has never diminished.

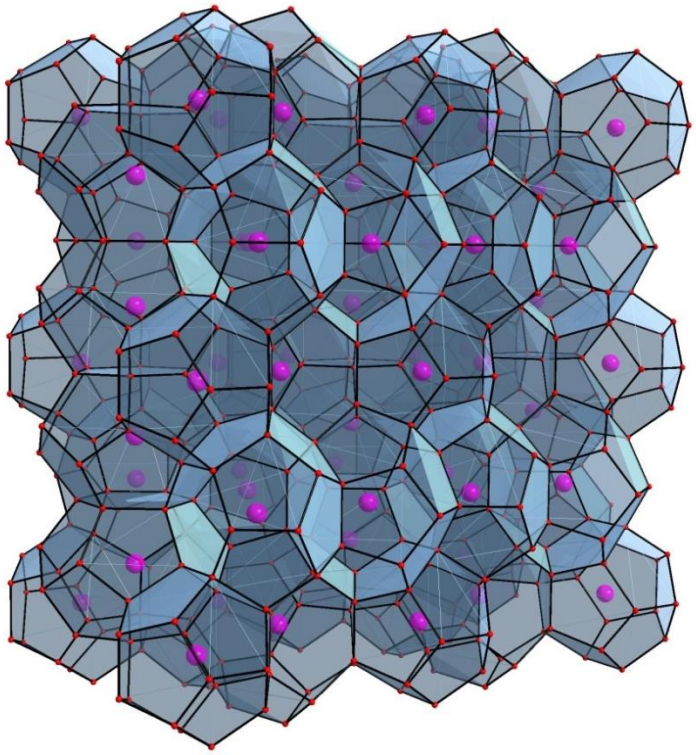


Figure 1.1: The structure of a Xenon Hydrate, $Xe_{3.27}[H_2O]_{23}$ (hydrogen atoms have been omitted for clarity).[15] Clathrate hydrates can exist as non-stoichiometric compounds or structures with fixed stoichiometry in which hydrogen-bonded H_2O molecules form a crystalline lattice.[1] The 3-D framework leaves cage-like voids that trap xenon atoms individually via weak van der Waals interactions. Heating the compound or lowering the outer pressure causes the collapse of the skeleton into liquid water and xenon gas evolution.

Nevertheless, there were several reasons why chemists believed that, by applying correct conditions, noble gases might react into authentic chemical compounds. The octet rule was known to have some exceptions and did not cover satisfactorily all known chemical compounds, which made it more a theory with explanatory rather than genuine predictive power. However, its general acceptance probably hindered many concentrated experimental attempts prior to 1962.

In the spring of 1962 at the University of British Columbia (UBC), Neil Bartlett and Derek Lohmann, when purifying PtF_4 by heating it in a stream of diluted fluorine, obtained a red sublimate, which was initially identified as platinum fluoride oxide, PtF_4O, but soon reformulated correctly as the ionic salt dioxygen hexafluoroplatinate, $O_2^+PtF_6$.[16] This important correction indicated clearly that PtF_6 is indeed a powerful oxidizer. Bartlett recognized the importance of this unexpected reaction, which was an authentic oxidation of oxygen into O_2^+. The essential requirement that the electron affinity of PtF_6 should exceed 7 eV was met with skepticism. Bartlett’s subsequent logical reasoning and experiments confirmed his extraordinary ability to

see problems in a broad context, worthy of a Nobel Prize, a recognition that was never awarded.[17,18] He noted that the first ionization potential of xenon atoms is comparable to that of oxygen molecules.[19] Driven by his creative thinking and curiosity, Bartlett tried reacting xenon gas with PtF_6 vapor. The reaction was successful, and the yellow-orange solid that suddenly formed was recognized as xenon hexafluoroplatinate ("$XePtF_6$"), which officially became the world's first authentic noble gas compound (Chapter 1.5.1, Figure 1.5).[20,21] Bartlett's achievement was later included in Ball's Elegant Solutions[22] and hailed by *Chemical & Engineering News* as "one of the 10 most beautiful experiments in the history of chemistry", and "one of the most important developments in inorganic chemistry in modern times".[23] Within months, other laboratories worldwide successfully repeated the experiment. The formula of the colorful solid was later modified to $[XeF][PtF_5]$. Although the exact composition and intriguing mechanism lying behind the formation of "$XePtF_6$" have not been deciphered yet, the significance of this achievement remained clear and textbooks had to be rewritten. Encouraged by Bartlett's discovery, other chemists soon (before the end of 1962) began to make new compounds from xenon[24,25,26] and later, radon and krypton.

This sub-chapter provides only a glimpse into the first steps towards noble-gas reactivity, which was launched by Bartlett's extraordinary experimental discovery. The avalanche that followed this event was then faced with a short period of silence, but only to see a new burst of startling breakthroughs in the 21st century, despite the relatively small number of laboratories involved. This still ongoing period has been legitimately referred to as "A Renaissance in Noble Gas Chemistry",[27] with more exciting possibilities yet to be discovered.

1.2 Estimating Lewis Acidity

Lewis acids are electron-deficient molecules, ions or carbocations, whereas Lewis bases are molecules that contain readily available nonbonding electron pairs for donation.[28] While the Brønsted acid-base interaction is always accompanied by the transfer of a proton, which allows a meaningful and easy quantitative comparison of the acidity, no such common denominator is present in the Lewis acid-base system. Consequently, the definition of strength has no well-defined meaning when assessing Lewis acidity.[28]

Moreover, the "strength" or "coordinating power" of different Lewis acids can strongly depend on the nature of the Lewis bases involved. For instance, BF_3 reacts best with fluorides, but not with other halides.[29] BCl_3 exhibits a greater Lewis acidity than BF_3 towards strong bases such as NH_3, whereas in case of weak bases (e.g. CO), the stronger acid is BF_3.[30] Since these are not isolated exceptions, a number of qualitative methods were developed to categorize Lewis acids.

To rationalize the behavior and reactivity of Lewis partners, Pearson introduced the *hard and soft acids and bases principle* (HSAB).[31,32] Hard acids are represented by small acceptor atoms with hard to excite outer electrons, which bear substantial positive charge. Acceptor atoms with lower positive charge, large size and easily excited outer electrons correspond to soft acids. Hard and soft bases are defined accordingly. This simple principle states that hard acids prefer to bind to hard bases while soft acids prefer soft bases. A vast number of chemical reactions involving Lewis acid-base interactions can be clarified by this concept,[33] which also proved to be very useful in coordination fluorochemistry, on both predictive and explanatory levels.[34]

More attempts to rank certain Lewis acids qualitatively were carried out measuring their catalytic activities in Friedel-Crafts-type reactions,[35,36] but again, such ratings strongly depend on the nature of reaction under study.

In a growing need for a quantitative treatment, determinations of the strength of Lewis acids of the type MF_n were made in different solvents using conventional techniques: conductivity and solubility measurements, cryoscopy, aromatic hydrocarbon extraction, kinetic parameters determinations, electrochemical titrations, IR and NMR spectroscopy, acidity function determinations using UV-visible spectroscopy, various gas-phase (complexometry with F_3NO, F^- affinity measurements, etc.) and solid-phase techniques. However, the obtained data is not consistent and shows large discrepancies when comparing results given by these different methods.

Later, the development of theoretical DFT, as well as more sophisticated *ab initio* high-level MP2-type calculations, enabled predictions of the intrinsic acidities and gas-phase deprotonation enthalpies for 39 neutral strong or superstrong Brønsted acids, Brønsted-Lewis conjugate superacids, and even acidic cluster of zeolites.[37,38] Almost simultaneously, a

quantitative scale for Lewis acidity ranking 170 compounds was reported.[39] The scale is based on fluoride ion affinities, which were calculated using *ab initio* methods at the MP2/B2 level of theory and defined as negative enthalpies for the following type (Eq.1) of reactions:

$$[LA] + F^- \longrightarrow [LA]F^- \quad (LA = \text{Lewis acid}) \qquad (1)$$

To simplify the calculations, the resulting relative F^- affinities were converted to an absolute scale by anchoring the calculations to the known[40] experimental value for COF_2. In this way, pF^- values are proposed as a measure for the Lewis acidity strength, but the definition totally differs from the logarithmic based pH scale and represents simply the fluoride affinities in kcal mol^{-1} divided by 10. Instead of the pF^- scale, the unscaled enthalpies in SI units (kJ mol^{-1}) of selected species are given in Table 1.1 and will be used for discussions in the present work.

In addition to the listed methods, Raman spectroscopy has been used to assess the Lewis acidity of the pnictogen pentafluorides $(PnF_5)_n$ by comparing key Ng-F_t stretching frequencies of several corresponding NgF^+ salts (ion pairs). This stretching frequency is assumed to increase with increasing acidity of the fluoride acceptor species $(PnF_5)_n$ as a consequence of a weaker cation-anion interaction.[41, 42, 43] On the ionization pathway from NgF_2 to NgF^+,[43] the corresponding covalent bonding model changes from 3c-4e to 2c-2e in agreement with the Ng-F bond order increase from 0.5 to 1 upon F^- abstraction from NgF_2. This method provides the increasing order $BiF_5 \approx AsF_5 < SbF_5 < Sb_2F_{10}$,[41] which is in good agreement with relative Lewis acidity orders obtained from measurements in HF solutions using the aforementioned traditional techniques.

Table 1.1: Abbreviated pF^- scale and corresponding fluoride ion affinities for selected species.

Species	pF^-	Fluoride Ion Affinity (kJ mol^{-1})	Reference
Sb_3F_{15}	13.18	551.5	44
Au_2F_{10}	12.88	538.9	45
	14.41	602.9	44
Bi_2F_{10}	12.13	507.5	44
Sb_2F_{10}	12.19	510.0	46
	12.69	530.9	44
	12.59	526.8	46
AuF_5	14.12	590.8	45
	12.88	538.9	44
BiF_5	11.59	466.9	46
	10.91	456.5	44
SbF_5	12.03	503.3	39
	11.83	495.0	46
	11.30	472.8	44
AlF_3	11.50	481.2	
$AlFCl_2$	11.50	481.2	
AlF_2Cl	11.47	479.9	
$AlCl_3$	11.46	479.5	39
$TeOF_4$	10.79	451.4	
InF_3	10.75	449.8	
GaF_3	10.70	447.7	
AsF_5	10.59	443.1	39
	10.51	439.7	44
SnF_4	9.82	410.9	39
PF_5	9.49	397.1	44
	9.43	394.7	46
	8.43	352.7	39
TeF_4	8.34	348.9	
BF_3	8.31	347.7	39
GeF_4	8.30	347.3	
ClF_5	7.47	312.5	

BrF_3	7.35	307.5
SiF_4	7.35	307.5
SeF_4	7.12	297.9
POF_3	5.86	245.2
XeF_4	5.71	238.9
SF_4	5.67	237.2
COF_2	4.99	208.8
PF_3	4.49	187.9
HF	3.68	154.0

1.3 The Chemistry of XeF_2

1.3.1 XeF_2

The chemistry of xenon is the most extensive and diverse among the noble gases because its oxidation states range from 0 till +VIII (up to +VI in fluorides), which is also the highest oxidation state for all main-group elements.[47] Compounds containing xenon bounded to fluorine, chlorine, oxygen, nitrogen, carbon, gold and even itself were isolated and structurally characterized. It was estimated that, despite the relatively small number of laboratories involved in this field, over 500 noble gas compounds (mainly xenon compounds) have been prepared by 2013.[48] Several comprehensive reviews and book chapters have been published to date on this topic,[21,49-55] however a full account of the chemistry of xenon exceeds the scope of the present work, which focuses on the fluoride ion donor properties of XeF_2 (see Chapter 1.3.2).

Ironically, the first noble gas compound reported[20] was not a simple binary fluoride. Behind a cloudy story of predictions and pioneering, the synthesis of XeF_2 was first published independently by two research groups[25,56] in 1962 and several effective syntheses were quickly reported.[57,58,59] Xenon(II) fluoride can be prepared from a gaseous mixture of xenon and fluorine by providing necessary activation energy. This can be achieved by irradiation with 10 MeV energy protons, electrons from a Van de Graaff accelerator, high-density γ radiation, electric discharge, heat, or UV exposure. Larger quantities of XeF_2 can be obtained using the static thermal method,[49] employing large excess of xenon over fluorine in order to prevent the formation of higher xenon fluorides.[53] The gaseous mixture is heated in a nickel or Monel vessel at 400 °C, quenched to room temperature, and the product XeF_2 isolated by vacuum sublimation. It has been shown[60] that high yields of pure product can be obtained with Xe : F_2 molar ratios of *ca.* 2 : 1. The heterogeneous thermal reaction between Xe and F_2 takes place on the walls of the reaction vessel or on the surface of the added fluoride.[61] Among all binary fluorides of the transition metals, NiF_2 was found to be the strongest catalyst (surface area of *ca.* 100 m^2). However, the best preparative method for quantities up to 1 kg of high-purity XeF_2 is a photochemical reaction using UV irradiation of xenon-fluorine gaseous mixture in the mole ratio Xe : F_2 of 2 : 1 and with a catalytic addition of about 1 molar % of HF in the fluorine.[62]

XeF_2 can be obtained as colorless crystals. The melting point of XeF_2 is 402.18 K and the vapor pressure of the solid at 25 °C is 600 Pa, which allows a facile sublimation already at room temperature. XeF_2 readily dissolves in different inorganic and even certain organic solvents without oxidation or reduction (BrF_5, BrF_3, IF_5, anhydrous HF, CH_3CN, etc.).[63] The very high solubility in aHF (167 g/100 g)[64] allows a variety of experiments with XeF_2 to be carried out in solution and makes this solvent a preferred choice in inorganic Xe(II) chemistry.

The structure of XeF_2 was intensively studied using IR, Raman and ^{19}F NMR spectroscopy, neutron and X-ray diffraction. A vibrational spectroscopic study showed a linear and centro-symmetric structure ($D_{\infty h}$) in the vapor phase,[65] which is in agreement with the predicted AX_2E_3 arrangement of the VSEPR (valence shell electron pair repulsion) model.[66,67,68,69] Such structural arrangement is also in agreement with the MO theory (molecular orbital theory), high enthalpy of sublimation (55.71 kJ/mol) and assumed charge distribution in XeF_2 molecules ($^{-0.5}F–Xe^{+1}–F^{-0.5}$).[70] This representation describes well the delocalization of the electron pair, the formation of single-electron bonds and fits most of the physical and chemical properties of XeF_2. Upon

interaction of the latter with a fluorine acceptor, the involvement of an electron pair in each bond between F and Xe atoms is assumed in the Lewis ionic model, where the bond scheme is shown as the resonance between two canonical forms F-Xe^+ F^- and F^- Xe^+-F. This representation predicts formal Xe–F bond orders of one-half for XeF_2 and one for the free XeF^+ cation and reflects many physical and chemical properties of XeF_2.[71]

In order to achieve meaningful comparisons of the Xe–F bond length with modern results, the crystal structure of XeF_2[72,73] was recently redetermined[74] with better accuracy (Figure 1.2). The elongation of the Xe–F bond (1.999(4) Å) measured at −173 °C against the length reported in the gas phase (Raman,[75] 1.9791(1) Å; IR,[76] 1.974365(7) Å) is attributed to the 8 intermolecular Xe···F contacts (3.338 Å), which can be found within the sum of the van der Waals radii (Xe 2.16 Å, F 1.47 Å).[77]

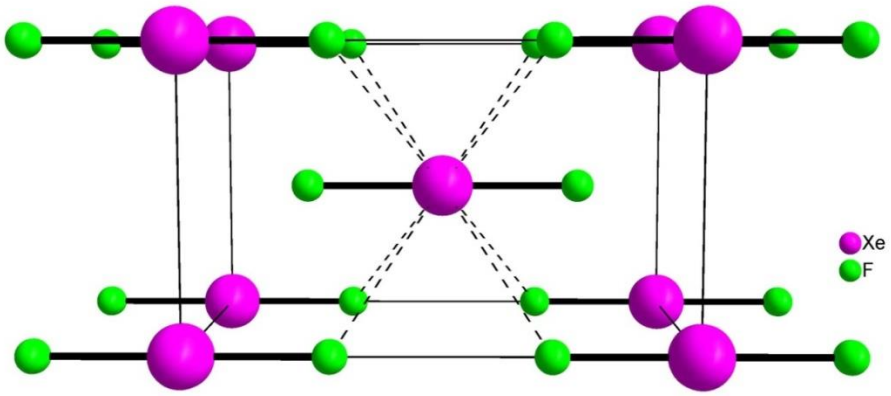


Figure 1.2: Unit cell of XeF_2 viewed along the a-axis, showing eight intermolecular Xe···F contacts (dashed lines).

XeF_2 is thermodynamically stable in a wide pressure and temperature range and it is commercially available today. Due to the inertness of its reduction product, xenon, XeF_2 has become a convenient oxidizer and fluorinator. These properties are even more pronounced when prepared as the cationic forms XeF^+, $Xe_2F_3^+$ in aHF. The electron affinity of its cationic species is greatly enhanced with respect to XeF_2 and the transfer of an electron to either of these cations generates the $XeF^\bullet$ radical as an effective source of atomic fluorine. In aHF, XeF_2 readily oxidizes many elements, lower fluorides, halides and halo complexes, oxides and carbonyls.[78] The oxidative ability is retained in aqueous solution, where XeF_2 is capable to oxidize chloride to chlorine, chlorate, bromate and iodate to the respective perhalates.[63] The interest in XeF_2 as a fluorinating agent is also growing in organic chemistry, with reports regarding the fluorination of fullerenes[79] and graphene.[80] Moreover, combinations XeF_2/fluoride ion acceptors have been recently proposed as versatile one-electron oxidants.[81]

Another very important aspect of the chemistry of XeF_2 is a rich series of coordination compounds, where XeF_2 acts as a ligand to the “naked” metal centers,[82] either as a non-bridging ligand interacting only with one metal center, or as a bridging ligand, connecting two metal centers. When specific conditions are met,[55] compounds of the type $[M^{n+}(XeF_2)_m[AF_6]^-_n]$ can form. Since the first complex of this type was reported[83] more than 20 years ago, several compounds of XeF_2 coordinated to monovalent (Li,[34,84] Ag[83,85]), divalent (Mg,[86-89] Ca,[90-92] Sr,[93,94] Ba,[34,95-98] Cu,[99,100] Zn,[100] Cd,[34,90,101-105] Hg,[104,106] Pb[93,94]) and trivalent (La,[107] Nd[88,108]) metal centers have been synthesized and structurally characterized.

Despite the abundancy of the coordination compounds given by XeF_2, no such tendency of a ligand behavior from KrF_2 towards metal centers has been reported until recently, where the first KrF_2 coordination to a metal has been observed in compounds $[Mg(KrF_2)_4(AsF_6)_2]\cdot 2BrF_5$ and $[Mg(KrF_2)_4(AsF_6)_2]$.[109] Similarly, the only example of XeF_4 as a metal ion ligand known thus far is $[Mg(XeF_2)(XeF_4)](AsF_6)_2$.[86]

There are also a few examples of XeF_2 coordinated to nonmetal centers, more specifically to the Xe(VI) atoms[43] of the XeF_5^+ cation in the compounds $2XeF_2\cdot[XeF_5][AsF_6]$, $XeF_2\cdot[XeF_5][AsF_6]$, $XeF_2\cdot 2[XeF_5][AsF_6]$, and to Br(V) of the $BrOF_2^+$ cation found in complexes $[BrOF_2][AsF_6]\cdot XeF_2$[110,111] and $[BrOF_2][AsF_6]\cdot 2XeF_2$.[111]

1.3.2 XeF^+ and $Xe_2F_3^+$ Compounds

XeF_2 acts as a moderately strong Lewis base and is a reasonably good fluoride ion donor.[112] The F^- donor ability among the binary xenon fluorides is well known: XeF_6 > XeF_2 >> XeF_4 and supported by the relative ratios of isolated compounds for each of these donors.

When the fluoride ion is abstracted from XeF_2 by a sufficiently strong Lewis acid, the bond between Xe^{II} and remaining F^- becomes a classical two-electron bond. The driving force for this process is the increase in the Xe–F bond energy during the cation formation (133.9 kJ/mol in XeF_2 compared to 195.9 kJ/mol in the cation XeF^+).[53] In fact, the Lewis acidity of the ionic metal in the aforementioned coordination compounds should not be strong enough to withdraw F^- from XeF_2, which would result in the salt formation. Compounds of composition $a$$XeF_2$·$b$$AF_5$ (A is a quinquevalent atom) have been known since 1963,[21,49] but several years passed before some of them were shown to be salts containing the cationic species.[112] XeF_2 reacts with pentafluorides of strong and moderate F^- acceptor strengths to give tight ionic pairs, which are best described as salts of XeF^+ and $Xe_2F_3^+$ cations with general formulations $XeF^+MF_6^-$ (M = Nb, Ta, Ru, Os, Pt, Ir, Au, As, Sb, Bi), $XeF^+M_2F_{11}^-$ (M = Nb, Ta, Ru, Pt, Ir, Sb, Bi) and $Xe_2F_3^+MF_6^-$ (M = Ta, Ru, Os, Pt, Ir, Au, As, Sb, Bi). Although most of these salts were extensively studied by vibrational and ^{19}F NMR spectroscopy, only the crystal structures of $[XeF][MF_6]$ (M = As,[113,74] Sb,[74] Bi,[74] Ir,[114], V[115,116], Ru[117]), $[XeF][M_2F_{11}]$ (M = Sb,[74,118,119] Bi[74]) and $[XeF][IrSbF_{11}]$[114], $[Xe_2F_3][MF_6]$ (M = As,[120,121,122] Sb[122], Ir,[123] Ru[123]) and $[Xe_2F_3][RuF_6]$·XeF_2[123] have been reported thus far.

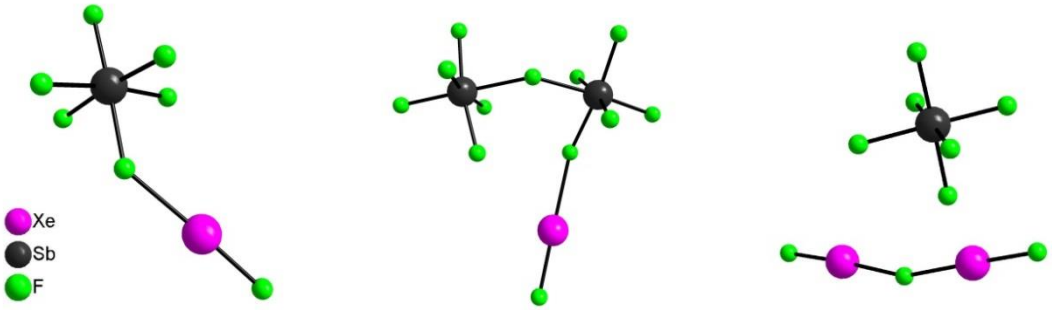


Figure 1.3: Three structural types of ion pairs demonstrated by the interactions of XeF_2 with SbF_5 (left to right): $[XeF][SbF_6]$,[74] $[XeF][Sb_2F_{11}]$,[74] $[Xe_2F_3][SbF_6]$[122].

In addition to the ionic pairs listed previously, a whole series of compounds, in which XeF_2 is found at the various stages of the ionization pathway,[43] have been reported. Examples, in which XeF_2 interacts with the metal by formation of asymmetric Xe-F-M bridges, are mostly represented by adducts formed by the reaction of XeF_2 with weak fluoride ion acceptors MF_4 (Chapters 1.4, 1.5) and MOF_4 ($a$$XeF_2$·$b$$MOF_4$, M = Mo, W;[124,125,126] crystal structures determined: XeF_2·$MoOF_4$,[127] XeF_2·WOF_4[128]).

The interaction of XeF_2 with even weaker fluoride ion donor acceptors results in a formation of compounds which are best described as molecular adducts (e.g. XeF_2·IF_5,[129] XeF_2·$XeOF_4$,[130,131] XeF_2·XeF_4[132]). In these cases, the molecular parameters of XeF_2 show little change to its solid-state form (Figure 1.2).

1.4 Metal Tetrafluorides and Fluoridometalates(IV)

Fluorine, the most electronegative element, is among the smallest and most rigid ligands. Therefore, the crystal structures of metal fluorides are relatively simple and governed mainly by geometric and electrostatic principles. It is not surprising that for many years the fluorides have been used for verifying the validity and limits of the rigid sphere concepts, where the

coordination numbers of the atoms strongly depend on the radius ratios. Additionally, the crystal structures of compounds and particularly those having transition-metal ions are affected by a variety of electronic effects, for instance Jahn-Teller distortion, covalency, back-bonding, etc. The coordination behavior, structural laws and bonding details in fluoride structures have been extensively studied during the past decades.[133]

Structures of the known metal tetrahalides MX_4 were classified[134,135] by the size of cations, coordination and dimensionality of the polyhedra formed. They were divided into four main groups. The first type belongs to small-sized cations, with tetrahedral coordination in molecular structures ($SnBr_4$ and SnI_4). The second type is valid for medium-sized cations, adopting mostly octahedral coordination. Several binary tetrafluorides can be found in this group and divided by the dimensionality of their solid-state structures: chains (α-NbI_4 and $TcCl_4$), columnar structures (isolated triple columns - TiF_4,[136] double columns of edge- and corner-sharing octahedra – α-CrF_4,[137] quadruple columns of corner sharing octahedra – β-CrF_4[138]), isolated layers of distorted octahedra sharing corners – VF_4,[139] MnF_4,[140] and RuF_4[141]), layered structures (SnF_4[142] and isotypic PbF_4,[142] $TaOF_3$ and NbF_4) and 3-D structures (IrF_4,[143,144] PtF_4[145]). The third and fourth groups are characterized by large-size cations and are represented by 2-D (layers – ThI_4[146]) and 3-D (8-coordinated metals; edge- and corner-sharing dodecahedra are found in 4 different structural types: U(Th)Cl_4,[147] α-ZrF_4,[148] β-ZrF_4,[149] γ-ZrF_4[135]) frameworks, respectively.

More details on the structural chemistry of TiF_4 and SnF_4, relevant to this work, are given in the following subsections.

1.4.1 TiF_4 and Fluoridotitanates(IV)

The solid-state structure of TiF_4[136] consists of individual columnar stacks of corner sharing TiF_6 octahedra in an infinite array. These columns are built from trimeric Ti_3F_{15} rings (Figure 1.4), where three TiF_6 octahedra share two *cis*-vertices. The relative low solubility in aHF and high melting point compared to other titanium(IV) halides reflect the polymeric structure in the solid phase, while the vapor contains tetrahedral molecules.[150]

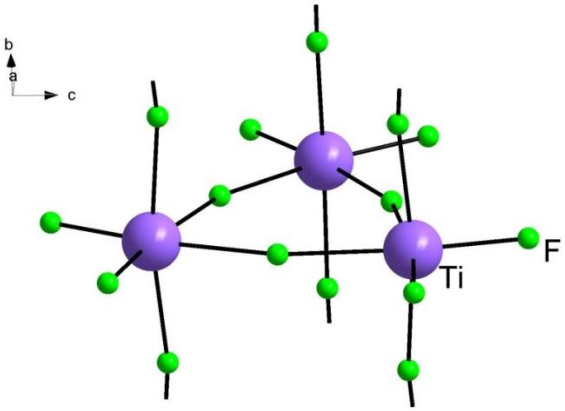


Figure 1.4: Ti_3F_{15} rings in the crystal structure of TiF_4.[136]

A few recent reviews[151,152,153] cover the chemistry of TiF_4, including reactions with Lewis bases and fluoride ion donors of different strength. The formation of the octahedral TiF_6^{2-} anion seems to be the most favorable in the majority of solvents and characterizations of a variety of compounds with monovalent and divalent metal cations, ammonium and several hybrid organic-inorganic complexes have been published.[154] However, a dramatic expansion of the known poly[perfluoridotitanate(IV)] anions has been achieved only recently with an extensive research work[155] delivering thirty nine new compounds. Nevertheless, especially polymeric fluoridotitanates with higher (2-D and 3-D) dimensionality remain poorly represented or ill-defined (Table 1.2).

Table 1.2: Overview of structurally determined oligomeric and polymeric fluoridotitanates(IV).

Anionic species and connectivity	Compound	Ref.
0-D DIMERIC AND OLIGOMERIC STRUCTURES		
dimeric $[Ti_2F_{11}]^{3-}$	$(ImH)_3[Ti_2F_{11}]$	156
	$(PyH)_2(H_3O)[Ti_2F_{11}]\cdot H_2O$	157
	$(NMe_4)_4[Ti_2F_{11}][Ti_2F_9(H_2O)_2]$	158
tetrameric rings $[Ti_4F_{20}]^{4-}$	α-$(ImH)_4[Ti_4F_{20}]$ β-$(ImH)_4[Ti_4F_{20}]$	156
	$(GuH)_4[Ti_4F_{20}]$ $(GuH)_4(H_3O)_4[Ti_4F_{20}][TiF_5]_4$	155
tetrameric $[Ti_4F_{19}]^{3-}$	$[XeF_5]_3[Ti_4F_{19}]$	159
Tetrahedral $[Ti_4F_{18}]^{2-}$	$[o\text{-}C_6H_4(PPh_2H)_2][Ti_4F_{18}]$	160
	$(Ph_4P)_2[Ti_4F_{18}]$	161
	$(NMe_4)_2[Ti_4F_{18}]$	161
	$[TiF_2([15]crown\text{-}5)]\ [Ti_4F_{18}]\cdot 0.5MeCN$	162
pentameric $[Ti_5F_{23}]^{3-}$	$(ImH)_3[Ti_5F_{23}]$	156
Trigonal prismatic $[Ti_6F_{27}]^{3-}$	$(GuH)_3[Ti_6F_{27}]\cdot SO_2$	155
Cubic $[Ti_8F_{36}]^{4-}$	$Rb_4[Ti_8F_{36}]\cdot 6HF$ $K_4[Ti_8F_{36}]\cdot 8HF$	163
	$(H_5O_2)_4[Ti_8F_{36}]$	155
Decameric $[Ti_{10}F_{45}]^{5-}$	β-$[XeF_5]_5[Ti_{10}F_{45}]$	164
1-D POLYMERIC STRUCTURES		
Chain, $[TiF_5]^-$	$(H_3O)[TiF_5]$	165
	$(NH_4)[TiF_5]$	166
	$(EnH_2)[TiF_5]_2$ $(GuH)_4(H_3O)_4[Ti_4F_{20}][TiF_5]_4$ $NaTiF_5$ and $NaTiF_5 \cdot HF$ $KTiF_5$ and $KTiF_5 \cdot HF$ $RbTiF_5 \cdot HF$ $CsTiF_5$	155
	$[XeF_5][TiF_5]$	164
Double chains, $[Ti_2F_9]^-$	$Cs[Ti_2F_9]$ α-$(H_3O)[Ti_2F_9]$	161
	β-$(H_3O)[Ti_2F_9]$	155
	α-$(ImH)[Ti_2F_9]$ β-$(ImH)[Ti_2F_9]$	156
	$(GuH)[Ti_2F_9]$ $NaTi_2F_9\cdot HF$ $RbTi_2F_9$ $CsTi_2F_9$	155
Columns, $[Ti_3F_{13}]^-$	$[XeF_5][Ti_3F_{13}]$	164
Columns, $[Ti_7F_{30}]^{2-}$	$(O_2)_2[Ti_7F_{30}]$	167
2-D POLYMERIC STRUCTURES		
Layers, $[Ti_8F_{33}]^-$	$Cs[Ti_8F_{33}]$	168
3-D POLYMERIC STRUCTURES		
3-D framework, $[Ti_6F_{27}]^{3-}$	not defined	155

1.4.2 SnF_4 and Fluoridostannates(IV)

Anhydrous SnF_4 is a white solid and has a polymeric *trans*-fluorine-bridged sheet structure[142] with octahedral Sn(IV) atoms (Figure 1.5). It sublimes at 978 K to give a vapor containing tetrahedral molecules[169].

Although it was reported that the Lewis acidity of the four Sn(IV) halides is greatest for SnF_4,[170] the coordination chemistry of this compound is still much less studied compared to other Sn(IV) halides. The polymeric nature of SnF_4 makes it unreactive towards neutral ligands and its coordination chemistry has been limited to strong O- and N-donor ligands for many years. This was changed by Tudela and co-workers, who reported[171,172] the reaction of SnF_2 with I_2 in MeCN to form $[SnF_4(MeCN)_2]$. This product is a soluble, efficient molecular source of SnF_4 and proved to be an excellent synthon,[151,173] which enables the introduction of soft donor ligands as well.

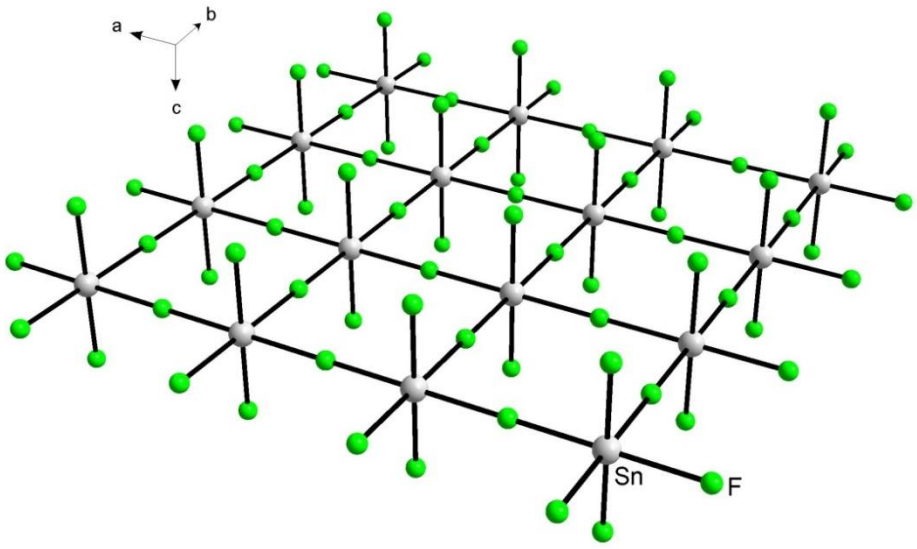


Figure 1.5: Octahedral SnF_6 units forming a layered structure in SnF_4.[142]

As in the case of TiF_6^{2-}, compounds with the SnF_6^{2-} anion are the most common among known fluoridostannates(IV) and basically the only being structurally characterized. Hexafluoridostannate(IV) salts of alkali and other monovalent metals[174, 175, 176, 177, 178, 179, 180, 181, 182, 183], divalent metals[184, 185, 186, 187, 188], mixed cations[189, 190], ammonium[180, 191, 192] and other nitrogen containing cations[193, 194, 195, 196] have been described and studied with different techniques, including X-ray crystal structure determination ($Li_2SnF_6{\cdot}2H_2O$[174], Na_2SnF_6[175,176], $K_2SnF_6{\cdot}KHF_2$[177], $K_2SnF_6{\cdot}H_2O$[177], Cs_2SnF_6[182], Tl_2SnF_6[183], $CaSnF_6$[184], $BaSnF_6$[186], $MSnF_6$ (M = Mn, Fe, Zn, Hg, Pb, Co, Ni, Cu[187], Cd)[185], $AgSnF_6$[188], $NaKSnF_6$[189], $NaRbSnF_6$,[190] $NaCsSnF_6$,[190] $(NH_4)_2SnF_6$[191], $(NH_4)_3FSnF_6$[192], $(N_2H_6)_2SnF_6F_2$[196], etc.), quantum chemical analysis[197], vibrational[198], Mössbauer[198,199], ^{119}Sn and ^{19}F NMR spectroscopy[200]. Although SnF_5^- and $Sn_2F_9^-$ are known[181, 201, 195, 202, 203], their structural nature remains ill-defined and mainly based on ^{19}F NMR studies and comparisons with polymeric fluoridotitanates(IV).[204,202]

1.5 XeF_2 – MF_4 Systems

1.5.1 XeF_2 – PtF_4 System

The first noble gas compound "$XePtF_6$" was prepared[20] by mixing equimolar quantities of red PtF_6 vapour and colourless Xe gas (Eq. 2). After breaking the seal (Figure 1.6) between these two compounds, a sticky, red-tinged yellow solid suddenly precipitated:

$$PtF_6(g) + Xe(g) \longrightarrow Xe(PtF_6)_x(s) \quad 1 \leq x \leq 2 \qquad (2)$$

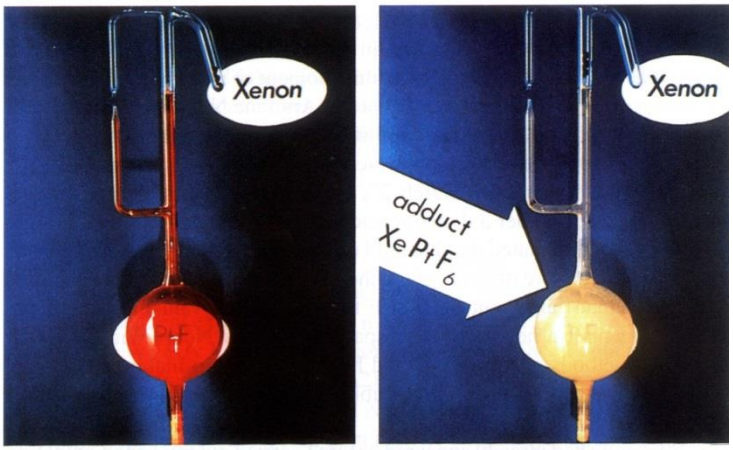


Figure 1.6: The historic experiment (recreated) producing the first noble-gas compound: when the glass seal separating the two gases (the red platinum hexafluoride at the bottom left and the colorless xenon in the small tube at the upper right) was broken using sphere magnets and the gases were allowed to mix, a bright yellow solid suddenly formed.

In their early studies of the oxidation of xenon by platinum hexafluoride, Bartlett and Jha found[21] that the stoichiometry of the product of that spontaneous reaction varied between $XePtF_6$ and $Xe(PtF_6)_2$, and was not 1:1 as had been concluded from the first preparation. More light on the reaction was thrown later[205] by performing additional experiments, where it was found that the X-ray powder diffraction pattern (XRDP) of the sticky red-tinged product $Xe(PtF_6)_X$ always exhibits the characteristic pattern of $XeF^+PtF_6^-$, which was found to be isostructural to $XeF^+RuF_6^-$. This means that first formed $XePtF_6$ (a Pt(IV) compound) interacts with additional platinum(VI) hexafluoride, giving two Pt(V) products: $XeF^+PtF_6^-$ and PtF_5 (Eq. 3):

$$XePtF_6 + PtF_6 \longrightarrow XeF^+PtF_6^- + PtF_5 \qquad (3)$$

PtF_5 does not crystallize easily, and its XRDP has never been observed in the $Xe(PtF_6)_X$ products. However, the colour as well as the stickiness of the solid is consistent[206] with its presence. Chemical evidence for this comes from the formation (Eq. 4, 5) of the orange-red, friable solid $XeF^+Pt_2F_{11}^-$, given by warming up the compound close to composition ~ $Xe(PtF_6)_2$ (XRDP of which show only $XeF^+PtF_6^-$):

$$Xe(PtF_6)_2 \xrightarrow{T \leq 60°C} XeF^+Pt_2F_{11}^- \quad \text{or:} \qquad (4)$$

$$XeF^+PtF_6^- + PtF_5 \xrightarrow{T \leq 60°C} XeF^+Pt_2F_{11}^- \qquad (5)$$

In addition, the interaction of XeF_2 with PtF_5 1:2 in BrF_5 solution was shown[112] to form the salt $XeF^+Pt_2F_{11}^-$. A vibrational study as well as XRDP showed it to be related to $XeF^+Sb_2F_{11}^-$(crystal structure obtained from single crystal data by Peacock et al.) and also to the structure of $XeF^+Ir_2F_{11}^-$.

A compound closest to the composition "$XePtF_6$" is best prepared[205] (Eq. 6) by mixing PtF_6 vapour, diluted with SF_6 gas in the ratio 1 : 6, with a large excess of Xe gas and quenching the product mixture at 77 K. $XePtF_6$, when pure, may be the relative of diamagnetic $XePdF_6$.[207] A mustard-yellow solid, obtained with this preparation technique, does not give the XRDP and is weakly paramagnetic, which indicates that small quantities of $XeF^+PtF_6^-$ and PtF_5 are present even in the best preparations.

PtF_6 (diluted 1 : 6 in SF_6) + Xe (in excess) $\longrightarrow$ "$XePtF_6$" (6)

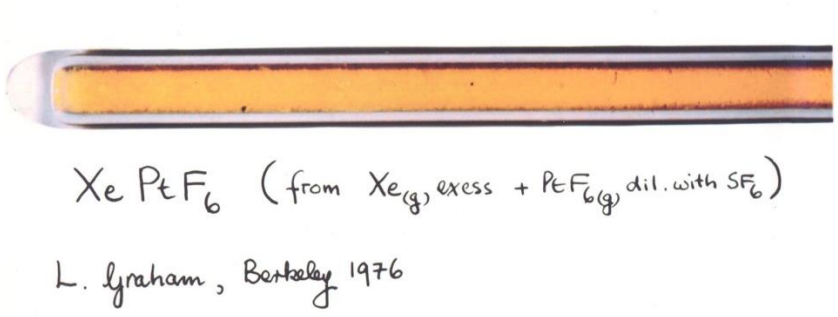


Figure 1.7: A sealed sample of a compound closest to the formulation "$XePtF_6$" prepared by Graham in 1976.

Another synthesis yielding a compound of composition close to the formulation of "$XePtF_6$" involves the dissolution of PtF_4 with a large excess of XeF_2 in aHF. ^{19}F NMR spectrum of the obtained yellow solution reveals the presence PtF_6^{2-}. PtF_6^{2-} in aHF is solvated with HF molecules and probably additionally stabilized by solvated and therefore less strongly polarizing cation $XeF^+_{(solv)}$, which after removal of aHF gives the strongly polarizing naked XeF^+(Eq. 7). This is capable of taking F^- from PtF_6^{2-} to yield PtF_5^- which could then oligomerize. Thus, the "$XePtF_6$" obtained from that solution is probably a XeF^+ salt of polymeric yield $(PtF_5^-)_n$ (Eq. 8).

$$2XeF_{2\,(solv)} + PtF_{4\,(s)} \xrightarrow{aHF} 2XeF^+_{(solv)} + PtF_6^{2-}{}_{(solv)} \quad (7)$$

$$n(XeF^+)_2PtF_6^{2-} \xrightarrow{\text{removal of aHF}} nXeF_2 + (XeF^+)_n(PtF_5^-)_n \quad (8)$$

"$XePtF_6$"

Some other, mostly thermal redox reactions were also investigated.[207] Liquid XeF_2 at 140-150 °C oxidized PtF_4 giving a Pt(V) $Xe_2F_3PtF_6$ (Eq. 9):

$$5XeF_{2\,(l)} + 2PtF_4 \xrightarrow{140\text{-}150\ °C} 2Xe_2F_3PtF_6 + Xe \quad (9)$$

The salt $Xe_2F_3^+PtF_6^-$ loses XeF_2 at 70 °C in *vacuo* (Eq. 10):

$$Xe_2F_3PtF_6 \xrightarrow{70\ °C} XeFPtF_6 + XeF_2 \quad (10)$$

Pyrolysis of $XeFPtF_6^-$ at 150-160 °C yields XeF_4 (Eq. 11). Xe(II) is oxidized to Xe(IV), Pt(V) goes to Pt(IV):

$$2XeFPtF_6 \xrightarrow{150\text{-}160\ °C} XePt_2F_{10} + XeF_4 \quad (11)$$

The Pt(IV) complex $XePt_2F_{10}$ loses XeF_2 at 430 °C; by liquid XeF_2 at 140-150 °C can be oxidized back to Pt(V) in $Xe_2F_3PtF_6$ compound:

$$XePt_2F_{10} \xrightarrow{430\ °C} PtF_4 + XeF_2 \quad (12)$$

$+ XeF_2$, 140-150 °C

$Xe_2F_3PtF_6 + Xe$

1.5.2 $XeF_2 – PdF_4$ System

The reaction between liquid XeF_2 at 140-150 °C and PdF_4 yielded a diamagnetic yellow material.[207] Changes in slope in a weight-loss time curve indicated that 4:1, 3:1, 2:1 and 1:1 XeF_2:PdF_4 complexes probably occur, however all but the 1:1 complex lose XeF_2 at or below 20° C. Experience with the XeF_2/PtF_4 system suggested that liquid XeF_2 might prove capable of oxidizing the mixed valence palladium fluoride Pd_2F_6. The reaction (Eq. 13) occurred.

$$(x+1)\,XeF_2 + Pd_2F_6 \xrightarrow{140\text{-}150\,^\circ C} xXeF_2{\cdot}PdF_4 + Xe \qquad (13)$$

This is a very convenient path since Pd_2F_6 is much easier to synthesize than PdF_4. Similarly to the reaction pathways of such compounds of platinum, the fluoride ion donor capability of XeF_2, coupled with its oxidizing power, are responsible for the oxidation of Pd_2F_6. The product in liquid XeF_2 (Eq. 14) is probably the salt $(Xe_2F_3^+)_2PdF_6^{2-}$ in accordance with the yellow color, characteristic of PdF_6^{2-} salts.

$$Pd_2F_6 + 9XeF_2(l) \xrightarrow{140\,^\circ C} 2(Xe_2F_3)_2PdF_6 \xrightarrow[-6XeF_2]{\text{RT, dynamic vacuum}} 2(XeF_2{\cdot}PdF_4) \qquad (14)$$

In $Xe_2F_3^+$ each Xe atom has two F atom neighbors connected approximately linearly to it and the electron-attracting capability, that such a Xe atom has, is much less than the XeF^+ cations possess. The consequence of the interaction of XeF^+ with one of the fluorides of the anion is to denude that ligand, and the entire anion, of some electron density, increasing the oxidative power of the metal fluoride part.[207]

A solution of XeF_2 in aHF reduces PdF_4 to Pd_2F_6, where only a part of the PdF_4 dissolves to give PdF_6^{2-}.[205] It was suggested that the fluoride ion donor capabilities of XeF_2 are in this case in competition with its ability to act as a reducing agent towards PdF_4, which is a very potent oxidizer and a fluorinating agent:

$$2XeF_{2\,(solv)} + PdF_{4\,(c)} \xrightarrow{\text{RT, aHF}} 2XeF^+_{(solv)} + PdF_6^{2-}{}_{(solv)} \qquad (15)$$

$$XeF_{2\,(solv)} + 2PdF_{4\,(c)} \xrightarrow{\text{RT, aHF}} XeF_{4\,(solv)} + Pd_2F_{6\,(c)} \qquad (16)$$

In contrast to XeF_2 dissolved in an aHF solution, liquid XeF_2 provided a route to pure $XePdF_6$ from Pd_2F_6.[207]

Pyrolysis of $XePdF_6$ ($XeF_2{\cdot}PdF_4$), which is thermally stable at room temperature, gives its "XeF_2 poor" relative (Eq. 17):

$$2XePdF_6 \xrightarrow{\text{140-150 °C, dynamic vacuum}} XePd_2F_{10} + XeF_2 \qquad (17)$$

$XePd_2F_{10}$ ($XeF_2{\cdot}2PdF_4$) is a close structural relative of $XePt_2F_{10}$ ($XeF_2{\cdot}2PtF_4$). Spectroscopic evidence suggests that both are salts of XeF^+ and a polymeric $(M_2F_9)_x^{x-}$.[207]

1.5.3 $XeF_2 – CrF_4$ System

1.5.3.1 $XeF_2{\cdot}CrF_4$

In 1971, investigations of the system chromium fluorides-xenon fluorides began[208,209] and the crystal structure of $XeF_2{\cdot}CrF_4$ was reported in 1992.[210] Since XeF_2 is capable of oxidizing chromium to only Cr(III), $XeF_2{\cdot}CrF_4$ was made by the reaction between CrF_5 and XeF_2. For the latter reaction a big excess of XeF_2 was necessary. Interestingly, in this reaction XeF_2 reduces Cr(V) to Cr(IV):

$$mCrF_5 + nXeF_2 \longrightarrow mXeF_2{\cdot}CrF_4 + 0.5mXeF_4 + (n\text{-}1.5m)XeF_2 \qquad (18)$$
$$n > 5m$$

$XeF_2 \cdot CrF_4$ is a deep blue, crystalline solid, stable in a dynamic vacuum to about 40 °C, where it starts to decompose slowly losing XeF_2. At higher temperatures (100 °C) beside XeF_2 also XeF_4 is obtained. The final product of decomposition is CrF_3. Obviously at a little higher temperatures, CrF_4 becomes an oxidizing agent strong enough to convert XeF_2 to XeF_4.

CrF_4, as a poor Lewis acid, in reaction with XeF_2, as a moderately strong fluoride ion donor, will not form an ionic compound of the formulation $XeF^+CrF_5^-$ but rather a molecular adduct like F–Xe–F–CrF_4, which is at the very beginning of the XeF_2 ionization pathway.[43] The Xe–F distance 1.93(2) Å is shorter than in XeF_2 itself (Xe–F = 2.01(1) Å) but longer than in known XeF^+ species.

$XeF_2 \cdot CrF_4$ crystallizes in the monoclinic space group $P2_1/n$ with a = 7.666(2) Å, b = 7.268(5) Å, c = 9.901(3) Å, β = 91.25(2)°, V = 551.5 Å^3, Z = 4 and d_c = 3.581 gcm^{-3}. The structure of $XeF_2 \cdot CrF_4$ consists of an infinite chain of distorted CrF_6 octahedra linked by trans-bridging fluorine atoms. XeF_2 molecules are alternating their position on this chain as shown in Figure 1.8.[210]

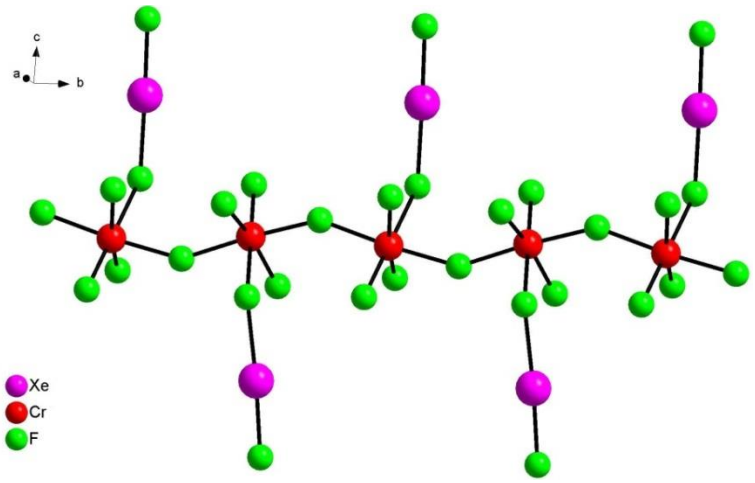


Figure 1.8: Crystal structure of $XeF_2 \cdot CrF_4$.[210]

1.5.3.2 $XeF_2 \cdot 2CrF_4$

The compound $XeF_2 \cdot 2CrF_4$ was prepared[211] by solvolysis of $XeF_2 \cdot CrF_4$ in aHF and subsequent decantation of the majority of dissolved XeF_2 in aHF. Remaining XeF_2 and a large excess of CrF_4 form $XeF_2 \cdot 2CrF_4$ after aHF is removed.

$$2(XeF_2 \cdot CrF_4) \xrightarrow{\text{partial solvolysis in aHF, RT}} XeF_{2\,(soln.)} + CrF_{4\,(s)} + XeF_2 \cdot CrF_4 \qquad (19)$$

$$XeF_{2\,(soln.)} + CrF_{4\,(s)} + XeF_2 \cdot CrF_4 \xrightarrow{\text{aHF removal, RT}} XeF_2 \cdot 2CrF_4 + \text{some } CrF_4$$

Ruby-red single crystals of $XeF_2 \cdot 2CrF_4$ may be obtained by two different methods, either by heating the solid for 2 months using a thermal gradient or by recrystallization from supercritical SF_6.[211]

The compound crystallizes in the triclinic space group $P\bar{1}$ with a = 8.551(3) Å, b = 9.221(3) Å, c = 10.438(3) Å, α = 76.02(2)°, β = 81.36(2)°, γ = 88.08(3)°, V = 0.7897(4) nm^3, d = 3.577 g/cm^3 and Z = 4 at 293 K. The basic structural unit is represented by two rings comprised of four independent Cr atoms, each octahedrally coordinated by six F atoms (Figure 1.9). The rings are joined by a CrF_6 unit carrying a XeF_2 molecule. In one type of tetrameric rings, two fluorine ligands are provided by two different XeF_2 molecules and the centrosymmetric arrangement recalls the RuF_5 type structure.[141] However, here the tetravalency of Cr requires additional six fluorine bridges from each ring to other units, which leads to a formation of a complicated three-dimensional network (Appendix A.1, Figure A. 1).

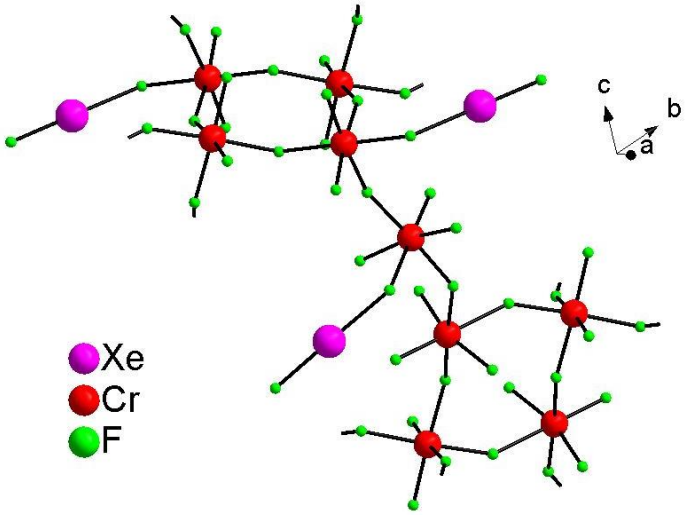


Figure 1.9: XeF_2 bonding and centrosymmetric rings found in the structure of $XeF_2 \cdot 2CrF_4$.211

1.5.4 $XeF_2 – MnF_4$ System

1.5.4.1 $XeF_2 \cdot MnF_4$

During the study of the catalytic effect of manganese trifluoride on the rate of reaction between xenon and fluorine it was found that a part of formed xenon difluoride reacts with manganese trifluoride and that the new formed compound catalyzes the xenon-fluorine reaction.[212] However it was impossible to isolate the pure compound using this method. Therefore, it was decided to react the manganese difluoride with an excessive amount of xenon difluoride since it was expected that XeF_2 would oxidize manganese difluoride and at the same time act as a fluoride ion donor. In this way (Eq. 20), pure $XeF_2 \cdot MnF_4$ was obtained and characterized[213] by chemical analysis, mass and IR spectrometry, magnetic susceptibility and later[214] by X-ray powder diffraction pattern.

$$MnF_2 + nXeF_2 \xrightarrow{120\ °C,\ 60\ h} XeF_2 \cdot MnF_4 + Xe + (n\text{-}2)XeF_2 \quad (20)$$
$$n \geq 4.7$$

The crystal structure was obtained several years later,[215] by partial solvolysis of the XeF_2 rich compound $3XeF_2 \cdot 2MnF_4$ in aHF at room temperature. After pumping off volatiles, wine-red crystals crystalized from aHF solution:

$$3XeF_2 \cdot 2MnF_4 \xrightarrow{aHF,\ RT} 2(XeF_2 \cdot MnF_4) + XeF_2 \quad (21)$$

An alternative synthetic pathway (Eq. 22),[215] starting from MnF_4 and XeF_2, was also successfully applied:

$$XeF_2 + MnF_4 \xrightarrow{aHF,\ RT} XeF_2 \cdot MnF_4 \quad (22)$$

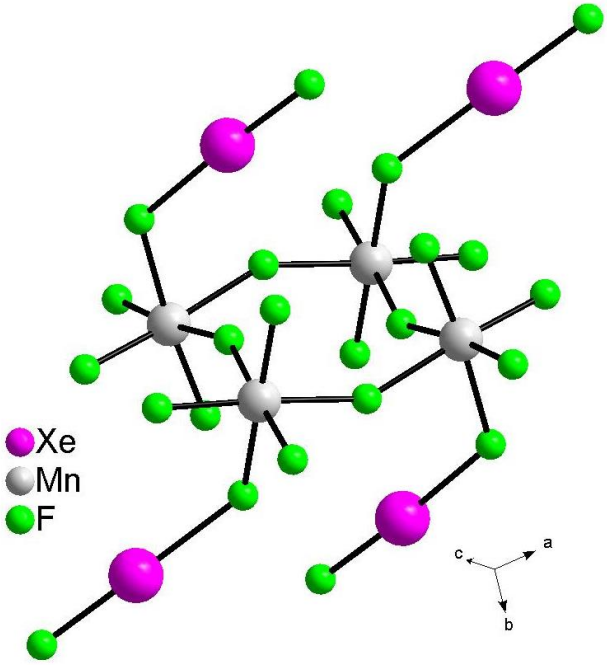


Figure 1.10: Four-membered ring with XeF_2 units in the crystal structure of $XeF_2 \cdot MnF_4$.

The wine-red product $XeF_2 \cdot MnF_4$ crystallizes in the monoclinic space group $P2_1/n$ (no. 14) with a = 9.6815(10) Å, b = 11.0473(9) Å, c = 9.8346(10) Å, β = 96,884(5)°, V = 1044.27(17) Å^3, Z = 4 and d_c = 3.819 gcm^{-3}. The structure (Figure 1.10) reveals four-membered rings of octahedra carrying trans-oriented XeF_2 molecules, which alternate respectively their position in pairs according to the ring-plane.[215]

1.5.4.2 $XeF_2 \cdot 2MnF_4$

$XeF_2 \cdot 2MnF_4$ was first synthesized[214] by thermal decomposition of $XeF_2 \cdot MnF_4$ at 120 °C under dynamic vacuum:

$$2(XeF_2 \cdot MnF_4) \xrightarrow{120\ °C,\ \text{in vacuum}} XeF_2 \cdot 2MnF_4 + XeF_2 \qquad (23)$$

Another synthetic approach[215] involved a partial solvolysis of the product $3XeF_2 \cdot 2MnF_4$ (Eq. 21) with a subsequent thermal decomposition of $XeF_2 \cdot MnF_4$ at 90 °C:

$$2(XeF_2 \cdot MnF_4) \xrightarrow{90\ °C} XeF_2 \cdot 2MnF_4 + XeF_2 \qquad (24)$$

Due to the poor crystallinity of the product, the crystal structure of $XeF_2 \cdot 2MnF_4$ has not been determined.

1.5.4.3 $3XeF_2 \cdot 2MnF_4$

The compound $3XeF_2 \cdot 2MnF_4$ was prepared[215] reacting MnF_2 with a large excess of XeF_2 in a nickel reaction vessel at 120–125 °C. The reaction was stopped by slowly cooling down to room temperature. After pumping off the excess volatiles, wine-red crystals were isolated:

$$5\ XeF_2 + 2\ MnF_2 \xrightarrow{120\text{-}125\ °C} 3XeF_2 \cdot 2MnF_4 + 2\ Xe \qquad (25)$$

The following reaction mechanism was proposed:[215]

$$XeF_2 + MnF_2 \longrightarrow MnF_4 + Xe \qquad (26)$$

$$3\ XeF_2 + 2\ MnF_4 \longrightarrow 3XeF_2 \cdot 2MnF_4 \qquad (27)$$

$3XeF_2 \cdot 2MnF_4$ is partially soluble in aHF, giving a pink solution. The product was characterized by Raman spectroscopy, magnetic susceptibility measurements and X-ray diffraction on the single crystal.

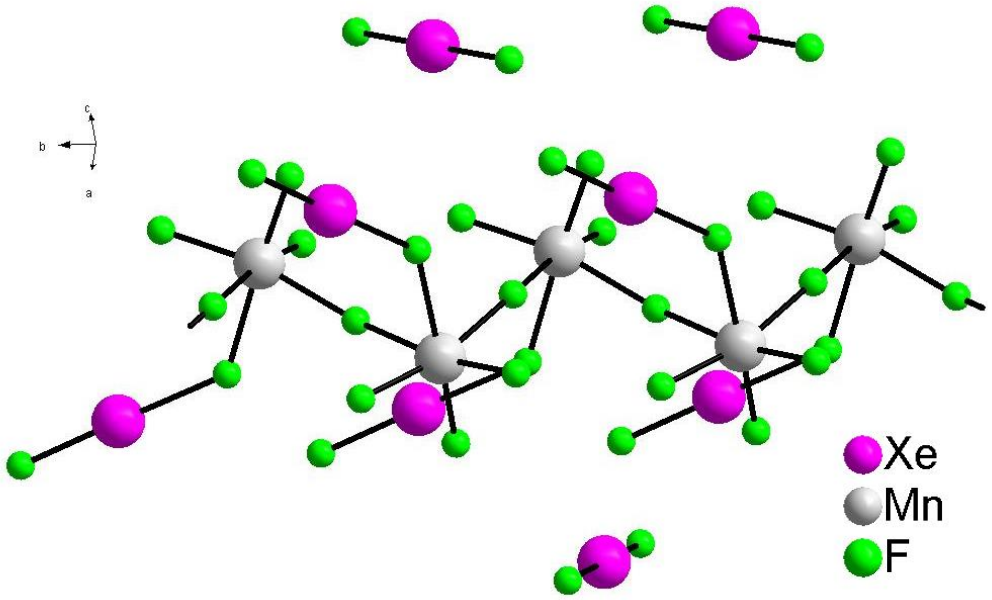


Figure 1.11: $3XeF_2 \cdot 2MnF_4$ is $XeF_2 \cdot MnF_4$ co-crystalized with XeF_2 molecules.

The compound $3XeF_2 \cdot 2MnF_4$ was found to crystallize in the monoclinic space group *P* $2_1/n$ *(no. 14)* with a = 10.28(3) Å, b = 4.998(4) Å, c = 12.51(2) Å, β = 96.93(3)°, V = 638.06(200) Å^3, Z = 2 and d_c = 4.007 gcm^{-3}. The main structural feature is a *cis*-chain of MnF_6^{2-} octahedra joined via two F-bridging atoms. Each manganese atom is additionally carrying a XeF_2 unit, which is in a *trans* position in respect to a XeF_2 of the neighbor manganese. Free non-bonded XeF_2 molecules, held by electrostatic interactions only, complete the crystal structure (Figure 1.11).

1.5.5 Other XeF_2 – MF_4 Systems

Xenon(II) fluoridozirconates(IV) and ***Xenon(II) fluoridohafnates(IV)***. The isolation of the reported[216] compounds $2XeF_2 \cdot ZrF_4$ and $2XeF_2 \cdot HfF_4$ has not been experimentally confirmed[217], even using the efficient route of hydrazinium fluorometalates and XeF_2 (thus preparing tetrafluorides in situ in the very reactive, so-called "molecular" form).

Xenon(II) fluoridorhodates(IV) – the synthesis of a single compound, $XeF_2 \cdot RhF_4$, was reported.[21] The product was obtained by reducing RhF_6 gas with elemental xenon. The stoichiometry of the reaction and consequently the product formulation was determined from the weight of adduct formed in the consumption of a tensimetrically measured quantity of xenon. The X-ray powder photographs of the deep red material showed only a faint, sharp pattern, which was supposed to belong to a minor phase present. No additional information on further studies or characterization attempts has been found in the available literature.

Overviews regarding the investigations on ***Xenon(II) fluoridotitanates(IV)*** and ***Xenon(II) fluoridostannates(IV)*** performed prior to this work are given as Backgrounds in Chapter 4.

1.6 XeF_6 – MF_4 Systems

Thus far, no products resulting from an interaction between metal tetrafluorides and xenon tetrafluoride (XeF_4) have been reported. This is not surprising, since XeF_4 is a much weaker

fluoride ion donor and only forms stable complex salts with the strongest fluoride ion acceptors.[54] On the other hand, xenon hexafluoride (XeF_6) that has been used to synthesize transition metal fluorides and oxide fluorides where the metal is in its highest oxidation state, acts both as a strong fluoride ion donor and acceptor.[54] To date, several crystal structures of compounds containing the square pyramidal $[XeF_5]^+$ or the $[Xe_2F_{11}]^+$ cation have been elucidated, moreover its exceptional F^- donor strength enables XeF_6 to overcome even the association energy barriers of many metal tetrafluorides as well as certain trifluorides, thus reacting in different molar ratios to form the corresponding salts. The published research results on XeF_6-MF_4 systems cover the isolation of different $[XeF_5]^+$ and $[Xe_2F_{11}]^+$ salts with general stoichiometric formulations $4XeF_6 \cdot MF_4$ (M = Ti, Mn, Ni, Pd, Ge, Sn, Pb, Ce, Pr, Tb), $2XeF_6 \cdot MF_4$ (M = Mn, Ni, Pd, Ge, Sn), $4XeF_6 \cdot 3MF_4$ (M = Sn), $XeF_6 \cdot MF_4$ (M = Ti, Zr, Hf, Cr, Mn, Ge), $3XeF_6 \cdot 4MF_4$ (M = Sn, Pb), $XeF_6 \cdot 2MF_4$ (M = Ti, Mn, Ce, Pr, Tb) and $XeF_6 \cdot 4MF_4$ (M = Sn, Pb, Pr).[53,55,218,219,220] Recently, an increase in the starting molar ratio in favor of MF_4 (before, the majority of experiments were carried out with a multifold excess of XeF_6 over the corresponding MF_4) delivered XeF_5^+ salts with oligo- and polymeric anions ($[MnF_5]^-$, $[Mn_8F_{36}]^{4-}$, $[Sn_5F_{24}]^{4-}$, $[TiF_5]^-$, $[Ti_3F_{13}]^-$, $[Ti_4F_{19}]^{3-}$, $[Ti_{10}F_{45}]^{5-}$).[159,164,165,221,222,223,224]

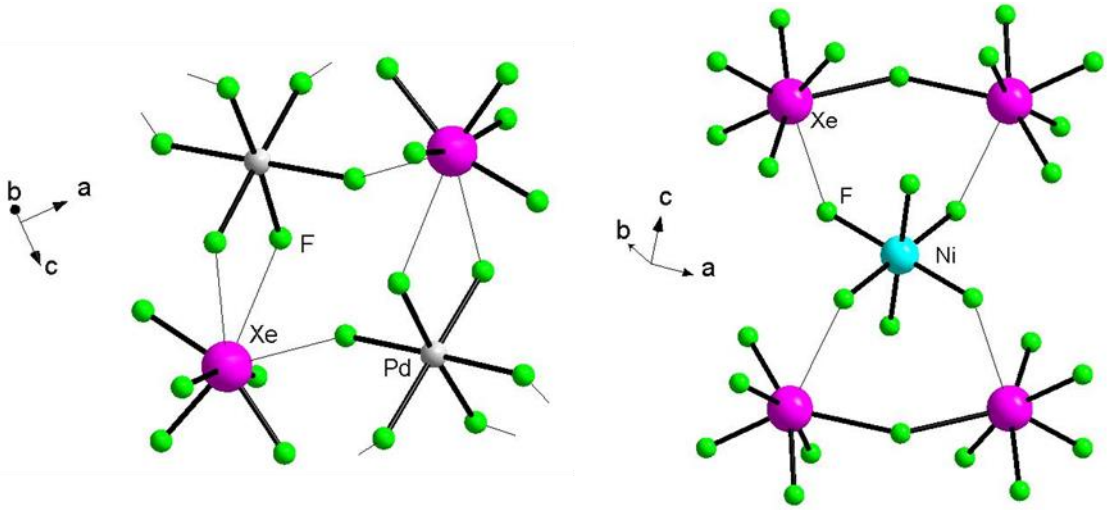


Figure 1.12: *Left* – $[XeF_5]^+$ coordination environment in $[XeF_5]_2[PdF_6]$.[225] *Right* – basic structural unit in $[Xe_2F_{11}]_2[NiF_6]$.[226]

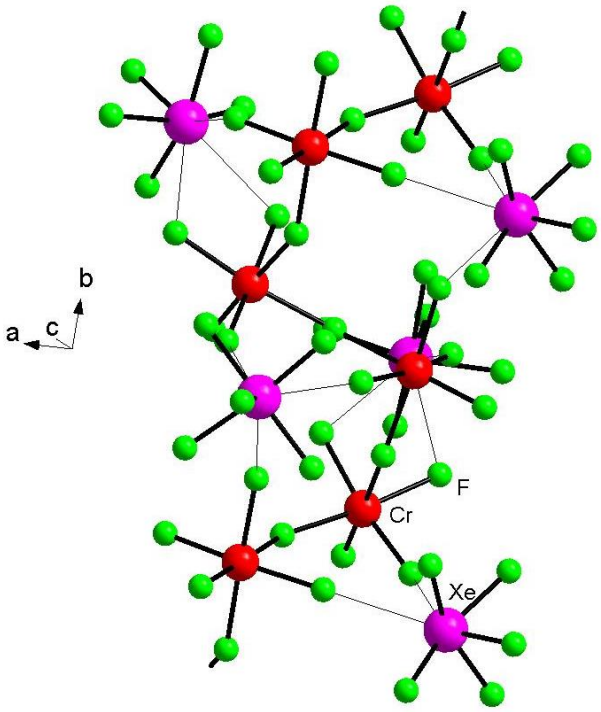


Figure 1.13: The polymeric CrF_5 anion found in the crystal structure of $[XeF_5][CrF_5]$ consists of highly distorted CrF_6 octahedra joined via cis vertexes. [211]

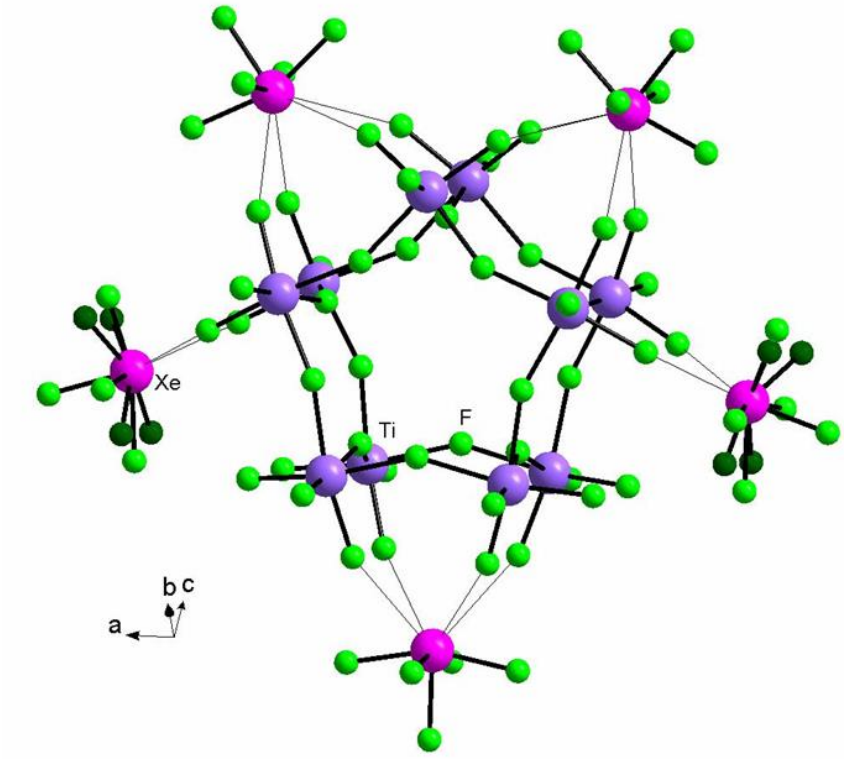


Figure 1.14: Ten TiF_6 units in a double star-like structural arrangement represent $[Ti_{10}F_{45}]^{5-}$, the largest observed discrete perfluoridometallate anion present in the recently isolated β-$[XeF_5]_5[Ti_{10}F_{45}]$.[164]

Chapter 2

Aims and Hypothesis

2.1 Aims

- Full structural characterization of some already known phases found in the systems XeF_2 – MF_4 (focusing on M = Sn and Ti).
- Synthesis and structural determination of potential novel compounds of general formulation $a XeF_2 \cdot b MF_4$.
- Improvement or development of new crystallization techniques, specifically designed for dealing with equilibrium concerns of the solution chemistry of the systems XeF_2 – MF_4.
- Development of new synthetic approaches with special emphasis on the study of key conditions that influence the type, yield and nature of the products.
- Comparison and interpretation of the results, integration of the obtained data into a wider context of the noble gas chemistry.
- Derivation of structure-directing principles and their potential application for targeted syntheses.

2.2 Hypothesis

Xenon(II) fluoride acts as a moderately strong Lewis base and fluoride ion donor. Strong fluoride ion acceptors like antimony pentafluoride are capable of abstracting a fluoride from XeF_2. In this case, XeF^+ species are formed and in case of excess XeF_2 over the Lewis acid used, $Xe_2F_3^+$ cations. Metal tetrafluorides MF_4 (M = Cr, Mn, Pb, Pd, Pt, Ti, Sn, etc.) are weaker fluoride ion acceptors than the pentafluorides and the formation of charged species or salts upon a reaction with XeF_2 is not expected. However, this interaction can produce adducts of the type $a XeF_2 \cdot b MF_4$, the majority of which have low solubilities in most of the solvents commonly used in this field of fluorine chemistry (aHF, SO_2ClF, BrF_5) and are consequently hard to crystallize and structurally characterize. Additionally, the fluoride ion acceptor capabilities of metal tetrafluorides are often hindered by their polymeric structures in the solid phase, while their vapors contain isolated tetrahedral molecules. Therefore, this research includes also thermal reactions occurring in those XeF_2 – MF_4 systems, of which the corresponding MF_4 is volatile enough at temperatures not exceeding 150 °C and is not susceptible to redox reactions with XeF_2. Of special interest are also "XeF_2 rich" $a XeF_2 \cdot b MF_4$ compounds, which can eventually decompose into crystalline "XeF_2 poorer" relatives at higher temperatures.

Chapter 3

Materials and Methods

3.1 Materials

A complete list of chemicals used within this research work is shown in alphabetic order in Table 3.1. An additional description on the preparation and treatment of certain compounds is given below the table.

Table 3.1: Overview of chemicals used in this work and their synthetic role.

Chemical	Specification	Role
aHF	*See details below*	Solvent
BrF_5	*See details below*	Solvent
F_2	Solvay Fluor and Derivate GmbH	Reagent
KrF_2	*See details below*	Reagent
NaF	Merck, 99%	Reagent
PbF_2	Merck, 99.7%	Reagent
SnF_2	Aldrich, 99%	Reagent
SnF_4	*See details below*	Reagent
SO_2ClF	*See details below*	Solvent
$TiCl_3$	Sigma Aldrich, 99.999%	Reagent
TiF_4	*See details below*	Reagent
TiO_2	Merck, 99%	Reagent
Xe	Messer Griesheim, 99.997%	Reagent, Solvent
XeF_2	*See details below*	Reagent, Solvent

aHF – Commercial HF (Linde, 99.995%) was treated with K_2NiF_6 (Ozark-Mahoning Co., 99%) for several hours or overnight prior to use. Such anhydrous conditions were maintained for months by keeping K_2NiF_6 with HF in the storage FEP vessel.

BrF_5 – Commercial bromine pentafluoride (Ozark-Mahoning Co.) was treated with fluorine at room temperature in order to eliminate BrF_3 and Br_2 impurities. The product was stored in the purification FEP vessel, loaded with KF (to complex HF as $K[HF_2 \cdot nHF]$) under 1000 Torr of 2 : 1 mixture of N_2 and F_2 at 78 °C.

KrF_2 – Krypton difluoride was prepared by the stainless steel hot-wire reactor method[227] at McMaster University (Department of Chemistry) from krypton and excess of fluorine. The product was purified by briefly warming the sample from −78 °C to 0 °C and flash distilling off the more volatile chromium oxifluorides. KrF_2 was stored in a FEP tube in dry-ice at −78 °C under 1000 Torr overpressure of N_2 or Ar until used.

SnF_4 – Tin tetrafluoride was synthesized by fluorination of SnF_2 with excess F_2 or reacting SnF_2 with an equimolar amount of XeF_2. Both procedures were carried out at room temperature in anhydrous HF. The purity of the product was assessed by Raman spectroscopy.

SO_2ClF – Purchased sulfuryl chloride fluoride (Allied Chemical Co., Baker and Adams Division, >90%) was purified by fractional distillation (to remove SO_2F_2) and treated with SbF_5 and XeF_2 (to eliminate impurities with reducing properties, i.e., SO_2) and dried KF (to complex residual HF). Each step of the process involved warming to room temperature followed by cooling to −78 °C. Finally, the liquid product was distilled by dynamic pumping at −78 °C into a glass vessel over a bed of dry KF. The purity was assessed by NMR spectroscopy at −80 °C, where only traces of SO_2F_2 were found.

TiF_4 – titanium tetrafluoride was prepared by two different synthetic methods. The first method used was a high-pressure fluorination of TiO_2 with excess F_2 in a nickel reaction vessel at high temperature (350 °C) as described elsewhere. The second method involved two steps – a reaction of $TiCl_3$ with HF to give TiF_3, followed by fluorination of the obtained TiF_3 in aHF with excess F_2 in the second step. The purity of the product was checked by chemical analysis and Raman spectroscopy.

XeF_2 – xenon difluoride was prepared by the photochemical reaction between gaseous xenon (excess) and gaseous fluorine at room temperature.[228] The purity of the product was assessed with Raman spectroscopy.

3.2 Synthetic Procedures

Several different synthetic techniques and crystallization methods were employed during the course of this work. Most of the compounds used and prepared were air and/or moisture sensitive and some of them were additionally thermally unstable at room temperature. Volatile materials were handled under rigorously anhydrous conditions in a nickel and PTFE vacuum line, which is a modified version of a vacuum system developed at the Department of Inorganic Chemistry and Chemical Technology (Jožef Stefan Institute). The working vacuum was achieved using a dual stage rotary vane oil pump (Edwards, model RV3), in conjunction with a mercury diffusion pump when necessary. A FEP trap cooled with liquid nitrogen was employed for solvent and by-product removal, while an additional trap containing soda lime scrubbers was used to intercept fluorine gas and highly volatile fluorides. The reaction vessels were usually attached to the PTFE part of the vacuum line, which was equipped with a fluorine resistant Helicoid pressure gauge (0 – 1500 Torr ± 0.25%). A glovebox with argon atmosphere (MBraun Lab-Star, the residual water content never exceeded 0.5 ppm) was employed for storage and manipulation of non-volatile and moisture-sensitive compounds.

The custom-made FEP vessels used within this work (Figure 3.1, Figure 3.2) were dried under dynamic vacuum and passivated with F_2 for several hours prior to use. T-shaped vessels were employed for crystallizations involving solvents. Typically, this process involved some crucial steps. Pre-calculated amounts of reactants were weighed into the larger diameter arm inside the glovebox and the solvent was condensed over the mixture on the vacuum line in the next step. After stirring for a defined period of time, only the clear, precipitate-free solution was carefully poured into the narrower – "crystallization" arm, where crystals were left to grow due to a slow, constant solvent evaporation maintained by the temperature difference between the two arms of the vessel. The final step, the isolation of the crystalline products, involved pumping off all volatiles on the vacuum line and covering the crystals with perfluorinated oil (ABCR, 99.5%, *cis* and *trans*), selecting a suitable single crystal under the stereo microscope (Leica Microsystems) and its fast transfer into a cold dry nitrogen stream of the X-ray diffractometer.

Specific experimental procedures and any variation of the equipment shown below are additionally described in the synthesis part of the corresponding chapters.

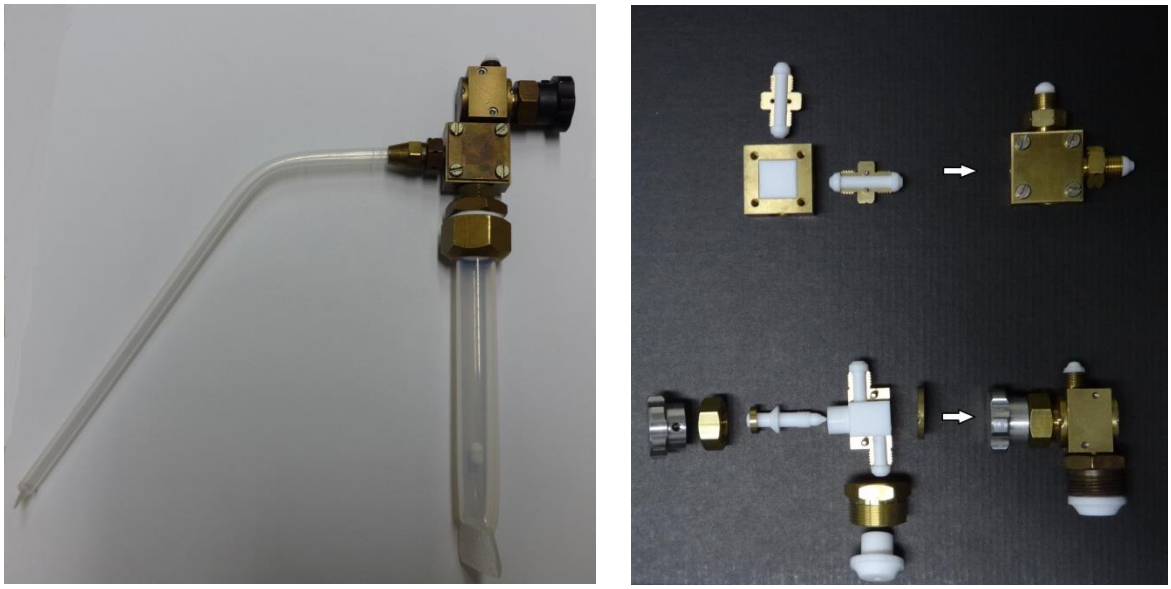


Figure 3.1: *Left* – a typical T-shaped crystallization vessel was comprised of two FEP (tetrafluoroethylene-hexafluoropropylene block copolymer, Polytetra GmbH) tubes sealed at one end. The wider – "reaction" arm (16 mm i.d., 19 mm o.d.; added inside, a PTFE-coated stirring bar) and the narrower – "crystallization" arm (6 mm i.d., 8 mm o.d.) were joined at the right angle through a PTFE T-connector and equipped with a PTFE valve. *Right* – All PTFE parts have been encased in full-metal housings.

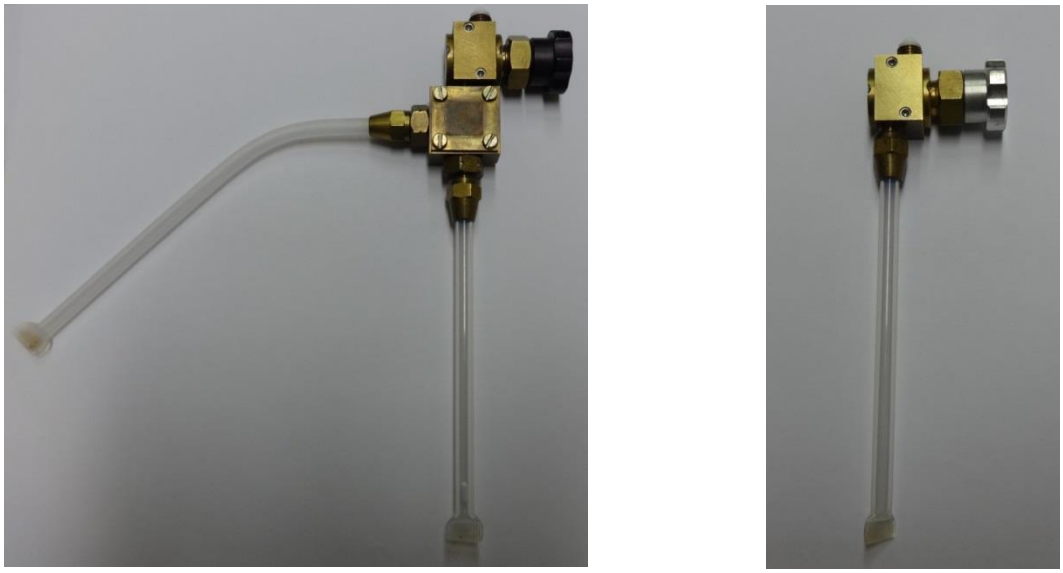


Figure 3.2: *Left* – a small T-shaped crystallization vessel allowed a better control over the reaction conditions and facilitated the visual following when experimenting with high concentrations of reactants in a small volume of solvent. *Right* – a typical small reaction vessel used mainly for the thermal studies of the XeF_2 – TiF_4 system. Both assemblies were made from 6 mm i.d. (8 mm o.d.) FEP tubing and connected similarly as presented in Figure 3.1.

3.3 Characterization

3.3.1 X-ray Crystal Structure Determinations

The single-crystal X-ray diffraction measurements of the compounds obtained during the course of this work were carried out using two different diffractometers.

The data for the first set of results described in Chapter 4 were collected using a Rigaku AFC7 diffractometer (graphite monochromatized Mo-Kα radiation (λ = 0.71069 Å) equipped with a Mercury CCD area detector at 150 K or 200 K (details are given for each individual product). The data were corrected for Lorentz, polarization and absorption effects and were processed using Rigaku CrystalClear software.[229] Crystal structures were solved by direct methods using the program SIR-92[230] (teXan software)[231] and refined with SHELXL-97 software[232] implemented in the program package WinGX.[233]

The data for the second set of compounds investigated within the present work were collected on a Gemini A diffractometer (Agilent Technologies), configured with an Atlas S2 CCD detector. The apparatus is provided with a dual-wavelength system with Enhance Mo and Cu fine focus X-ray sources. The data were treated using the CrysAlis^{Pro} suite program package[234]. Structures were solved by the charge flipping method using the structure solution program Superflip[235] implemented in the Olex2[236] crystallographic software and refined with SHELXL-2013[237] (program package WinGX)[238]. The program DIAMOND 3.2[239] was used for structure visualization and graphical representations; publCIF[240] was employed for data formatting and preparation of customized geometry tables.

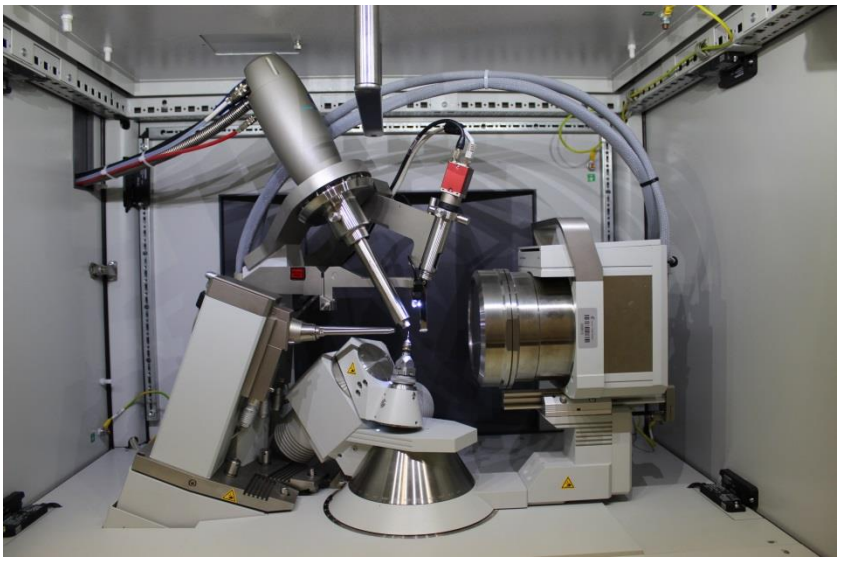


Figure 3.3: Agilent Gemini A diffractometer with a 4-circle kappa goniometer, Atlas S2 CCD detector and Cryojet5 (Oxford Instruments) cryogenic device.

3.3.2 Raman Spectroscopy

Due to the translucency of the FEP vessels, Raman spectroscopy enabled a fast and reliable identification of the reaction products, and proved to be very useful in following the reaction rate and/or estimating the composition of the product mixture between the various steps during the experiment.

The spectra were obtained from powdered samples or samples of randomly oriented single crystals. Powdered samples were prepared by grinding the desired products inside the glovebox. If the reaction was not selective, but the products could be easily distinguished by crystal morphology, pure phases were manually separated with the help of a surgical microscope (OPTON, West Germany) mounted outside the glovebox by focusing through the glovebox window panel. The samples were usually loaded into 0.3-mm quartz capillaries, previously

vacuum dried and pre-treated with F_2. These capillaries were temporarily sealed with Halocarbon 25-5S grease (Halocarbon Corp.) and subsequently heat-sealed outside the glovebox. The spectra were acquired using the LabSpec Version 5.78.24 (Horiba Scientific) software and formatted using OriginPro 8 (OriginLab, Northampton, MA).

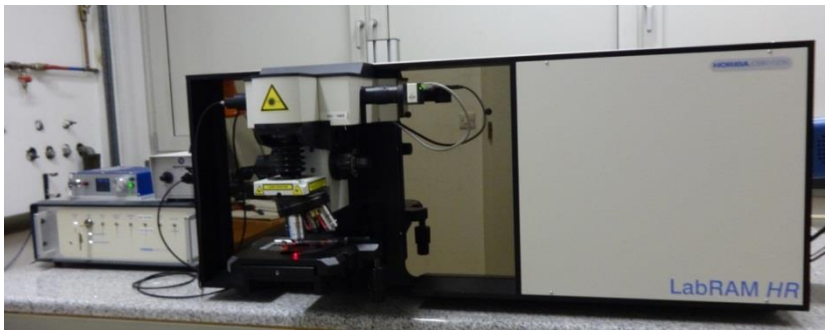


Figure 3.4: Raman spectra were recorded at room temperature on a Horiba Jobin Yvon Labram-HR spectrometer coupled with an Olympus BXFM-ILHS microscope. Samples were excited by the red 633 nm emission line of a 24.3 mW He−Ne laser with a power output of 14 mW on the sample.

Chapter 4

Results and Discussion

4.1 XeF_2 - TiF_4 System

4.1.1 Background

Xenon difluoride reacts with titanium tetrafluoride in different molar ratios. The first compound of composition $aXeF_2 \cdot bTiF_4$ reported was $2XeF_2 \cdot TiF_4$.[241] The existence of this compound was established only by measurements of the electrical conductivity of a XeF_2/TiF_4 melt. The same product was also claimed to form upon the reaction of XeF_2 and $TiCl_4$.[216] The color was reported to be light yellow in both cases. The formation of $2XeF_2 \cdot TiF_4$ has never been confirmed by other laboratories.

A few years later, during the study[212] of the catalytic effect of titanium tetrafluoride on the rate of reaction between xenon and fluorine at 120 °C, it was found that besides $2XeF_2 \cdot TiF_4$ more compounds could be found in the system XeF_2-TiF_4. Soon, the compounds of the following compositions: $3XeF_2 \cdot 2TiF_4$, $XeF_2 \cdot TiF_4$ and $XeF_2 \cdot 2TiF_4$ were prepared[242] by two different synthetic pathways – by reaction between hydrazinium(II) hexafluoridotitanate(IV) and XeF_2 at 120 °C as well as reacting directly TiF_4 and excessive XeF_2 at room temperature. Both reactions initially yielded the compound $3XeF_2 \cdot 2TiF_4$, which decomposed at 60 °C under dynamic vacuum to give XeF_2 and $XeF_2 \cdot TiF_4$. The latter decomposed further at 75 °C to give again XeF_2 and $XeF_2 \cdot 2TiF_4$. All the compounds were identified as diamagnetic white solids, which turn yellowish when exposed to air. Consequently, it was suggested that the previously reported[241,**Error! Bookmark not defined.**] yellowish color of $2XeF_2 \cdot TiF_4$ might be due to the partial hydrolysis of the product as well.

The volatiles were followed by mass spectrometry (Xe, N_2) and IR spectroscopy (xenon fluorides, HF), while the products $3XeF_2 \cdot 2TiF_4$, $XeF_2 \cdot TiF_4$ and $XeF_2 \cdot 2TiF_4$ were characterized[242] by chemical analysis, IR spectroscopy and magnetic susceptibility measurements. The unexpected, preferable formation of $3XeF_2 \cdot 2TiF_4$ over the previously predicted $2XeF_2 \cdot TiF_4$ was attributed to the facile decomposition of the latter under dynamic vacuum at room temperature, by releasing XeF_2 and consequently giving the compound $3XeF_2 \cdot 2TiF_4$.

Another study reported[243] the formation of $XeF_2 \cdot TiF_4$ upon reaction of excessive XeF_2 over $(NH_4)_2TiF_6$ at 453 K (180 °C), along with oxidized nitrogen by-products N_2 and unexpectedly, even some NF_3.

Table 4.1: Characterization results obtained from the previous studies of the system XeF_2 -TiF_4.

	$3XeF_2 \cdot 2TiF_4$		$XeF_2 \cdot TiF_4$		$XeF_2 \cdot 2TiF_4$	
	Chemical analyses					
	Calcd.(%)	Found (%)	Calcd. (%)	Found(%)	Calcd. (%)	Found(%)
Ti	12.68	12.8	16.34	15.7	22.97	24.6
Xe	52.12	51.3	44.78	44.2	31.48	30.9
F	35.20	34.7	38.88	39.1	45.55	45.2

	I.R. absorption frequencies	
/	710 s, 660 s, 568 vs, 530 m, 512 s	690 w, 640 s, 587 m, 542 m
	Intensity: s-strong, m-medium, w-weak, vs-very strong	

4.1.2 $(XeF_2 \cdot TiF_4)_2 \cdot XeF_2$

Colorless crystals of the phase $3XeF_2 \cdot 2TiF_4$, better formulated as $(XeF_2 \cdot TiF_4)_2 \cdot XeF_2$, were firstly obtained from an equimolar aHF solution of XeF_2 (0.27 mmol, 46 mg) and TiF_4 (0.30 mmol, 37 mg) using a typical T-shaped crystallization vessel (Figure 3.1) as described previously in the Methods section. The 16-day long crystallization process was driven by a temperature difference of 7 °C between the two arms of the FEP crystallization reactor, which was raised to 22 °C at the end of the first week in order to compensate the lowering of the vapor pressure over the concentrated solution left in the narrower arm. The compound was isolated by pumping off anhydrous HF on the vacuum line while keeping the narrower arm at 0 °C. The formed crystalline deposit was immersed in the perfluorinated oil inside the glovebox and a suitable single crystal was isolated and quickly transferred into a cold dry-nitrogen stream of the X-ray diffractometer.

The structure of the compound was solved in the non-standard $P2_1/n$ cell setting of the monoclinic space group number 14 with two formula units per unit cell. Ten crystallographically independent atoms form the asymmetric unit (Figure 4.1). Seven fluorine atoms, one titanium and one xenon atom lie on general positions (Wyckoff 4e), while Xe1 resides on an inversion center (Wyckoff 2a). More details on the X-ray structural analysis are given in Table 4.2, fractional atomic coordinates are found in Appendix B.1, Table B. 1.

The compound $(XeF_2 \cdot TiF_4)_2 \cdot XeF_2$ was found to be isostructural to its manganese analogue $(XeF_2 \cdot MnF_4)_2 \cdot XeF_2$ (phase $3XeF_2 \cdot 2MnF_4$, section 1.5.4). Similarly, the main structural feature appeared to be again the formation of a zig-zag chain of *cis* connected $FXeFTiF_3F_{2/2}$ units by single fluorine bridges. A list of associated bond distances and angles is given in Table 4.3.

Table 4.2: Crystal structure determination* and refinement details for compound $(XeF_2 \cdot TiF_4)_2 \cdot XeF_2$.

Crystal data	*Data collection*	*Refinement*
$Xe_3Ti_2F_{14}$	Rigaku AFC7 diffractometer	$R_1[F^2 > 2\sigma(F^2)] = 0.036$
$M_r = 755.7$	Mercury CCD detector	$wR_2\ (F^2) = 0.107$
Crystal system: monoclinic	λ = 0.71069 Å (Mo K_α)	1526 reflections
Space group: $P2_1/n$	2824 measured reflections	89 parameters
a = 10.4210 (12) Å	1526 independent reflections	GOF = 1.07
b = 5.0926 (9) Å	1345 observed reflections (I > 2 σ (I))	$\Delta\rho_{max}$ = 1.07 e/Å^3
c = 12.691 (2) Å	R_{int} = 0.031	$\Delta\rho_{min}$ = −1.56 e/Å^3
β = 97.258 (9)°	θ_{max} = 29.2°, θ_{min} = 2.7°	
V = 668.10 (17) Å^3	$-12 \leq h \leq 14$	
Z = 2	$-6 \leq k \leq 6$	
ρ_{calc} = 3.757 g/cm^3	$-7 \leq l \leq 16$	
$3.6° \leq \theta \leq 28.9°$		
Cell parameters from 311 reflections		
μ = 8.82 mm^{-1}		
T = 200 K		
F(000) = 664		
Size: 0.08×0.07×0.04 mm		

* The crystal structure has been redetermined with higher accuracy at lower temperature on a Bruker SMART APEX II diffractometer at the Department of Chemistry at McMaster University (Canada). The dataset is still being processed and the partial results obtained are not included in this work.

Appearance: Colorless, chunk

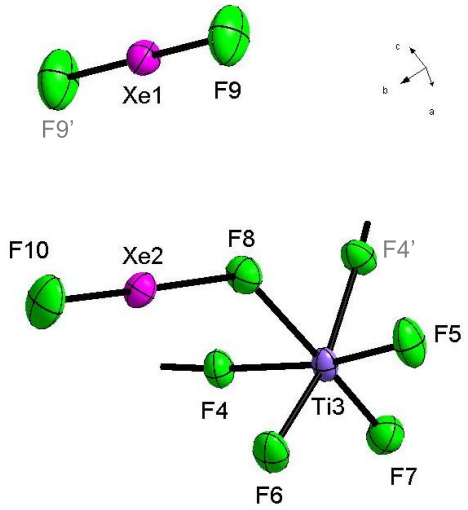


Figure 4.1: The asymmetric unit (black labeled atoms) in the compound $(XeF_2 \cdot TiF_4)_2 \cdot XeF_2$. Thermal ellipsoids are drawn at the 50 % probability level.

Certain geometrical parameters were previously found to be crucial when elucidating the nature of chemical bonding present in XeF_2 adducts and salts. For instance, the deviation from the $D_{\infty h}$ symmetry of the molecular XeF_2 can indicate the degree of interaction between this molecule acting as a moderately strong fluoride donor and the fluoride acceptor counterpart. In this way, the firstly linear symmetrical molecule is deformed, which can be observed as an elongation of Xe−F_b and shortening of Xe−F_t bonds. In $(XeF_2 \cdot TiF_4)_2 \cdot XeF_2$ the Xe–F_t and Xe–F_b bond distances of bonded XeF_2 are 1.922(4) and 2.133(3) Å, respectively. These values indicate that the aforementioned bonding is at the beginning of the ionization pathway[43], and are comparable with the corresponding values found in compounds like $XeF_2 \cdot VF_5$,[116] $XeF_2 \cdot CrF_4$[210] or $XeF_2 \cdot VOF_3$,[34] which gives more legitimacy to the adduct formulation, rather than describing the compound as an ionic $([XeF][TiF_5])_2 \cdot XeF_2$. The bond angle of the F8–Xe2–F10 moiety equals to 178.94(15)° which is also in good agreement with the Fb–Xe–Ft values previously determined in various $[XeF][MF_6]$ compounds (ranging from 177.4(2)° (M = Ir)[114] to 179.1(2)° (M = As)[74]). On the other hand, the F–Xe–F (F9–Xe–F9') bond angle (180°) belonging to the "free" XeF_2 replicates the linear geometry of the pure, solid and gas phase XeF_2 (Figure 1.2).

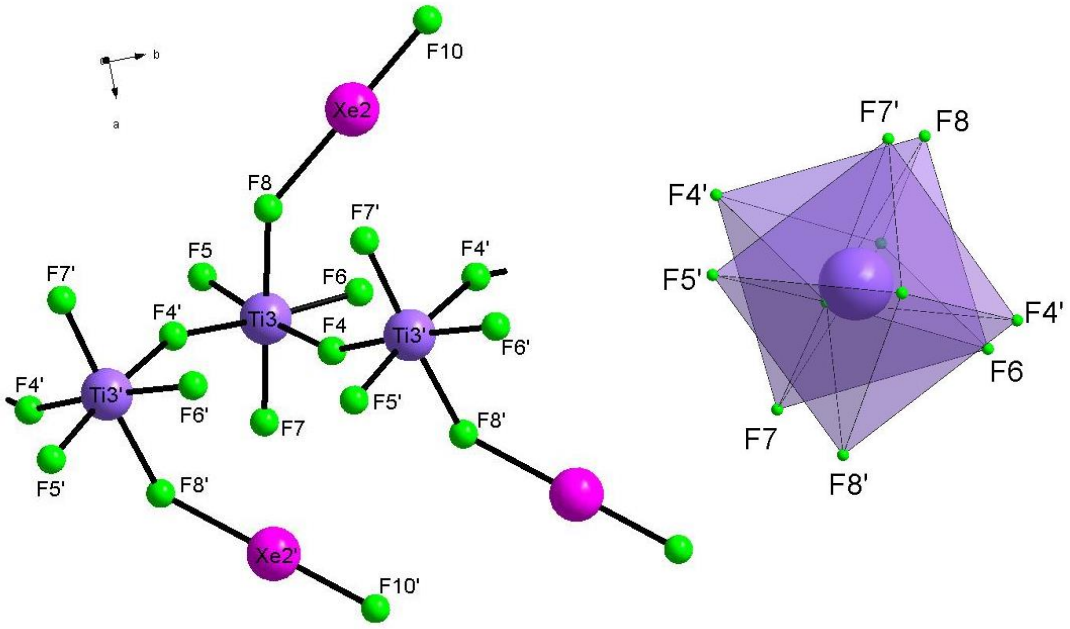


Figure 4.2: Selected part of the polymeric chain showing the connectivity of the $FXeFTiF_3F_{2/2}$ units (*left*) and torsion of neighboring TiF_6 octahedra (*right*) observed in the compound $(XeF_2{\cdot}TiF_4)_2{\cdot}XeF_2$.

The F8 atom shared by the XeF_2 molecule completes the octahedral arrangement around the Ti3 atom. A regular octahedron is a Platonic solid with eight faces that are equilateral triangles and six corners, while each bond is 90° from four other bonds and 180° from one other bond. Since three equivalent planes can be defined by four-fold symmetry axes, all ligands are geometrically equivalent and the axial/equatorial distinction as in triangular bipyramidal structures is impossible. However, most octahedra observed in various oligomeric and polymeric fluoridometalates(IV) are distorted by different ligands or vertex-, edge- or face-sharing connectivity. For salts $[XeF][M_2F_{11}]$ (M^v = Bi, Sb), the equatorial positions of four F atoms were defined on a plane perpendicular to the fluorine bridge between the two pseudo-octahedrally coordinated pnictogen atoms.[74] Unlike the octahedral MF_6^- anions derived from strong MF_5 (M = As, Sb, Bi, etc.) fluoride acceptors, where all six fluorine vertexes have equivalent fluorobasicities, the M–F_b bonds present in oligomeric and polymeric assemblies induce a *trans*-influence on the axial fluorine ligands and thus lowering their fluorobasicity in respect to the equatorial ones. Coordination of the cation to an equatorial fluorine position is therefore clearly preferred and experimentally supported by the solved structures of $[XeF]^{+}$[74,114], $[XeF_3]^{+}$[244] and $[OsO_2F_3]^{+}$[245] salts investigated thus far. Likewise, this tendency is followed by $(XeF_2{\cdot}TiF_4)_2{\cdot}XeF_2$, although the equatorial plane cannot be as previously defined due to the *cis*-bridging (via F4 and F4') construction of the $^1_\infty[FTiF_3F_{2/2}]$ chain. In this way, the *trans*-influence exercised by the fluorine bridges on F5 and F6 positions makes them less fluoro-basic, and thus less attractive as anchoring sites for the $F_tXe^{\delta+}$ moiety. This leaves the bonding possibilities open for F7 and F8, which are in fact not equivalent due to the torsion angle between the neighboring octahedra (Figure 4.2). The anchored $F_tXe^{\delta+}$ moieties alternate their positions on the F8 (F8') apex on neighboring TiF_6 octahedra along the chain, roughly *trans* to each other (Figure 4.5). However, the difference in fluorobasicity between F7 and F8 atoms seems to be minimal, taking into account that the symmetrically generated F8' atoms occupy very similar positions to F7 along the chain. Each TiF_6 octahedron therefore consists of three bridging fluorine ligands and three terminal fluorines, both sets in *fac*-arrangement. The Ti3–F8 bond length forming the connective apex is the longest (2.034(4) Å) among the Ti-F lengths observed in $(XeF_2{\cdot}TiF_4)_2{\cdot}XeF_2$. The elongation of the M–F_b(Xe) bond is indicative of a substantial cation-anion interaction and is correlated to a lesser degree of fluoride ion transfer to the anion as a result of the lower Lewis acidity of the parent TiF_4. Similarly, the significant difference observed between the Ti–F_b(Xe) length and other non-bridging Ti–F_t (average length: 1.763 Å) lengths is typical of a lower fluoride

ion acceptor strength of the parent Lewis acid. The Ti3–F8–Xe2 angle equals to 133.1(2)°, which is comparable to the corresponding M–F_b–Xe angles found in [NgF][MF_6] (Ng = Xe, M = As: 133.6(2)°; Sb: 136.9(1)°; Ir: 119.3-141.9°; Ru: 137.2(5)°. Ng = Kr, M = As: 133.7(3)°; Sb: 139.2(2)°; Bi: 138.3(3)°; Au: 125.3(7)°)[74,114], although the deviation from the ideal tetrahedral angle predicted for an $AXYE_2$ (A = F_b, X = Xe, Y = M) VSEPR arrangement was attributed[74] to the high ionic characters of these compounds.

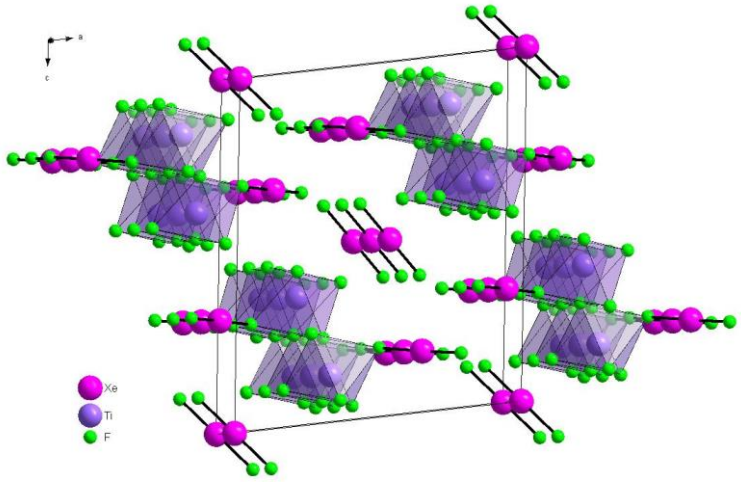


Figure 4.3: The unit cell of compound $(XeF_2{\cdot}TiF_4)_2{\cdot}XeF_2$ viewed along the *b*-axis.

The F_t–Xe–F_b–M moiety is in practically eclipsed conformation with respect to the [F4', F7, F6, F8]-plane, in terms of the very small torsion angle Xe2–F8–Ti3–F6 (−0.4°), which maximizes the steric interaction between the partially positive $F_tXe^{\delta+}$ fragment and the nearest fluorine ligand (F6) of the negatively charged chain.

Table 4.3: Selected geometric parameters for the compound $(XeF_2{\cdot}TiF_4)_2{\cdot}XeF_2$.

Bond Lengths (Å)			
Xe1—F9^{i}	1.986 (4)	Ti3—F6	1.774 (4)
Xe1—F9	1.986 (4)	Ti3—F4^{ii}	1.951 (3)
Xe2—F10	1.922 (4)	Ti3—F4	2.013 (3)
Xe2—F8	2.133 (3)	Ti3—F8	2.034 (4)
Ti3—F5	1.746 (4)	F4—Ti3^{iii}	1.951 (3)
Ti3—F7	1.769 (4)		
Bond Angles (°)			
F9^{i}—Xe1—F9	180.00	F6—Ti3—F4	87.0(2)
F10—Xe2—F8	178.9(2)	F4^{ii}—Ti3—F4	84.2(2)
F5—Ti3—F7	100.0(2)	F5—Ti3—F8	89.0(2)
F5—Ti3—F6	96.4(2)	F7—Ti3—F8	169.2(2)
F7—Ti3—F6	96.9(2)	F6—Ti3—F8	88.0(2)

F5—Ti3—F4^{ii}	91.0(2)	F4^{ii}—Ti3—F8	82.6(2)
F7—Ti3—F4^{ii}	91.2(2)	F4—Ti3—F8	82.0(2)
F6—Ti3—F4^{ii}	167.9(2)	Ti3^{iii}—F4—Ti3	156.0(2)
F5—Ti3—F4	170.2(2)	Ti3—F8—Xe2	133.1(2)
F7—Ti3—F4	88.67(2)		

Symmetry codes: (i) −*x*+2, −*y*, −*z*+2; (ii) −*x*+5/2, *y*−1/2, −*z*+3/2; (iii) −*x*+5/2, *y*+1/2, −*z*+3/2.

Nevertheless, the fluoridotitanate backbone $([TiF_3F_{2/2}]^-)_\infty$ resembles closely a variety of zig-zag chains of vertex-sharing octahedra found in different compounds containing the well-known polymeric $[TiF_5]^-$ and $[CrF_5]^-$ anions.[155,246]Despite the similarity, many geometrical conformers exist, while the main impact on the structural arrangement appears to come from different Ti-Fb-Ti angles and torsion angles between the crystallographically non-equivalent TiF_6 octahedra, which in turn generate a number of twisted and alternating motifs depending on the symmetry operations involved (Figure 4.4).

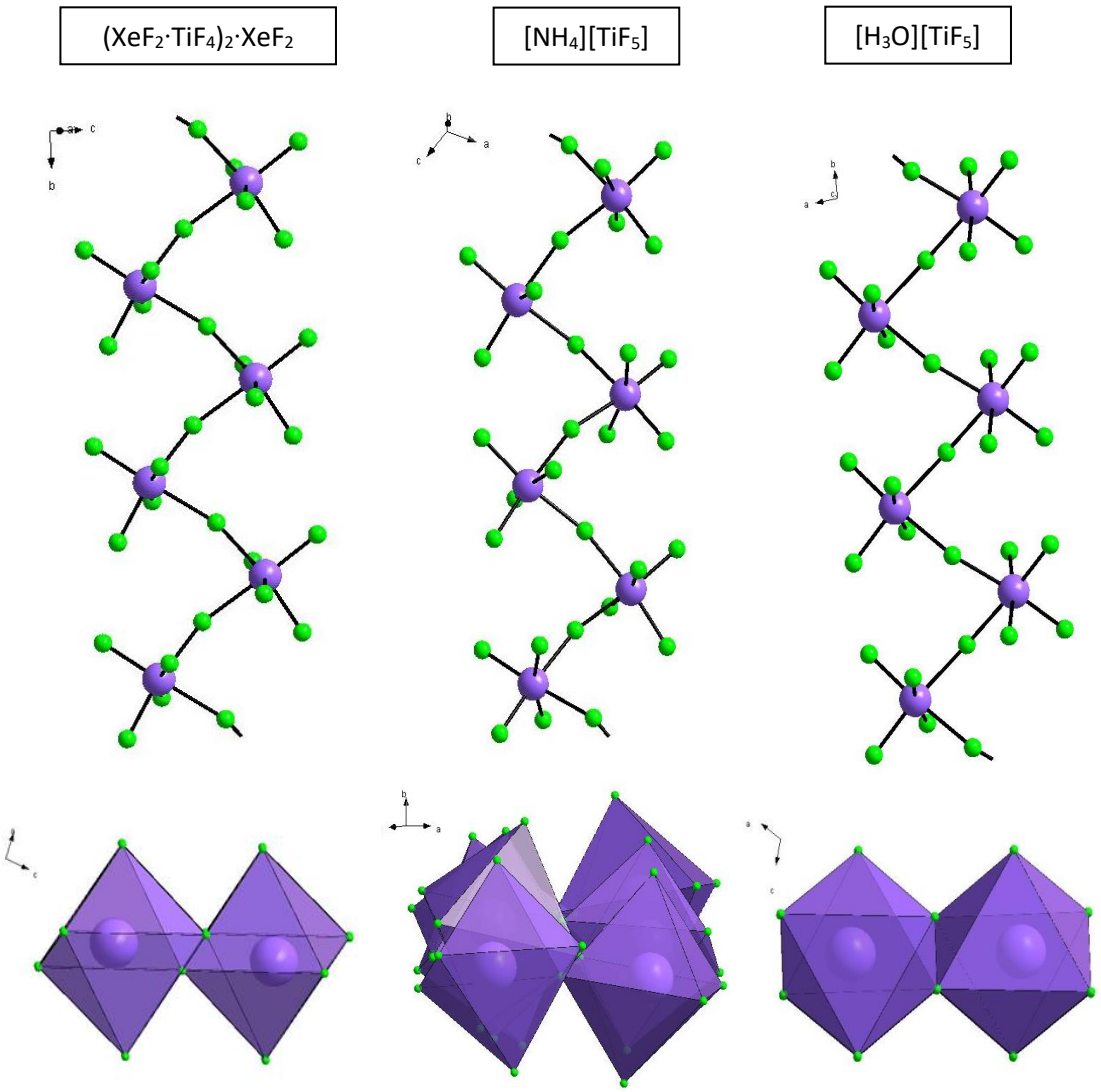


Figure 4.4: Isoformulaic $[TiF_5]$-type architectures found in compounds $(XeF_2{\cdot}TiF_4)_2{\cdot}XeF_2$, $[NH_4][TiF_5]$[166] and $[H_3O][TiF_5]$[165]. Different views along the chains reveal different geometrical conformers. Although the graphical representation creates an optical illusion of edge sharing connectivity, all octahedra are joined exclusively through common vertices.

The fluoridotitanate chain in $(XeF_2 \cdot TiF_4)_2 \cdot XeF_2$ is built from octahedral TiF_6 units, *cis*-connected by F4 bridging atoms. Although a periodic zig-zag pattern is observed, all titanium atoms do not lie on the same level parallel to the *bc*-plane but sequentially change their heights according to the orientation difference between the Ti3–F4–Ti3' and Ti3'–F4'–Ti3 bridging angles (with a unique value of 156.0(2)°) pointing towards two different directions (Figure 4.2). The Ti–F_t distances are in the 1.746(4) – 1.774(4) Å range and as expected shorter than Ti–Fb (Ti–Fb(Xe): 2.034(4) Å, Ti–Fb(Ti): 1.951(3)-2.013(3) Å), which corresponds to the values found in different polymeric $[TiF_5]^-$–anions (see references listed in Table 1.2). Due to moderate octahedral distortions, the torsion angles between nearby octahedra differ significantly (Figure 4.2) depending on the set of atoms considered, which gives an average of 20°.

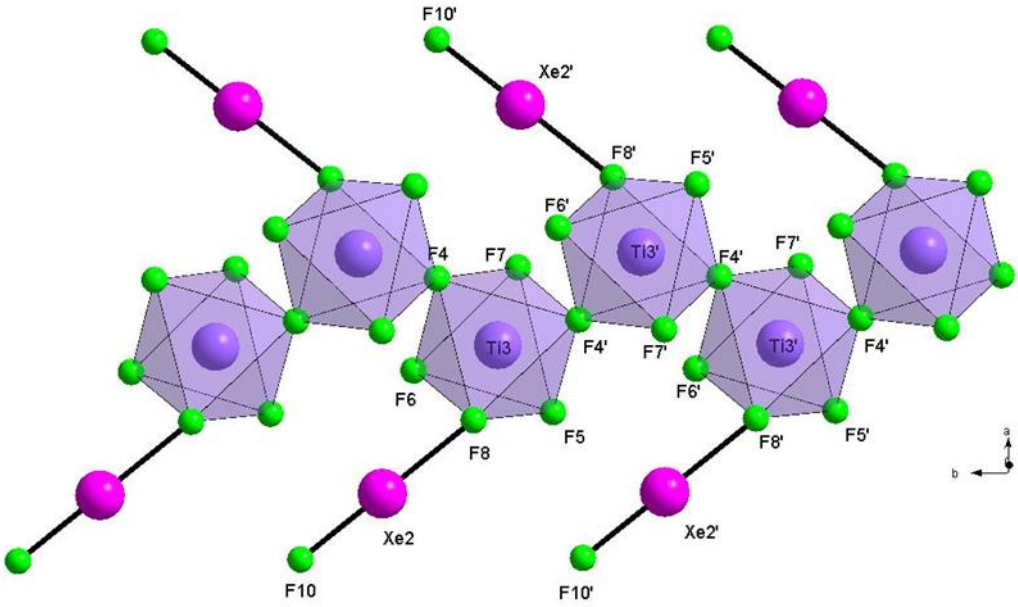


Figure 4.5: Selected part of the crystal structure of $(XeF_2 \cdot TiF_4)_2 \cdot XeF_2$, illustrating the $([FXeFTiF_4])_\infty$ chain.

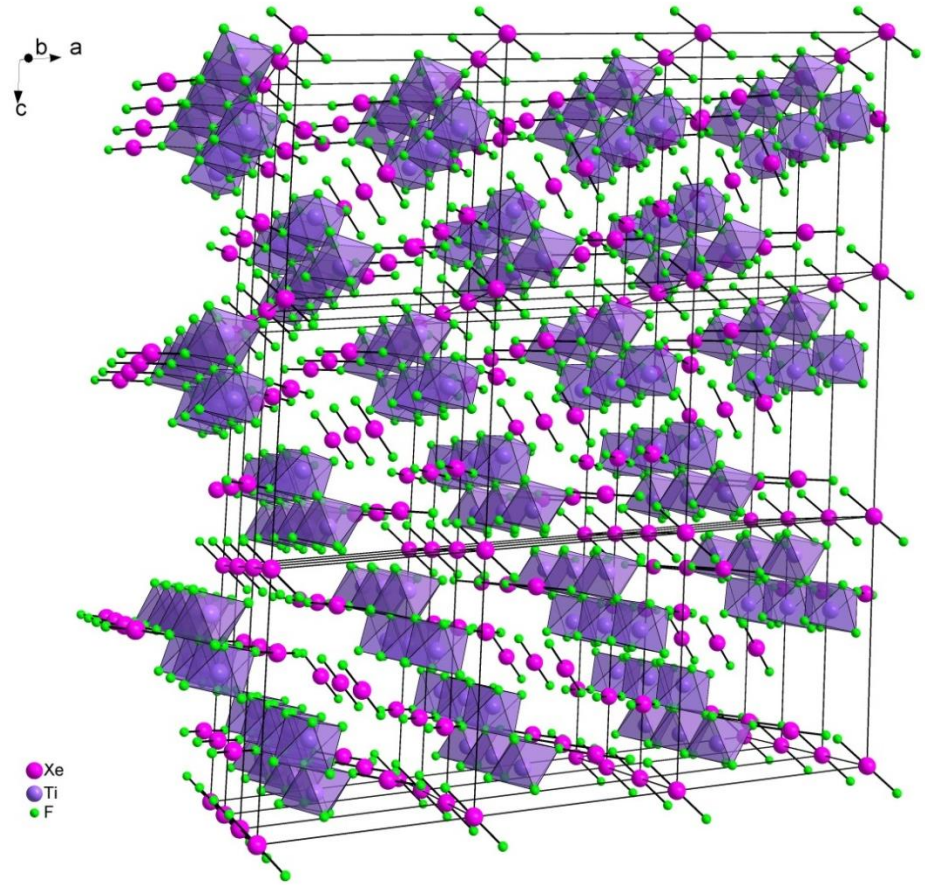


Figure 4.6: Packing of $([FXeFTiF_4])_\infty$ chains and XeF_2 molecules in the crystal structure of $(XeF_2{\cdot}TiF_4)_2{\cdot}XeF_2$.

Moreover, two crystallographically independent xenon atoms exhibit rich secondary coordination spheres defined within the sum of the F and Xe van der Waals radii (3.63 Å).[247]

Xe1, belonging to the co-crystalized XeF_2 molecule, resides on an inversion center and forms six symmetry related long contacts ranging from 3.233 (4) to 3.523 (4) Å. In this way, two separate $([FXeFTiF_4])_\infty$ chains are connected by three contacts reaching two TiF_6 units per each chain, as shown in Figure 4.7. The F9 and F9' atoms associated with Xe1 provide four additional contacts (two per each F atom) with the two Xe2 atoms belonging to two different chains (Figure 4.7).

As expected, the Xe2 secondary coordination sphere is not as symmetric as in the previous case (Figure 4.8). The Xe2 atom provides nine long-range (3.175 (4) - 3.506 (3) Å) contacts: two with two non-bonded XeF_2 molecules and seven more reaching three different $(TiF_5)^-$ chains. Among the latter, four contacts reach three neighboring octahedra (via terminal F5, F6, F7 and bridging F4) situated on the same parental $([FXeFTiF_4])_\infty$ chain, while two connections link the terminal F5 and F6 atoms of the closest non-neighboring TiF_6 units belonging to the next $(TiF_5)^-$ chain. In addition, the fragment Xe2 – F10 provides two more contacts with the corresponding Xe2' - F10 atom-couple belonging to the third $(TiF_5)^-$ chain, as depicted in Figure 4.8.

Table 4.4: Xe1 and Xe2 coordination environment in the compound $(XeF_2{\cdot}TiF_4)_2{\cdot}XeF_2$.

Bonds and Contacts (Å)			
Xe1		Xe2	
Xe1–F9^i	**1.986 (4)**	**Xe2–F8**	**2.133 (3)**

Xe1–F9	**1.986 (4)**	**Xe2–F10**	**1.922 (4)**
Xe1–F7^{v}	3.233 (4)	Xe2—F6^{xii}	3.175 (4)
Xe1–F7^{iii}	3.233 (4)	Xe2—F9^{xiii}	3.186 (4)
Xe1–F7^{iv}	3.353 (4)	Xe2—F9^{x}	3.241 (5)
Xe1–F7^{ii}	3.353 (4)	Xe2-F5^{xi}	3.258 (4)
Xe1–F6^{iv}	3.523 (4)	Xe2-F10^{vi}	3.347 (4)
Xe1–F6^{ii}	3.523 (4)	Xe2-F7^{iii}	3.383 (4)
F9–Xe2^{vi}	3.186 (4)	Xe2-F6	3.436 (4)
F9^{i}–Xe2^{viii}	3.186 (4)	Xe2-F5^{x}	3.484 (4)
F9–Xe2^{vii}	3.241 (5)	Xe2-F4^{iii}	3.506 (3)
F9^{i}–Xe2^{ix}	3.241 (5)	F10-Xe2^{xiii}	3.347 (4)

Symmetry codes: (i) −*x*+2, −*y*, −*z*+2; (ii) −*x*+2.5, *y*−0.5, −*z*+1.5; (iii) −*x*+2.5, *y*+0.5, −*z*+1.5; (iv) *x*−0.5, −*y*+0.5, *z*+0.5; (v) *x*−0.5, −*y*−0.5, *z*+0.5; (vi) –*x*+1.5, *y*−0.5, −*z*+1.5; (vii) *x*, *y*−1, *z*; (viii) *x*+0.5, −*y*+0.5, *z*+0.5; (ix) –*x*+2, −*y*+1, −*z*+2; (x) *x*, *y*+1, *z*; (xi) –*x*+2, −*y*, −*z*+1; (xii) –*x*+2, −*y*+1, −*z*+1; (xiii) –*x*+1.5, *y*+0.5, −*z*+1.5.

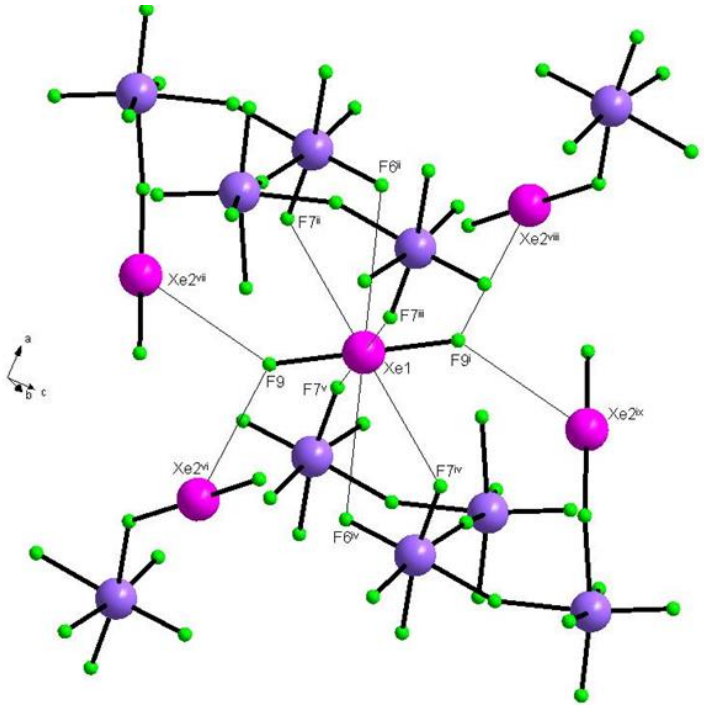


Figure 4.7: Xe1 coordination sphere in the compound $(XeF_2{\cdot}TiF_4)_2{\cdot}XeF_2$. Thin bonds denote long contacts. Symmetry codes: (i) −*x*+2, −*y*, −*z*+2; (ii) −*x*+2.5, *y*−0.5, −*z*+1.5; (iii) −*x*+2.5, *y*+0.5, −*z*+1.5; (iv) *x*−0.5, −*y*+0.5, *z*+0.5; (v) *x*−0.5, −*y*−0.5, *z*+0.5; (vi) –*x*+1.5, *y*−0.5, −*z*+1.5; (vii) *x*, *y*−1, *z*; (viii)

x+0.5, −*y*+0.5, *z*+0.5; (ix) –*x*+2, −*y*+1, −*z*+2.

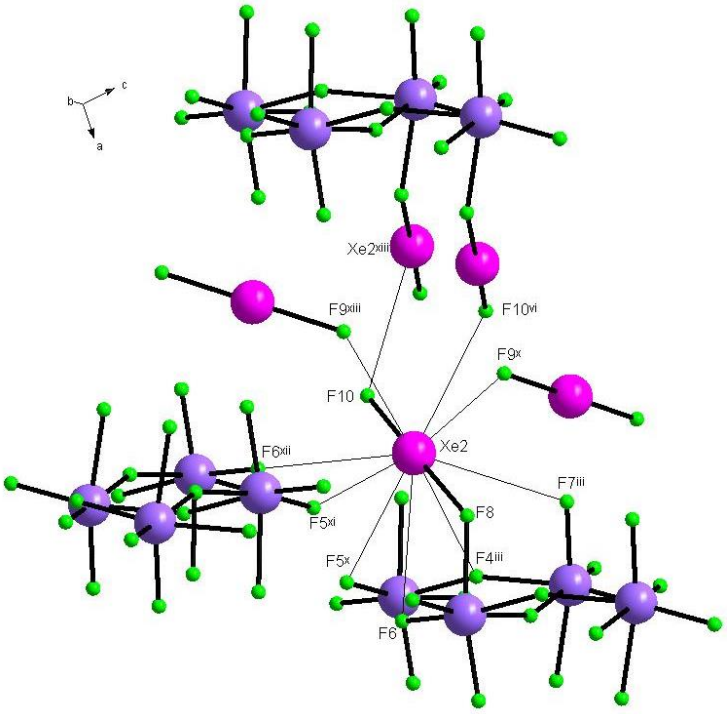


Figure 4.8: Xe2 coordination sphere in the compound $(XeF_2 \cdot TiF_4)_2 \cdot XeF_2$. Thin bonds denote long contacts. Symmetry codes: (iii) −*x*+2.5, *y*+0.5, −*z*+1.5 (vi) –*x*+1.5, *y*−0.5, −*z*+1.5; (x) *x*, *y*+1, *z*; (xi) –*x*+2, −*y*, −*z*+1; (xii) –*x*+2, −*y*+1, −*z*+1; (xiii) –*x*+1.5, *y*+0.5, −*z*+1.5.

The Raman spectrum of the product resembles that of $(XeF_2 \cdot MnF_4)_2 \cdot XeF_2$[215] and is essentially identical to the spectrum previously assigned to $XeF_2 \cdot TiF_4$.[116] The most prominent signal (505 cm^{-1}) can be attributed to the well-known Xe-F stretching vibration of weakly associated XeF_2, where the corresponding lines are slightly shifted towards higher frequencies relative to that of pure solid phase XeF_2 (496 cm^{-1}, ν_1 (A_{1g}))[72]. Examples of this bonding mode include molecular addition compounds like $XeF_2 \cdot XeF_4$ (where the intense lines at 503 cm^{-1} and 508 cm^{-1} have been tentatively assigned to a factor-group split XeF_2 mode) or co-crystalized XeF_2 molecules found in $(XeF_2 \cdot MnF_4)_2 \cdot XeF_2$ (505 cm^{-1}) or $[Xe_2F_3][MF_6] \cdot XeF_2$, where M = Ru (506 and 515 cm^{-1}) or Ir (506 and 516 cm^{-1}).[123]

The second most intense line at 566 cm^{-1} can be readily assigned to the Xe–F_t stretching frequency of the fluorine bridged $F_bXe(2)F_t$ moiety. This value is comparable with Xe–F_t frequencies found in the analogous $(XeF_2 \cdot MnF_4)_2 \cdot XeF_2$ (572 cm^{-1})[215], $XeF_2 \cdot CrF_4$ (574 cm^{-1})[210] and $XeF_2 \cdot VF_5$ (562 cm^{-1})[116] adducts, which additionally confirms a substantial covalent contribution to the bonding nature.

The lines at 701 cm^{-1} and 749 cm^{-1} correspond to Ti–F stretching frequencies found in various compounds containing the $(TiF_5)^-$ anion. The variation of intensities of bands at ~700 cm^{-1}, ~720 cm^{-1} and ~750 cm^{-1} is commonly observed among their Raman spectra.

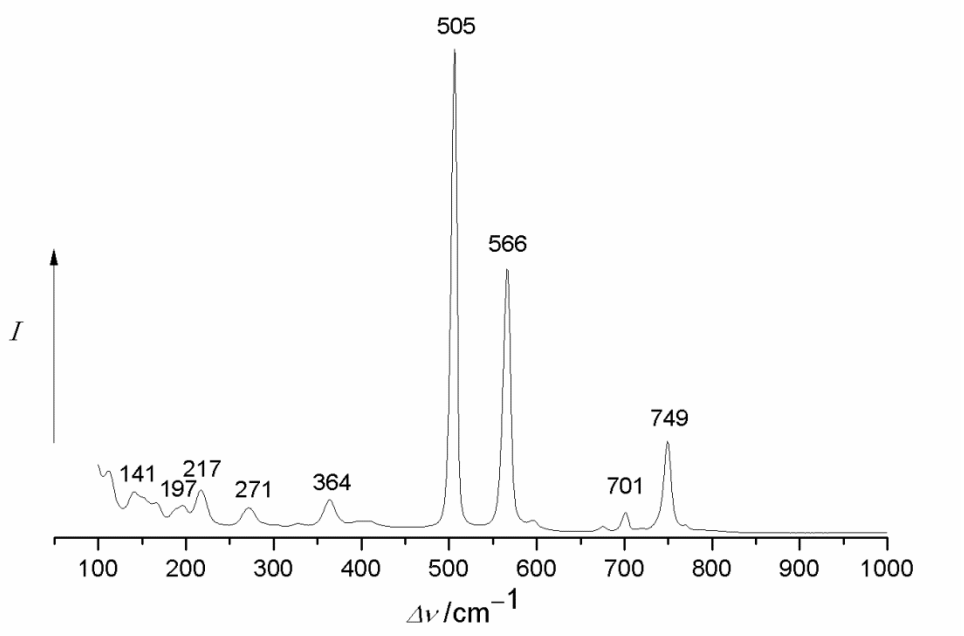


Figure 4.9: Raman spectrum of $(XeF_2 \cdot TiF_4)_2 \cdot XeF_2$ recorded at room temperature on randomly oriented crystals.

By using the previously described synthesis approach, a moderate amount of unreacted XeF_2 prevails in the product mixture, and most probably the reaction itself occurs during the last step of crystallization, when a clear XeF_2 oversaturated solution is left in the crystallization arm. The high solubility of XeF_2 and consequently the low yield of the colorless crystalline product may have prevented many successful isolation attempts in the past. In the final period of the experimental work covered hereby, a novel synthetic approach was developed based on observations made during the crystallization process, which provided a quantitative route to the product $(XeF_2 \cdot TiF_4)_2 \cdot XeF_2$ (Appendix B.1, Figure B. 1). This method consists of carrying out the reaction using a five-fold excess of XeF_2 over TiF_4 in enough aHF to let a sticky, viscous gel-like precipitate form (the chemical nature of this material is discussed in Section 4.1.4, the low-temperature Raman spectrum is given in Appendix B.1, Figure B. 2). Then, aHF is carefully evaporated until all the precipitate dissolves leaving a clear solution (usually half of the solvent, the solution with noticeable higher surface tension begins frothing). This phenomenon illustrates an interesting synthetic peculiarity as it seems that the formation and solvation of $(XeF_2 \cdot TiF_4)_2 \cdot XeF_2$ product requires a very high concentration of XeF_2, which holds the reaction equilibrium towards its favor. The temperature of such concentrated solution is then lowered stepwise (~0.5 °C/h) until the first crystal seeds begin to visibly appear on the walls. This temperature should be maintained for at least 12 h, which enables a slow, constant crystal growth. If the crystals dissolve again during the process or no further growth occurs, more aHF is carefully pumped out and the procedure repeated as described previously. Since this approach is meant to be a preparative technique, the crystal quality is not the main priority; however, a fast evaporation can result in XeF_2 crystallization from the oversaturated solution instead of the desired product. The remaining solution is finally decanted into the side arm as it contains mostly dissolved XeF_2 and all volatiles pumped off at room temperature. The best choice for this experimental method is a small T-shaped FEP reactor as it allows a better visual following, as well as better control over the process.

As mentioned in the Background section, the existence of compound $2XeF_2 \cdot TiF_4$ was also reported, but poor evidence was given and the results raised several doubts. In order to explore this possibility, a five-fold excess of XeF_2 was left to react with TiF_4 at room temperature in aHF for 24 h. The reaction mixture was then slowly cooled down to −78 °C and after 6 h the low-temperature (−150 °C) Raman spectrum of the frozen solution was recorded. The band positions coincide with the spectrum of $(XeF_2 \cdot TiF_4)_2 \cdot XeF_2$, overlapped with unreacted XeF_2 (Appendix B.1,

Figure B. 3). Therefore, the formation of compound $2XeF_2 \cdot TiF_4$ in aHF, neither at very low temperatures, cannot be confirmed.

4.1.3 $[Xe_2F_3][Ti_8F_{33}]$

Targeted studies of the system XeF_2 – TiF_4 began 40 years ago with the isolation of phases $n XeF_2 \cdot TiF_4$ (n = 1.5, 1, 0.5), synthesized from TiF_4 and excess XeF_2 at 120 °C. While the XeF_2-rich compound (n = 1.5, $3XeF_2 \cdot 2TiF_4$) formed readily at room temperature, others were prepared by thermal decomposition (60 and 75 °C, respectively) of the parent compound under dynamic vacuum (see Background). The crystal structure of the XeF_2-rich compound, $(XeF_2 \cdot TiF_4)_2 \cdot XeF_2$, has been determined on crystals grown from aHF solution within the present work and described in the previous section. However, using aHF as a solvent did not work for the other two aforementioned phases. Mixing stoichiometric amounts of TiF_4 and XeF_2 in aHF always resulted in the formation of an amorphous precipitate or unknown glassy solid.

The solubility and the F^--accepting potential of metal tetrafluorides in the solid state are strongly affected by their polymeric nature. Previous attempts to overcome these association energies by carrying out gas-phase reactions between TiF_4 and XeF_2 were not successful.[116] The failure was attributed to the heating temperature, which might not had been sufficient (398 K) to reach a satisfactory vapor pressure of TiF_4 and consequently to ensure enough contact with XeF_2 molecules in the gaseous phase (at 398 K, P_{TiF_4} = 40 Pa, while P_{XeF_2} = 400-500 Pa). In fact, the reaction temperature should be low enough to prevent the thermal decomposition of the potentially formed products and high enough for the used MF_4 to be at least partially volatile, since the majority of the aforementioned MF_4 compounds exist as tetrahedral molecules in the gas phase.

In the present work, thermal reactions between XeF_2 and TiF_4 were carried out adopting different approaches and several more experiments were needed in order to improve the selectivity of the reactions and the crystallinity of the products. This extensive study involved variations in the heating and cooling rates, different molar ratios of the starting material, reaction times, the lengths and type (nickel, quartz, FEP) of the reactors used, as well as quenching at different temperatures. Moreover, it was found that even the reaction atmosphere (argon, aHF) and its pressure have a significant effect on the formation and crystal quality of the products. In order to detect any potential new phase formed, the contents of the reactor tubes were meticulously screened after each run with Raman spectroscopy and special attention was given to classify all the different morphologies present.

Short (8-19 cm) translucent sealed FEP tubes provided the most suitable synthetic environment (high probability of chemical contacts in the gaseous phase along a short confined space) and allowed an easy and fast control over the reaction conditions as well as visual following of the entire process.

Different molar ratios of the reactants were tested, ranging from XeF_2 : TiF_4 = 5:1 to XeF_2 : TiF_4 = 1:5. In a typical run, the temperature of the reaction mixture was held above the triple point of XeF_2 (129.03 °C),[248] at ~135 °C, for several hours. Where the molar ratio exceeded 1:1 in favor of the TiF_4, crystals of the first product[249], determined as $[Xe_2F_3][Ti_8F_{33}]$, started to grow on the wall of the fluoroplastic tube after approximately 2–3 h at 135 °C. The best yield and crystal quality was achieved using the following procedure: A FEP reaction vessel (tubing, 6 mm i.d, 8 mm o.d.), equipped with a PTFE valve, was filled with TiF_4 (23 mg, 0.19 mmol) and XeF_2 (16 mg, 0.09 mmol) in a glove box under argon atmosphere. Subsequently, the reaction vessel assembly, along with the contents, was evacuated at –196 °C on a vacuum line and the FEP tube was sealed. The sealed reaction tube was then heated to 135 °C for 12 h. Initially, the mixture turned into a pale-yellow gel-like material, which began to slowly decompose during the heating process. Careful cooling to 110 °C (2 °C/h) afforded colorless, rod-like crystals (Figure 4.10), which were isolated from the reaction vessel and immersed in perfluorinated oil inside the glove box. A suitable crystal was selected at low temperature (−15 °C) under the microscope and transferred into the cold nitrogen stream of the X-ray diffractometer.

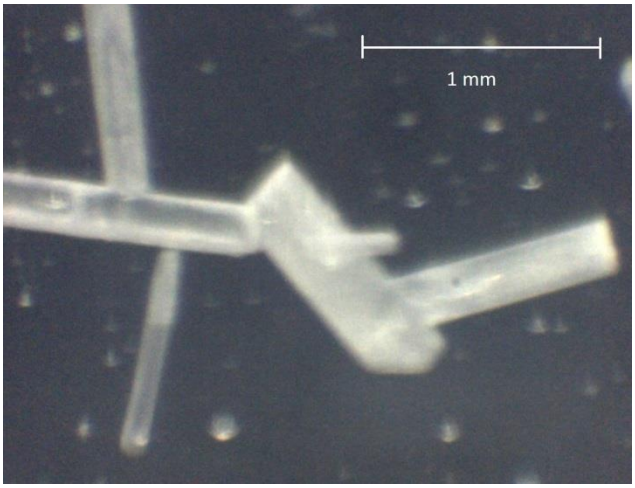
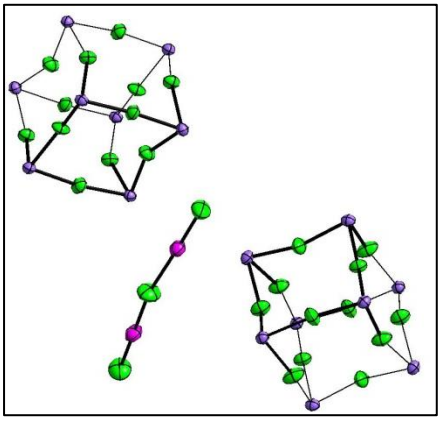


Figure 4.10: Crystals of $[Xe_2F_3][Ti_8F_{33}]$ growing on the inner wall of the FEP reactor.

Table 4.5: Crystal structure determination and refinement details for compound $[Xe_2F_3][Ti_8F_{33}]$.

Crystal data	*Data collection*	*Refinement*
$Xe_2Ti_8F_{36}$	Rigaku AFC7 diffractometer	$R_1[F^2 > 2\sigma(F^2)] = 0.052$
$M_r = 1329.54$	Mercury CCD detector	$wR_2\ (F^2) = 0.155$
Crystal system: monoclinic	λ = 0.71069 Å (Mo K_α)	6602 reflections
Space group: *P*2/*a*	23240 measured reflections	416 parameters
a = 17.6347 (5) Å	6602 independent reflections	GOF = 1.14
b = 8.4106 (2) Å	5573 observed reflections (I > 2 σ (I))	$\Delta\rho_{max}$ = 2.18 e/Å^3
c = 19.9028 (5) Å	R_{int} = 0.029	$\Delta\rho_{min}$ = −1.98 e/Å^3
β = 97.140 (1)°	θ_{max} = 29.2°, θ_{min} = 2.1°	
V = 2929.06 (13) Å^3	$-24 \leq h \leq 23$	
Z = 4	$-9 \leq k \leq 10$	
ρ_{calc} = 3.016 g/cm^3	$-25 \leq l \leq 25$	
$2.1° \leq \theta \leq 29.1°$		
Cell parameters from 9928 reflections		
μ = 4.56 mm^{-1}		
T = 150 K		
F(000) = 2432		
Size: 0.1×0.06×0.04 mm		
Appearance: Colorless, chunk		

The compound $[Xe_2F_3][Ti_8F_{33}]$ crystallizes in the monoclinic centrosymmetric *P*2/*a* space group with 4 formula units per unit cell. Additional details on the crystal, data collection and refinement are given in Table 4.5. Forty-seven atoms define the asymmetric unit – forty-five atoms are situated on general positions (Wyckoff 4g), while the fluorine atoms F4 (Wyckoff 2e) and F29 (Wyckoff 2f) reside on a 2-fold rotational axis.



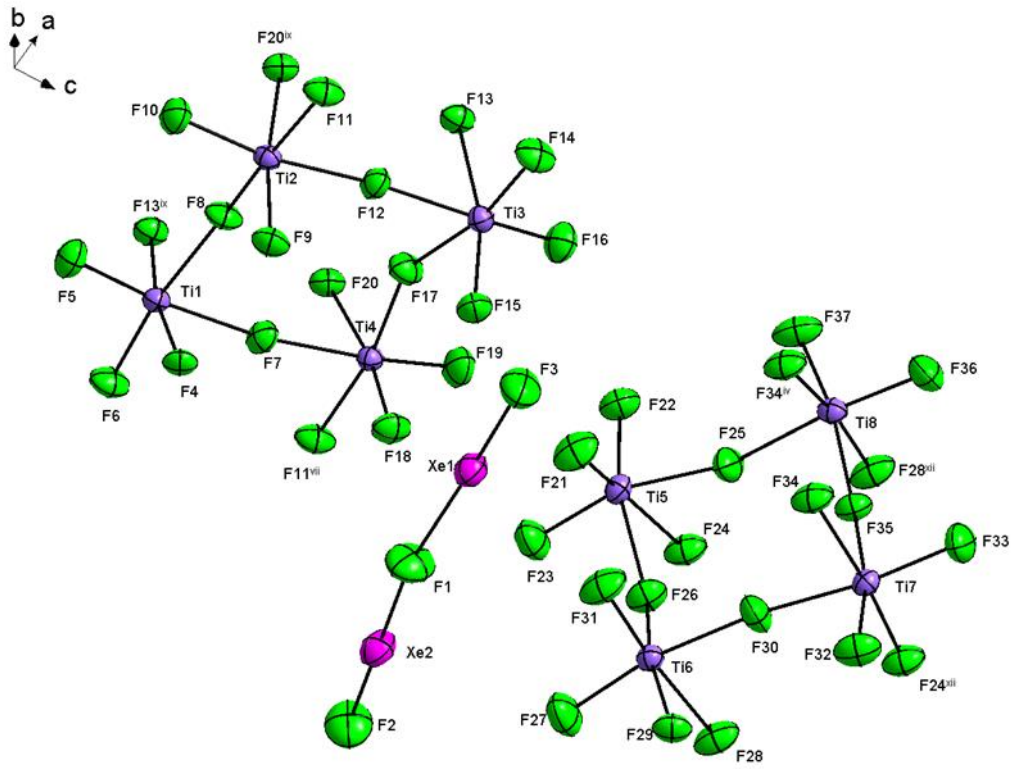


Figure 4.11: The asymmetric unit of the compound $[Xe_2F_3][Ti_8F_{33}]$ consists of two separate tetrameric rings and a Xe_2F_3 unit (ellipsoids are drawn at the 50% probability). Each ring represents a square face in two symmetrically generated cubic architectures (framed above; thick bonds are used for asymmetric tetramers, the terminal F atoms are omitted for clarity). Symmetry codes: (iv) −*x*+1, −*y*+1, −*z*+1; (vii) *x*, *y*−1, *z*; (ix) −*x*+1, −*y*+1, −*z*; (xii) −*x*+1, −*y*, −*z*+1.

The $Xe_2F_3^+$ cation is known since 1968, when its hexafluoridoarsenate salt $[Xe_2F_3][AsF_6]$ was synthesized by the thermal decomposition of the $[XeF][AsF_6]$ as a result of the volatile nature of AsF_5.[112,120] Thus far, the formation of cationic species $Ng_2F_3^+$ (Ng = Kr, Xe) has been observed only when ensuring an excess of NgF_2 over the corresponding fluoride acceptor, and not the other way around. The surplus of XeF_2 has always been achieved either by the initial reaction stoichiometry or by the reaction intermediates releasing XeF_2 during their solvolysis in aHF.[122] Already the compound formulation $[Xe_2F_3][Ti_8F_{33}]$ itself is a striking surprise, since the required XeF_2 : TiF_4 ratio for the overall chemical reaction would be 1 : 4. Moreover, high temperatures have been required in most previous studies only to provide the molten XeF_2 (which can act as solvent and/or as reactant) and never with the specific aim to carry out thermal chemical reactions, where the instability of such compounds has to be taken in consideration.

One plausible explanation for the formation of the cationic part of the title product is the genesis of the $Xe_2F_3^+$ in the gas phase due to the overabundance of XeF_2 vapors at the early stage of the reaction. Strong evidence for the formation of $Xe_2F_3^+$ ions in the gas phase has already been reported [250] – a new asymmetric isomer with connectivity $[F–Xe–XeF_2]^+$ cation was prepared by high-pressure chemical ionization (CI) of XeF_2 and structurally assayed by collisionally activated decomposition (CAD) and MS/MS/MS mass spectrometry.

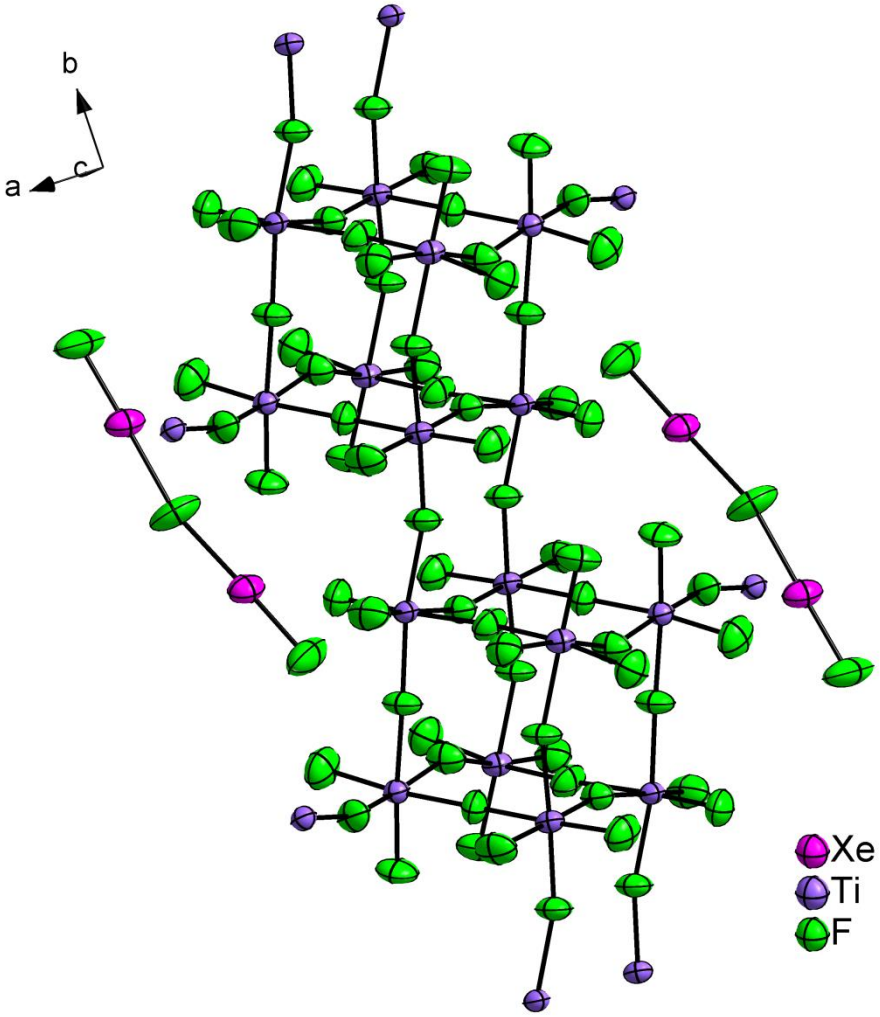


Figure 4.12: Representative structural part of the compound $[Xe_2F_3][Ti_8F_{33}]$. Ellipsoids are drawn at the 50% probability.

The knowledge regarding the formation, connectivity and geometry of the $Xe_2F_3^+$ ions is limited to only five related structures solved by X-ray crystallography: $[Xe_2F_3][MF_6]$ (M = As (monoclinic and trigonal)[120,121,122], Sb[122], Ir[123], Ru[123]) and $[Xe_2F_3][RuF_6]\cdot XeF_2$[123]. The crystal structure of $[Xe_2F_3][Ti_8F_{33}]$ revealed a roughly symmetrical V-shaped cation with the widest Xe−F_b−Xe angle (164.3(3)°) among the $Xe_2F_3^+$ compounds (previously found to vary from 139.8(8) to 160.3(3)° in trigonal $[Xe_2F_3][AsF_6]$ and $[Xe_2F_3][SbF_6]$, respectively). The deviation from linearity and the facile deformation of this angle in the crystals were attributed to the presence of counterions and additionally confirmed using DFT methods.[122] While a Hartree-Fock study[251] predicted a linear Xe−F−Xe bridge for the free cation, our result is in perfect agreement with the previous Christiansen-Ermler ECP (effective core potential) calculation,[122] which gave a non-linear geometry with a Xe−F_b−Xe angle of 168°.

The main contribution to a slight asymmetric arrangement arises from the inequality of the two F_b−Xe bonds (Xe1−F1: 2.194(4) Å, while Xe2−F1: 2.158 (4) Å). Here it should be noted that all five atoms constructing the $Xe_2F_3^+$ cation in $[Xe_2F_3][Ti_8F_{33}]$ are crystallographically independent. Nevertheless, the Xe−F_t bond lengths (Xe1–F3: 1.901 (4) Å; Xe2–F2: 1.905 (4) Å) and essentially linear angles of the two F_b–Xe–F_t moieties (178.2(2) and 179.4(2)°) are

comparable with the corresponding values found in the previously reported structures of $Xe_2F_3^+$ salts.[122,]**Error! Bookmark not defined.**

A basic structural motif repeating in $[Xe_2F_3][Ti_8F_{33}]$ is shown in Figure 4.12. Despite an isoformulaic polymeric anion $[Ti_8F_{33}]^-$ has already been found in the alkali metal salt $CsTi_8F_{33}$,[168] the substitution of spherical Cs^+ with the planar V-shaped $Xe_2F_3^+$ cations impacts dramatically its structure. A nearly regular hexahedron observed resembles a recently reported isolated cubic $[Ti_8F_{36}]^{4-}$ anion[163] comprising eight TiF_6 octahedra, and similar architectures were also found in some other polyfluoridotitanates(IV)[155,164] (Figure 4.14). The atoms that complete the tetrameric rings of the asymmetric unit into distorted cubes are symmetry related with a center of inversion situated in the middle of each cubic assembly.

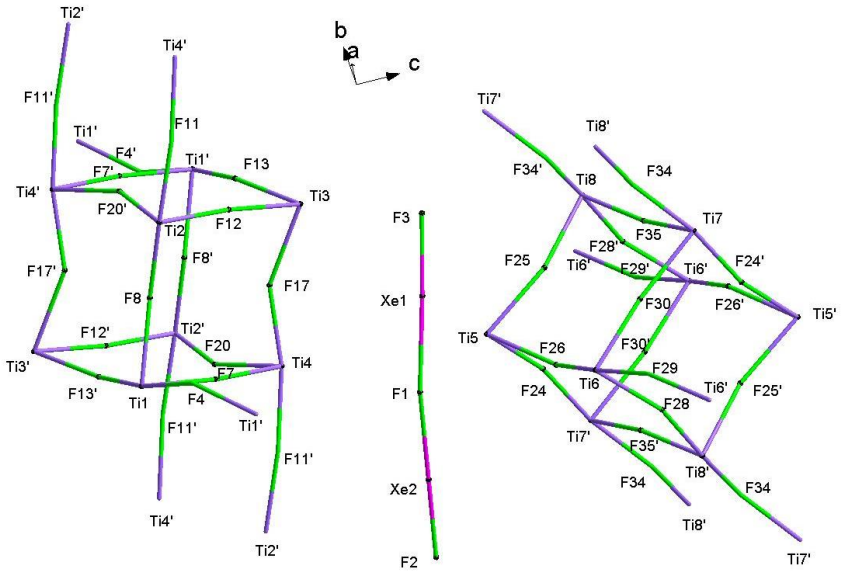


Figure 4.13: Labeling scheme and connectivity of two crystallographically independent cubic assemblies found in $[Xe_2F_3][Ti_8F_{33}]$. The notation (') indicates a symmetrically generated atom.

In $[Xe_2F_3][Ti_8F_{33}]$, the cube-like assemblies are further linked through six shared fluorine atoms – four nearly straight bridges (Ti2–F11–Ti4' angle: 169.9(2) °, Ti8'–F34–Ti7 angle: 154.2 (2)°) are made roughly along the crystallographic *b*-axis, in pairs situated on opposite edges, thus connecting the cubes into a columnar structure. These columns are additionally connected with two fluorine bridges (*via* F4 and F29 situated on a 2-fold rotational axis, Ti1'—F4—Ti1 angle equals 152.3(3)° and $Ti6^v$—F29—Ti6 161.8(3)°) originating from vertexes lying on the cubic body diagonal along the *a*-axis, forming a complex polyanion layer.

Table 4.6: Selected geometric parameters for the compound $[Xe_2F_3][Ti_8F_{33}]$.

Bond Lengths (Å)			
Xe1—F3	1.901 (4)	Ti4—F20	1.975 (3)
Xe1—F1	2.194 (4)	Ti4—F7	1.984 (3)
Xe2—F2	1.905 (4)	Ti5—F21	1.742 (4)
Xe2—F1	2.158 (4)	Ti5—F22	1.741 (4)
Ti1—F6	1.740 (3)	Ti5—F23	1.748 (4)
Ti1—F5	1.748 (3)	Ti5—F25	1.985 (3)

Ti1—F13^{ix}	1.861 (3)	Ti5—F24	2.046 (3)
Ti1—F4	1.9352 (14)	Ti5—F26	2.077 (3)
Ti1—F7	1.949 (3)	Ti6—F31	1.731 (4)
Ti1—F8	2.007 (3)	Ti6—F27	1.742 (4)
Ti2—F10	1.738 (3)	Ti6—F26	1.851 (3)
Ti2—F9	1.737 (3)	Ti6—F29	1.9239 (12)
Ti2—F8	1.904 (3)	Ti6—F30	1.942 (3)
Ti2—F11	1.929 (3)	Ti6—F28	2.012 (3)
Ti2—F12	1.952 (3)	Ti7—F33	1.727 (4)
Ti2—F20^{ix}	1.976 (3)	Ti7—F32	1.737 (3)
Ti3—F15	1.744 (3)	Ti7—F24^{xii}	1.858 (3)
Ti3—F14	1.750 (3)	Ti7—F34	1.945 (3)
Ti3—F16	1.755 (4)	Ti7—F35	1.967 (3)
Ti3—F12	1.972 (3)	Ti7—F30	1.981 (3)
Ti3—F17	2.060 (3)	Ti8—F36	1.721 (4)
Ti3—F13	2.070 (3)	Ti8—F37	1.732 (4)
Ti4—F19	1.732 (3)	Ti8—F28^{xii}	1.896 (3)
Ti4—F18	1.741 (3)	Ti8—F34^{iv}	1.938 (3)
Ti4—F17	1.873 (3)	Ti8—F25	1.950 (3)
Ti4—F11^{vii}	1.934 (3)	Ti8—F35	1.972 (3)
Bond Angles (°)			
F3—Xe1—F1	178.2 (2)	F22—Ti5—F24	89.0 (2)
F2—Xe2—F1	179.4 (2)	F23—Ti5—F24	88.7 (2)
F6—Ti1—F5	98.1 (2)	F25—Ti5—F24	80.6 (2)
F6—Ti1—F13^{ix}	96.01 (15)	F21—Ti5—F26	89.5 (2)
F5—Ti1—F13^{ix}	93.8 (2)	F22—Ti5—F26	164.2 (2)
F6—Ti1—F4	92.1 (2)	F23—Ti5—F26	86.3 (2)
F5—Ti1—F4	90.78 (15)	F25—Ti5—F26	78.64 (15)
F13^{i}—Ti1—F4	170.04 (12)	F24—Ti5—F26	77.97 (14)

F6—Ti1—F7	90.8 (2)	F31—Ti6—F27	97.3 (2)
F5—Ti1—F7	170.0 (2)	F31—Ti6—F26	94.6 (2)
F13^{i}—Ti1—F7	89.58 (14)	F27—Ti6—F26	94.9 (2)
F4—Ti1—F7	84.48 (11)	F31—Ti6—F29	93.1 (2)
F6—Ti1—F8	171.9 (2)	F27—Ti6—F29	90.3 (2)
F5—Ti1—F8	88.5 (2)	F26—Ti6—F29	170.07 (13)
F13^{i}—Ti1—F8	88.10 (14)	F31—Ti6—F30	91.3 (2)
F4—Ti1—F8	83.18 (14)	F27—Ti6—F30	169.8 (2)
F7—Ti1—F8	82.16 (14)	F26—Ti6—F30	89.9 (2)
F10—Ti2—F9	100.4 (2)	F29—Ti6—F30	83.64 (13)
F10—Ti2—F8	94.5 (2)	F31—Ti6—F28	173.6 (2)
F9—Ti2—F8	93.43 (15)	F27—Ti6—F28	88.6 (2)
F10—Ti2—F11	90.9 (2)	F26—Ti6—F28	87.27 (15)
F9—Ti2—F11	92.42 (15)	F29—Ti6—F28	84.5 (2)
F8—Ti2—F11	171.18 (15)	F30—Ti6—F28	82.6 (2)
F10—Ti2—F12	169.2 (2)	F33—Ti7—F32	99.5 (2)
F9—Ti2—F12	89.82 (14)	F33—Ti7—F24^{xii}	95.0 (2)
F8—Ti2—F12	88.43 (15)	F32—Ti7—F24^{xii}	94.3 (2)
F11—Ti2—F12	84.99 (15)	F33—Ti7—F34	92.0 (2)
F10—Ti2—F20^{ix}	88.90 (15)	F32—Ti7—F34	91.1 (2)
F9—Ti2—F20^{ix}	170.70 (15)	F24^{xii}—Ti7—F34	170.3 (2)
F8—Ti2—F20^{ix}	85.35 (13)	F33—Ti7—F35	90.1 (2)
F11—Ti2—F20^{ix}	87.81 (14)	F32—Ti7—F35	169.4 (2)
F12—Ti2—F20^{ix}	80.93 (13)	F24^{xii}—Ti7—F35	89.22 (14)
F15—Ti3—F14	102.2 (2)	F34—Ti7—F35	84.12 (14)
F15—Ti3—F16	101.1 (2)	F33—Ti7—F30	170.8 (2)
F14—Ti3—F16	97.5 (2)	F32—Ti7—F30	89.4 (2)
F15—Ti3—F12	90.21 (15)	F24^{xii}—Ti7—F30	86.3 (2)

F14—Ti3—F12	93.0 (2)	F34—Ti7—F30	85.7 (2)
F16—Ti3—F12	162.5 (2)	F35—Ti7—F30	80.79 (14)
F15—Ti3—F17	89.61 (15)	F36—Ti8—F37	99.2 (2)
F14—Ti3—F17	166.67 (15)	F36—Ti8—F28^{xii}	93.5 (2)
F16—Ti3—F17	86.1 (2)	F37—Ti8—F28^{xii}	95.0 (2)
F12—Ti3—F17	80.62 (14)	F36—Ti8—F34^{iv}	91.3 (2)
F15—Ti3—F13	165.19 (15)	F37—Ti8—F34^{iv}	92.0 (2)
F14—Ti3—F13	88.12 (15)	F28^{iii}—Ti8—F34^{iv}	170.8 (2)
F16—Ti3—F13	87.9 (2)	F36—Ti8—F25	171.6 (2)
F12—Ti3—F13	78.52 (13)	F37—Ti8—F25	88.9 (2)
F17—Ti3—F13	79.17 (13)	F28^{xii}—Ti8—F25	88.0 (2)
F19—Ti4—F18	99.3 (2)	F34^{iv}—Ti8—F25	86.2 (2)
F19—Ti4—F17	94.6 (2)	F36—Ti8—F35	89.8 (2)
F18—Ti4—F17	94.9 (2)	F37—Ti8—F35	170.7 (2)
F19—Ti4—F11^{vii}	92.6 (2)	F28^{xii}—Ti8—F35	86.61 (14)
F18—Ti4—F11^{vii}	91.9 (2)	F34^{iv}—Ti8—F35	85.54 (14)
F17—Ti4—F11^{vii}	169.17 (15)	F25—Ti8—F35	82.00 (14)
F19—Ti4—F20	89.6 (2)	Xe2—F1—Xe1	164.3 (3)
F18—Ti4—F20	170.31 (15)	Ti1—F7—Ti4	170.5 (2)
F17—Ti4—F20	88.24 (14)	Ti2—F8—Ti1	156.6 (2)
F11^{vii}—Ti4—F20	83.78 (14)	Ti2—F11—Ti4^{ii}	169.9 (2)
F19—Ti4—F7	170.0 (2)	Ti2—F12—Ti3	175.1 (2)
F18—Ti4—F7	90.50 (15)	Ti1^{ix}—F13—Ti3	161.4 (2)
F17—Ti4—F7	86.35 (15)	Ti4—F17—Ti3	150.2 (2)
F11^{vii}—Ti4—F7	85.12 (15)	Ti4—F20—Ti2^{ix}	151.9 (2)
F20—Ti4—F7	80.53 (13)	Ti7^{xii}—F24—Ti5	163.0 (2)
F21—Ti5—F22	102.3 (2)	Ti8—F25—Ti5	160.9 (2)
F21—Ti5—F23	97.2 (2)	Ti6—F26—Ti5	151.3 (2)

F22—Ti5—F23	101.7 (2)	Ti8^{xii}—F28—Ti6	160.4 (2)
F21—Ti5—F25	90.5 (2)	Ti6—F30—Ti7	171.6 (2)
F22—Ti5—F25	91.4 (2)	Ti8^{iv}—F34—Ti7	154.2 (2)
F23—Ti5—F25	163.0 (2)	Ti7—F35—Ti8	164.2 (2)
F21—Ti5—F24	165.8 (2)		

Symmetry codes: (i) −*x*+1/2, *y*, −*z*; (ii) *x*, *y*+1, *z*; (iii) *x*−1/2, −*y*+1, *z*; (iv) −*x*+1, −*y*+1, −*z*+1; (v) −*x*+1/2, *y*, −*z*+1; (vi) *x*−1/2, −*y*, *z*; (vii) *x*, *y*−1, *z*; (viii) −*x*+1/2, *y*−1, −*z*; (ix) −*x*+1, −*y*+1, −*z*; (x) *x*+1/2, −*y*+1, *z*; (xi) *x*+1/2, −*y*, *z*; (xii) −*x*+1, −*y*, −*z*+1; (xiii) −*x*+1/2, *y*+1, −*z*.

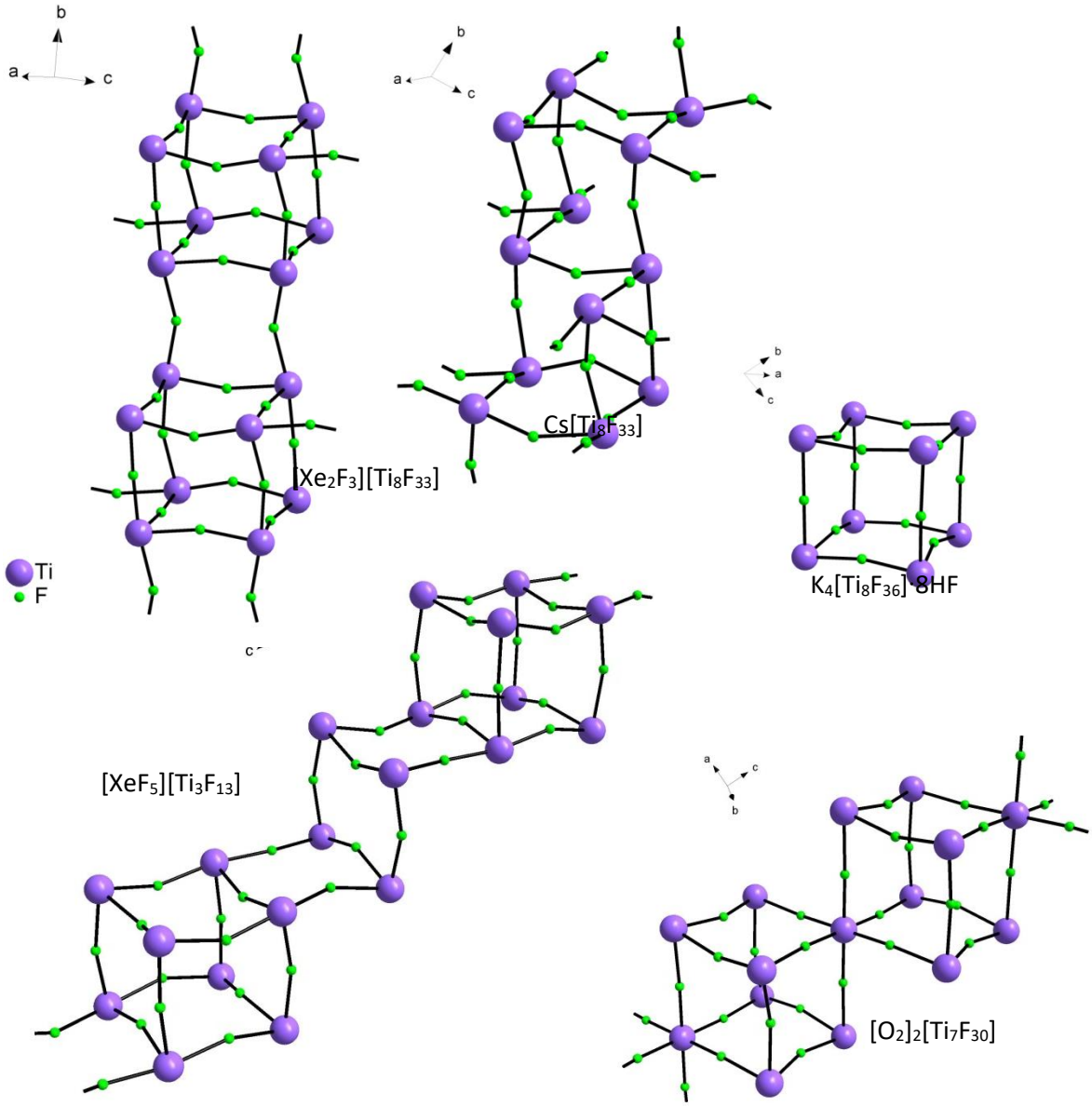


Figure 4.14: Cube-like architectures found in different fluoridotitanates(IV). The terminal F atoms have been omitted for clarity and broken-off bonds represent further connections to the neighboring Ti atoms. The $[Ti_8F_{32+x}]^{x-}$-type anions were determined as two structurally very different but isoformulaic $^{2}_{\infty}[(Ti_8F_{33})^{-}]$ ions in compounds $[Xe_2F_3][Ti_8F_{33}]$ and $Cs[Ti_8F_{33}]$ and

additionally as an isolated $[Ti_8F_{36}]^{4-}$ cube in $K_4[Ti_8F_{36}]\cdot 8HF$.[163,168,249] Other examples of cubic [–Ti–F–Ti–] grouping can be found in the structures of $^1_\infty[(Ti_7F_{30})^{2-}]$ and recently isolated $^1_\infty[(Ti_3F_{13})^-]$ anion.[164,167]

The $Xe_2F_3^+$ cations are situated in semi-closed channels arising from indentations between the anion layers. These voids are generated by single Ti1'—F4—Ti1 and Ti6^v—F29—Ti6 bridges, where the layer is narrowest, and restricted by cubic arrangements, where the layer thickness equals approximately the distance of terminal F atoms lying at the ends of the cubic body diagonal (~8 Å). The resulting extended structure of $[Xe_2F_3][Ti_8F_{33}]$ consists of alternating anion and cation layers parallel to the *ab*-plane. Different views of cation-anion packing are depicted in Figure 4.15, Figure 4.17 and Figure 4.18.

A list of associated bond distances and angles is given in Table 4.6. As expected, the Ti – F_t bond lengths, ranging from 1.721(4) to 1.755(4) Å are considerably shorter than the Ti – F_b bond lengths (1.851(3) – 2.077(3) Å). Both sets of distances are comparable to the corresponding bond lengths found in various fluoridotitanate(IV) salts and other titanium fluoride complexes.[154,155] The distances of bridging Ti–F_b bonds which connect the cubic assemblies vertically into columns and horizontally into layers do not differ from other Ti–F_b lengths defining the cubic edges. The mentioned regularity of hexahedrons is justified by the low variation of the nonbonding Ti···Ti distances (3.801(1) – 3.921(1) Å) and Ti···Ti···Ti angles close to the requested right angle of 90° (85.91(2) – 94.31(3)°). Both crystallographically independent cubes are oriented towards opposite directions with a torsion angle of 55.5°.

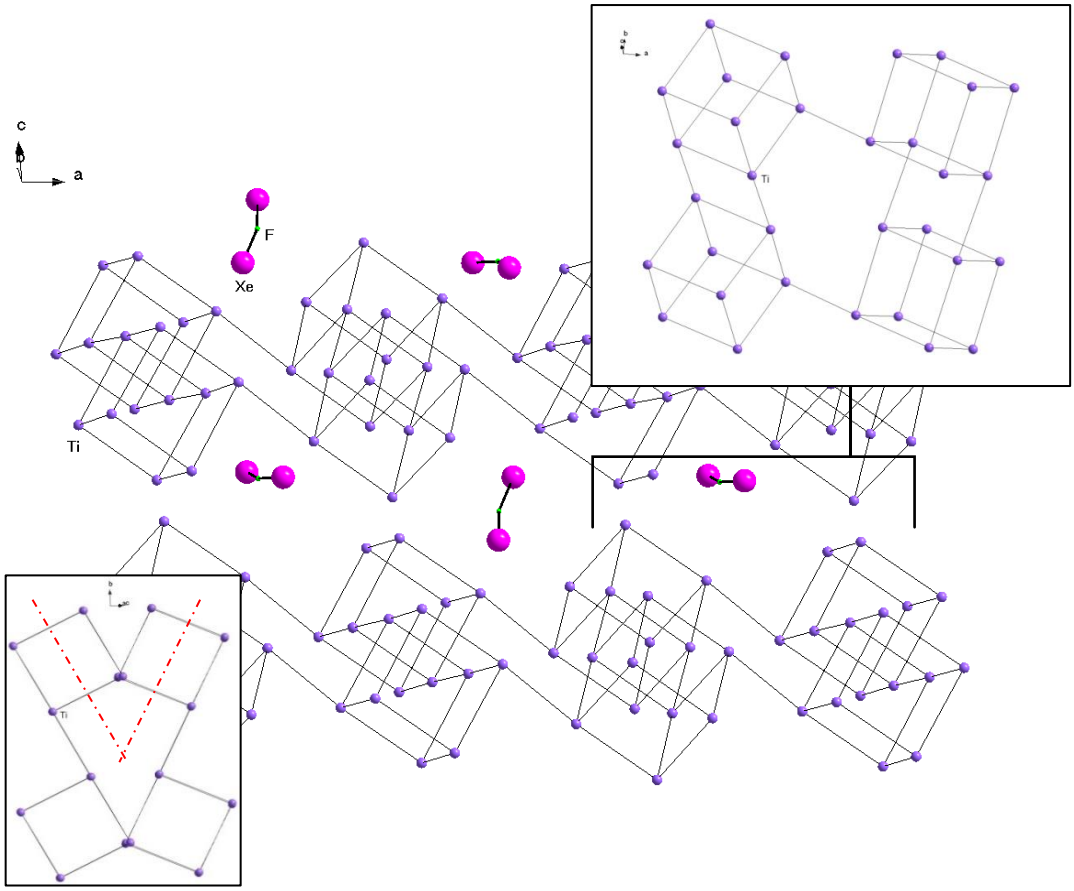


Figure 4.15: Layered structure, cubic assemblies and different cation orientations found in $[Xe_2F_3][Ti_8F_{33}]$. All fluorine atoms, except the bridging ones of the $Xe_2F_3^+$ cations, have been omitted for reasons of clarity and imaginary Ti–Ti bonds have been drawn.

The "naked" layer representation in Figure 4.15 showing only imaginary Ti–Ti connections reveals exclusively quadrilateral faces (rectangles), which can also be described as almost square

tiles with two vertex configurations[†]: 4^3 ("free" apexes on each cube) and 4^4 (shared apexes).[252,253,254]

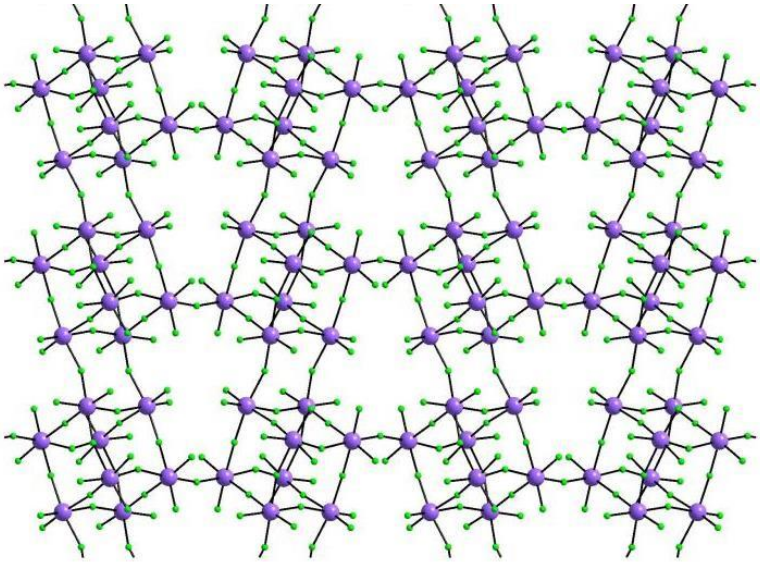


Figure 4.16: The layered structure of $^{2}_{\infty}[(Ti_8F_{33})^-]$ anion.

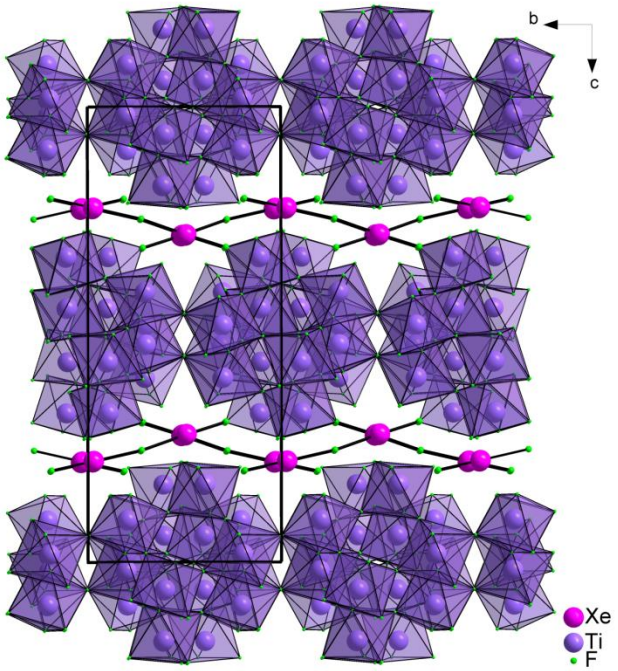


Figure 4.17: Packing diagram and the unit cell of $[Xe_2F_3][Ti_8F_{33}]$; view along the *a*-axis.

[†] The descriptions used for vertex configurations (also *vertex type* or *vertex symbol*) refer to O'Keeffe & Hyde,[253] using Schläffli notation[252] modified by Cundy & Rollet.[254]

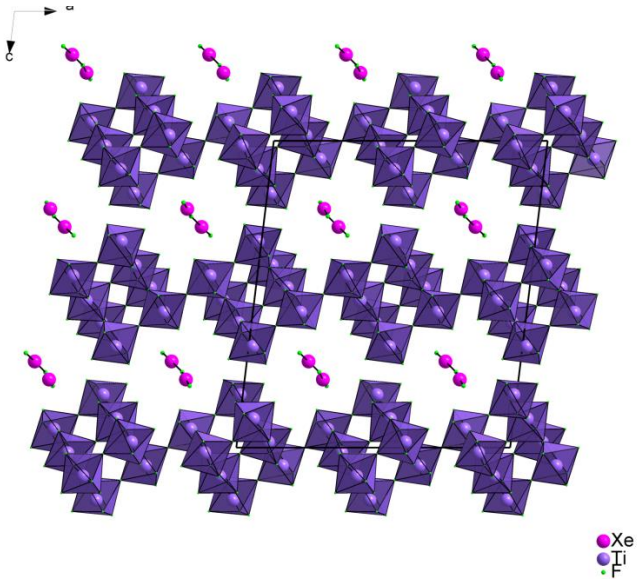


Figure 4.18: Unit cell edges and packing diagram of $[Xe_2F_3][Ti_8F_{33}]$; view along the *b*-axis.

Table 4.7: Xe1 and Xe2 coordination environment in the compound $[Xe_2F_3][Ti_8F_{33}]$.

Bonds and Contacts (Å)			
Xe1		Xe2	
Xe1–F3	**1.901 (4)**	**Xe2–F2**	**1.905 (4)**
Xe1–F1	**2.194 (4)**	**Xe2–F1**	**2.158 (4)**
Xe1–F31	3.047 (3)	Xe2–F6^{i}	3.213 (3)
Xe1–F5^{i}	3.147 (3)	Xe2–F27	3.302 (4)
Xe1–F2^{ii}	3.177 (4)	Xe2–F22^{vi}	3.323 (4)
Xe1–F15	3.272 (3)	Xe2–F14^{iii}	3.371 (3)
Xe1–F21	3.443 (4)	Xe2–F3^{vii}	3.528 (4)
Xe1–F16^{iii}	3.537 (4)	Xe2–F10^{viii}	3.534 (3)
Xe1–F36^{iv}	3.590 (4)	F2–Xe1^{vii}	3.177 (4)
Xe1–F32^{v}	3.601 (3)		
F3–Xe2^{ii}	3.528 (4)		

Symmetry codes: (i) $-x+1/2, y, -z$; (ii) $x, y+1, z$; (iii) $x-1/2, -y+1, z$; (iv) $-x+1, -y+1, -z+1$; (v) $-x+1/2, y, -z+1$; (vi) $x-1/2, -y, z$; (vii) $x, y-1, z$; (viii) $-x+1/2, y-1, -z$.

The $Xe_2F_3^+$ cation provides 12 long Xe···F contacts (from 3.047(3) to 3.601(3) Å) lying within the sum of the Xe and F van der Waals radii[247] (3.63 Å) to the anion layers and two more interactions (3.177(4) Å, 3.528(4) Å) with the neighboring cations (Table 4.7, Figure 4.19). The essentially linear angles of the $F_t - Xe\cdots F_b$ moieties (178.2(2) and 179.4(2)°) are comparable with the corresponding angles found in the previously reported structures of $Xe_2F_3^+$ salts.[122,**Error! Bookmark not defined.**] These values are in agreement with the AX_2E_3 valence-shell electron-

pair repulsion (VSEPR) arrangement,[66-69] which also supports the observed geometry of Xe···F longer contacts, thus avoiding xenon's three electron lone pairs in the equatorial positions.

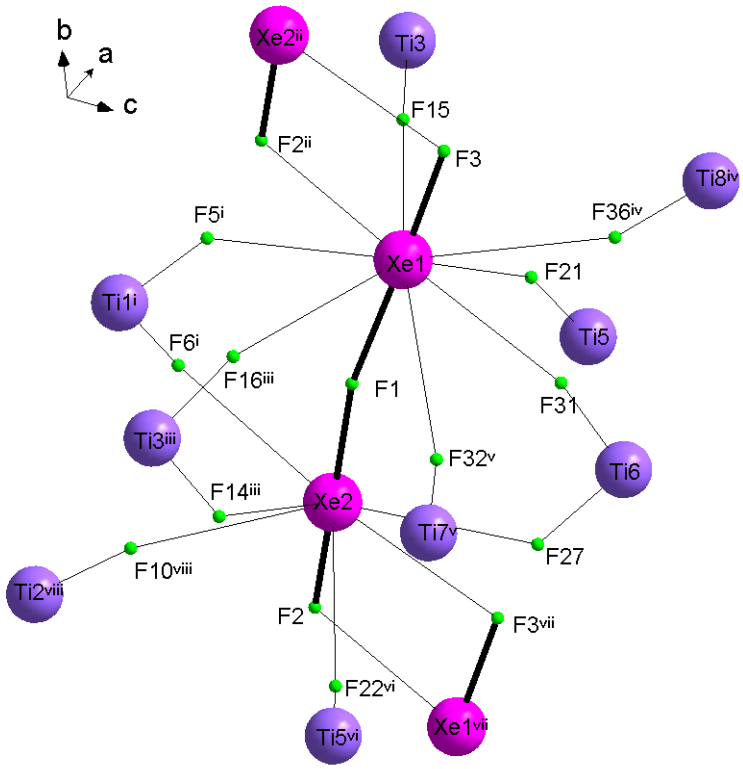


Figure 4.19: Xe1 and Xe2 coordination environment in $[Xe_2F_3][Ti_8F_{33}]$. The Xe2F3 moieties are graphically depicted with thick bonds, while thin lines are used for long contacts within the van der Waals sphere.

The Raman spectra were taken on several randomly oriented single crystals, of which the identity was additionally confirmed by the unit-cell measurement on the diffractometer. Another compound, namely $[XeF]_2[Ti_9F_{38}]$, described in the next subchapter, was regularly accompanying the product $[Xe_2F_3][Ti_8F_{33}]$ in varying yields depending on the reaction conditions (i.e. temperature gradient, reaction time, starting ratio of reactants) during most experimental runs. Thus, the phases had to be adequately separated, which was possible due to the evident difference in their morphologies. The powdered samples were prepared by grinding pure phases of both products, which was accomplished by isolating the crystalline material from the product mixture and physically separating more than 100 crystals of consistent crystal habit and distinct morphology of each phase. The selection procedure was carried out inside the glove box with the help of a surgical microscope, where the selected crystals were afterwards carefully grinded in a dry, mini agate mortar. The spectra obtained from the powdered samples corresponded completely with the spectra taken on single crystals.

The Raman spectrum of $[Xe_2F_3][Ti_8F_{33}]$ features a strong line at 594 cm^{-1}, which fits in the characteristic Xe–F_t stretch region (ca. 575–600 cm^{-1}) of the $Xe_2F_3^+$ cations.[120,121,122,]**Error! Bookmark not defined.** The observed strong band at 795 cm^{-1} can also be readily assigned to the symmetric in-phase Ti–F_t stretching mode of the $[Ti_8F_{33}]^-$ anion (usually found to vary between 700 and 800 cm^{-1} in polyfluoridotitanate(IV) salts).[155,156,161,163,164]

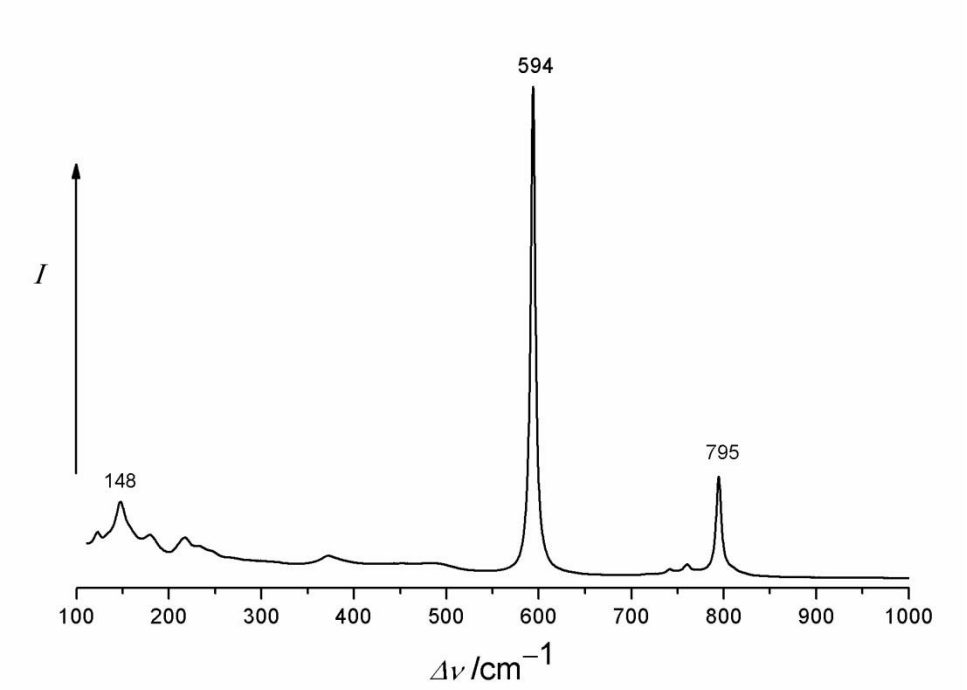


Figure 4.20: Raman spectrum of $[Xe_2F_3][Ti_8F_{33}]$ recorded at room temperature on a powdered sample.

4.1.4 $[XeF]_2[Ti_9F_{38}]$

The thermal reactions described in the previous section were not selective. Another compound, identified as $[XeF]_2[Ti_9F_{38}]$, was found accompanying the product $[Xe_2F_3][Ti_8F_{33}]$ in most experimental runs. The presence of a second product was firstly detected by Raman spectroscopy and usually becomes visually evident only later as another phase with distinct morphology that always succeeds the formation of rod-like $[Xe_2F_3][Ti_8F_{33}]$ crystals. An earlier appearance of $[XeF]_2[Ti_9F_{38}]$ was achieved by raising the starting TiF_4 : XeF_2 ratio in favor of TiF_4 or faster heating, otherwise it was observed only later during the syntheses.

Although the same procedure for the synthesis, crystallization and isolation as described for $[Xe_2F_3][Ti_8F_{33}]$ was applied, the best crystal quality in good yield (visually estimated) gave the reaction between TiF_4 (32 mg, 0.26 mmol) and XeF_2 (15 mg, 0.09 mmol) at 135 °C (12 h). Slow cooling to 110 °C (2 °C/h) afforded colorless prismatic crystals of $[XeF]_2[Ti_9F_{38}]$.

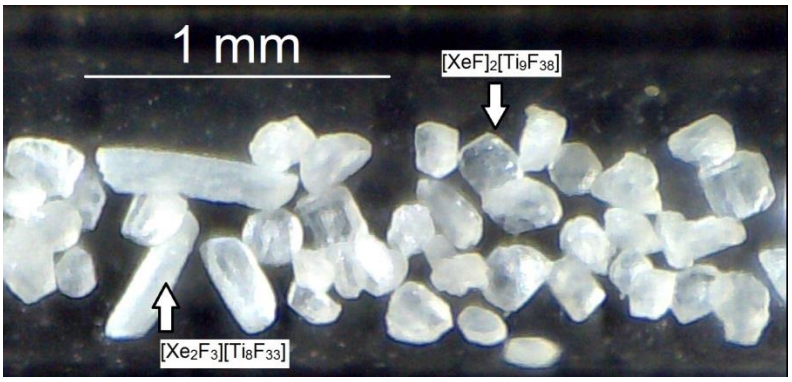


Figure 4.21: A magnified view on different crystal morphologies of $[Xe_2F_3][Ti_8F_{33}]$ and $[XeF]_2[Ti_9F_{38}]$ inside a sealed quartz capillary. The pale-white shade on some crystals is related to a partial decomposition on their surface.

The crystal structure $[XeF]_2[Ti_9F_{38}]$ was solved in the non-centrosymmetric polar *Cc* space group. However, an ambiguous value of the Flack parameter has shown a possible merohedral twinning and the final refinement of the racemic twin led to a 0.33(2) BASF parameter. The checkCIF procedure[255] warned about possible additional pseudo symmetry, thus the refinement of this structure was attempted in a centrosymmetric *C2/c* space group, but due to a strong (~ 0.1 against 0.035) *R*-value increase, the *Cc* space group was left as the correct choice.

The asymmetric unit of the compound $[XeF]_2[Ti_9F_{38}]$ is constructed from two Xe, nine Ti and forty F atoms. All 51 atoms reside on general positions (Wyckoff 4a) and together form a trigonal prismatic fluoridotitanate(IV) framework with two crystallographically independent XeF_2 ligands (Figure 4.22).

Table 4.8: Crystal structure determination and refinement details for compound $[XeF]_2[Ti_9F_{38}]$.

Crystal data	*Data collection*	*Refinement*
$Xe_2Ti_9F_{40}$	Rigaku AFC7 diffractometer	$R_1[F^2 > 2\sigma(F^2)] = 0.035$
$M_r = 1453.7$	Mercury CCD detector	$wR_2\ (F^2) = 0.086$
Crystal system: monoclinic	λ = 0.71069 Å (Mo K_α)	6713 reflections
Space group: *Cc*	12053 measured reflections	461 parameters
a = 17.5967 (8) Å	6713 independent reflections	GOF = 1.10

b = 15.3862 (6) Å	6346 observed reflections (I > 2 σ (I))	$\Delta\rho_{max}$ = 1.09 e/Å^3
c = 11.9529 (6) Å	R_{int} = 0.036	$\Delta\rho_{min}$ = −1.39 e/Å^3
β = 108.280 (2)°	θ_{max} = 29.2°, θ_{min} = 1.8°	
V = 3072.9 (2) Å^3	$-22 \leq h \leq 22$	
Z = 4	$-20 \leq k \leq 14$	
ρ_{calc} = 3.142 g/cm^3	$-15 \leq l \leq 15$	
1.8° ≤ θ ≤ 28.7°		
Cell parameters from 974 reflections		
μ = 4.62 mm^{-1}		
T = 150 K		
F(000) = 2664		
Size: 0.12×0.1×0.06 mm		
Appearance: Colorless prism		

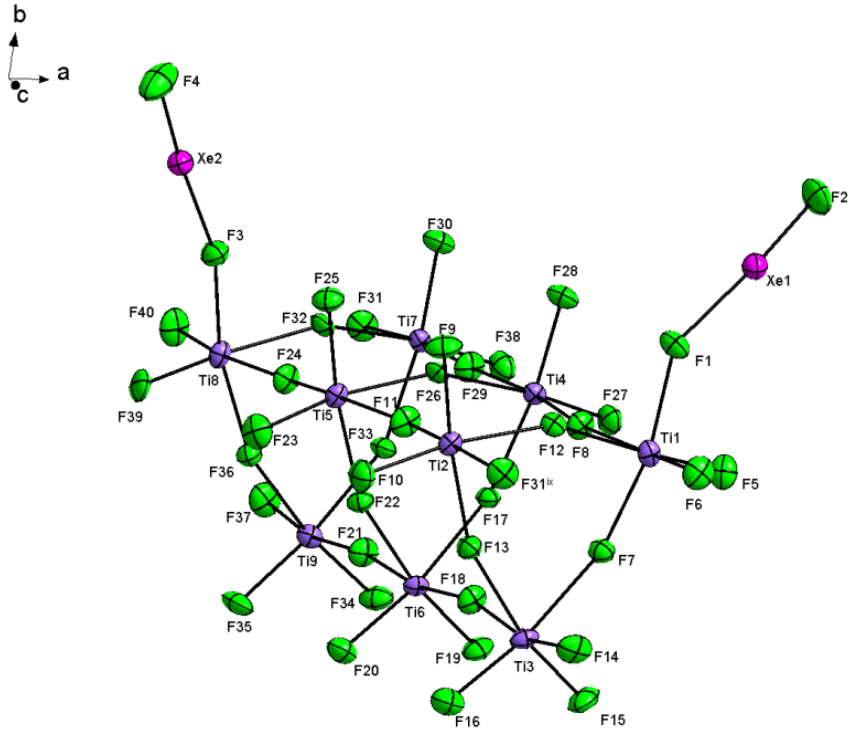
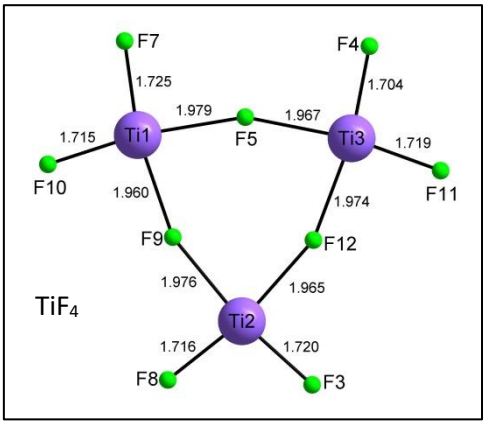
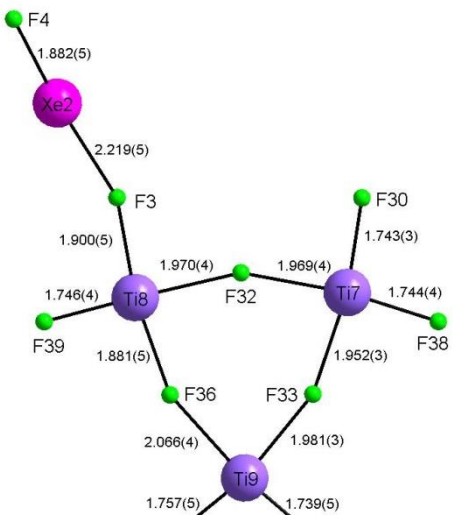


Figure 4.22: The asymmetric unit of the compound $[XeF]_2[Ti_9F_{38}]$ (ellipsoids are drawn at the 50% probability level).





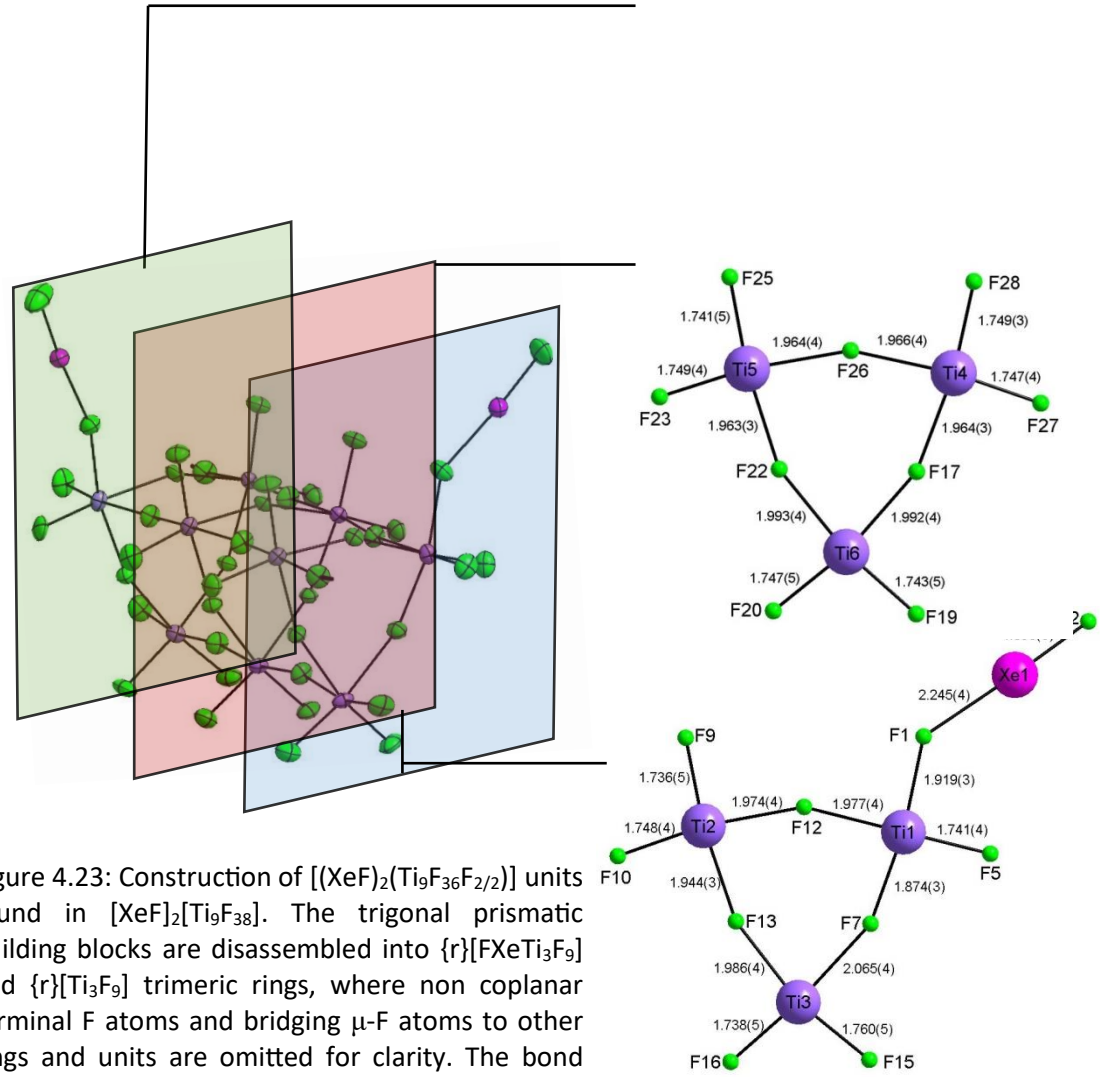


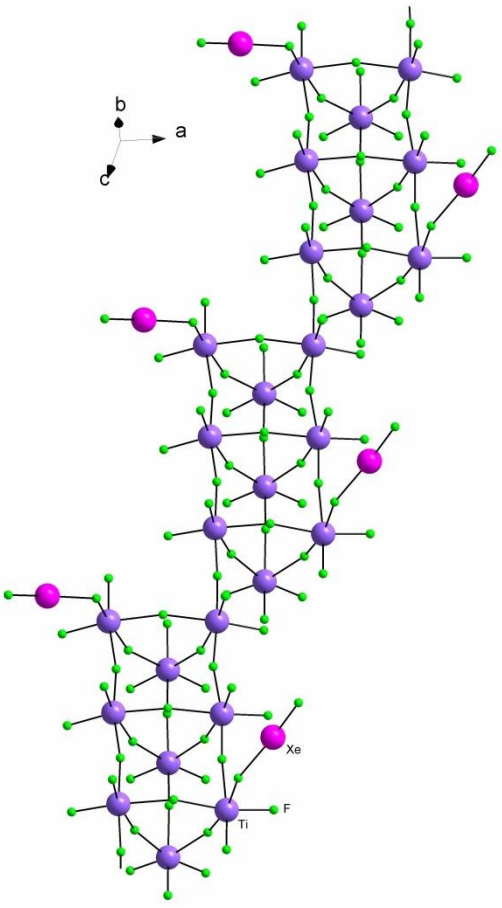
Figure 4.23: Construction of $[(XeF)_2(Ti_9F_{36}F_{2/2})]$ units found in $[XeF]_2[Ti_9F_{38}]$. The trigonal prismatic building blocks are disassembled into {r}$[FXeTi_3F_9]$ and {r}$[Ti_3F_9]$ trimeric rings, where non coplanar terminal F atoms and bridging μ-F atoms to other rings and units are omitted for clarity. The bond lengths are given in Å. The framed figure above depicts the corresponding crystallographically unique {r}$[Ti_3F_9]$ ring fragment in the TiF_4 columnar structure.

igure 4.22 also defines the main repeating]$_2$[Ti_9F_{38}]. Although a classical trigonal prism olygonal faces, the [$Ti_9F_{36}F_{2/2}$] results from association of nine crystallographically independent TiF_6 units into three crystallographically independent trimeric rings (Figure 4.23) joined through three common fluorine vertices, forming a double trigonal prismatic frame. A similar trimeric [$Ti_3F_9F_{6/2}$] ring (Figure 4.23) was found to comprise infinite columns in the crystal structure of TiF_4 and can provide an important anchor point for comparisons of the Ti–F bond length data.

As expected, the most symmetrical polygon assembling the [$Ti_9F_{36}F_{2/2}$] unit is the middle ring (confined by the atom set Ti4···Ti5···Ti6), as it remains almost unaffected by the XeF_2 molecules and neighboring prismatic units. While the Ti–Fb–Ti bridges of the unique trigonal ring in TiF_4 are highly symmetric (or at least within the experimental error range, which was not provided), a significant elongation of the lower apex belonging to the aforementioned middle ring is reflected in the *cis*-Ti6-F_b bond lengths (Ti6–F17: 1.992(4) Å; Ti6–F22: 1.993(4) Å, other Ti–F_b bonds lie within the 1.963(3)-1.966(4) Å range), which extend to compensate the deformations present in the outer rings. Another noteworthy difference can be observed when comparing the Ti–F_t lengths of both structures. The Ti–F_t values in [$Ti_9F_{36}F_{2/2}$] units (all bonds to terminal fluorine atoms considered) are ranging from 1.727(4) to 1.764(4) Å, which are substantially longer than those found in TiF_4 with distances spanning between 1.704 and 1.725 Å. However, the ring assemblies in both structures are forced to adopt a trigonal geometry, which requires the sum of internal angles to invariably equal to 180° or in case of an equilateral (regular) triangle all

internal angles have to be congruent to each other and each 60°. While this is observed and valid for Ti···Ti···Ti angles (~ 59.7-60.1°) of rings with almost equidistant Ti vertices (Ti···Ti distances ~ 3.87-3.88 Å), the F_b–Ti–F_b angles actually defining the ring corners assume values (range 80.5-80.7° and 79.6(2)-84.4(2)° in TiF_4 and $[XeF]_2[Ti_9F_{38}]$, respectively) between the geometrical constraint and the right angle required by the ideal octahedral (O_h) coordination of two *cis*-ligands around the Ti metal center. Thus, the ring edges cannot exist as straight symmetrical couples of bonds, but bent Ti–F_b–Ti connections with obtuse angles ranging from 155.2(2) to 160.6(2)° in $[XeF]_2[Ti_9F_{38}]$ (159.2-159.6° in TiF_4) and pointing outside the rings. The *cis* - F_t–Ti–F_t angles of terminal fluorine atoms lying in the ring plane are considerably more open (up to 100.4(2)°) than their corresponding coplanar *cis* - F_b–Ti–F_b angles, which is consistent with higher sterical requirements due to larger electron domains of short terminal bonds.[66,69]

Nevertheless, the trigonal geometry is not rare among the fluoridotitanate(IV) anions and it seems that associates involving an odd number (or a multiple of 3) of Ti atoms (TiF_4, $[Ti_6F_{27}]^{3-}$, $[Ti_9F_{38}]^{2-}$) prefer to adopt triangular polygons in their crystal structures, in contrast to anions with an even number of Ti atoms ($[Ti_2F_9]^-$, $[Ti_4F_{20}]^{4-}$, $[Ti_8F_{33}]^-$, $[Ti_8F_{36}]^{4-}$), which are more likely to preserve the octahedral geometry demands by association into rectangular/square (or corresponding cuboid/cubic) motifs. Anyway, some exceptions to this assumption demonstrate that the energy difference between the two types of assemblage is indeed very small and recently isolated compounds ($[Ti_5F_{23}]^{3-}$, $[Ti_{10}F_{45}]^{5-}$) possessing a combination of pseudo-octahedra with different degrees of distortion additionally confirm the facile adaptation of the Ti^{4+}- coordination sphere to other factors affecting the structure (e.g. cation nature, presence of solvates, hydrogen bonding, etc.). More evidence comes from the vertex configuration of the $[Ti_9F_{38}]^{2-}$ itself, where the combination of triangles and rectangles defined by Ti atoms can be described with Schläffli notations 3.4^2 (six Ti atoms belonging to the outer rings) and 4^4 (three Ti atoms of the middle ring).



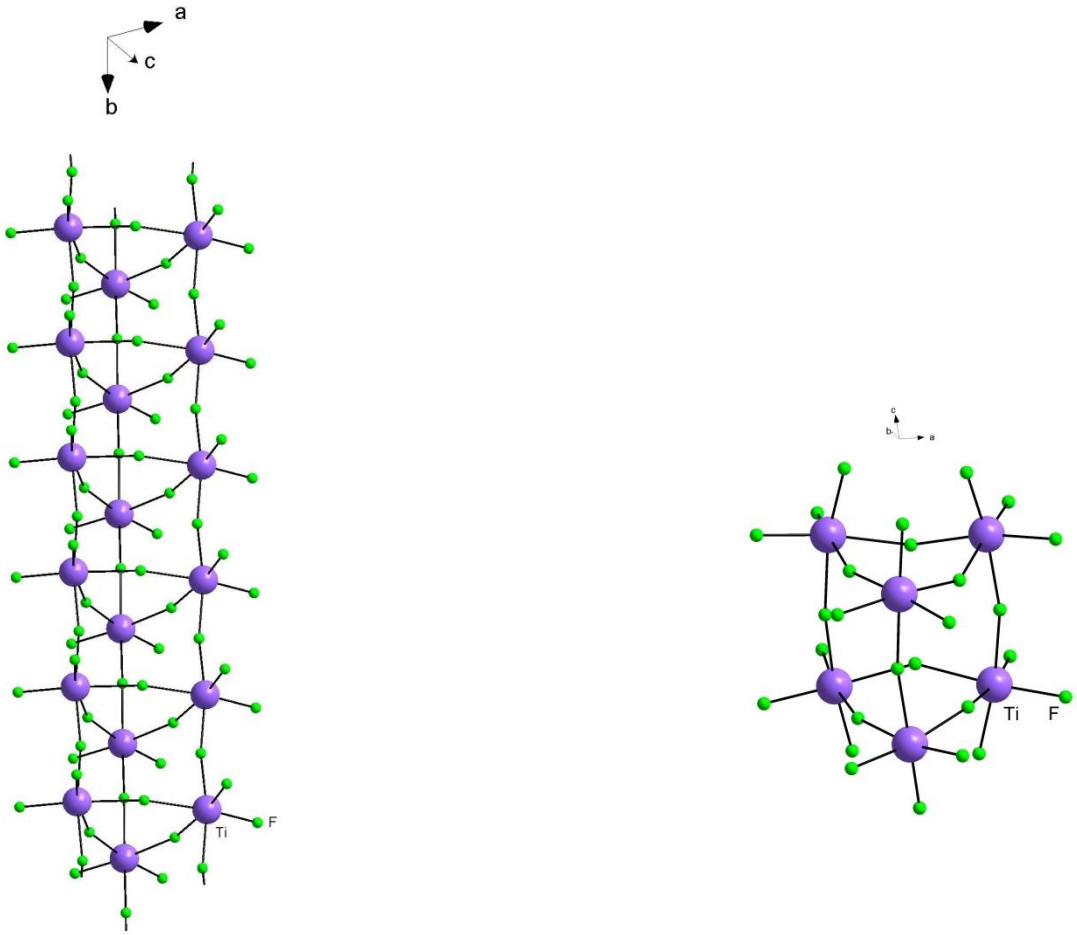


Figure 4.24: Columns found in crystal structures of TiF_4 (*left*)[136] and $[XeF]_2[Ti_9F_{38}]$ (*middle*).[249] On the *right*, the trigonal prismatic anion $[Ti_6F_{27}]^{3-}$ determined in $[GuH]_3[Ti_6F_{27}] \cdot SO_2$.[155]

The three rectangular faces present in the prismatic building blocks $[Ti_9F_{36}F_{2/2}]$ are outlined by six Ti–F_b–Ti bridges with Ti–F_b bond lengths ranging from 1.857(4) Å to 2.067(3) Å and nearly straight Ti–F_b–Ti angles (166.4(3)-173.3(2) Å). The most symmetrical are the F_b–Ti–F_b bridges belonging to the middle ring, which are not exposed to the trans-influence of the terminal fluorine atoms of the outer rings, and the μ-F31 bridges between the outer rings and neighboring $[Ti_9F_{36}F_{2/2}]$ units (Ti2–F31: 1.933(5) Å; F31–Ti7: 1.923(5) Å). This single, almost linear (Ti2–F31–Ti7 angle: 171.8(2)°) fluorine bridge emerges from the closest apex to the XeF_2 carrying TiF_6 octahedron (both octahedra form the short edge of the rectangular face parallel to the *ac*-plane) and links the prismatic units into columns in an infinite array along the *c* crystallographic axis.

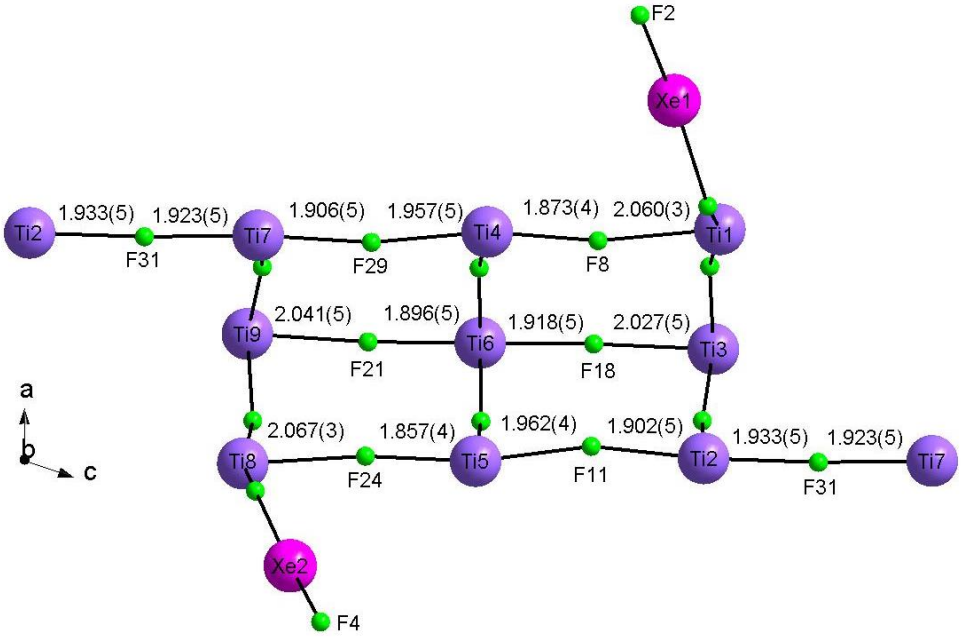


Figure 4.25: The trimeric $[Ti_3F_9F_{6/2}]$-rings in $[XeF]_2[Ti_9F_{38}]$ are connected through μ-F bridges into a prismatic skeleton, which is further linked to neighboring $[Ti_9F_{36}F_{2/2}]$ units by single-vertex sharing. Some transversally bridging and terminal fluorine atoms have been removed for clarity.

The two crystallographically independent XeF_2 molecules provide two fluorine atoms (F1 and F3) to complete the octahedral coordination around Ti1 and Ti8 metal centers, which lie on the face (parallel to the *ac*-plane) diagonal of each prismatic $[Ti_9F_{36}F_{2/2}]$ unit. The F_bXeF_t moieties deform the ring structures mainly due to the *trans*-influence exercised by Ti–Fb(Xe) on Ti–Fb(Ti) bonds, thus causing a contraction of Ti1–F7 and Ti8–F36 distances down to 1.874(3) Å and 1.881(5) Å, respectively. Consequently, this leads further to the aforedescribed elongation of all lower prismatic apexes, where the middle ring is also affected as the octahedral arrangement is likely forced to follow the given pattern in order to maintain the prism-shaped framework.

Although the "classic" stoichiometric formulation of the title product would be $XeF_2{\cdot}4TiF_4$, it can be confidently written as $[XeF]_2[Ti_9F_{38}]$. In fact, a closer look at some geometrical parameters of $Ti–F_b–Xe–F_t$ fragments reveals the presence of XeF_2 in an asymmetric, ionized form F-Xe—F, where the degree of deviation from the original $D_{\infty h}$ symmetry (with two equidistant Xe–F bonds measuring 1.999(4) Å at 100 K)[74] is seen as an elongation of $Xe–F_b$ and shortening of $Xe–F_t$ bonds. In $[XeF]_2[Ti_9F_{38}]$, the $Xe–F_t$ (Xe1–F2: 1.890(6) Å; Xe2–F4: 1.882(5) Å) and $Xe–F_b$ (Xe1–F1: 2.245(4) Å; Xe2–F3: 2.219(5) Å) bond lengths are comparable with the XeF^+ salts of the strongest Lewis acids (Table 4.9). Similarly, the almost linear F–Xe–F bond angles (μ-Xe1: 176.2(2)°; μ-Xe2: 175.5(2)°) are also in excellent agreement with the corresponding angles observed in the crystal structures of XeF^+ compounds reported thus far,[74,114] and that determined for the bonded FXeF moiety in $(XeF_2{\cdot}TiF_4)_2{\cdot}XeF_2$ (178.94(15)°).

The efficiency of the fluorine ion transfer can be deduced from the $M–F_b$(Xe) bond lengths. Although these bonds are longer than other non-bridging $Ti–F_t$ bonds present, the difference (Ti1–F1: 1.919(3) Å and Ti8–F3: 1.900(5) Å *vs*. $Ti–F_t$ average length: 1.745 Å), is considerably smaller than in $(XeF_2{\cdot}TiF_4)_2{\cdot}XeF_2$ ($Ti–F_b$(Xe): 2.034(4) Å *vs*. $Ti–F_t$ average length: 1.763 Å), where a lower cation-anion interaction is also expected from the parent fluorine acceptor with higher Lewis acidity. Nevertheless, this coordination is still evidently strong, which is also the main reason why these compounds are rather addressed as tight ion-pairs.

Table 4.9: An overview of reported Xe−F_t (F_t, terminal fluorine) and Xe−F_b (F_b, bridging fluorine) bond lengths and Xe−F_t vibrational assignments among selected XeF^+ compounds and $[XeF]_2[Ti_9F_{38}]$.

Compound	Xe−F_t [Å]	Xe−F_b [Å]	T [K][a]	$\Delta\nu$ [cm^{-1}][b]	T [K][c]	Ref.
$[XeF][AsF_6]$	1.888(3)	2.208(3)	100	607 (96) 611 (100)	110	74
$[XeF][SbF_6]$	1.885(2)	2.278(2)	100	616 (100) 621 (66)	110	74
$[XeF][Sb_2F_{11}]$	1.888(4)	2.343(4)	100	621 (100)	RT	74, 112
$[XeF][IrF_6]$	1.854(4) 1.854(5) 1.867(5)	2.220(4) 2.245(5) 2.272(4)	133	602 (60) 608 (44)	RT	112, 114
$[XeF][Ir_2F_{11}]$[d]	/	/	/	601 (68)[e] 612 (100)	RT	112
$[XeF][BiF_6]$	1.913(7)	2.204(7)	100	602 (48) 608 (11)	110	74
$[XeF][Bi_2F_{11}]$	1.909(6)	2.253(5)	100	605 (49) 609 (74)	77	42, 74
$[XeF]_2[Ti_9F_{38}]$	1.890(5) 1.882(4)	2.245(4) 2.219(4)	150	612 (100)	RT	249
$[XeF][V_4O_4F_{13}]$	1.905(4)	2.159(3)	200	598 (100)	RT	34

[a] X-ray data collection temperature. [b] Values in parentheses denote relative intensities. [c] Raman spectra acquisition temperature. [d] No crystallographic data available. [e] The band might not be found in the pure phase; the authors remarked a possibility of attributing the peak to the $[XeF][IrF_6]$ impurity.[112]

Besides M–F_b(Xe) bonds, the Xe−F_b lengths have also been reported[74] to be susceptible to the fluoride ion acceptor strengths (even more than Xe−F_t) of the Lewis acids used. Figure 4.26 shows the correlation between the increase in measured Xe−F_b bond lengths determined in XeF^+ salts and calculated fluoride ion activities (abbreviated: FIAs, Table 1.1, the most recently reported values have been considered) of the parent MF_5 and M_2F_{10} (M = Sb, Bi) Lewis acids. The higher FIAs of these species were attributed to a greater dispersal of the negative charge among the fluorine atoms of the corresponding $[M_2F_{11}]^-$ anions. It should be noted that the polymeric nature of the parent Lewis acids delivering the type of compounds discussed within this work additionally intensifies the *trans*-influence on the M–F_b(Xe) bonds by holding the bridging fluorine atom more tightly to the mother skeleton, away from the Xe–F_t fragment, thus raising their ability to maintain the final products in ionized forms.

Although a linear trend line ((FIA) = 391.59·d(Xe−F_b) - 389.03, with a coefficient of determination R^2 = 0.794) was supposed due to the lack of experimental results, it might provide a very rough estimation of this dependence for other related compounds of this type. Thus, a simple linear extension down to the Xe−F_b length (2.133(3) Å) of $(XeF_2{\cdot}TiF_4)_2{\cdot}XeF_2$, gave an approximate FIA value for TiF_4 of 446.2 kJ mol^{-1}. Similarly, taking into account the average Xe−F_b bond length (2.232(4) Å) in $[XeF]_2[Ti_9F_{38}]$, the FIA was linearly extrapolated for an imaginary intermediate $[XeF][Ti_9F_{37}]$. Since the final product characterized possesses two XeF-moieties on a prismatic assembly of nine TiF_6 octahedra, another fluorine ion has to be abstracted from a second XeF_2 molecule. Assuming the same increase rate, the combined, total strength of the parent Lewis acid Ti_9F_{36} should be twice the FIA value of the intermediate, which amounts to 970 kJ mol^{-1}. Although this prediction is extremely inaccurate, there is no doubt that the actual fluoride ion accepting ability of Ti_9F_{36} must be immense, reaching and possibly exceeding the acidity value that was calculated[256] for a combination of four monomeric (non-fluorine-bridged)

SbF_5 molecules in the gas-phase (855 kJ mol^{-1}). If the consistency of such bold suppositions is experimentally confirmed in the forthcoming studies, many new possibilities might open especially if a synthetic method that preserves the integrity of the polymeric anion with at least partial solvation in polar anhydrous solvents will be developed. In this sense, a potential compound $[H_2F]_2[Ti_9F_{38}]$ (as well as $[H_2F]Ti_8F_{33}$) derived from an aHF solution containing the aforementioned anion would confidently rank among the strongest known superacids, while several applications which see $[Ti_9F_{38}]^{2-}$ as a weakly coordinating anion (WCA) or structure directing building block can arise.

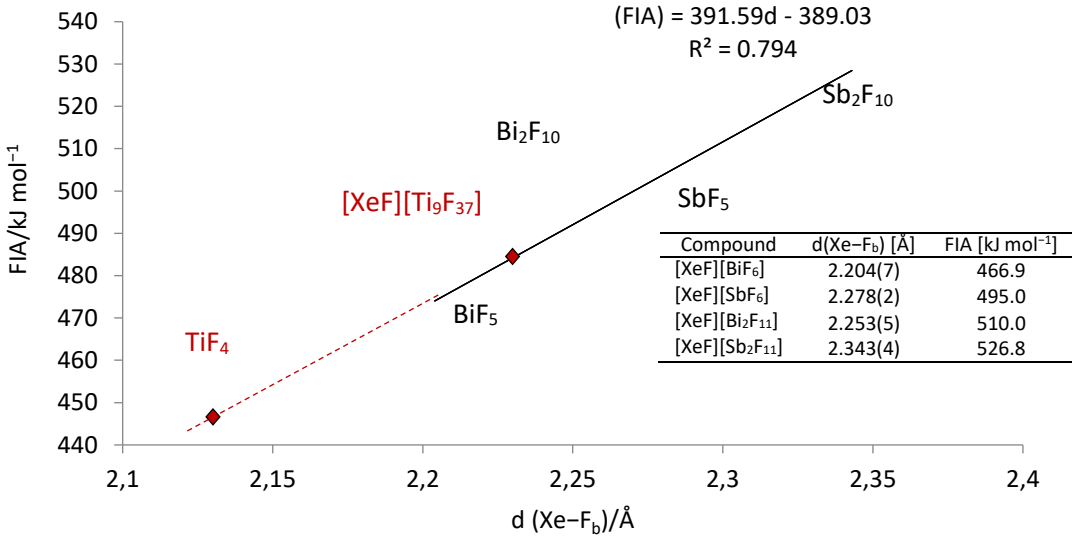


Figure 4.26: Correlation between measured Xe–F_b (F_b-bridging fluorine) bond lengths of some XeF^+ compounds[74] and calculated FIA (fluoride ion activity) values of their parent MF_5 and M_2F_{10} Lewis acids (see references in Table 1.1). The missing FIAs of fluoride ion acceptors relevant to this work are estimated by extrapolation assuming a linear relationship (source data for linear regression supplied in table within the diagram).

determined in various $[NgF][MF_6]$ (Ng = Xe, M = As: 133.6(2)°; Sb: 136.9(1)°; Ir: 119.3-141.9°; Ru: 137.2(5)°. Ng = Kr, M = As: 133.7(3)°; Sb: 139.2(2)°; Bi: 138.3(3)°; Au: 125.3(7)°) compounds[74,114] and comparable to that in $(XeF_2{\cdot}TiF_4)_2{\cdot}XeF_2$ (133.1(2)°), while the Ti8–F3–Xe2 angle (156.9(2)°) basically equals to the one determined in $[XeF][BiF_6]$ (156.1(4)°). The larger angle in the latter case has been attributed to the crystal packing resulting in a unique near-eclipsed Xe–F_b–Bi–F*(F* = next nearest fluorine atom) arrangement, however, no such correlation is observed in case of $[XeF]_2[Ti_9F_{38}]$ (torsion angle Xe1–F1–Ti1–F5: 7.1°; torsion angle Xe2–F3–Ti8–F39: 17.0°), as it would require a larger Ti1–F1–Xe1 angle relative to that of Ti8–F3–Xe2. More bond lengths and bond angles determined in $[XeF]_2[Ti_9F_{38}]$ are summarized in Table 4.10.

Table 4.10: Selected geometric parameters for the compound $[XeF]_2[Ti_9F_{38}]$.

Bond Lengths (Å)			
Xe1—F2	1.890(5)	Ti5—F24	1.857(4)
Xe1—F1	2.245(4)	Ti5—F11	1.962(4)
Xe2—F4	1.882(4)	Ti5—F26	1.964(4)
Xe2—F3	2.219(4)	Ti5—F22	1.964(4)

Ti1—F6	1.727(4)	Ti6—F19	1.743(4)
Ti1—F5	1.741(4)	Ti6—F20	1.746(5)
Ti1—F7	1.873(4)	Ti6—F21	1.895(4)
Ti1—F1	1.919(4)	Ti6—F18	1.918(4)
Ti1—F12	1.977(4)	Ti6—F22	1.992(4)
Ti1—F8	2.060(4)	Ti6—F17	1.993(4)
Ti2—F9	1.736(4)	Ti7—F30	1.743(4)
Ti2—F10	1.748(4)	Ti7—F38	1.744(4)
Ti2—F11	1.902(4)	Ti7—F29	1.906(4)
Ti2—F31^{ix}	1.933(5)	Ti7—F31	1.923(5)
Ti2—F13	1.943(4)	Ti7—F33	1.951(4)
Ti2—F12	1.973(4)	Ti7—F32	1.968(4)
Ti3—F16	1.737(5)	Ti8—F40	1.730(4)
Ti3—F15	1.761(5)	Ti8—F39	1.746(4)
Ti3—F14	1.764(4)	Ti8—F36	1.880(4)
Ti3—F13	1.986(4)	Ti8—F3	1.900(4)
Ti3—F18	2.027(4)	Ti8—F32	1.970(4)
Ti3—F7	2.066(4)	Ti8—F24	2.067(4)
Ti4—F27	1.746(4)	Ti9—F34	1.739(4)
Ti4—F28	1.750(4)	Ti9—F37	1.747(4)
Ti4—F8	1.874(4)	Ti9—F35	1.757(4)
Ti4—F29	1.957(4)	Ti9—F33	1.981(4)
Ti4—F17	1.964(4)	Ti9—F21	2.041(4)
Ti4—F26	1.966(4)	Ti9—F36	2.067(4)
Ti5—F25	1.741(4)	F31—Ti2^{xiv}	1.933(5)
Ti5—F23	1.749(4)		

Bond Angles (°)			
F2—Xe1—F1	176.2(2)	F14—Ti3—F18	166.4(2)
F4—Xe2—F3	175.5(2)	F13—Ti3—F18	80.9(2)
F6—Ti1—F5	99.0(2)	F16—Ti3—F7	170.4(2)

F6—Ti1—F7	96.5(2)	F15—Ti3—F7	86.4(2)
F5—Ti1—F7	95.8(2)	F14—Ti3—F7	87.5(2)
F6—Ti1—F1	94.7(2)	F13—Ti3—F7	79.6(2)
F5—Ti1—F1	90.4(2)	F18—Ti3—F7	81.8(2)
F7—Ti1—F1	166.3(2)	F27—Ti4—F28	97.0(2)
F6—Ti1—F12	92.3(2)	F27—Ti4—F8	98.4(2)
F5—Ti1—F12	168.6(2)	F28—Ti4—F8	92.7(2)
F7—Ti1—F12	84.4(2)	F27—Ti4—F29	89.9(2)
F1—Ti1—F12	87.2(2)	F28—Ti4—F29	92.1(2)
F6—Ti1—F8	173.4(2)	F8—Ti4—F29	169.8(2)
F5—Ti1—F8	87.5(2)	F27—Ti4—F17	90.9(2)
F7—Ti1—F8	83.8(2)	F28—Ti4—F17	171.7(2)
F1—Ti1—F8	84.2(2)	F8—Ti4—F17	88.7(2)
F12—Ti1—F8	81.2(2)	F29—Ti4—F17	85.3(2)
F9—Ti2—F10	98.1(2)	F27—Ti4—F26	168.5(2)
F9—Ti2—F11	92.0(2)	F28—Ti4—F26	90.1(2)
F10—Ti2—F11	92.1(2)	F8—Ti4—F26	90.2(2)
F9—Ti2—F31^{ix}	92.6(2)	F29—Ti4—F26	80.8(2)
F10—Ti2—F31^{ix}	90.6(2)	F17—Ti4—F26	81.7(2)
F11—Ti2—F31^{ix}	174.3(2)	F25—Ti5—F23	96.5(2)
F9—Ti2—F13	172.4(2)	F25—Ti5—F24	94.7(2)
F10—Ti2—F13	89.4(2)	F23—Ti5—F24	98.2(2)
F11—Ti2—F13	86.1(2)	F25—Ti5—F11	91.8(2)
F31^{ix}—Ti2—F13	88.9(2)	F23—Ti5—F11	89.6(2)
F9—Ti2—F12	90.9(2)	F24—Ti5—F11	169.2(2)
F10—Ti2—F12	171.0(2)	F25—Ti5—F26	90.8(2)
F11—Ti2—F12	88.6(2)	F23—Ti5—F26	168.5(2)
F31^{i}—Ti2—F12	87.9(2)	F24—Ti5—F26	90.0(2)
F13—Ti2—F12	81.7(2)	F11—Ti5—F26	81.2(2)
F16—Ti3—F15	99.6(2)	F25—Ti5—F22	172.4(2)

F16—Ti3—F14	99.1(2)	F23—Ti5—F22	90.1(2)
F15—Ti3—F14	97.8(2)	F24—Ti5—F22	88.1(2)
F16—Ti3—F13	93.5(2)	F11—Ti5—F22	84.5(2)
F15—Ti3—F13	164.2(2)	F26—Ti5—F22	82.18(14)
F14—Ti3—F13	88.8(2)	F19—Ti6—F20	99.6(2)
F15—Ti3—F18	90.0(2)	F16—Ti3—F18	90.6(2)
F20—Ti6—F21	92.1(2)	F40—Ti8—F24	172.7(2)
F19—Ti6—F18	92.1(2)	F39—Ti8—F24	86.5(2)
F20—Ti6—F18	94.8(2)	F36—Ti8—F24	84.5(2)
F21—Ti6—F18	169.42(15)	F3—Ti8—F24	83.4(2)
F19—Ti6—F22	170.4(2)	F32—Ti8—F24	81.2(2)
F20—Ti6—F22	89.7(2)	F34—Ti9—F37	99.0(2)
F21—Ti6—F22	86.9(2)	F34—Ti9—F35	100.4(2)
F18—Ti6—F22	85.1(2)	F37—Ti9—F35	98.1(2)
F19—Ti6—F17	90.2(2)	F34—Ti9—F33	91.8(2)
F20—Ti6—F17	170.0(2)	F37—Ti9—F33	89.1(2)
F21—Ti6—F17	85.3(2)	F35—Ti9—F33	164.7(2)
F18—Ti6—F17	86.5(2)	F34—Ti9—F21	90.3(2)
F22—Ti6—F17	80.52(12)	F37—Ti9—F21	166.5(2)
F30—Ti7—F38	99.3(2)	F35—Ti9—F21	89.7(2)
F30—Ti7—F29	92.6(2)	F33—Ti9—F21	80.8(2)
F38—Ti7—F29	92.1(2)	F34—Ti9—F36	168.8(2)
F30—Ti7—F31	93.9(2)	F37—Ti9—F36	88.2(2)
F38—Ti7—F31	90.3(2)	F35—Ti9—F36	87.0(2)
F29—Ti7—F31	172.6(2)	F33—Ti9—F36	79.7(2)
F30—Ti7—F33	170.0(2)	F21—Ti9—F36	81.2(2)
F38—Ti7—F33	90.7(2)	Ti1—F1—Xe1	136.8(2)
F29—Ti7—F33	86.3(2)	Ti8—F3—Xe2	156.9(2)
F31—Ti7—F33	86.7(2)	Ti1—F7—Ti3	156.3(2)
F30—Ti7—F32	87.9(2)	Ti4—F8—Ti1	169.7(2)

F38—Ti7—F32	172.6(2)	Ti2—F11—Ti5	166.4(3)
F29—Ti7—F32	89.0(2)	Ti2—F12—Ti1	155.2(2)
F31—Ti7—F32	87.7(2)	Ti2—F13—Ti3	160.6(2)
F33—Ti7—F32	82.1(2)	Ti4—F17—Ti6	158.5(2)
F40—Ti8—F39	100.5(2)	Ti6—F18—Ti3	167.6(2)
F40—Ti8—F36	96.8(2)	Ti6—F21—Ti9	169.5(3)
F39—Ti8—F36	95.2(2)	Ti5—F22—Ti6	158.3(2)
F40—Ti8—F3	94.2(2)	Ti5—F24—Ti8	173.3(2)
F39—Ti8—F3	91.6(2)	Ti5—F26—Ti4	157.7(2)
F36—Ti8—F3	165.7(2)	Ti7—F29—Ti4	171.3(3)
F40—Ti8—F32	91.8(2)	Ti7—F31—Ti2^{xiv}	171.8(2)
F39—Ti8—F32	167.8(2)	Ti7—F32—Ti8	155.7(2)
F36—Ti8—F32	83.6(2)	Ti7—F33—Ti9	158.7(2)
F3—Ti8—F32	87.1(2)	Ti8—F36—Ti9	156.3(2)
F19—Ti6—F21	94.7(2)		

Symmetry codes: (ix) *x*, *y*, *z*+1; (xiv) *x*, *y*, *z*−1.

The extended structure of $[XeF]_2[Ti_9F_{38}]$ resembles the solid-state structure of TiF_4 itself.[136] However, unlike TiF_4, where the trimeric rings form uniform continued columns, each vertex-sharing prismatic assembly of three rings in $[XeF]_2[Ti_9F_{38}]$ is interrupted by single fluorine bridges emerging from the prism corners lying on the face parallel to the *ac*-plane, so that the neighboring $[Ti_9F_{36}F_{2/2}]$ units are shifted by one proper width (Ti···Ti distance ~ 3.85 Å) along the crystallographic *a*-axis. The nearest columns along the *a*- and *b*-axis alternate in these directions their reflected and translated positions, which are symmetrically generated by two *c*-glide planes perpendicular to [0, 1, 0] (b-axis) with glide components [0, 0, 0.5] and [0.5, 0, 0.5]. In this way, both FXeF moieties of each chiral $[Ti_9F_{36}F_{2/2}]$ assembly point towards the voids left by the indentations at each side of the column. Such arrangement also maximizes the secondary intermolecular contacts as described in more detail hereinafter.

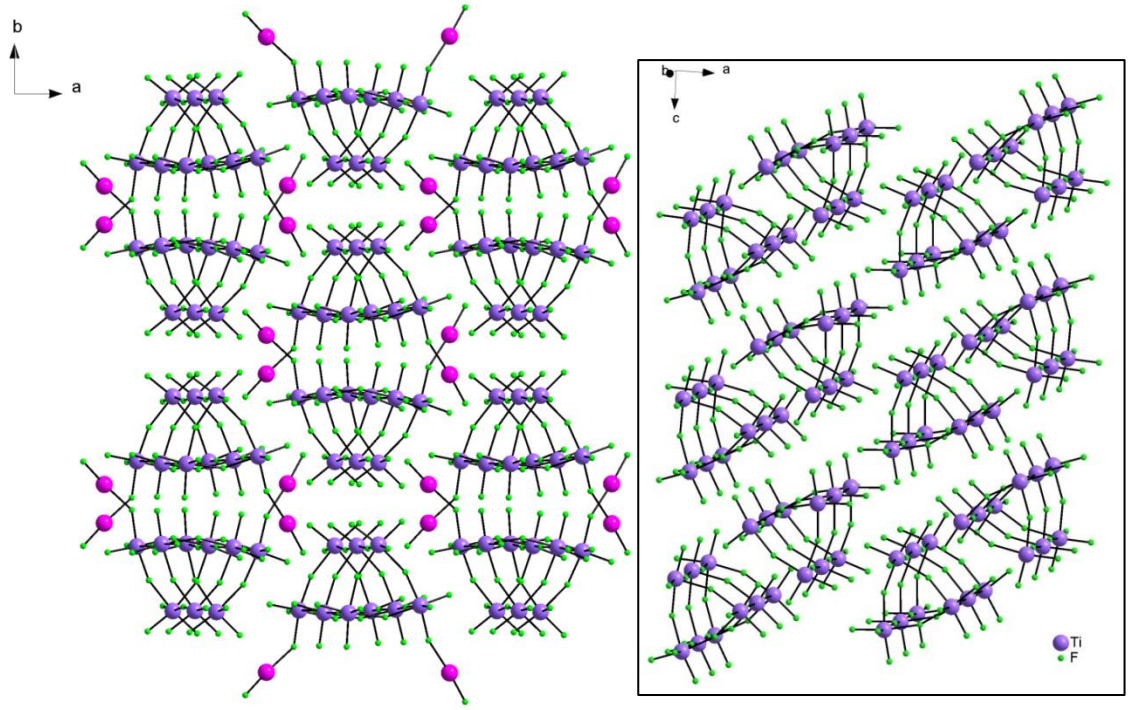


Figure 4.27: Columnar structures of $[XeF]_2[Ti_9F_{38}]$ (*left*) and TiF_4 (*right*).[136]

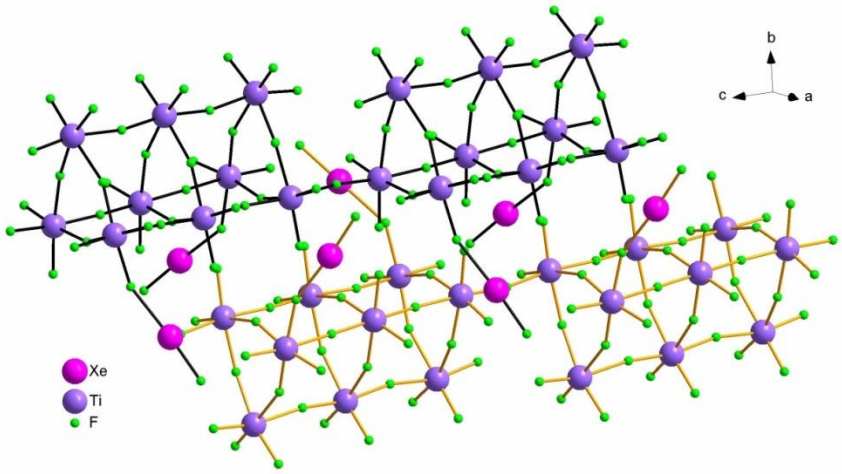


Figure 4.28: Columns in $[XeF]_2[Ti_9F_{38}]$ are comprised of chiral prismatic $[Ti_9F_{36}F_{2/2}]$-units multiplied and stacked by axial glide planes perpendicular to the *b*-axis.

The higher thermal stability of this product might be attributed to some degree to the relative abundance, distribution and orientation of additional interactions between the $[(Ti_9F_{38})^{2-}]$ columns and the secondary coordination spheres of two crystallographically independent Xe atoms, where a number of Xe···F contacts with distances ranging from 3.024(4) to 3.628(5) Å were identified (Table 4.11).

Table 4.11: Xe1 and Xe2 coordination environment in the compound $[XeF]_2[Ti_9F_{38}]$.

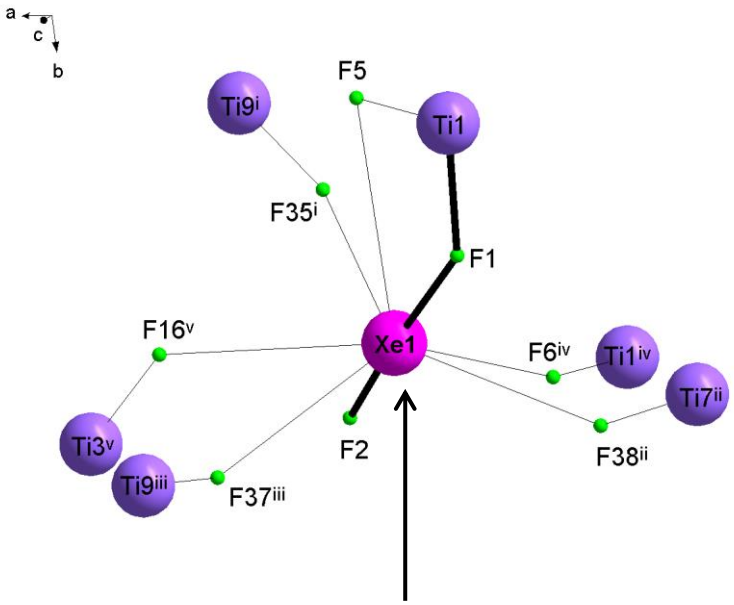
Bonds and Contacts (Å)

Xe1		Xe2	
Xe1—F2	**1.890(5)**	**Xe2—F4**	**1.882(4)**
Xe1—F1	**2.245(4)**	**Xe2—F3**	**2.219(4)**
Xe1···F35^{i}	3.024(4)	Xe2···F14^{vi}	3.029(4)
Xe1···F38^{ii}	3.039(4)	Xe2···F10^{iv}	3.070(4)
Xe1···F37^{iii}	3.174(4)	Xe2···F15^{vii}	3.071(4)
Xe1···F6^{iv}	3.330(4)	Xe2···F34^{viii}	3.319(5)
Xe1···F5	3.578(4)	Xe2···F40^{ii}	3.462(4)
Xe1···F16^{v}	3.628(5)	Xe2···F19^{vii}	3.549(4)

Symmetry codes: (i) *x*+1/2, −*y*+3/2, *z*+1/2; (ii) *x*, −*y*+2, *z*+1/2; (iii) *x*+1/2, *y*+1/2, *z*+1; (iv) *x*, −*y*+2, *z*−1/2; (v) *x*+1/2, *y*+1/2, *z*; (vi) *x*−1/2, *y*+1/2, *z*−1; (vii) *x*−1/2, −*y*+3/2, *z*−1/2; (viii) *x*−1/2, *y*+1/2, *z*; (ix) *x*, *y*, *z*+1; (x) *x*+1/2, *y*−1/2, *z*+1; (xi) *x*−1/2, *y*−1/2, *z*−1; (xii) *x*+1/2, *y*−1/2, *z*; (xiii) *x*−1/2, *y*−1/2, *z*; (xiv) *x*, *y*, *z*−1.

The Xe1 atom exhibits 5 long Xe···F interactions (Figure 4.29) between the "mother" column (intramolecular) and 3 adjacent columns (intermolecular contacts). Similarly, the Xe2 secondary coordination sphere consists of 6 Xe···F long contacts (Figure 4.30) with 3 neighboring columns (2 interactions per each column).

Unlike $(XeF_2{\cdot}TiF_4)_2{\cdot}XeF_2$, terminal fluorine atoms of the XeF^+ cations in $[XeF]_2[Ti_9F_{38}]$ do not have any residual charge left to share in the secondary sphere coordination, which is consistent with a higher degree of ionization observed for the F_b—Xe-F_t moiety in this product.



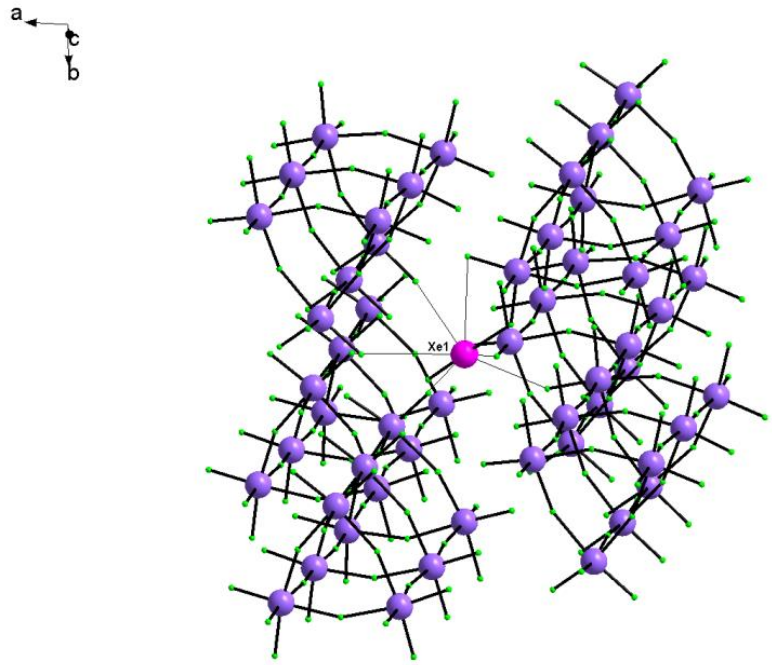
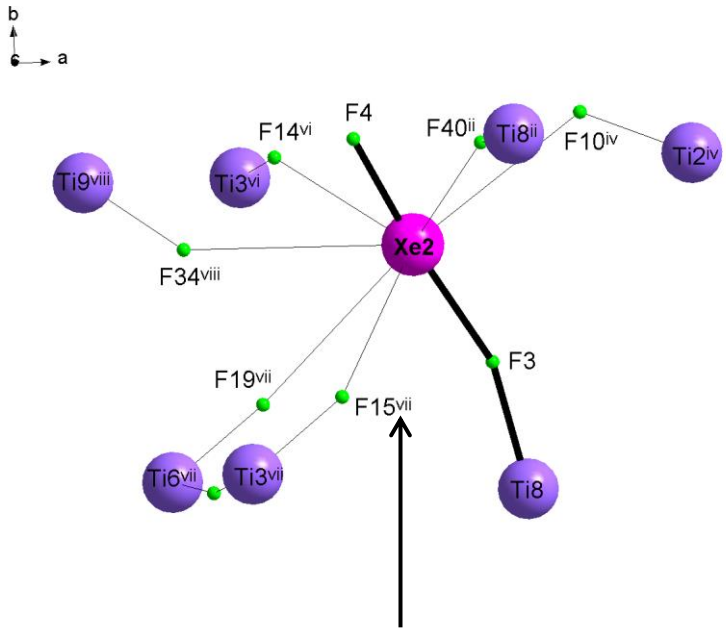


Figure 4.29: Xe1 coordination environment with long intra- and intermolecular contacts (*thin* bonds) in $[XeF]_2[Ti_9F_{38}]$.



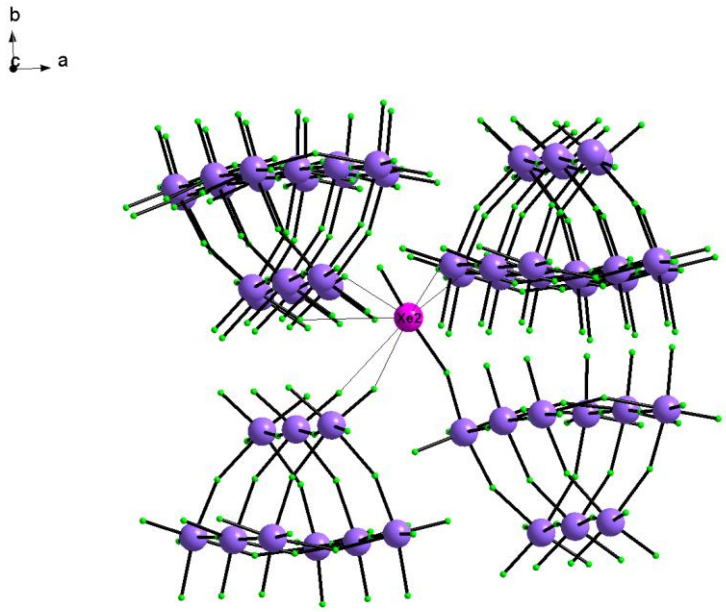


Figure 4.30: Xe2 coordination environment including long intermolecular contacts (*thin* bonds) in $[XeF]_2[Ti_9F_{38}]$.

The Raman spectrum of $[XeF]_2[Ti_9F_{38}]$ is given in Figure 4.31. It is dominated by a sharp peak at 612 cm^{-1}, which can be readily assigned to the Xe−F_t stretching frequency. Despite that two different Xe−F_t bonds are present, their lengths are basically identical (within $\pm$ 3σ) and thus not distinguishable by vibrational spectroscopy (at least not at room temperature). The same value was reported for $[XeF][Ir_2F_{11}]$ and some other $[XeF]^+$ compounds have similar corresponding frequencies (see Table 4.9), which additionally supports that both anchored XeF_2 ligands in $[XeF]_2[Ti_9F_{38}]$ are in the late stage of their ionization pathway ($XeF_2 \rightarrow XeF^+ + F^-$).

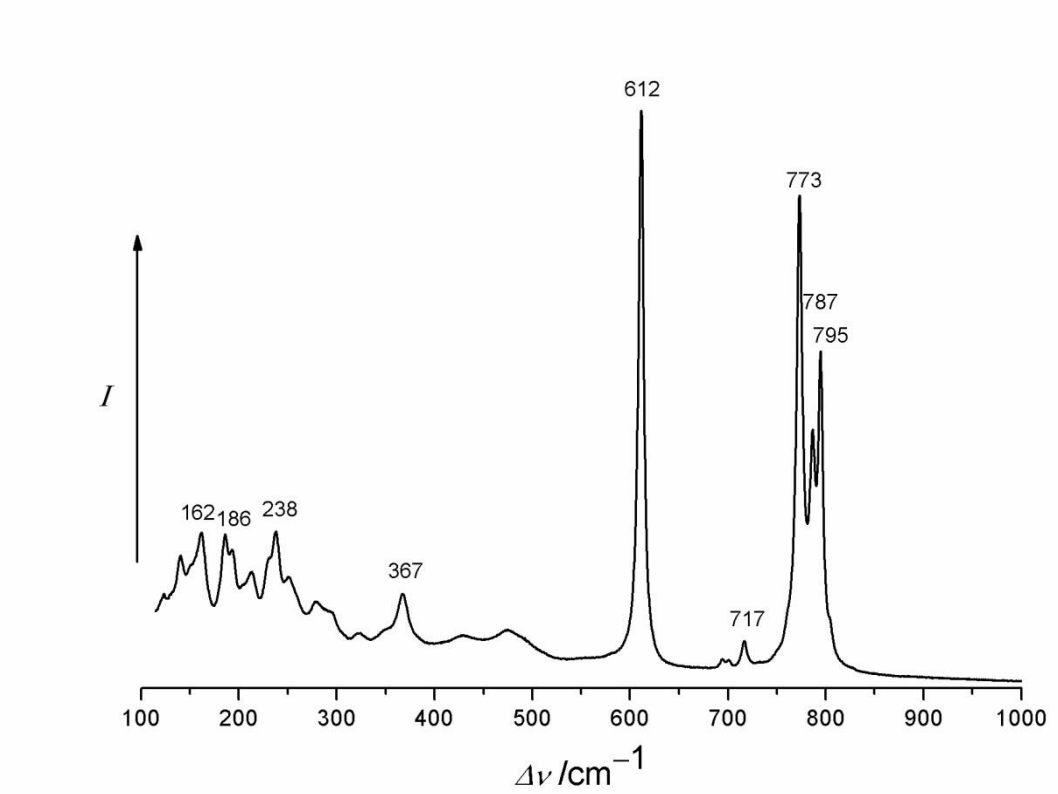


Figure 4.31: Raman spectrum of $[XeF]_2[Ti_9F_{38}]$ recorded at room temperature on a powdered sample.

Already 40 years ago, it was found[257] that the symmetric, in-phase, terminal Ti–F stretching mode, which results in a narrow and very intense Raman band, can be used for the identification of different perfluoridotitanate(IV) anions. The assumption was based on the interesting observation that the frequency of this band increases with increasing TiF_4 content and decreasing negative charge of the anion, which was exemplified on a row TiF_6^{2-} < $Ti_2F_{10}^{2-}$ < $Ti_2F_9^-$ < $Ti_3F_{13}^-$ < $Ti_6F_{25}^-$ < $(TiF_4)_n$. Since then, a number of novel compounds involving polyfluoridotitanates(IV) have been structurally characterized and such a ready identification of the anion nature has been additionally confirmed by a recent report,[163] where the calculated *x/n* ratios (*x* – total anion charge, *n* – number of TiF_6 octahedra present in the anion) for several compounds containing $[(Ti_nF_{4n+x})^{x-}]$ anions were correlated with their measured Raman frequencies. The observed strong band at 773 cm^{-1} for $[(Ti_9F_{38})^{2-}]$ (*x/n* = −0.22), as well as the 795 cm^{-1} in the case of $[(Ti_8F_{33})^-]$ (*x/n* = −0.125*)* are in accordance with the trend described previously, thus providing more experimental evidence on the dependence between the partial charges on the TiF_6 octahedra and the corresponding Raman shifts. In this aspect, more validity is also provided to the question raised by the authors (Bialowons and Müller) in their research paper[136] – whether $CsTi_8F_{33}$ is the last step on the way to TiF_4. From this point of view, $[(Ti_8F_{33})^-]$ is basically Ti_8F_{32} (TiF_4) with an additional F^- and this similarity is reflected in their Raman spectra. Moreover, this simple rule might explain another result – in case of $(XeF_2{\cdot}TiF_4)_2{\cdot}XeF_2$, the band at 749 cm^{-1} tentatively assigned the symmetric in-phase Ti−F_t stretching mode does not follow this tendency if assuming the formation of a singly charged $[(TiF_5)^-]$ anion, but fits well in the model when taking into consideration a significant covalent contribution, for instance by taking away half of the negative charge on each octahedra and writing the compound core formulation as $[(XeFF_{1/2})^{0.5+}][(TiF_4F_{1/2})^{0.5-}]$ rather than $[(XeF)^+][(TiF_5)^-]$. This assumption would result in an *x/n* value of −0.5, which would in turn place the observed frequency into the predicted range (745-756 cm^{-1}).[163] Nevertheless, the discussed frequency interval is the widest among polyfluoridotitanates(IV) only for $[(TiF_5)^-]$ anions (701-757 cm^{-1}) found in different compounds and caution should be taken in interpreting the shifts to a higher field, as more information

should always be considered when assessing the degree and nature of interactions with the cation, which can seriously influence the vibration outcome. This reflection may possibly provide an explanation or even a correction on the proposed model, since some obvious deviations from the trend remain unexplained (Figure 4.32).

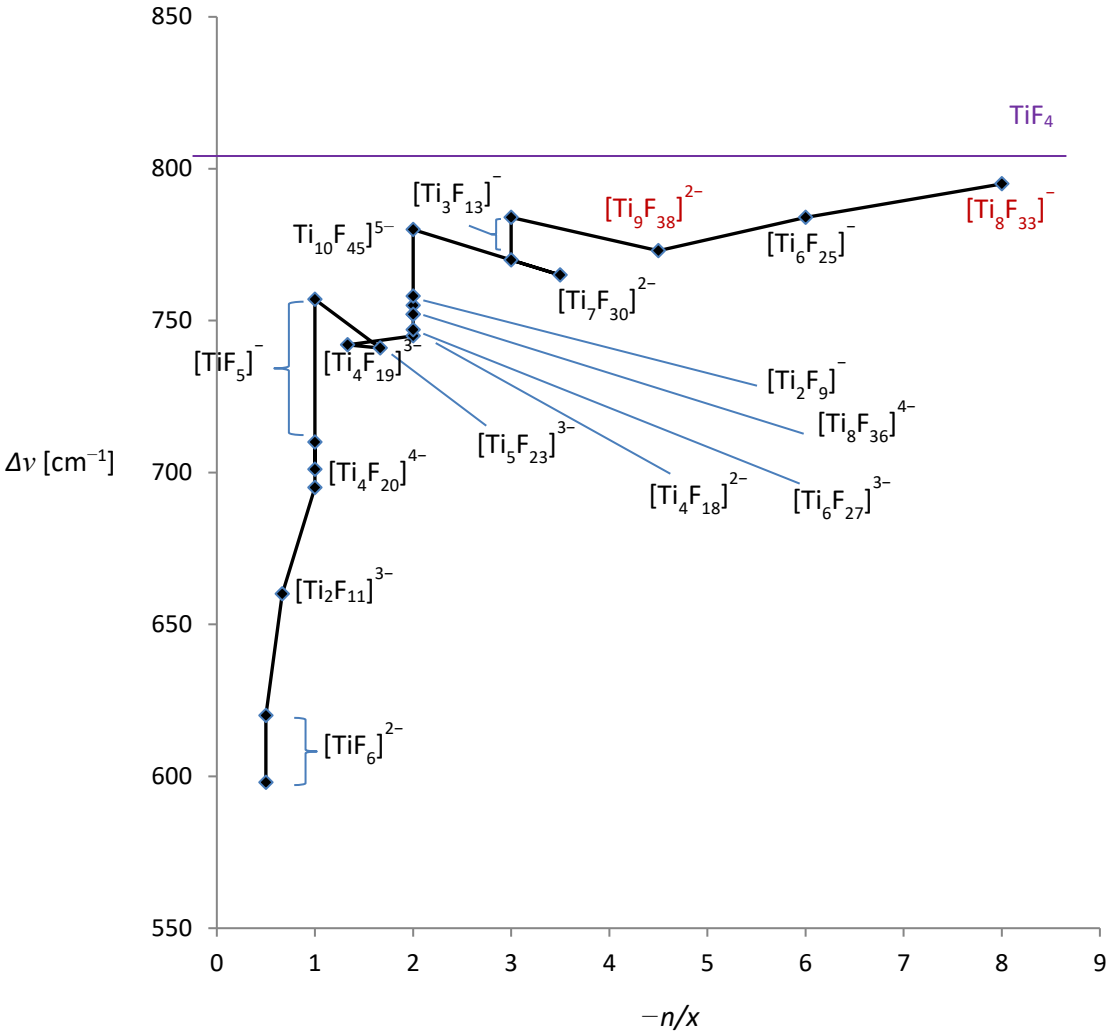


Figure 4.32: Scatter plot showing the correlation between observed Ti – F_t stretching frequencies and calculated $-n/x$ ratios (n – number of TiF_6 octahedra in the anion, x – total anion charge) for various fluoridotitanates(IV). If more than one value exists for an individual anion, only the endpoints of a range are depicted. The Raman frequencies are taken from references listed in Table 1.2 and combined with prior spectroscopic data for $[TiF_6]^{2-}$, $[Ti_3F_{13}]^-$ and $[Ti_6F_{25}]^-$.[257,258]

In previous studies (see 4.1.1 Background), the 3:2 phase $((XeF_2{\cdot}TiF_4)_2{\cdot}XeF_2)$ was the first product identified upon thermal reaction between XeF_2 and TiF_4. Here it should be noted that essentially in every experimental run covered by this sub-chapter, $(XeF_2{\cdot}TiF_4)_2{\cdot}XeF_2$ was detected by Raman spectroscopy at the very beginning of the heating process, and soon followed by the formation of an amorphic "gel-like" product. This material solidifies into a glassy product upon cooling to room temperature, and does not give any XRD pattern (see Appendix B.3, Figure B. 4). Its Raman spectrum (Figure 4.33-*d*, Figure 4.34-*a* – *c*) features a broad band between 550 and 620 cm^{-1}, indicating multiple Xe−F modes of a complex composition or more likely of a mixture of compounds. As soon as the preparative synthetic method for $(XeF_2{\cdot}TiF_4)_2{\cdot}XeF_2$ was developed, a series of experimental runs aimed at preparing compounds with lower XeF_2 content, with special interest in the 1:1 stoichiometry, of which the manganese analogue has

been obtained[215] by solvolysis of the parent $(XeF_2 \cdot MnF_4)_2 \cdot XeF_2$. Albeit all attempts in aHF failed to deliver any crystalline product, the thermal treatment of 3:2 revealed its decomposition and the slow stepwise formation of the gel-like material (Figure 4.33).

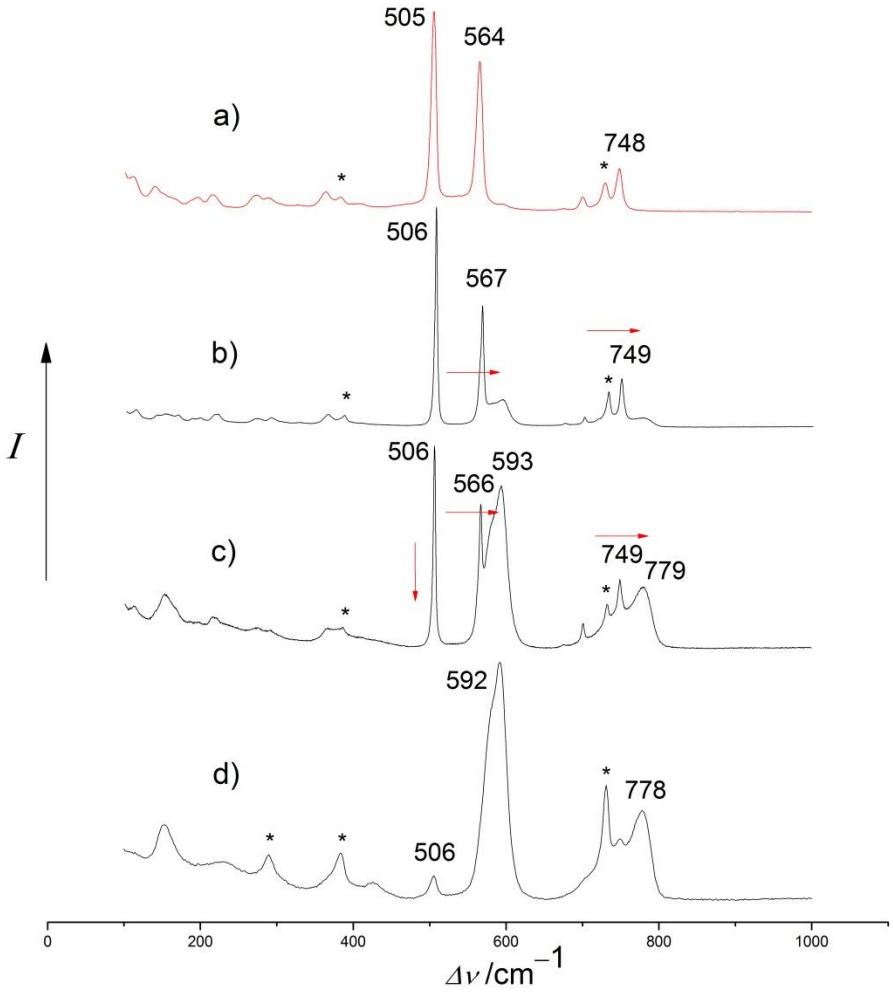


Figure 4.33: Thermal degradation of $(XeF_2 \cdot TiF_4)_2 \cdot XeF_2$ (*a* - red spectrum) and conversion to the gel-like material (spectra *b* – *d*) followed with the Raman spectroscopy. The spectra were recorded after heating the sample at 72 °C for 14 h (*b*), 34 h (*c*) and 58 h (*d*). FEP tube lines are marked with (*) symbols.

The negative shifts of $Xe{-}F_t$ and $Ti{-}F_t$ stretching bonds, from 564 to 592 cm^{-1} and from 749 to 778 cm^{-1}, respectively, are in perfect agreement with an increase of XeF_2 ionization due to the dispersal of the negative charge over growing anionic assemblies of TiF_6-octahedra.

Similarly, a viscous product also formed and covered crystals of $XeF_2 \cdot MnF_4$ made upon solvolysis of $(XeF_2 \cdot MnF_4)_2 \cdot XeF_2$ in aHF.[215] The Raman spectrum of the analogous substance found after $(XeF_2 \cdot TiF_4)_2 \cdot XeF_2$ has been rinsed twice with aHF is consistent with the gel-like product described in the ensuing discussion.

In addition, an attempt to determine the melting interval of this glassy material of unknown composition provided us unexpectedly with a remarkable insight into the early stage of the crystallization process.

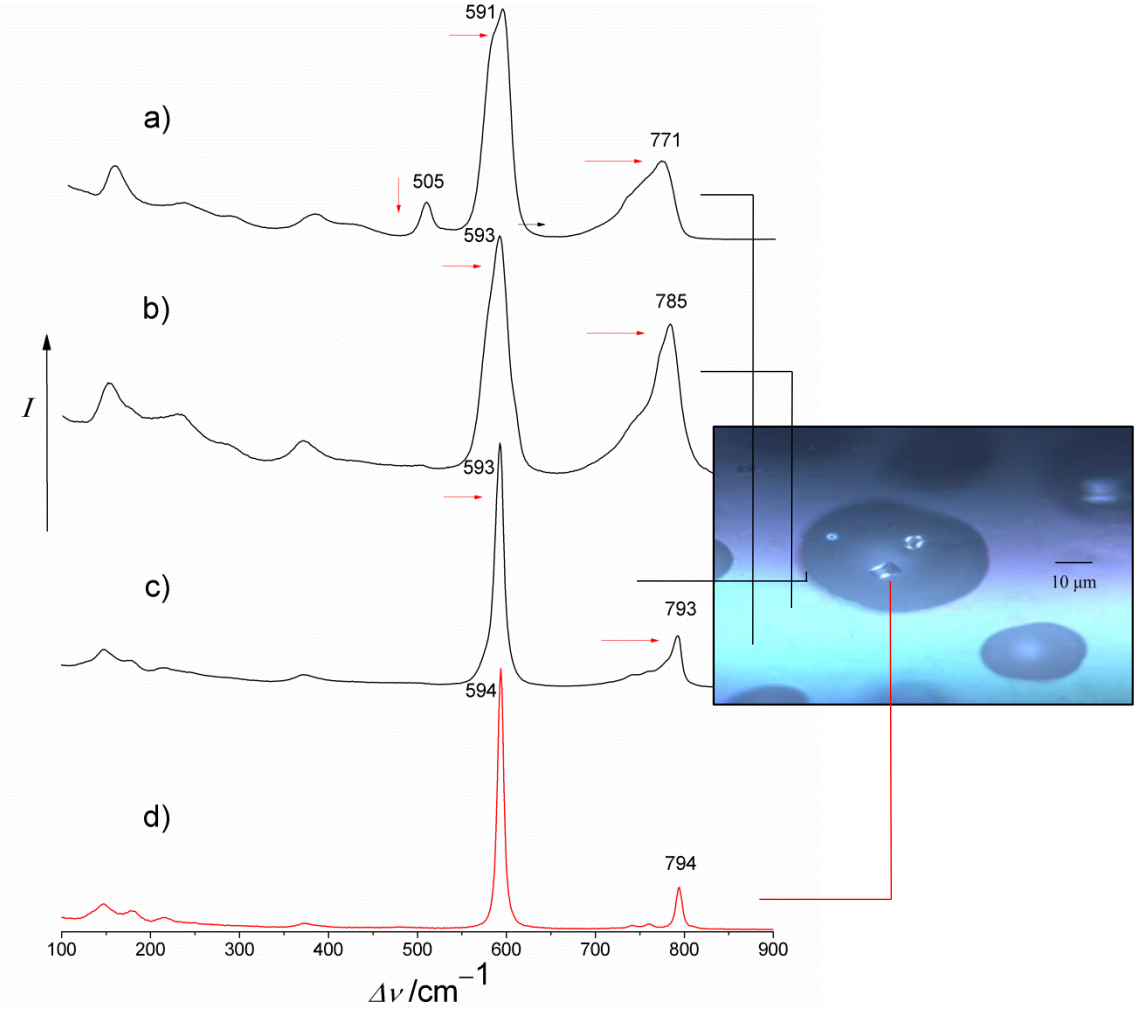


Figure 4.34: Formation of compound $[Xe_2F_3][Ti_8F_{33}]$ followed by Raman spectroscopy. The spectra (*a*-*c*) were recorded on the glassy material of unknown composition using a stepwise approach towards microcrystals of $[Xe_2F_3][Ti_8F_{33}]$ (*d*) formed on the wall of a sealed quartz capillary used for the melting-point determination. Although the contents were extensively screened, no trace of $[XeF]_2[Ti_9F_{38}]$ was detected. *Right*: Crystal seeds of $[Xe_2F_3][Ti_8F_{33}]$ growing on the capillary wall inside clear spherical regions of the glassy matrix.

A precise Raman study of the semi-molten matrix obtained after the thermal treatment (up to 142 °C) demonstrates unambiguously that microscopic crystal seeds of compound $[Xe_2F_3][Ti_8F_{33}]$ (Figure 4.34, Figure 4.35) are formed first. Figure 4.34 shows a gradual decomposition of the glassy material as a function of the distance from the crystal seeds of product $[Xe_2F_3][Ti_8F_{33}]$. Basically the same result was obtained if focusing and recording spectra consecutively on the same spot over a time period needed to form the crystals from the gel-like matrix.

Again, the wavenumber shift from 771 cm^{-1}, through 785 cm^{-1} to 794 cm^{-1}, which is indicative of an undergoing ordering towards larger polyanion associates and/or of a decrease of the anion charge, is consistent with a slight increase in the XeF_2 ionization. The latter is best represented by the Xe–F_t stretch frequency being shifted and sharpened from a broad 591 cm^{-1} band of the glassy material to a 594 cm^{-1} peak obtained on microcrystals of $[Xe_2F_3][Ti_8F_{33}]$.

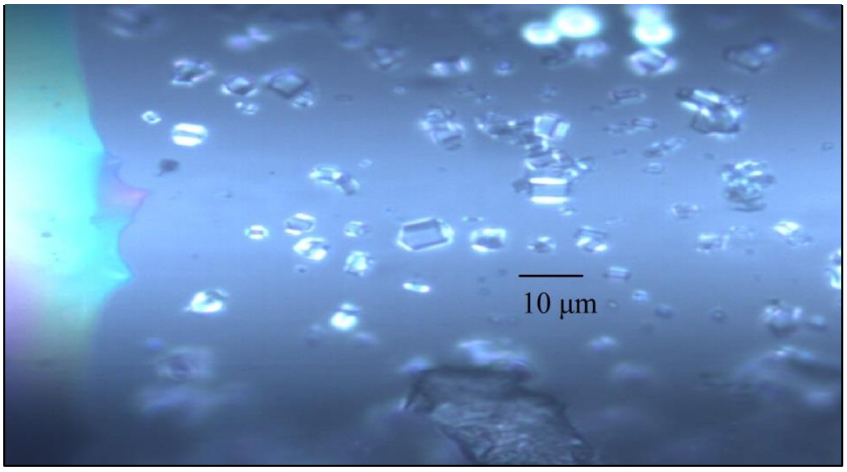


Figure 4.35: Crystalogenesis of product $[Xe_2F_3][Ti_8F_{33}]$ from the gel-like matrix observed through the microscope of the Raman spectrometer. Microcrystals were growing on the wall of the quartz capillary used for the melting point determination. Crystalline seeds typically formed inside bubble-like regions of the glassy matrix or were seen in clear regions, as they were left behind after the glassy material retracted (or decomposed) during the thermal treatment.

Most probably, the synthetic pathways leading to the product $[XeF]_2[Ti_9F_{38}]$ involve either a direct formation from the gel-like matrix after $[Xe_2F_3][Ti_8F_{33}]$ has left a deficiency of available XeF_2 (while more $XeF_{2(g)}$ additionally diffused through the semipermeable FEP reactor walls) or an equimolar gas-phase reaction of $[Xe_2F_3][Ti_8F_{33}]$ with TiF_4, affording crystals of $[XeF]_2[Ti_9F_{38}]$. The proposed reaction routes are in agreement with the visual (morphology-based) and spectroscopic observations that were made by carefully following the experimental runs, thus witnessing the formation and accumulation of $[XeF]_2[Ti_9F_{38}]$ during prolonged exposure to high temperatures (~130 °C) or when using higher molar ratios of TiF_4. Finally, exposing the product mixture to 148 °C for 48 hours left only TiF_4 in the FEP reactor.

At this point, thermal analysis as a powerful complementary method in an effort to elucidate the complex aggregation mechanism under question should definitely be considered. The investigation of energetics has been planned already at the early stage of this study, since both of the reported compounds, $[Xe_2F_3][Ti_8F_{33}]$ and $[XeF]_2[Ti_9F_{38}]$, were prepared at relatively high temperatures and showed a remarkable thermal stability. However, the realization of this characterization step would require not only overcoming all the obstacles that have hindered this kind of analysis for most of the noble-gas salts isolated thus far, but also surmounting specific problems, which arise from the complex nature of the XeF_2-TiF_4 system.

Generally, the Xe(II) cationic species are, along with their krypton analogues, among the most powerful oxidizers known. Besides the challenging synthesis, the handling of these compounds is extremely difficult and much effort is already required for a successful isolation and their structural characterization. Accordingly, the very first problem is an effective transfer of the samples into the apparatus for analysis. These salts are very reactive and undergo a rapid decomposition immediately after being exposed to air or traces of moisture. The operators responsible for the analytical equipment are usually reluctant to analyze such samples, even in small amounts, due to the aggressive properties of their decomposition products (e.g. HF, F_2, etc.). Consequently, the thermodynamic data regarding these systems available thus far are confined to only a few calorimetric studies. The standard enthalpies of formation of $[XeF][MF_6]$, $[XeF][M_2F_{11}]$ (M = Sb, Ta or Nb) and $[Xe_2F_3][MF_6]$ (M = Sb or Ta) were roughly estimated[119,259] from their heats of alkaline hydrolyses, where the thermochemical results confirmed the iconicity order of these compounds (Sb > Ta > Nb) adducted previously from vibrational spectroscopy. Nearly two decades later, adopting the same approach through hydrolysis in alkaline or neutral solution, the enthalpies of formation of the complexes $XeF_2{\cdot}VF_5$, $XeF_2{\cdot}MnF_4$ and $XeF_6{\cdot}CrF_4$ were estimated to be −1664, −1292 and −1620 kJ mol^{-1}, respectively.[260]

To compensate the resulting shortfall of experimental results, the volume-based thermodynamics (VBT) approach was developed and successfully applied on a number of noble-

gas salts with simple molecular fluoridoanions.[74] Although our basic idea was to perform the reactions in the gas phase, where the tetrahedral TiF_4 has better F^- accepting and the XeF_2 better F^- donating capabilities, all the presented evidence shows that the elevated temperature plays a key role mainly in the last stage of the synthesis/crystallization, when most probably the decomposition of the glassy solid into (unknown) volatile precursors takes place. In fact, already at room temperature, where the vapor pressure of TiF_4 is negligible, an oily substance forms upon mixing the reactants in the glove-box and covers the reaction mixture, the Raman spectrum of which is very similar to the spectrum d) in Figure 4.33, with an intensified band at 506 cm^{-1} showing a considerable amount of weakly associated XeF_2. This finding suggests a solid-gas reaction for the initial step. Interestingly, besides the oily substance, the $[XeF_2{\cdot}TiF_4]_2{\cdot}XeF_2$ could be always identified with Raman spectroscopy after leaving the reaction mixture (using excess XeF_2) for several days at room temperature. Thus, a gas-phase reaction for the initial step: $TiF_4(g) + 2\ XeF_2\ (g) \rightarrow TiF_5^-\ (g) + Xe_2F_3^+\ (g)$ is very unlikely to occur and can be ruled out. Since even the polymeric TiF_5^- does not ionize efficiently the XeF_2 molecule, it is not expected from a gaseous molecular TiF_5^- species of being capable of sustaining the $Xe_2F_3^+$ cation. Reformulating the reaction above according to our findings could possibly lead to the adduct $XeF_2{\cdot}TiF_4$. In this case, the VBT approach with the ionic model implied in the calculation of the lattice energy (omitting substantial covalent contributions) would not offer a reliable guidance. Additionally, the support from theoretical calculations is currently limited for the salts containing novel polymeric anions and therefore unlikely to deliver meaningful approximations. Anyway, more experimental data is needed in order to speculate on the nature and dimensionality of the intermediates and to narrow the wide variety of possible molecular fluoridotitanate(IV) anions present in the gas phase and to clarify the mechanism underlying the chemical process delivering both aforedescribed products.

Moreover, it should be remembered again that in previous studies (see 4.1.1 Background), after the formation of $(XeF_2{\cdot}TiF_4)_2{\cdot}XeF_2$, two more phases with molar stoichiometries $XeF_2{\cdot}TiF_4$ (1:1) and $XeF_2{\cdot}2TiF_4$ (1:2) were isolated, where no further decomposition was reported for the latter although the heating limit reached was 120 °C. Since the experimental runs described in this work were not carried out in dynamic vacuum, there is a high probability that both elusive compounds remain hidden in the glassy solid (and therefore in the viscous material reported if aHF is used as a solvent) mentioned previously. A question, however, remains whether even more unknown phases are co-melted in this intriguing product and what type of structures have the highest probabilities to be found in this system at the given conditions.

In case of $XeF_2{\cdot}TiF_4$, one possibility would be retention of the chain-like $(XeF_2{\cdot}TiF_4)_2{\cdot}XeF_2$ core structure after removal of the co-crystalized XeF_2 molecules, with FXeF-moieties alternating on octahedra as in $XeF_2{\cdot}CrF_4$. The possibility to keep the original arrangement has been well illustrated recently, where the removal of two considerably larger BrF_5 molecules from the solvated $[Mg(KrF_2)_4(AsF_6)_2]{\cdot}2BrF_5$ did not have any serious impact on its crystal structure.[109] However, based on a similarity of $(XeF_2{\cdot}TiF_4)_2{\cdot}XeF_2$ with its manganese analogue, it is more likely that the crystal structure of the XeF_2-rich compound breaks in aHF or at elevated temperatures after XeF_2 is released and the octahedral chains close, forming four-membered rings of cis-linked TiF_6-units with XeF_2 molecules anchored to titanium atoms. In addition, such four-membered rings are already known to exist in the form of $[Ti_4F_{20}]^{4-}$ anions determined in two polymorphic modifications of $[ImH]_4[Ti_4F_{20}]$.[155]

The resemblance with fluoridomanganates(IV) might as well help to decipher the crystal structure of $XeF_2{\cdot}2TiF_4$. In fact, the 1:2-phase in the XeF_6 - MnF_4 system was found to be $[XeF_5]_4[Mn_8F_{36}]$[224]. Also in the titanium case, the isolated cubic $[Ti_8F_{36}]^{4-}$ anion has already been structurally characterized and from here on it is not difficult to imagine the polymerization of such associates into $[Xe_2F_3][Ti_8F_{33}]$ in the next step. In spite of this, several results discussed herein show that also the formation of trimeric rings is common among fluoridotitanates(IV), which can be further joined together through common TiF_6-octahedra as observed in the complicated 3-D network of $XeF_2{\cdot}2CrF_4$, thus this additional possibility should not be ruled out completely. Nevertheless, caution should be taken with such predictions, as the reported stoichiometries might be as well mixtures of phases of other molar ratios with very similar thermal stability.

4.1.5 Other Fluoridotitanate(IV) Salts and By-Products

4.1.5.1 $KrF_2 - TiF_4$ System

Except xenon, krypton is thus far the only noble gas that forms chemical compounds isolable in macroscopic amounts. All krypton chemistry is derived from the binary fluoride KrF_2, which is an extraordinary strong oxidative fluorinating agent, capable of oxidizing elemental xenon to XeF_6 and iodine to IF_7 at room temperature.[261] Unlike their xenon(II) analogues, and because of their strong oxidative-fluorination properties and thermodynamic instabilities with respect to redox decomposition, krypton(II) compounds are extremely difficult to synthesize, isolate, manipulate and characterize. The chemistry of KrF_2 resembles, to some extent, that of XeF_2. Their fluoride ion donor properties were established[262] as intermediate with respect to XeF_6 and XeF_4, where XeF_2 was found to exhibit slightly higher Lewis basicity than KrF_2,[111] altogether resulting in the F^- donating strength sequence $XeF_6 > XeF_2 \geq KrF_2 >> XeF_4$. Krypton(II) fluoride reacts with pentafluorides of platinum, gold and elements belonging to group 5 and 15, forming salts of the KrF^+ and/or $Kr_2F_3^+$ cations best described with general formulations $[KrF][MF_6]$ (M = Ta, Ru, Rh, Pt, Au, As, Sb, Bi), $[KrF][M_2F_{11}]$ (M = Nb, Ta, Ru, Pt, Sb) and $[Kr_2F_3][MF_6]$ (M = Ta, Au, As, Sb)[227]. Among the afore-listed, only the crystal structures of $[KrF][MF_6]$ (M = As, Sb, Bi, Au), of the double salt $[Kr_2F_3][AsF_6]\cdot[KrF][AsF_6]$ and of two KrF_2-solvates $[Kr_2F_3][SbF_6]\cdot KrF_2$ and $([Kr_2F_3][SbF_6])_2\cdot KrF_2$, have been determined up to now, using aHF as the synthetic and crystallization medium[227].

The data regarding reactions between KrF_2 and metal tetrafluorides are scarce, although molecular adducts with weak fluoride ion acceptors, mainly with some metal oxide fluorides MOF_4 (M = Cr, Mo, W) are known.[227] Many metals (e.g. Cr, Pt, Ru, Rh, etc.) are oxidized in aHF by KrF_2 beyond their tetravalency, while on the other hand, KrF_2 can provide an access to the +4 oxidation state of certain other metals (e.g. Ni[226]), which is unreachable with the use of XeF_2 and basically impossible in typical $XeF_2 - MF_4$ systems without a corresponding redox reaction.

Thus far, only two KrF_2 adducts with metal tetrafluorides have been prepared[263], but not structurally characterized: the compound $2KrF_2\cdot MnF_4$, which decomposes at –45 °C under dynamic vacuum yielding KrF_2 and the product $KrF_2\cdot MnF_4$, which is stable in a dynamic vacuum up to –25 °C and undergoes further decomposition at room temperature to form Kr, F_2, KrF_2 and high-purity MnF_4. Due to the analogy with titanium(IV) discussed previously in this work, similar products can also be expected in the $KrF_2 - TiF_4$ system and results of reactions between KrF_2 and some binary fluorides, including TiF_4, have already been discussed[264], but no further information is available. Another report[265] described the reaction of NF_3, KrF_2 and TiF_4 in a molar ratio 2:2:1 in aHF, which yielded after 3 h at room temperature only polytitanate salts of undefined composition $[NF_4][TiF_5\cdot n TiF_4]$.

In the present work, the possibility of formation of any $a KrF_2\cdot b TiF_4$-type product was further explored. The experiments were based on a slightly modified synthetic approach as described in the Methods section. The T-reactors used were constructed from two thin-walled 6.35 mm o.d. FEP tubing, joined (fused) at 90° at the cross section and heat-sealed at both ends. The reaction vessels were fitted with Kel-F valves encased in aluminium housings and then connected to a glass vacuum line through 6.35 mm stainless steel Swagelok Ultratorr unions and rigorously dried by pumping for 8 h under dynamic vacuum. Once dried, T-reactors were passivated with ~1000 Torr of fluorine overnight and once passivated the vessels were evacuated and back-filled with ~1000 Torr of dry nitrogen prior to use.

TiF_4 (22.2 mg; 0.179 mmol) was weighed inside the glovebox into the vessel and aHF (0.6 mL) was condensed onto the sample at −196 °C by vacuum distillation from the storage vessel, on a metal vacuum line through FEP-connections, while KrF_2 (149.5 mg; 1.227 mmol) was added to the frozen reaction mixture under static vacuum. Upon slow warming to −78 °C, a yellow-orange viscous layer formed at the bottom of the solution. Partial aHF removal or temperature variations (in −78 °C – RT range) resulted in multiple interchanges from a viscous layer to white precipitate. All attempts of crystallization from either the yellow-orange layer or clear solution failed; the only crystalline material found by X-ray unit cell determination in the product mixture was KrF_2. However, the Raman spectrum of the bulk recorded at −150 °C indicated a formation of an adduct $a KrF_2\cdot b TiF_4$ of undefined composition with two bands at 596.9 cm^{-1} and 579.2 cm^{-1}, which can be tentatively assigned to the $Kr_2F_3^+$ cation (corresponding $\nu(KrF_t{+}KrF_t)$ and $\nu(KrF_t{-}KrF_t)$ values (cm^{-1}) assigned[266] for $Kr_2F_3^+$ in C_{2v} point group found in $[Kr_2F_3][AsF_6]$: 594(100),

600(80), 610(43), 567(31); ([Kr_2F_3][SbF_6]: 603(100), 594(89), 555(34); [Kr_2F_3][AsF_6]·*n*KrF_2 602(100), 575(23), 553(50); [Kr_2F_3][SbF_6]·*n*KrF_2: 599(100), 557(50); values in parentheses denote relative Raman intensities)[41]. The existence of such ion pairs in the KrF_2 – TiF_4 system should not be surprising considering that [Kr_2F_3][BF_4]·*n*KrF_2, derived from the relatively weak fluoride ion acceptor BF_3 (FIA 347.3 kJ mol^{-1}, see Table 1.1), has been ascertained by Raman spectroscopy.[265] Again, an aggregation of TiF_6-octahedra into larger polyanionic assemblies, probably efficiently solvated by aHF and KrF_2 molecules, with a consequent increase of the fluoride ion acceptor ability of the parent Lewis acid, is supposed.

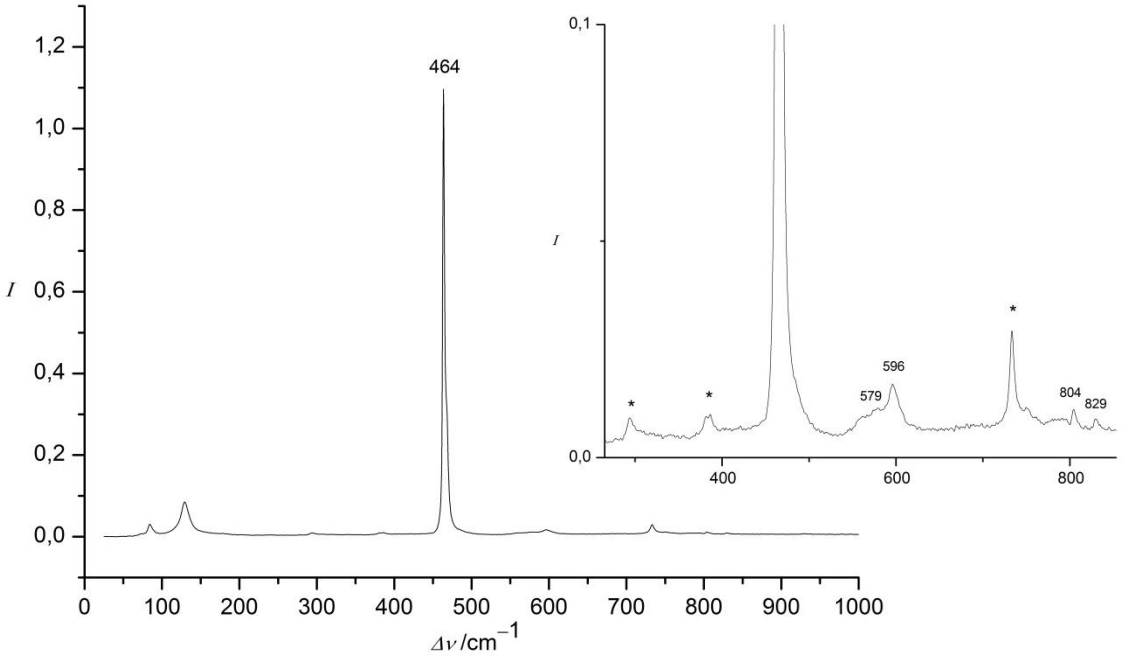


Figure 4.36: The Raman spectrum is dominated by unreacted KrF_2 (464 cm^{-1}) and TiF_4 (804 and 829 cm^{-1}). *Upper right* – the magnified region of interest, with signals at 596 cm^{-1} and 579 cm^{-1}, which cannot be attributed to FEP lines (denoted with (*) symbols). Although weak FEP bands are found in this frequency region, their intensities are considerably low in comparison with the strongest FEP band at 733 cm^{-1}).

For the aforedescribed experimental attempt, a 6.8-fold molar excess of KrF_2 over TiF_4 was used, while an equimolar reaction of KrF_2 and TiF_4 in 0.4 mL aHF did not proceed and only reactants were re-identified in the reaction mixture.

4.1.5.2 *β*-[H_3O][Ti_2F_9]

The compound *β*-[H_3O][Ti_2F_9] was found among the products [XeF]$_2$[Ti_9F_{38}] and [Xe_2F_3][Ti_8F_{33}] inside one reactor tube during a prolonged thermal treatment. H_2O molecules diffused through the FEP wall, which was made even more permeable at high temperatures (135 °C), while the whole surface of the used reactor was exposed to the (moist) air of the laboratory.[267]

The title compound crystalizes in the monoclinic crystal system as the second polymorph of the previously reported[161] orthorhombic *α*-[H_3O][Ti_2F_9] (*Pnma* space group). The asymmetric unit is constructed from 15 crystallographically independent atoms (2 Ti, 9 F, 1 O and 3 H atoms, all atoms reside on general Wyckoff 4e positions, fractional atomic coordinates are given in Appendix B.4, Table B. 4) where the two Ti atoms (Ti1 and Ti2) belong to two infinite *cis*-chains of TiF_6-octahedra, which mutually connect *via* μ-F bridges to form a ladder-like [Ti_2F_9]$^{-1}$ anionic structure.

Table 4.12: Crystal structure determination and refinement details for compound β-$[H_3O][Ti_2F_9]$.

Crystal data	*Data collection*	*Refinement*
$H_3OTi_2F_9$	Rigaku AFC7 diffractometer	$R_1[F^2 > 2\sigma(F^2)] = 0.058$
$M_r = 285.76$	Mercury CCD detector	$wR_2\ (F^2) = 0.14$
Crystal system: monoclinic	λ = 0.71069 Å (Mo K_α)	1824 reflections
Space group: $P2_1/c$	1824 measured reflections	109 parameters
a = 5.3219(12) Å	1824 independent reflections	GOF = 1.046
b = 16.004(3) Å	1258 observed reflections (I > 2 σ (I))	$\Delta\rho_{max}$ = 1.02 e/Å^3
c = 8.891(2) Å	$R_{int} = 0$	$\Delta\rho_{min}$ = −0.61 e/Å^3
β = 91.38(13)°	θ_{max} = 29.2°, θ_{min} = 3.8°	
V = 757.0 (3) Å^3	$-7 \leq h \leq 7$	
Z = 4	$0 \leq k \leq 21$	
ρ_{calc} = 2.508 g/cm^3	$0 \leq l \leq 12$	
$2.6° \leq \theta \leq 25.4°$		
Cell parameters from 208 reflections		
μ = 2.23 mm^{-1}		
T = 200 K		
F(000) = 544		
Size: 0.1×0.09×0.07 mm		
Appearance: Colorless chunk		

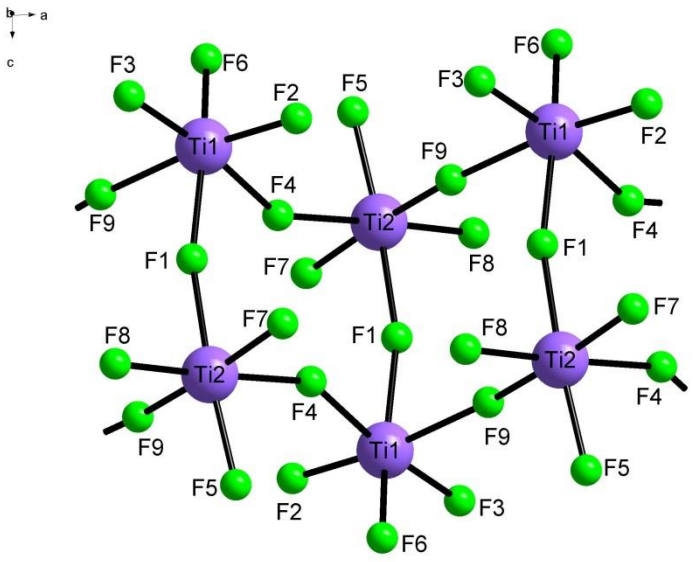


Figure 4.37: Construction of the double-chained $[Ti_2F_9]^{-1}$ anion found in β-$[H_3O][Ti_2F_9]$. The corresponding geometric parameters are given in Table 4.13.

Table 4.13: Selected geometric parameters for the compound β-$[H_3O][Ti_2F_9]$.

Bond Lengths (Å)

Ti1—F2	1.757 (3)	Ti2—F9^{ii}	1.921 (3)
Ti1—F6	1.762 (3)	Ti2—F1	1.952 (3)
Ti1—F3	1.793 (3)	Ti2—F4	1.988 (3)
Ti1—F1	1.960 (3)	F4—Ti1^{i}	1.965 (3)
Ti1—F4^{i}	1.965 (3)	F9—Ti2^{ii}	1.921 (3)
Ti1—F9	2.001 (3)	O1—H1	0.917 (3)
Ti2—F8	1.765 (3)	O1—H2	0.936 (3)
Ti2—F5	1.784 (3)	O1—H3	0.933 (3)
Ti2—F7	1.795 (3)		
Bond Angles (°)			
F2—Ti1—F6	99.20 (14)	F8—Ti2—F9^{ii}	90.07 (13)
F2—Ti1—F3	92.64 (13)	F5—Ti2—F9^{ii}	90.87 (14)
F6—Ti1—F3	96.95 (13)	F7—Ti2—F9^{ii}	171.79 (13)
F2—Ti1—F1	91.11 (13)	F8—Ti2—F1	92.52 (12)
F6—Ti1—F1	167.18 (12)	F5—Ti2—F1	169.94 (12)
F3—Ti1—F1	90.12 (12)	F7—Ti2—F1	88.46 (14)
F2—Ti1—F4^{i}	90.70 (13)	F9^{ii}—Ti2—F1	84.65 (12)
F6—Ti1—F4^{i}	88.65 (12)	F8—Ti2—F4	175.23 (12)
F3—Ti1—F4^{i}	172.95 (12)	F5—Ti2—F4	87.15 (12)
F1—Ti1—F4^{i}	83.60 (11)	F7—Ti2—F4	88.03 (13)
F2—Ti1—F9	172.47 (13)	F9^{ii}—Ti2—F4	86.78 (11)
F6—Ti1—F9	87.75 (13)	F1—Ti2—F4	83.62 (11)
F3—Ti1—F9	89.40 (12)	Ti2—F1—Ti1	166.25 (16)
F1—Ti1—F9	81.63 (12)	Ti1^{i}—F4—Ti2	149.92 (15)
F4^{i}—Ti1—F9	86.52 (11)	Ti2^{ii}—F9—Ti1	161.10 (15)
F8—Ti2—F5	96.49 (13)	H1—O1—H2	108.9 (3)
F8—Ti2—F7	94.69 (14)	H1—O1—H3	113.4 (3)
F5—Ti2—F7	95.22 (15)	H2—O1—H3	115.1 (4)

Symmetry codes: (i) −*x*+1, −*y*+2, −*z*+1; (ii) −*x*+2, −*y*+2, −*z*+1.

Each octahedron has three bridging F-ligands in *fac* arrangement and three terminal fluorine atoms. The latter interact with H_3O^+ cations through hydrogen bonding (Figure 4.38). Hydrogen bonds can be described as moderate[268,269] (H···F distances ranging from 1.682(2) to 1.977(2) Å and O···F from 2.538(4) to 2.757(4) Å).

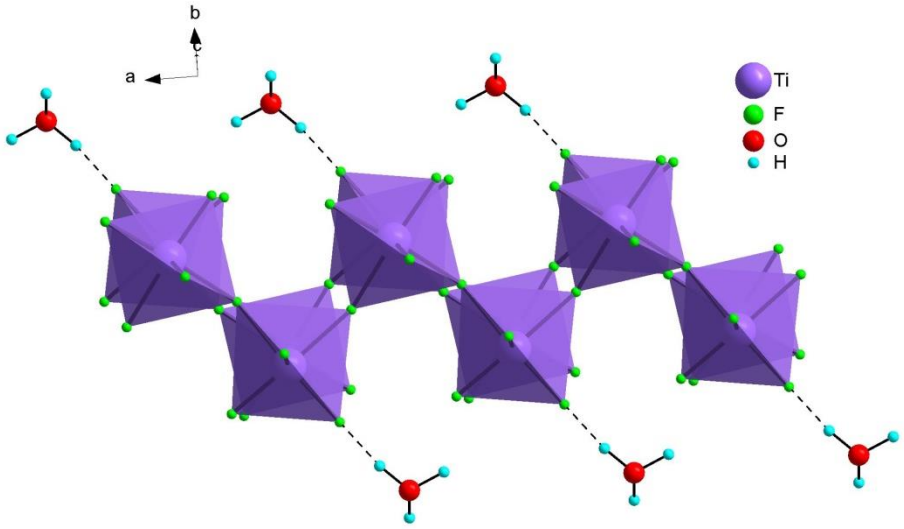


Figure 4.38: Selected part of the crystal structure of β-$[H_3O][Ti_2F_9]$. Several H_3O^+ cations were omitted for clarity.

The main structural difference between the two modifications is in the arrangement of TiF_6-octahedra belonging to the two infinite chains which comprise the $[Ti_2F_9]^-$ anion. The double chain found in α-$[H_30][Ti_2F_9]$ is eclipsed, while the two chains of the herein reported β-phase are in gauche conformation to each other, featuring a torsion angle of approximately $-16°$ (Figure 4.38). Similar gauche conformations have been previously observed in $[Ti_2F_9]^-$ anions of compounds $CsTi_2F_9$[161] and α-$[ImH][Ti_2F_9]$[156].

4.2 $XeF_2 – SnF_4$ System

4.2.1 Background

While the $XeF_6 – SnF_4$ system (see Section 1.6), where six phases with general formulations $4XeF_6 \cdot SnF_4$, $2XeF_6 \cdot SnF_4$, $4XeF_6 \cdot 3SnF_4$, $3XeF_6 \cdot 4SnF_4$, $4XeF_6 \cdot 5SnF_4$ and $XeF_6 \cdot 4SnF_4$ have been isolated so far, has been extensively studied[219], the results in the $XeF_2 – SnF_4$ system are hitherto limited to only two products: $3XeF_2 \cdot 4SnF_4$ and $XeF_2 \cdot 2SnF_4$.[270]

The compound $XeF_2 \cdot 2SnF_4$ was obtained upon redox reaction between tin difluoride and an excess of liquid xenon difluoride at 140 °C. The same compound was also prepared at 60 °C using hydrazinium(II) fluoridostannate(II), $N_2H_6SnF_4$, as starting material, with an evolution of gaseous HF, Xe and N_2 accompanying the reaction.

Table 4.14: Characterization results obtained from previous studies[270] of the system $XeF_2 – SnF_4$.

	$XeF_2 \cdot 2SnF_4$		$3XeF_2 \cdot 4SnF_4$	
	Chemical analyses			
Element	Calcd.(%)	Found (%)	Calcd. (%)	Found (%)
Sn	42.49	41.9	36.51	37.1
Xe	23.50	24.2	30.80	30.0
F	34.01	34.3	32.69	32.2
	IR spectroscopy			
	670 m, 627 m, 595 sh, 585 s, 550 vs, 475 s, 420 sh		675 m, 625 m, 582 s, 550 sh, 530 vs, 475 s, 420 sh	
	Intensity: s-strong, m-medium, w-weak, vs-very strong, sh-shoulder			
	Raman spectroscopy			
	619 (34), 594 (100), 580 (25), 284 (2), 150 (18)		619 (38), 594 (66), 588 (100), 574 (sh), 509 (34), 309 (2), 283 (2), 160 (12)	
	Values in parentheses denote relative intensities; sh-shoulder			

During the preparation of $XeF_2 \cdot 2SnF_4$, the weight of the mixture in the reaction vessel was followed during the course of pumping off the volatiles. It was found that there is a change in slope of the curve corresponding to the composition $3XeF_2 \cdot 4SnF_4$. This phase was reported to be unstable at room temperature, losing XeF_2 under dynamic vacuum at the rate of about 4 mole % per hour, slowly approaching the $XeF_2 \cdot 2SnF_4$ composition. Both xenon(II) fluoridostannates(IV) were identified as white diamagnetic solids, with negligible vapour pressure at 0 °C ($3XeF_2 \cdot 4SnF_4$) and at room temperature ($XeF_2 \cdot 2SnF_4$). The results of thermal decomposition indicated that $3XeF_2 \cdot 4SnF_4$ starts to lose XeF_2 even below room temperature (but can be successfully isolated at 0 °C), while $XeF_2 \cdot 2SnF_4$ is stable up to ~50 °C and that the final product at decomposition temperatures lower than 300 °C is SnF_4 in both cases.

The characterization of products was made by X-ray powder diffraction, Raman and IR spectroscopy (Table 4.14), chemical analysis and magnetic susceptibility measurements. An earlier report[216] on the existence of a yellowish $2XeF_2 \cdot SnF_4$ was debunked[270], since the claimed XeF_2-rich phase turned out to give an identical infrared spectrum as $XeF_2 \cdot 2SnF_4$. Moreover, although the structural determination of the isolated phases was not undertaken, several possibilities regarding the nature of the two products were discussed. These assumptions will be addressed together with the obtained results of the present work in the ensuing section.

4.2.2 $[Xe_2F_3][Sn_4F_{17}]\cdot XeF_2\cdot HF$

The title compound was prepared in a small T-shaped FEP reactor by the reaction between XeF_2 (84 mg, 0.5 mmol) and SnF_4 (19 mg, 0.1 mmol) in aHF. The reactants were weighed inside the glovebox and then aHF (1.1 ml) was condensed onto the reaction mixture at -196 °C. Upon warming to room temperature, a white precipitate, identified with Raman spectroscopy as the phase 1:2 ($XeF_2\cdot 2SnF_4$), formed. This solution was left stirring for 30 minutes and aHF was then carefully evaporated (~0.4 ml) until all the precipitate dissolved forming a clear, dense solution (see Section 4.1.2). Afterwards, the temperature of the solution was slowly lowered (−1 °C/h) to −20 °C. Despite no precipitate formation or crystallogenesis was observed in the next hours, holding this temperature overnight finally afforded thin colorless plate-like crystals of $[Xe_2F_3][Sn_4F_{17}]\cdot XeF_2\cdot HF$. The remaining solution containing dissolved XeF_2 was decanted into the side arm and pumped off. The crystalline material was quickly isolated in the glove-box and a suitable crystal for X-ray diffraction analysis was selected under perfluorinated oil at −14 °C using a stereo microscope. Results from the X-ray diffraction data collection are given in Table 4.15.

Table 4.15: Crystal structure determination and refinement details for compound $[Xe_2F_3][Sn_4F_{17}]\cdot XeF_2\cdot HF$.

Crystal data	*Data collection*	*Refinement*
$Xe_3Sn_4F_{23}H$	Agilent Gemini diffractometer	$R_1[F^2 > 2\sigma(F^2)] = 0.018$
$M_r = 2613.44$	Atlas CCD detector	$wR_2\ (F^2) = 0.036$
Crystal system: orthorhombic	λ = 0.71073 Å (Mo K_α)	2946 reflections
Space group: *Pbcm*	32873 measured reflections	156 parameters
a = 9.40492(14) Å	2946 independent reflections	GOF = 1.056
b = 21.3328(3) Å	3660 observed reflections (I > 2 σ (I))	$\Delta\rho_{max}$ = 1.13 e/Å^3
c = 10.27566(16) Å	R_{int} = 0.040	$\Delta\rho_{min}$ = −1.49 e/Å^3
V = 2061.64 (6) Å^3	θ_{max} = 29.8°, θ_{min} = 3.5°	
Z = 2	$-13 \leq h \leq 12$	
ρ_{calc} = 4.210 g/cm^3	$-28 \leq k \leq 29$	
$3.6° \leq \theta \leq 29.7°$	$-14 \leq l \leq 13$	
Cell parameters from 15922 reflections		
μ = 9.83 mm^{-1}		
T = 150 K		
F(000) = 2280		
Size: 0.17×0.11×0.05 mm		
Appearance: Colorless plate		

Similarly as in the case of $(XeF_2\cdot TiF_4)_2\cdot XeF_2$, the crucial requirement for the formation of the XeF_2 rich phase seems to be a very high concentration of XeF_2, which can be achieved with a multifold excess of XeF_2 (specifically a five-fold molar surplus was needed for $[Xe_2F_3][Sn_4F_{17}]\cdot XeF_2\cdot HF$ in a relatively small volume of aHF. It has already been observed in separate experiments that the resulting dense medium that formed behaves somewhat differently than the solvent alone, which can be attributed to the high degree of hydrogen bonding involved, also accountable for the high solubility of XeF_2 in aHF.

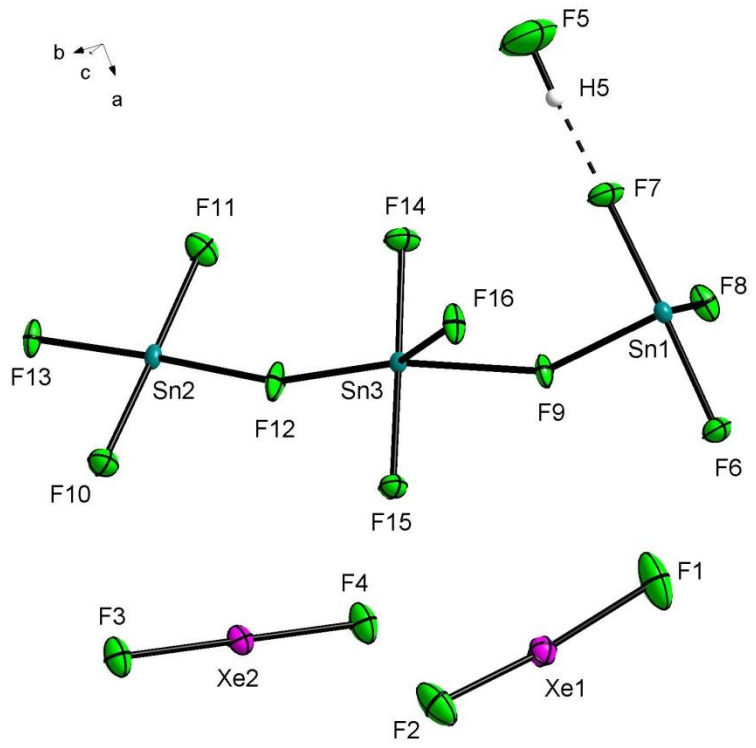


Figure 4.39: The atoms in the asymmetric unit of $[Xe_2F_3][Sn_4F_{17}]\cdot XeF_2\cdot HF$. Thermal ellipsoids are drawn at the 50 % probability level. A standard representation model is used for the hydrogen atom.

The compound $[Xe_2F_3][Sn_4F_{17}]\cdot XeF_2\cdot HF$ crystallizes in the orthorhombic centrosymmetric *Pbcm* space group with 2 formula units per unit cell. The asymmetric unit (Figure 4.39) consists of twenty-two atoms (2 Xe, 3 Sn, 16 F and one H atom). Only 9 atoms are situated on general positions (Wyckoff 8e), while the rest reside mainly on mirror planes (Wyckoff 4d).

Non-tetrahedral structures of organic derivatives of the silicon subgroup are often caused by inter- or intra-molecular coordination interaction X→M, where X is an electronegative, electron-withdrawing (non-carbon) substituent, which has at least one unshared electron pair (X = N, P, O, S, halogen) and is directly bonded to M.[271] Since the heavier Group 14 elements silicon, germanium, tin and lead tend to exceed more readily the usual four-coordination than their lighter congener carbon[272], the donor-acceptor interaction X→M results in a rise of the coordination number of the M atom. Particularly tin may exhibit coordination numbers of five, six or seven in numerous neutral, cationic or anionic organyl complexes and even a few examples of octacoordinated tin from pure inorganic chemistry are known (e.g. $Sn(NO_3)_4$[273]). For coordination numbers 4, 5, 6, 7 and 8, the central Sn atom was found to adopt a configuration of a tetrahedron, trigonal bipyramid or square pyramid, octahedron or skew trapezoid, pentagonal bipyramid and distorted cube or square antiprism, respectively[274].

Examples of a seven-coordinated tetravalent tin with a pentagonal bipyramidal geometry can be found only in certain organotin complexes[271,274]. In spite of a large number of characterized compounds derived from TiF_4, where all perfluoridotitanate(IV) anions reported to date were found to be constructed exclusively from octahedral TiF_6-units, the structural knowledge of perfluoridostannates(IV) has been thus far limited to the octahedral SnF_6^{2-} anion (see Section 1.4.2). Here it should be noted that the previously reported[275] compound $(NH_4)_3SnF_7$, of which the structure is best formulated as $[NH_4]_2[SnF_6]\cdot NH_4F$, and compounds $M^{III}SnF_7$ (M = Eu, Y, La, Sm, Gd, Yb, Lu, Tl)[276,277] contain only "ordinary" SnF_6 groups. The Sn1 and Sn2 atoms in $[Xe_2F_3][Sn_4F_{17}]\cdot XeF_2\cdot HF$ follow this established octahedral geometry, while Sn3 atoms adopt a coordination of seven fluorine ligands in a pentagonal bipyramidal arrangement, which is the first reported case of a heptacoordinated Sn(IV) in a fluorine environment. The bond lengths associated to the Sn3 coordination sphere are given in Figure 4.40.

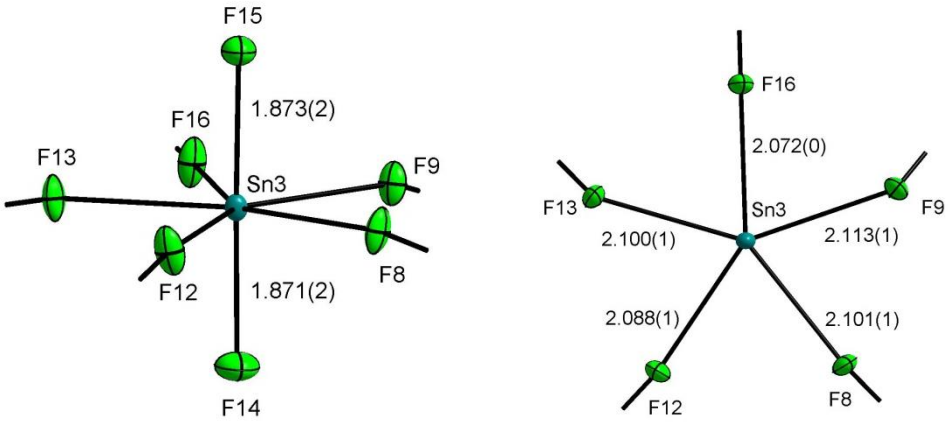


Figure 4.40: Pentagonal bipyramidal geometry of the Sn(3) atom found in $[Xe_2F_3][Sn_4F_{17}]\cdot XeF_2\cdot HF$ with Sn–F bond lengths (Å) of axial (*left*) and equatorial (*right*) fluorine atoms. Thermal ellipsoids are shown at the 50% probability level. Further bridging connections to neighboring Sn atoms are drawn with broken-off bonds.

The Sn–F bond lengths of the heptacoordinated Sn3 do not differ significantly from those of the octahedral $Sn1F_6$- and $Sn2F_6$-units, although terminal fluorine atoms representing the axial apexes of the $Sn3F_7$-pentagonal bipyramids are slightly shorter. Considering both geometries, the Sn–F_t bond lengths range from 1.871(2) to 1.899(2) Å (the maximum value belongs to the Sn2–F7, where the terminal F7 is additionally hydrogen bonded to HF), while the Sn–F_b bonds are expectedly longer, in the 1.991(2) – 2.113(2) Å range. The difference however is not as pronounced as in the aforediscussed fluoridotitanates(IV).

All axial F atoms of the octahedral (if equatorial planes of four F atoms are defined as those comprising the formed anionic layer described in the ensuing discussion) and pentagonal bipyramidal arrangements are terminal, while all equatorial ones are bridged. The average F_b–Sn3–F'_b angle amounts to 72.01(6)°, the average F_t–Sn3–F_b angle is 90.00(7)° (average F14–Sn3–F_b, 90.86(7)°; average F15–Sn3–F_b, 89.13(7)°) and the F14–Sn3–F15 bond angle equals to 176.83(7)°. These parameters are in perfect agreement with the 72°, 90°, and 180° angle values required by the ideal D_{5h} symmetry. Despite the inequality of bond lengths, the O_h symmetries of the Sn1 and Sn2 coordination spheres are also well reproduced by means of angular demands, with cis F–Sn1–F' angles ranging from 88.21(8)-92.36(7)° and trans F–Sn1–F in the 177.30(6)-178.15(10)° range. The analogous parameters observed for Sn2 are similar, 85.89(9)-92.43(8)° and 176.54(6)-179.11(10)°.

The equatorial F atoms comprising the pentagonal base of $Sn3F_7$-units are further connected to four octahedral assemblies (vertex-sharing with two $Sn1F_6$- and two $Sn2F_6$-units) and to another $Sn3F_7$-unit, as shown in Figure 4.41.

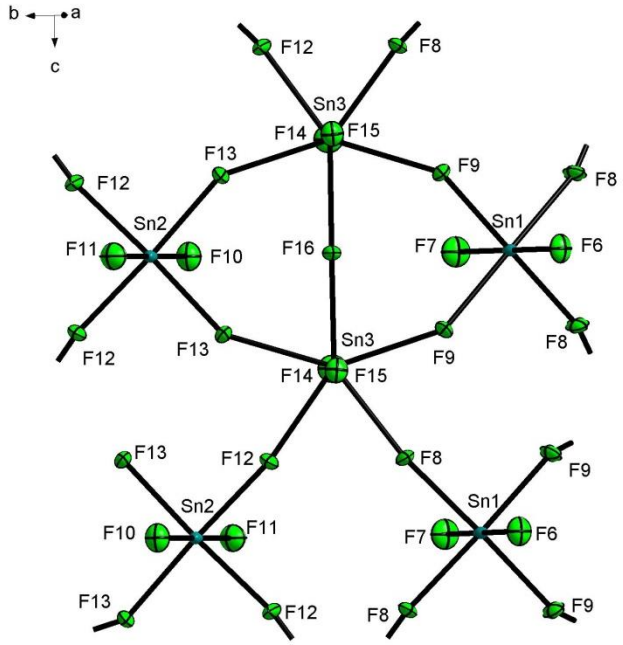


Figure 4.41: Extended coordination environment of the $(Sn3)F_2F_{5/2}$ –unit. HF molecules are omitted for clarity; the probability of the thermal ellipsoids is 50 %. Broken-off bonds denote further connections.

Similarly, each octahedral SnF_6-unit is in turn further connected through single μ-F bridges to four nearest $(Sn3)F_2F_{5/2}$ –units. In this way, all three crystallographically unique polyhedra form a complex 2-D network parallel to the *bc*-plane (Figure 4.42). Two types of trimeric and two types of tetrameric rings can be found comprising polygons of different size and shape. The Sn atoms form an undulated plane net (Figure 4.42) with vertex configurations $[3.4^3]$ (Sn1 and Sn2) and $[3^2.4^3]$ (Sn3). Other important bond lengths and angles associated to the cation and anion are given in Table 4.16.

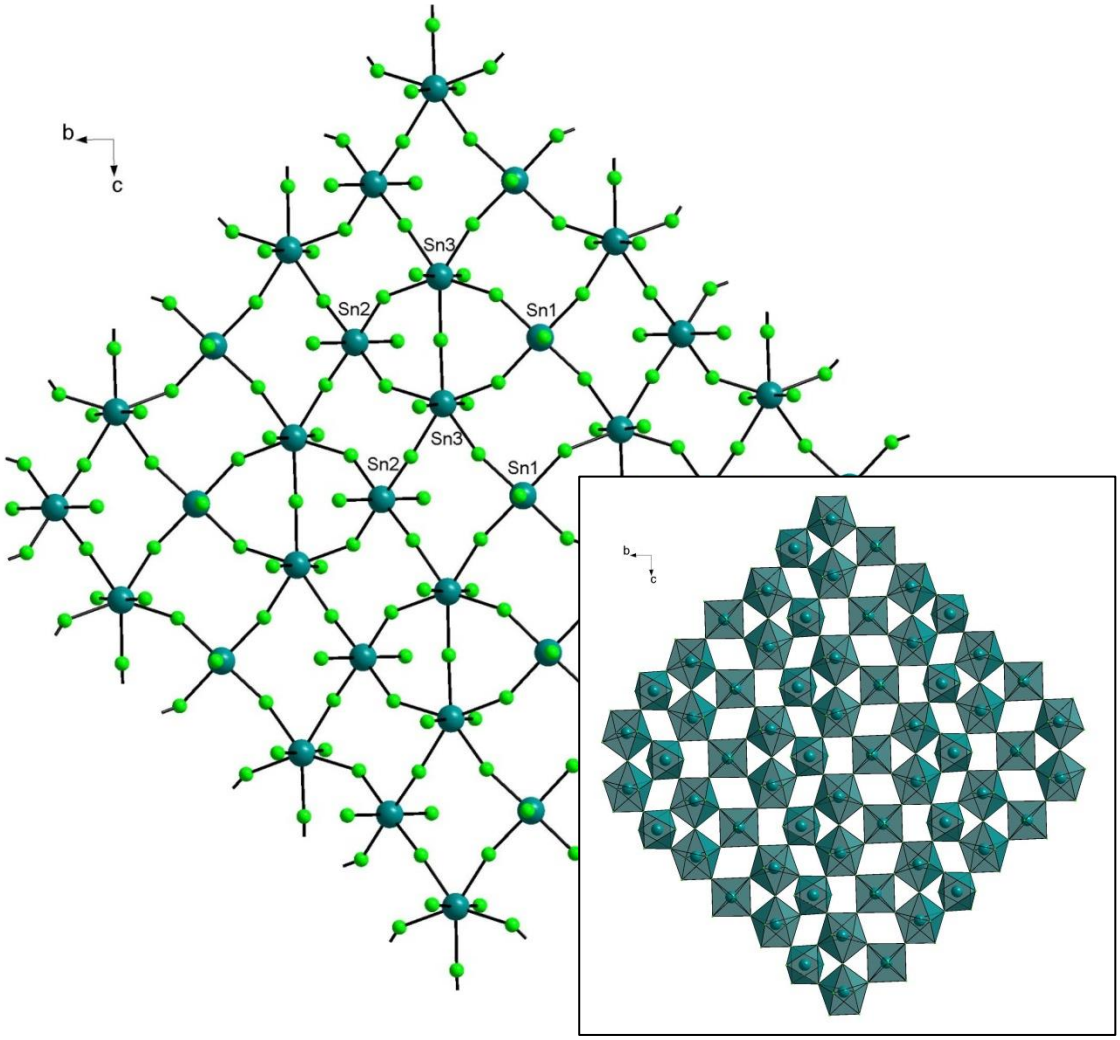


Figure 4.42: The $^{2}_{\infty}[(Sn_4F_{17})^{-}]$ anion found in $[Xe_2F_3][Sn_4F_{17}]\cdot XeF_2\cdot HF$ exhibits a layered structure of vertex-sharing octahedral and pentagonal bipyramidal units.

Table 4.16: Selected geometric parameters for the compound $[Xe_2F_3][Sn_4F_{17}]\cdot XeF_2\cdot HF$.

Bond Lengths (Å)			
Xe1—F1^{i}	2.1425 (9)	Sn2—F12	2.0030 (14)
Xe1—F2	1.9108 (17)	Sn2—F12^{iii}	2.0030 (14)
Xe2—F3	1.988 (2)	Sn2—F13^{iii}	2.0073 (14)
Xe2—F4	1.991 (2)	Sn2—F13	2.0073 (14)
Sn1—F6	1.877 (2)	Sn3—F8^{i}	2.1006 (14)
Sn1—F7	1.899 (2)	Sn3—F9	2.1126 (14)
Sn1—F8	1.9909 (14)	Sn3—F12	2.0882 (14)

Sn1—F8^{ii}	1.9909 (14)	Sn3—F13^{iv}	2.0997 (14)
Sn1—F9	2.0043 (14)	Sn3—F14	1.8705 (16)
Sn1—F9^{ii}	2.0043 (14)	Sn3—F15	1.8731 (15)
Sn2—F10	1.880 (2)	Sn3—F16^{ii}	2.0716 (2)
Sn2—F11	1.882 (2)	F5—H5	0.95 (2)
Bond Angles (°)			
F2—Xe1—F1^{i}	175.13 (11)	F13—Sn2—F12	176.54 (6)
F4—Xe2—F3	179.91 (11)	F13^{iii}—Sn2—F13	92.43 (8)
F7—Sn1—F6	178.15 (10)	F9—Sn3—F8^{i}	70.88 (6)
F8^{ii}—Sn1—F6	92.36 (7)	F12—Sn3—F8^{i}	72.25 (6)
F8—Sn1—F6	92.36 (7)	F12—Sn3—F9	143.10 (6)
F8—Sn1—F7	88.97 (7)	F13^{iv}—Sn3—F8^{i}	143.87 (6)
F8^{ii}—Sn1—F7	88.97 (7)	F13^{iv}—Sn3—F9	144.98 (6)
F8—Sn1—F8^{ii}	88.21 (8)	F13^{iv}—Sn3—F12	71.88 (6)
F9—Sn1—F6	89.99 (7)	F14—Sn3—F8^{i}	91.04 (7)
F9^{ii}—Sn1—F6	89.99 (7)	F14—Sn3—F9	90.22 (7)
F9—Sn1—F7	88.72 (7)	F14—Sn3—F12	88.95 (7)
F9^{ii}—Sn1—F7	88.72 (7)	F14—Sn3—F13^{iv}	92.54 (7)
F9—Sn1—F8	90.37 (6)	F15—Sn3—F8^{i}	86.19 (6)
F9—Sn1—F8^{ii}	177.30 (6)	F15—Sn3—F9	90.33 (6)
F9^{ii}—Sn1—F8^{ii}	90.37 (6)	F15—Sn3—F12	88.73 (7)
F9^{ii}—Sn1—F8	177.30 (6)	F15—Sn3—F13^{iv}	88.80 (6)
F9—Sn1—F9^{ii}	90.97 (8)	F15—Sn3—F14	176.83 (7)
F11—Sn2—F10	179.11 (10)	F16^{ii}—Sn3—F8^{i}	143.31 (7)
F12^{iii}—Sn2—F10	89.90 (7)	F16^{ii}—Sn3—F9	72.51 (7)
F12—Sn2—F10	89.90 (7)	F16^{ii}—Sn3—F12	144.39 (7)
F12—Sn2—F11	90.75 (7)	F16^{ii}—Sn3—F13^{iv}	72.52 (7)
F12^{iii}—Sn2—F11	90.75 (7)	F16^{ii}—Sn3—F14	91.53 (8)
F12—Sn2—F12^{iii}	85.89 (9)	F16^{ii}—Sn3—F15	91.62 (8)
F13^{iii}—Sn2—F10	88.99 (7)	Xe1—F1—Xe1^{i}	153.50 (19)

F13—Sn2—F10	88.99 (7)	Sn3^{i}—F8—Sn1^{ii}	163.87 (9)
F13^{iii}—Sn2—F11	90.40 (7)	Sn3—F9—Sn1^{ii}	143.45 (8)
F13—Sn2—F11	90.40 (7)	Sn3—F12—Sn2^{iii}	161.62 (9)
F13^{iii}—Sn2—F12^{iii}	176.54 (6)	Sn3^{v}—F13—Sn2^{iii}	145.02 (8)
F13^{iii}—Sn2—F12	90.83 (6)	Sn3—F16—Sn3^{ii}	178.16 (13)
F13—Sn2—F12^{iii}	90.83 (6)		

Symmetry codes: (i) *x*, −*y*+1/2, −*z*+1; (ii) *x*, *y*, −*z*+1/2; (iii) *x*, *y*, −*z*+3/2; (iv) −*x*, −*y*+1, *z*−1/2; (v) −*x*, −*y*+1, *z*+1/2.

Moreover, an interesting wave-like pattern can be observed immediately after positioning the polyanionic structure shown in Figure 4.42 into view along the *c*-axis. The small gradual elevation and descent give rise to a regular undulating layer, reminiscent of a sine wave. Thus, a selected series of atoms, besides being generated by symmetry operations as discrete points, also lie on a continuous periodic function, which can be described with a mathematical model. Details on the sinusoidal approximation are given in Appendix C.1.2.

$$x(y) = 0.27598\, sin(6.28505y)$$

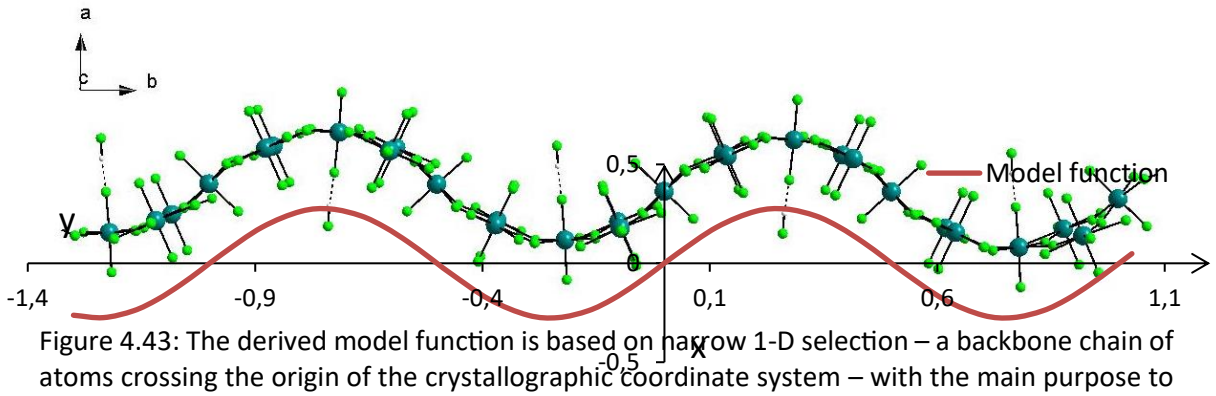


Figure 4.43: The derived model function is based on narrow 1-D selection – a backbone chain of atoms crossing the origin of the crystallographic coordinate system – with the main purpose to show the surprising wave nature of the polymeric anion. The *x* and *y* variables in the calculated equation denote fractional atomic coordinates. Since the wave propagation of the stacked anionic layers along the *ab*-plane can be mathematically described as an "in phase" fluctuation, the model function for each layer can be derived simply by adding the vertical offset to the (original) equation given above.

The initial rise at the foothill of each layered network is enabled by bridging Sn3^{i}–F8–Sn1^{ii} (163.87(9)°) and Sn3–F9–Sn1^{ii} (143.45(8)°) angles, while the opposing curvature beyond the inflection point results from Sn3–F12–Sn2^{iii} (161.62(9)° and Sn3^{v}–F13–Sn2^{iii} (145.02(8)°. Only the $Sn3F_7$-units are linked transversely along the crystallographic *c*-axis with almost linear μ-F16 bridges (Sn3—F16—Sn3^{ii}, 178.16(13)°).

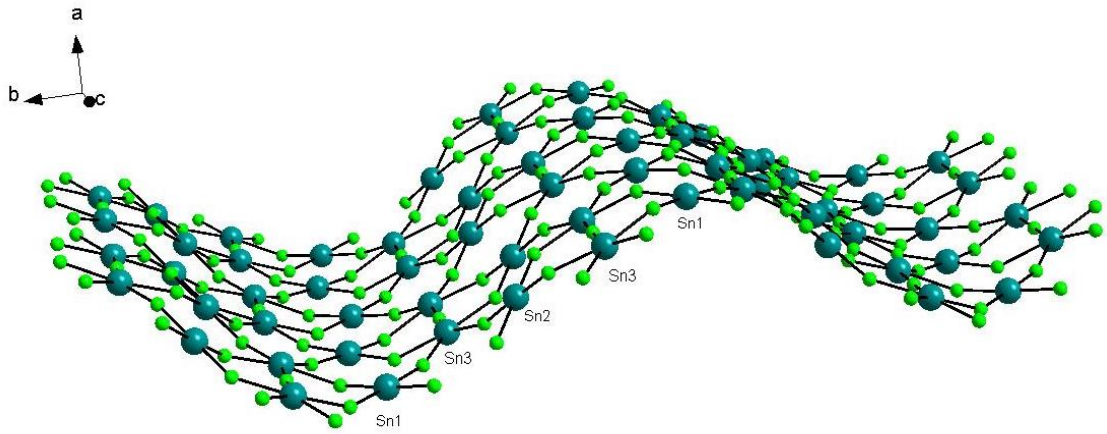


Figure 4.44: The wave-like 2-D structure of the polymeric $[Sn_4F_{17}]^-$ anion found in $[Xe_2F_3][Sn_4F_{17}]\cdot XeF_2\cdot HF$. Terminal F atoms are omitted for clarity.

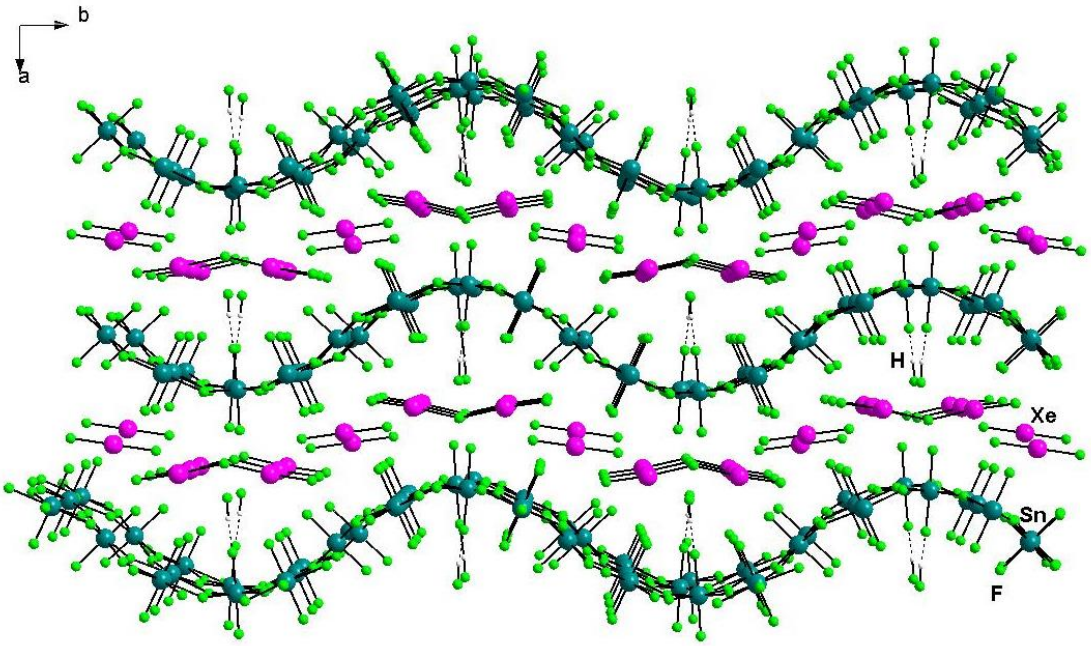


Figure 4.45: Layered structure of $[Xe_2F_3][Sn_4F_{17}]\cdot XeF_2\cdot HF$.

A continuous layered void of steady thickness (interlayer spacing: Sn···Sn distance ~9.4 Å, F–F distance ~5.6 Å) A is maintained between the neighboring anionic networks, interrupted only by F7···H5F5 moieties (F7···H5 distance: 1.58 Å; F7···F5 distance: 2.53 Å, F7···H5–F5 angle: 176(2)°) pointing perpendicularly into the voids. Confined in this space, a network of $Xe_2F_3^+$ cations and co-crystallized XeF_2 molecules alternate their positions, roughly following the wave-like pattern of the anionic layers. The resulting unique crystal structure is shown in Figure 4.45.

Moreover, several long intermolecular interactions between the cations, fluoridostannate(IV) networks, HF and XeF_2 molecules are found within the sum of the F and Xe van der Waals radii (3.63 Å).[77] The secondary coordination spheres of both crystallographically independent Xe atoms are depicted in Figure 4.46 and Figure 4.47, while the associated contact distances are summarized in Table 4.17.

Table 4.17: Xe1 and Xe2 coordination environment in the compound $[Xe_2F_3][Sn_4F_{17}]\cdot XeF_2\cdot HF$.

Bonds and Contacts (Å)			
Xe1		Xe2	
Xe1–F1	**2.1425(9)**	**Xe2–F3**	**1.988(2)**
Xe1–F2	**1.911(2)**	**Xe2–F4**	**1.991(2)**
Xe1–F3	3.117(1)	Xe2—F15''	3.183 (2)
Xe1–F4	3.181(1)	Xe2—F15''	3.183 (2)
Xe1–F14'	3.197(2)	Xe2—F10	3.233 (2)
Xe1-F15	3.299(1)	Xe2-F2''	3.406(2)
Xe1-F11'	3.495(2)	Xe2-F2''	3.406(2)
Xe1-F5''	3.509(3)	Xe2-F2	3.487(2)
Xe1-F5'	3.523(2)	Xe2-F2	3.487 (2)
Xe1-F6'	3.536(1)	Xe2-F15	3.559(2)
F2–Xe2'	3.406(2)	Xe2-F15'	3.559(2)
F2–Xe2	3.487(2)	F3-Xe1''	3.117(1)
		F3-Xe1''	3.117(1)
		F4-Xe1'	3.181(2)
		F4-Xe1	3.181(2)

Symbols (' and '') denote symmetrically generated atoms.

Among the atoms residing on special positions, the Xe is the only one lying on a 2-fold rotational axis, which symmetrically completes the $Xe_2F_3^+$ cation. Its expected V-shaped geometry is given by the Xe1–F1–Xe1^i bond angle (153.5(2)°), which is intermediate between the two extremes defining the large variation of this angle among the $Xe_2F_3^+$ salts determined thus far (ranging from 139.8(8)° in trigonal $[Xe_2F_3][AsF_6]$ to 164.3(3)° in $[Xe_2F_3][Ti_8F_{33}]$). The F2–Xe1–F1^i moieties are slightly more bent (175.13(11)°) than the essentially linear F_b–Xe–F_t arrangements observed in other $Xe_2F_3^+$ cations (~177-179°), while the F_b–Xe (F1-Xe1, 2.1425(9) Å) and Xe–F_t (Xe1-F2, 1.911(2) Å) bond lengths compare well with the corresponding values reported in the literature.

Each $Xe_2F_3^+$ cation provides sixteen long Xe…F intermolecular contacts ranging from 3.117 to 3.536 Å; four to two HF molecules, four to four "free" XeF_2 molecules and eight reaching the anionic layers (four interactions on each side of the cation along the *a*-axis). The strongest Xe···F contacts (3.117 and 3.181 Å) are observed with the neighboring XeF_2 molecules, which are additionally linked by the cation through four F2···Xe2 interactions (3.406-3.487 Å) arising from both terminal fluorine atoms of the $Xe_2F_3^+$.

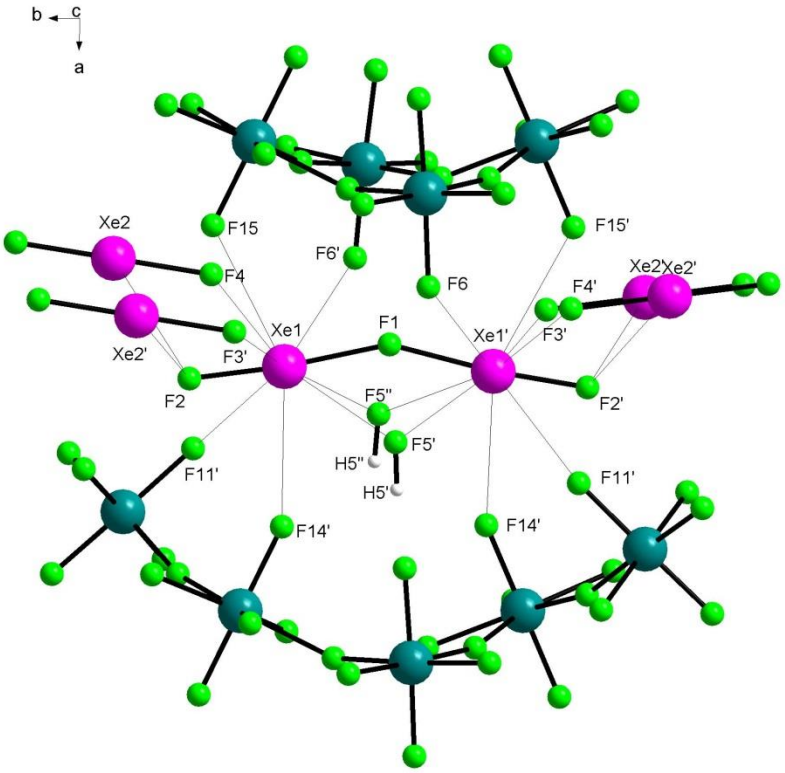


Figure 4.46: Coordination environment of the $Xe_2F_3^+$ cation in $[Xe_2F_3][Sn_4F_{17}]\cdot XeF_2\cdot HF$. Long contacts lying within the sum of the F and Xe van der Waals radii (3.63 Å) are drawn as thin bonds.

Similarly as in $(XeF_2\cdot TiF_4)_2\cdot XeF_2$, the "free", co-crystallized molecules of XeF_2 essentially retain the geometric parameters of pure solid XeF_2 (linear (F-Xe-F, 180°) geometry with two equidistant Xe–F bonds (Xe-F, 1.999(4) Å) and eight equidistant long Xe···F contacts (3.338 Å) in a symmetrical arrangement), with F4—Xe2—F3 angle measuring 179.91(11)° and nearly equal Xe-Ft bond lengths (Xe2-F3, 1.988(2) Å; Xe2-F4, 1.991(2) Å). The XeF_2 molecule in $[Xe_2F_3][Sn_4F_{17}]\cdot XeF_2\cdot HF$ exhibits a rich coordination environment with nine Xe2···F contacts ranging from 3.183 to 3.559 Å and 4 additional long contacts from terminal F3 and F4 atoms to 4 nearest $Xe_2F_3^+$ cations (in 3.117-3.181 Å range). Five Xe2···F interactions connect two stacked anionic layers, while four additional Xe2···F2 contacts (3.406-3.487 Å) link the XeF_2 molecules and $Xe_2F_3^+$ cations into a 2-D network in an infinite array (Figure 4.48).

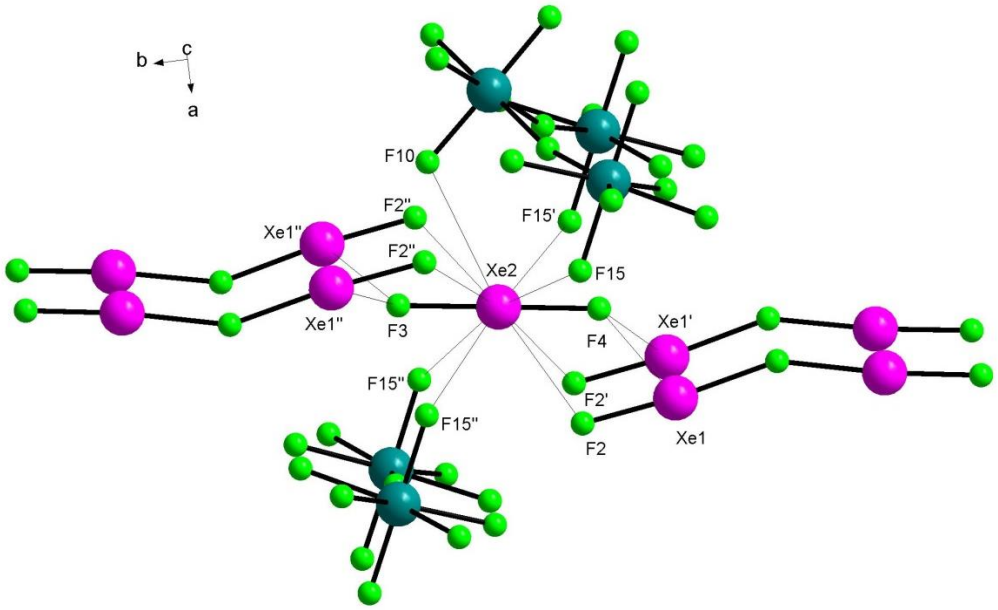


Figure 4.47: Coordination sphere of the XeF_2 molecule in the crystal structure of $[Xe_2F_3][Sn_4F_{17}]\cdot XeF_2\cdot HF$. Thin bonds denote long intermolecular contacts.

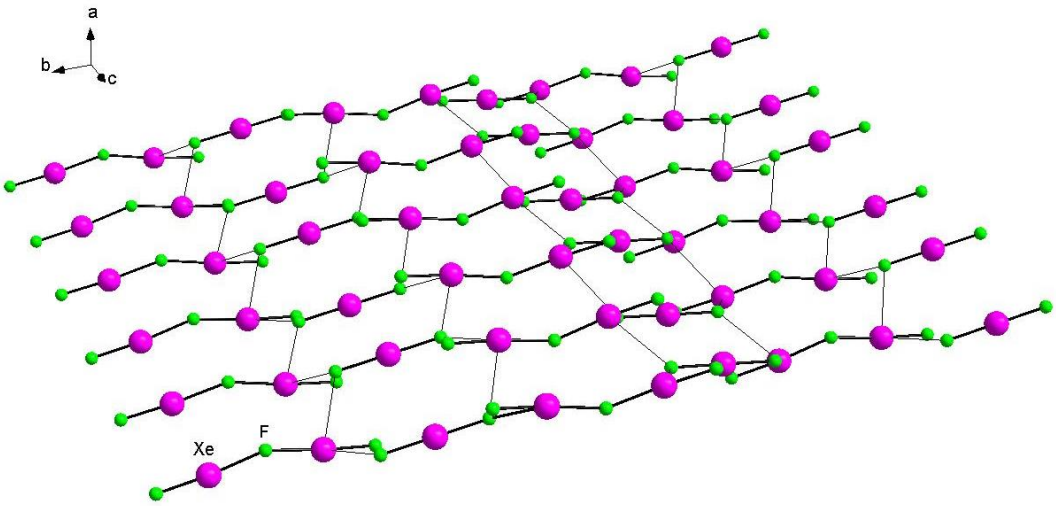


Figure 4.48: Cationic $\{Xe_2F_3^+ \cdots XeF_2\}$ networks follow the wave-like pattern between anionic layers in compound $[Xe_2F_3][Sn_4F_{17}]\cdot XeF_2\cdot HF$. Long interactions are depicted with thin bonds.

The interactions between NgF_2 molecules and $Ng_2F_3^+$ cations have already been observed in crystal structures of $[Kr_2F_3][SbF_6]\cdot KrF_2$, $[Kr_2F_3]_2[SbF_6]_2\cdot KrF_2$ and $[Xe_2F_3][RuF_6]\cdot XeF_2$. In both krypton salts, it was concluded that the effects of secondary contacts on the geometries of the $Kr_2F_3^+$ cations are difficult to assess, but their angular distribution is generally consistent with avoidance of the three valence lone pair domains of krypton. In all three aforementioned compounds, however, the molecules forming a complex 3-D network through long contacts which are more or less randomly oriented, usually in perpendicular mutual arrangements, in contrast with the ordered 2-D networks of $Xe_2F_3^+$ and XeF_2 units in $[Xe_2F_3][Sn_4F_{17}]\cdot XeF_2\cdot HF$, where their alignment is sterically forced by the anionic layers.

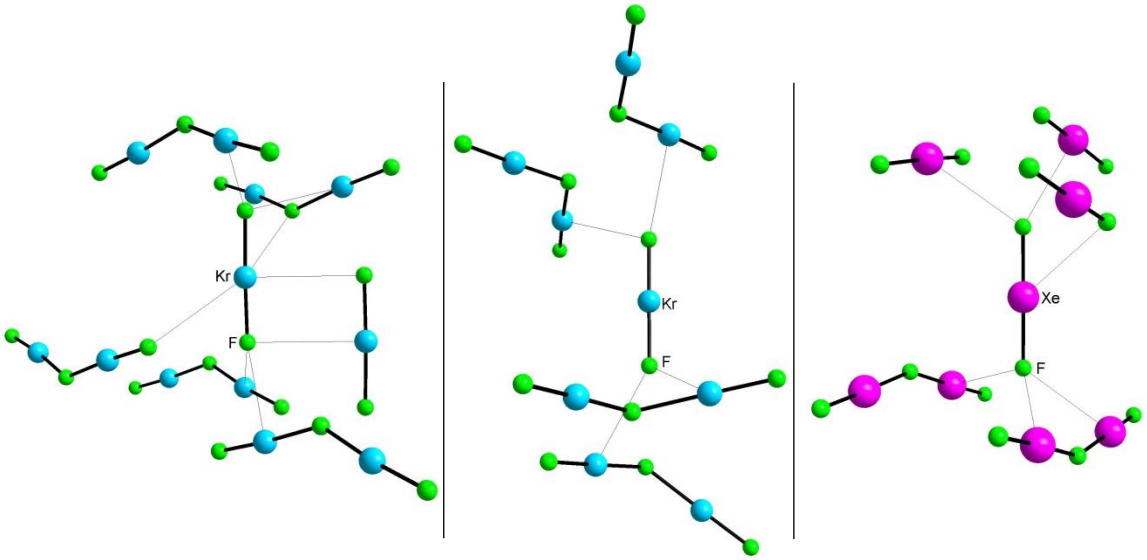


Figure 4.49: Comparison of $Ng_2F_3^+\cdots NgF_2$ contacts (only NgF_2 secondary spheres are shown) found in analogous compounds $[Kr_2F_3][SbF_6]\cdot KrF_2$ (*left*), $[Kr_2F_3]_2[SbF_6]_2\cdot KrF_2$ (*middle*) and $[Xe_2F_3][RuF_6]\cdot XeF_2$ (*right*).

Similarly as in $[Xe_2F_3][Ti_8F_{33}]$, the association into larger anionic associates in $[Xe_2F_3][Sn_4F_{17}]\cdot XeF_2\cdot HF$ considerably increases the F^- accepting strength of the parent Lewis acid, Sn_4F_{16}. A closer look at Figure 4.41 reveals that the one net negative charge of $[Sn_4F_{17}]^-$ anion can be found dispersed over tetrameric $\{(Sn(3)F_2F_{5/2})^{0.5-}(Sn(2)F_2F_{4/2})(Sn(3)F_2F_{5/2})^{0.5-}(Sn(1)\ F_2F_{4/2})\}$ ring fragments, which surprisingly offers enough stabilization to sustain the cationic $Xe_2F_3^+$ species.

The incorporation of XeF_2 and HF solvates into the crystal lattice of the firstly formed XeF_2-poorer compound obviously facilitates the dissolution and is necessary for crystallization of such strongly networked large polyanions from the polar solvent aHF. A very large excess of XeF_2 is needed to force this process, which also explains why, despite correct and successful synthetic approaches, all structural characterization attempts thus far have failed, as were unable to deliver products of sufficient crystal size and quality.

The compound $[Xe_2F_3][Sn_4F_{17}]\cdot XeF_2\cdot HF$ was additionally characterized by Raman spectroscopy. The spectrum shown in Figure 4.50 was obtained on a single crystal (with checked unit-cell parameters) immersed in perfluorodecalin, only seconds before the protective layer evaporated, thus exposing the sample to moist air. In a limited time window, only the most important 400-800 cm^{-1} range measurement has been efficiently performed before the compound decomposed. The Raman spectrum in a 50-800 cm^{-1} range recorded through a thicker layer of protective oil is given in Figure C. 1 (Appendix C.1.1), where the sample signals are significantly overlapped with band lines of the perfluorinated liquid used.

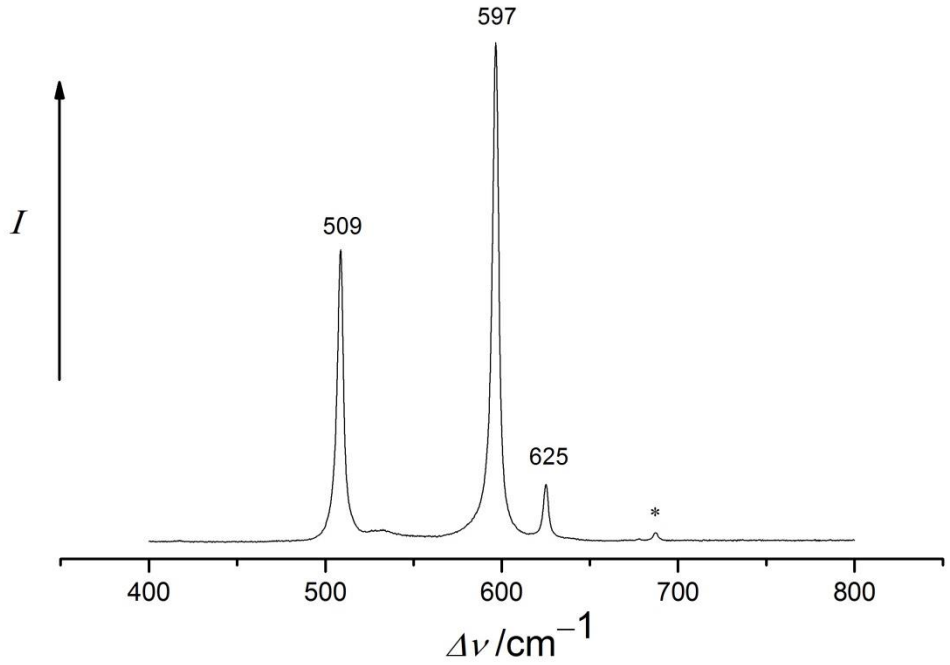


Figure 4.50: Raman spectrum of $[Xe_2F_3][Sn_4F_{17}]\cdot XeF_2\cdot HF$ recorded on a single crystal under a thin protective layer of perfluorinated liquid (peak denoted by asterisk(*)) at room temperature.

The Raman spectrum of $[Xe_2F_3][Sn_4F_{17}]\cdot XeF_2\cdot HF$ is dominated by an intense line at 597 cm^{-1}, which can be readily assigned to the Xe−F_t stretching frequency of the $Xe_2F_3^+$ cation (typically found in the 575–600 cm^{-1} region)[120,121,122,**Error! Bookmark not defined.**]. Similarly, the strong band at 509 cm^{-1} belongs undoubtedly to the Xe-F stretching mode of the weakly associated XeF_2, while the peak at 625 cm^{-1} can be attributed to the Sn−F_t stretching vibrations of the $[Sn_4F_{17}]^-$ anion.

Thermal solid-state reactions between XeF_2 and SnF_4 were studied adopting a similar experimental approach as used for thermal runs in the XeF_2-TiF_4 system (see Chapter 4.1). The reactions employing different starting XeF_2 : SnF_4 molar ratios (1:2, 1:1, 2:1 and 5:1) were carried out at 135 °C and the products were screened by Raman spectroscopy upon cooling the reaction mixture to 29 °C with a cooling rate of 2 °C/h. The 1:2 initial ratios and equimolar runs always resulted in white SnF_4 powder (unreacted XeF_2 easily diffused through the FEP walls at high temperatures). A two-fold excess of XeF_2 was necessary in order to obtain a synthetic product, which was, according to the Raman spectroscopy, identified as the 3:4 phase reported[270] previously. The same compound also formed with the highest XeF_2 : SnF_4 (1:5) ratio tested. The Raman spectrum is given in Figure 4.51.

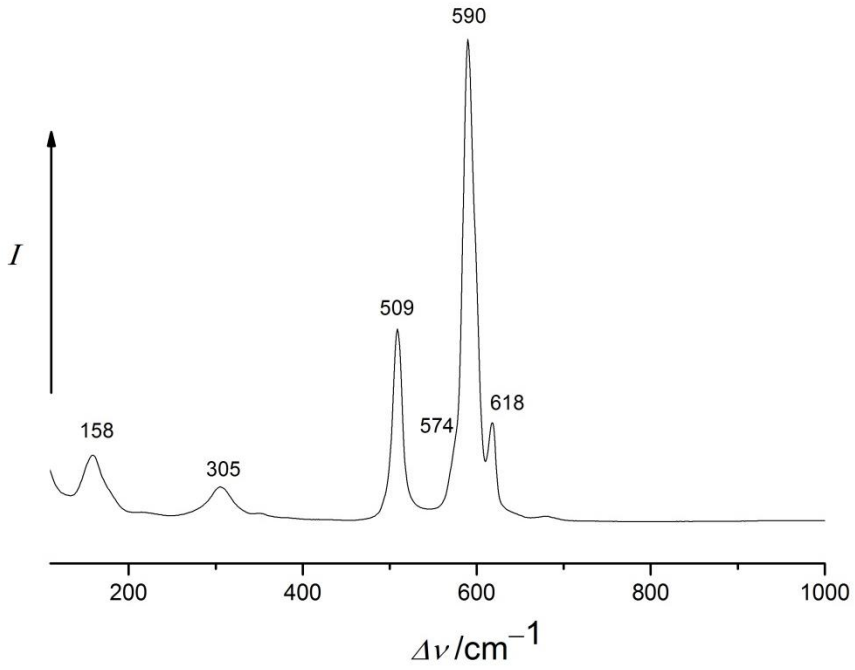


Figure 4.51: The Raman spectrum of thermally obtained XeF_2-rich product corresponds to the $3XeF_2{\cdot}4SnF_4$ phase reported previously.

The solved crystal structure is in excellent agreement with the formulation proposed previously[270], describing the $3XeF_2{\cdot}4SnF_4$ phase as $XeF_2{\cdot}(XeF_2{\cdot}2SnF_4)_2$. Taking into account that the aforementioned study was performed in XeF_2 melt, thus without HF, their formulation defines exactly $[Xe_2F_3][Sn_4F_{17}]{\cdot}XeF_2$. Since the two major Raman lines reported (and reproduced within this work) for 3:4 differ from the spectrum of $[Xe_2F_3][Sn_4F_{17}]{\cdot}XeF_2{\cdot}HF$, it is difficult to confidently assume that this formulation best describes the reported thermally obtained unsolvated product as well. Although the band at 619 cm^{-1} (or 618 cm^{-1} obtained in this study) belongs probably to unreacted SnF_4 (Figure C. 2, Appendix C.1.1), the negative shift of the Xe–F mode from 597 cm^{-1} to 588 cm^{-1} (or 590 cm^{-1}, see Figure 4.51), indicative of a lower degree of XeF_2 ionization, still needs to be addressed.

Moreover, the authors correctly predicted the presence of a polymeric anion, resembling the noble metal MF_4 (M = Ir, Rh, Pd) structures[144] with corner sharing octahedra, and also left open the possibility for discrete species, expecting the simplest of which to be $[Sn_8F_{36}]^{4-}$. Interestingly, an analogous $[Mn_8F_{36}]^{4-}$ anion was observed recently in the compound $[XeF_5]_4[Mn_8F_{36}]$ (phase $XeF_5{\cdot}2MnF_4$)[224].

Although the stability of a coordination bond X→M increases with the atomic number of M: Si<Ge<Sn<Pb, which also reflects in higher coordination numbers due to an increase of its steric accessibility[271], attempts, even with large excess of XeF_2 (200 mg, 1.18 mmol) over PbF_4 (36 mg, 0.127 mmol) in aHF (0.6 ml), failed and only the Raman spectrum (Figure 4.52) of the starting tetrafluoride was obtained after stirring the reaction suspension for several hours at room temperature. Despite having the same layered structure like SnF_4, the molecular solubility of PbF_4 seems to be negligible in aHF at room temperature, while the fluoride donor strength of XeF_2 is obviously too low to enable the dissolution of PbF_4 into any anionic form.

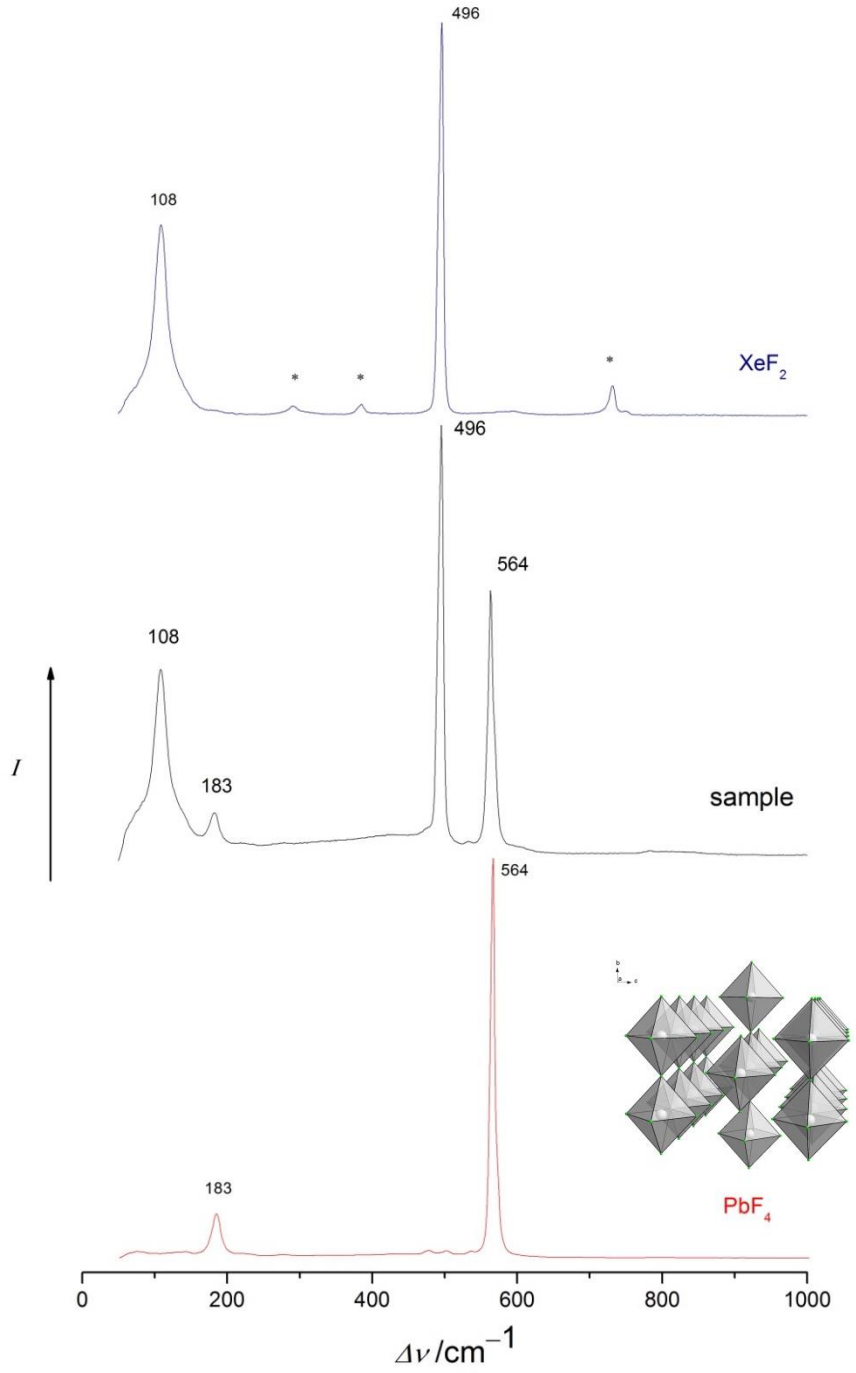


Figure 4.52: Raman spectroscopy analysis of a synthetic attempt (middle spectrum) in the system XeF_2 – PbF_4. Peaks arising from FEP sample tube are denoted by asterisks (*).

4.2.3 $XeF_2 \cdot 2SnF_4$

4.2.3.1 Reactions in Anhydrous HF

The product having the lowest solubility in aHF in principle precipitates first from its aHF-solution. The corresponding phase in the XeF_2 – SnF_4 system is most probably the 1:2 compound, which suddenly forms in diluted solutions of XeF_2 and SnF_4 in aHF as a white poorly crystalline suspension. After sedimentation, the precipitate can be isolated by decanting the remaining aHF

– XeF_2 solution into the side arm of a T-reactor and pumping off all volatiles in the next step. According to the results from the Raman spectroscopy, the same compound forms in a solventless degradation already below room temperature from the parent XeF_2-rich 3:4 phase in dynamic vacuum.

The Raman spectrum given in Figure 4.53 was recorded on a product sample prepared from XeF_2 (56 mg, 0.33 mmol) and SnF_4 (65 mg, 0.33 mmol) in aHF (0.9 mL), by isolating the precipitate as described above. The obtained spectrum corresponds to the one reported for the 1:2 phase (Table 4.14 in Section 4.2.1 Background). The X-ray powder diffraction analysis of this sample (Figure 4.54) shows a considerable amount of reactants in the reaction mixture. Although the crystal structure determination from PXRD was not attempted at that time, comparison with the simulated powder pattern of $[Xe_2F_3][Sn_4F_{17}]\cdot XeF_2\cdot HF$ structure shows a notable structural relationship.

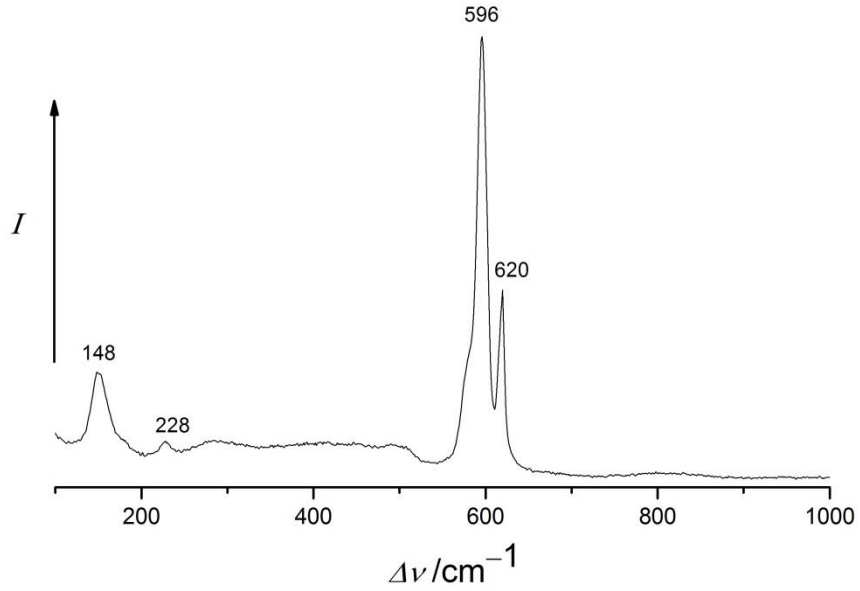


Figure 4.53: The Raman spectrum of the white product, which precipitates first from XeF_2-SnF_4 systems of diluted aHF solutions, indicates the previously reported 1:2 phase and the presence of initial SnF_4 (lines 228 cm^{-1} and 620 cm^{-1}, Figure C. 2, Appendix C.1.1).

More than two-hundred experimental attempts were carried out in order to obtain single crystals of 1:2 of sufficient crystal quality. For this purpose, besides aHF, SO_2ClF and mixtures of aHF/SO_2ClF in different volume ratios were unsuccessfully employed, giving only amorphic or poorly crystalline material, while crystallizations from BrF_5 afforded only XeF_2 crystals from the clear supernatant.

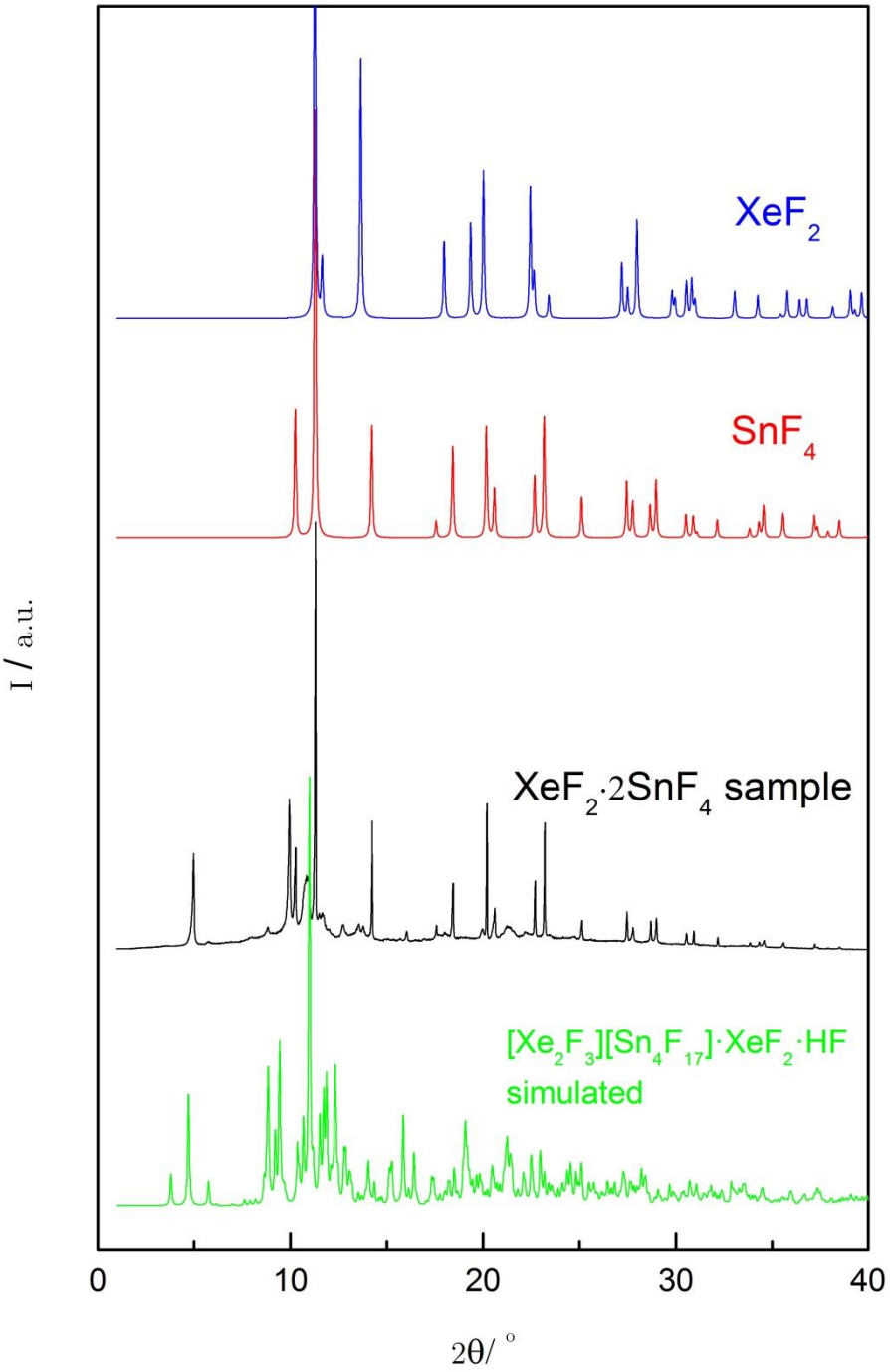


Figure 4.54: X-ray powder diffractograms of the reactants, powdered sample[‡] of $XeF_2 \cdot 2SnF_4$ and simulated diffraction pattern of $[Xe_2F_3][Sn_4F_{17}] \cdot XeF_2 \cdot HF$.

In the first report on the existence of xenon(II) fluoridostannates(IV), the authors proposed the 3:4 to be a molecular adduct between XeF_2 and the 1:2 compound and based their assumption on the similarity between the vibrational spectra of both compounds, which differed only in the prominent Raman band at 509 cm^{-1} and strong IR band at 530 cm^{-1}, tentatively assigned to the symmetric and asymmetric stretching vibration of weakly associated molecular XeF_2. However, in this case, it is unlikely to obtain meaningful structural data only by

[‡] PXRD measurements were performed at the Department of Chemistry, Durham University (UK), on a Bruker D8 Advance diffractometer using Mo *Kα* radiation (λ = 0.7093187 Å), a step size of 0.01° and scan step time of 12.3384 s. The diffraction patterns were recorded in the range 2θ = 1-50° (total scan time 17 h 8 min 12 s).

comparisons, since the original bands are overlapped with the initial SnF_4, which indicates a partial decomposition or incomplete reaction. Similar difficulties have been encountered in product mixtures from the isolated bulk precipitates from aHF solutions, possibly as a result of an observed equilibrium present between different phases and the reactants.

4.2.3.2 Reactions in Liquid Xenon

The structural determination of noble gas compounds often depends on an efficient experimental route to single crystals, where the aggressiveness, reactivity and oxidizing power of these products severely restrict the choice of a suitable solvent for this purpose to a few inorganic (mainly BrF_5, IF_5, aHF, XeF_2 and SO_2ClF) and in some cases organic (CH_3CN, fluorotrichloromethane, etc.) liquids. Nevertheless, several noble gas complexes, especially those with large polyionic parts[205], remain insoluble in the abovementioned solvents. After numerous unsuccessful attempts with $XeF_2 \cdot 2MF_4$ (M = Mn, Ti, Sn) phases, it was clear that a new approach is required in order to overcome the elusiveness of this type of compounds. The efficient application of SF_6 as a recrystallization medium delivering ruby-red single crystals of $XeF_2 \cdot 2CrF_4$ (the structural determination of which revealed a complex 3-D network, Figure A. 1 in Appendix A.1) within two days under supercritical conditions, inspired the herein described experimental study aiming to explore the solvent capabilities of liquid and near-supercritical xenon on the phase $XeF_2 \cdot 2SnF_4$.

After methods have been worked out for the purification of xenon and techniques have been developed for its use in technology and medicine, the idea of using liquefied noble gases, especially xenon, as spectroscopic solvents began already in the fifties[278] and evolved in the subsequent decades with a few studies on a small-molecule solutes, like hydrogen halides[279,280], which were limited to a narrow temperature range around the xenon melting point. Later in 1981, the experimental evidence[281] in the form of UV, visible, IR and NMR spectra proved that liquid xenon can be used as a fluid solvent for several biological and organic molecules in a wide temperature range from near RT to almost –100 °C.

Among the noble gases, elemental xenon is particularly useful because its liquid phase occurs in the fairly convenient conditions of 16 °C and 58 atm (Figure 4.55) so that solubility studies can be carried out near RT. Xenon also exhibits a polarizability of $4.01 \cdot 10^{-24}$ cm^3,[282] which is relatively large when compared to the other rare gases[281]. Thus, xenon is a very weakly coordinating inert solvent and very different to the polar solvent aHF. Xenon did not possess distinct properties of cleaving polar covalent, nor ionic bonds. Moreover, because of its optical transparency in most of the vacuum UV and all of the UV, visible and IR spectral regions, spectra may be recorded in xenon over a very wide spectral range, leaving the character of the molecular environment intact.[283] In addition, change in spectral features arising from environmental change, solvent fluorescence or spectral interference, is also avoided, which enables well resolved and intense spectra to permit vibrational assignments and kinetic studies with visible, UV, Raman and NMR spectroscopy even at low solubility[284]. Soon after the discovery of solvent properties of liquid xenon, many experiments were done to determine the solubility of various organic substances in liquid and supercritical Xe (T_c = 16 °C)[285], covering the pressure range of 60–95 atm at temperatures from 0 °C to 40 °C for liquid and 100–225 atm in a 34.9–45 °C range for supercritical conditions. The authors reported that large organic neutral species dissolved readily, while attempts to dissolve ion pairs or free ions failed.[284] In subsequent years, other research groups have continued using liquid[286,287,288,289] and supercritical[286,290] Xe as a solvent for chemical reactions.

However, the literature describing liquid and/or supercritical xenon used as a solvent for noble gas or inorganic compounds is so far limited to only some cryospectroscopic investigations of unsubstituted carbonyl dihydrogen complexes $M(CO)_5(H_2)$[286], organometallic noble gas complexes $M(CO)_5L$ (M = Cr, Mo, and W; L = Ar (W only), Kr, Xe, and CO_2)[290] and binary noble gas fluorides[291]. In addition, only a few papers[292,293,294] describe reactions with liquefied xenon in the role of a reactant-reducing agent or complex ligand giving novel noble gas compounds, though with very scarce information on the potential solvent effects.

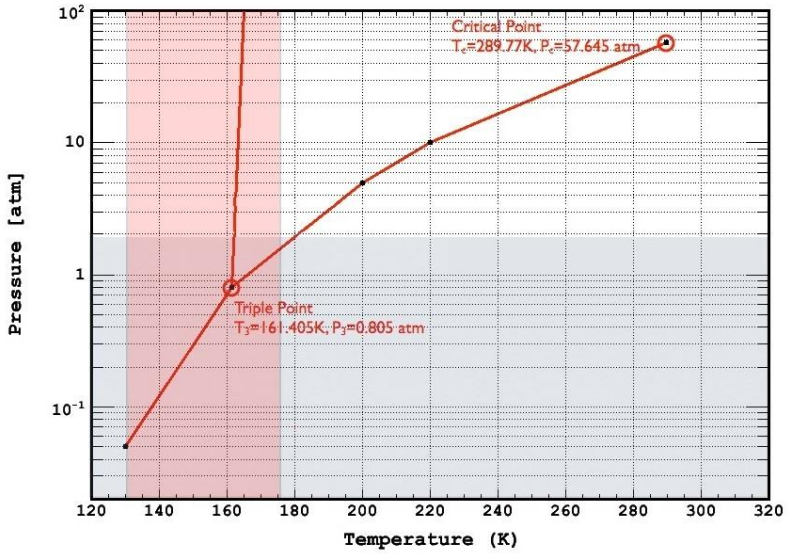


Figure 4.55: Xenon phase diagram. Adapted from Solid Xenon R&D Project by J. Yoo (FERMILAB, LBNL)[295].

An argon arc welded nickel pressure and weighing vessel (Figure 4.56a, volume 5.8 mL), equipped with a PTFE-packed nickel valve, was constructed and tested up to 110 atm for experiments with xenon under near supercritical conditions. For investigations with xenon between its melting (-112 °C) and boiling point (-108 °C), a reaction vessel was made of 16 mm i.d. (19 mm o.d.) FEP tubing and equipped with a PTFE valve and a PTFE-coated stirring bar. The volume of this vessel was 64 mL, which allowed 7.7 mmol of Xe to expand to ~3.5 atm at room temperature. A smaller reaction vessel (Figure 4.56b) was made of 3 mm i.d. (6 mm o.d.) thick-walled FEP tubing, also equipped with a metal-encased PTFE valve. This vessel (working volume 0.74 mL) was tested up to 45.4 atm and allowed experiments with liquid xenon (Figure 4.56c) in a temperature range from -112 °C to -19 °C (the maximum pressure effectively reached was 25 atm). All reaction vessels were passivated with 1100 torr F_2 for several hours prior to use. The transfer of all volatiles (aHF, Xe) was carried out by condensation under vacuum at –196 °C, using a PTFE/nickel vacuum line and system as described in the Methods section. Xenon gas was efficiently recuperated after each experimental run and reused.

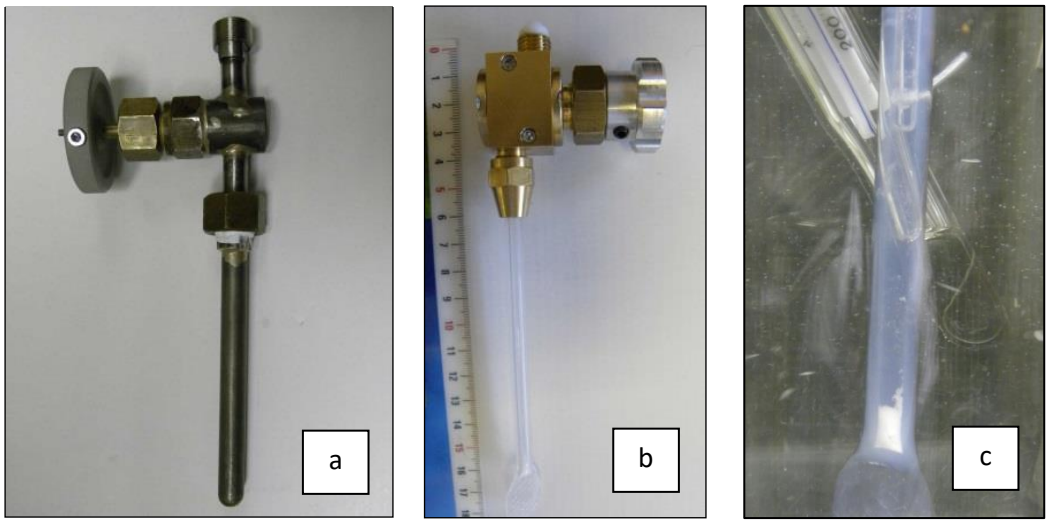


Figure 4.56: a – Nickel vessel for experiments in supercritical xenon. b – Thick walled FEP reaction vessel for studies in liquid xenon. c – Synthesis and sedimentation in liquid xenon viewed through a transparent Dewar flask filled with cold ethanol.

On 17 mg (0.03 mmol) of amorphous white $XeF_2 \cdot 2SnF_4$ (synthesized from XeF_2 and SnF_4 in aHF as described before), 6200 mg (47 mmol) of xenon was condensed reaching a solvent density of 1.07 g/cm^3 (ρ_c = 1.11g/cm^3)[296], which gave approximately 90 atm of pressure at RT. After 79 days, xenon was slowly pumped off at -20 °C and the reaction vessel was opened in the glovebox. A white, poorly crystalline material was accumulated on the top of the vessel and inside the PTFE valve. Attempts to isolate a suitable crystal for X-ray structural analysis were unsuccessful. The Raman spectrum of this material corresponded to the unaltered, starting compound $XeF_2 \cdot 2SnF_4$.

Before carrying out experiments with liquid xenon, the process of liquefying was studied at low temperatures and pressures in the long FEP reaction vessel in order to obtain a general impression on the behavior of xenon near its melting and boiling points (expansion rate, amounts, liquefying and boiling speed, possible unexpected interactions with $XeF_2 \cdot 2SnF_4$ or FEP walls, etc.). Using liquid nitrogen, a pre-calculated amount of gaseous xenon from this vessel was then quantitatively condensed into the smaller thick-walled FEP reaction vessel, so that liquid xenon reached half of its height as the temperature increased to -19 °C. A mixture of XeF_2 (15 mg, 0.09 mmol) and SnF_4 (25 mg, 0.13 mmol) was weighed into the small thick-walled vessel prior to the experiment. The reaction vessel was held overnight in the cryostat at –25 °C and the next day a few crystals appeared on the liquid-gas interface, but were lost during slow removal of Xe on the vacuum line. However, some crystalline material was found under microscope magnification (Figure 4.57) and the Raman analysis of the sample (Figure 4.58) showed that a reaction between XeF_2 and SnF_4 in liquid xenon actually occurred, giving an unknown product, possibly a new $a XeF_2 \cdot b SnF_4$ phase. The compound decomposes by solvolysis in aHF or after a 30 min exposure to dynamic vacuum, giving mainly SnF_4 $XeF_2 \cdot 2SnF_4$ and some XeF_2-rich phase (Appendix C.2, Figure C. 4). The band at 613 cm^{-1} can be tentatively assigned to a different fluoridostannate(IV) anion than those present in spectroscopically characterized $a XeF_2 \cdot b SnF_4$ phases, while the line at 546 cm^{-1} probably indicates a XeF_2 molecule somewhere in the middle of its ionization pathway ($XeF_2 \rightarrow XeF^+ + F^-$)[43]. Additionally, the bands at 513 cm^{-1} and 585 cm^{-1} most likely belong to weakly associated and at least partially ionized XeF_2 molecules, respectively. In these conditions, the formation of Xe_n^{+} [293,294] or $[M^{n+}Xe_m]^{n+}$ [297] species is unlikely (calculated symmetric and antisymmetric stretching frequencies of linear D_{8h} structures Xe_2^+, Xe_3^+, Xe_3^{2+} and Xe_4^+ ranging from 31-180 cm^{-1}; experimentally observed at 123 cm^{-1} for Xe_2^+ and at 110 cm^{-1} for Xe_4^+)[293,294] since the presence of “magic” acid HF/SbF_5 has always been required for such reactions.

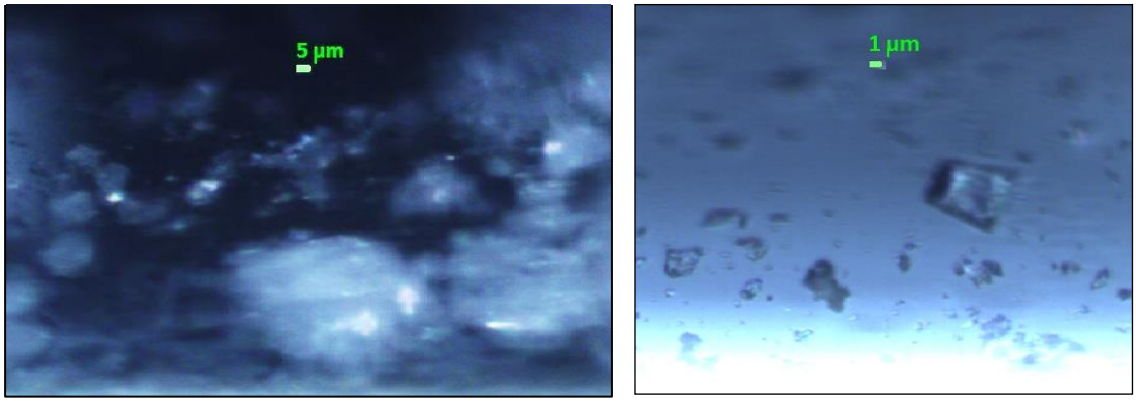


Figure 4.57: Isolated crystals (sealed in quartz capillary, magnified view) of undefined composition grown upon reaction of XeF_2 and SnF_4 in liquid xenon.

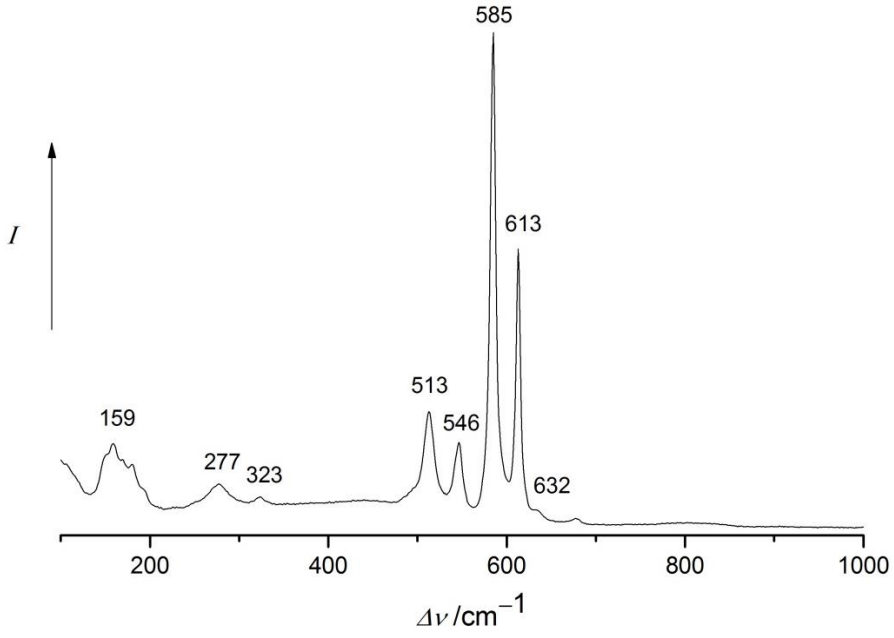


Figure 4.58: Raman spectrum of undefined crystalline product obtained by reaction of XeF_2 with SnF_4 in liquid xenon.

Most probably, the high pressure of xenon forces XeF_2 into a change of coordination mode by somehow altering the original structure of $XeF_2 \cdot 2SnF_4$. Similar solvent effects have already been encountered when using noble gases as cryogenic solvents, where noble gas solutions do not behave as "pseudo gas phase" model solutions as is often assumed, but are able, for instance, to significantly shift rotational equilibria if the conformers have different dipolarities.[298] Moreover, xenon offers other interesting possibilities[299] that do not evince chemical bonds. In such situations, xenon atoms may be viewed as isolated guest molecules enclosed by the host lattice (clathrates, see Section 1.1, Figure 1.1), trapped between layers (intercalation compounds) or adsorbed in large regular frameworks (zeolites).

In any case, further research providing more data is needed and future attempts might eventually reveal the nature of this product, possibly trying also with aHF-Xe mixtures or other binary systems. Certainly xenon, due to its chemical inertness, relative high density and

polarizability combined with convenient working temperature and pressure behavior, remains an attractive candidate as a solvent (or co-solvent) for this type of coordination complexes.

4.2.4 Other Fluoridostannate(IV) Salts and By-Products

Within the present work, five additional fluoridostannate(IV) compounds were identified during the studies of XeF_2-MF_4 (M = Sn, Ti) systems. Many factors and specific difficulties related to these systems, especially low solubility and poor crystallinity of the desired products, contributed to the preferential formation of by-products, while their detection and identification were often achieved only by meticulous screening and inspection under magnification of each product batch.

The two main routes delivering H_3O^+ salts in aHF acidified with strong Lewis acids as AsF_5 or SbF_5 are dissolution of various metal oxides[300,301,302,303,304,305], where chemically bound oxygen is converted *in situ* to water and protonated or the presence of water itself during the reaction/crystallization process (either upon addition or contamination). Thus far, a number of oxonium fluorido compounds, including salts of fluoridometalates(IV) (mostly fluoridotitanates(IV): $[H_3O]_2[TiF_6]$[158], $[H_3O][H_5O_2][TiF_6]$ [306], $[H_3O][TiF_5]$[165], $[H_3O][Ti_2F_9]$[155,161,267], $[GuH]_4[H_3O]_4[Ti_4F_{20}][TiF_5]_4$[155]), fluoridometalates(V) ($[H_3O][AsF_6]$ [307], $[H_3O][SbF_6]$[307], $[H_3O][Sb_2F_{11}]$ [308]), mixed ligand complexes ($(H_3O)M(AsF_6)_3$ (M = Mn, Co, Ni, Fe, Zn)[300,302,304], $(H_3O)MF(AsF_6)_2$ (M = Fe, Cu)[304], $(H_3O)_2Hg_2F(AsF_6)_5$[304], $(H_3O)M(SbF_6)_3$ (M = Mg, Fe, Co, Ni, Cu, Zn)[305], $(H_3O)_3M(SbF_6)_5$ (M = Mn, Pd, Cd)[305], $(H_3O)_3[Cr(SbF_6)_6](Sb_2F_{11})\cdot HF$[305], $(H_3O)_3La_2F(AsF_6)_8$[301], $(H_3O)_8La_2F(AsF_6)_{13}$[301], $(H_3O)_4La_2F(AsF_3)_2(AsF_6)_9$[301], $(H_3O)Cd(SbF_6)(Sb_2F_{11})_2$[303], $(H_3O)_2Cd(SbF_6)_3(Sb_2F_{11})$[303], $(H_3O)Cd_2F(SbF_6)_5$[303], $(H_3O)[Cd(HF)]_4(SbF_6)_9$[303]) and others (e.g. $[H_3O][BF_4]$[309], etc.) have been structurally characterized and many more ($[H_3O][AF^-_6]$ (A = U[310],

Bi[311], Ir[312], Pt[312], Ru[312], Nb[313], Ta[313]), $[H_3O]_2[PtF_6]$[312], $[H_3O][WOF_5]$[313]) have been reported. The particular interest in this type of compounds has been attributed[307] to the strong hydrogen bonding observed (O–F distances found ~ 2.5-2.6 Å[165,309]), the nature of which is strongly temperature dependent, so that oxonium salts show phase transitions, exhibit unexpected high thermal stability and present interesting structural problems. This is not surprising, since the bond dissociation enthalpy for normal hydrogen bonds is ca. 13-42 kJ/mol, while covalent single bonds have dissociation enthalpies ranging from 210 to 420 kJ/mol[298]. Therefore, hydrogen bonds are approximately ten times weaker than covalent single bonds, but also approximately ten times stronger than the non-specific intermolecular interactions[298].

The prolonged crystallizations and temperature variations combined with the well-known permeability of FEP fluoroplastic[314] to moisture and other aforementioned contributions led to the unwanted formation of oxonium compounds described in this work. The sodium salts were probably generated by a NaF impurity in the XeF_2. Although only traces of NaF, arising from ordinary glass used for the XeF_2 photosynthesis (see 3.1 Materials), are present, the compound eventually concentrated over the past years at the bottom of the XeF_2 stock vessel. Immediately after the first Na^+ side products have been identified from non-sodium systems, XeF_2 was re-sublimed and stored in a new vessel.

Nevertheless, due to the considerable paucity of structurally determined fluoridostannates(IV) and, most importantly, in order to obtain additional information on their anionic behavior in aHF solutions, targeted syntheses of $[H_3O]_2[SnF_6]$, $[H_3O][SnF_5]$, $Na[SnF_5]$, $Na[Sn_2F_9]\cdot HF$ and studies of the H_2O-HF-SnF_4 and Na-HF-SnF_4 systems were undertaken after these compounds had been unexpectedly obtained and structurally characterized; the results are summarized in the following sub-chapters.

4.2.4.1 $[H_3O]_2[SnF_6]$

The title compound was firstly obtained during an attempted preparation of $XeF_2\cdot 2SnF_4$. In order to increase the crystal quality and size of $XeF_2\cdot 2SnF_4$ precipitated crystals, the temperature of the solution was consecutively raised and lowered in a 0-49 °C range by exposing repeatedly the unprotected T-shaped FEP reactor to a warm and cold water bath. After 20 such cycles in a two-week period, all precipitate dissolved (due to H_2O diffusion through the FEP reactor wall) to form a clear solution, which yielded the compound $[H_3O]_2[SnF_6]$ upon crystallization. Later, the oxonium salt $[H_3O]_2[SnF_6]$ was purposively synthesized by condensing H_2O (36.5 mg, 2.03 mmol) onto a frozen mixture of SnF_4 (194 mg, 0.996 mmol) and aHF (1,2 mL) under static vacuum and its crystal structure re-determined (Table 4.18). An attempt to prepare a hydrate of this salt by using excess H_2O (188.5 mg, 10.47 mmol) over SnF_4 (94 mg, 0.483 mmol) resulted in a viscous gel-like material (left after 7 months of crystallization by slow solvent evaporation (closed system) driven by an average temperature difference of 40 °C), which remained unchanged after 8 hours under dynamic vacuum and was not further characterized.

Table 4.18: Crystal structure determination and refinement details for compound $[H_3O]_2[SnF_6]$.

Crystal data	*Data collection*	*Refinement*
$SnF_6O_2H_6$	Agilent Gemini diffractometer	$R_1[F^2 > 2\sigma(F^2)] = 0.014$
$M_r = 270.75$	Atlas CCD detector	$wR_2\ (F^2) = 0.030$
Crystal system: monoclinic	λ = 0.71073 Å (Mo K_α)	854 reflections
Space group: *C*2/*c*	4951 measured reflections	56 parameters
a = 12.5762(17) Å	854 independent reflections	GOF = 1.088
b = 5.1714(2) Å	700 observed reflections (I > 2 σ (I))	$\Delta\rho_{max}$ = 0.34 e/Å^3
c = 10.8702(8) Å	R_{int} = 0.024	$\Delta\rho_{min}$ = −0.44 e/Å^3
β = 110.394(8)°	θ_{max} = 29.9°, θ_{min} = 3.5°	
V = 662.64(11) Å^3	$-18 \leq h \leq 18$	
Z = 4	$-7 \leq k \leq 6$	

ρ_{calc} = 2.714 g/cm^3	$-14 \leq l \leq 13$
$4.3° \leq \theta \leq 29.7°$	
Cell parameters from 2761 reflections	
μ = 3.92 mm^{-1}	
T = 150 K	
F(000) = 504	
Size: 0.1×0.06×0.04 mm	
Appearance: Colorless chunk	

The compound crystallizes in the monoclinic *C*2/*c* space group with four formula units per unit cell. The presence of two additional formula units in comparison with $Na_2[SnF_6]$ (*P*2/*a*; *a* = 11.31 Å, *b* = 5.06 Å, *c* = 5.06; *V* = 258.93 Å^3, *Z* = 2) results in a two-fold elongation of the *c*-edge dimension, and consequently in a larger unit cell, where the volume increase is not directly proportional to the increase of the *Z*-value since the Na^+ cations are considerably smaller. The size of H_3O^+ is roughly comparable to that of K^+ cation, however in the absence of a reported crystal structure for the un-solvated $K_2[SnF_6]$ in the literature, it would be difficult to make meaningful comparisons.

The structure of $[H_3O]_2[SnF_6]$ consists of isolated octahedral SnF_6-units and tetrahedral H_3O-groups. The octahedral coordination sphere around each tin atom is completed by three symmetrically generated F ligands through an inversion center located on the Sn (Wyckoff 4a), all other atoms reside on general positions forming the two aforementioned crystallographically unique ions.

The Sn–F bond lengths (1.9470(11)-1.9593(11) Å, Table 4.19) are somewhat intermediate to those found in $[Xe_2F_3][Sn_4F_{17}]\cdot XeF_2\cdot HF$. In fact, despite all F-ligands in $[H_3O]_2[SnF_6]$ are terminal, they are strongly hydrogen bonded with the H_3O^+ cations, where all H atoms are involved in hydrogen bonding to adjacent SnF_6-units (Figure 4.59 and Figure 4.60). The distances and bond angles associated with hydrogen bonding in $[H_3O]_2[SnF_6]$ are given in Table 4.20.

Table 4.19: Selected geometric parameters for the compound $[H_3O]_2[SnF_6]$.

Bond Lengths (Å)			
Sn1—F2^i	1.9470 (11)	Sn1—F1^i	1.9521 (12)
Sn1—F2	1.9471 (11)	Sn1—F3	1.9593 (11)
Sn1—F1	1.9521 (12)	Sn1—F3^i	1.9593 (11)
Bond Angles (°)			
F2^i—Sn1—F2	180.0	F1^i—Sn1—F3	89.01 (5)
F2^i—Sn1—F1	90.34 (6)	F2^i—Sn1—F3^i	87.93 (5)
F2—Sn1—F1	89.66 (6)	F2—Sn1—F3^i	92.06 (5)
F2^i—Sn1—F1^i	89.66 (6)	F1—Sn1—F3^i	89.01 (5)
F2—Sn1—F1^i	90.34 (6)	F1^i—Sn1—F3^i	90.99 (5)
F1—Sn1—F1^i	180.0	F3—Sn1—F3^i	180.0
F2^i—Sn1—F3	92.07 (5)	H1A—O1—H1B	110 (3)
F2—Sn1—F3	87.94 (5)	H1A—O1—H1C	111 (3)

F1—Sn1—F3	90.99 (5)	H1B—O1—H1C	110 (3)

Symmetry code: (i) −*x*+1, −*y*+1, −*z*+1.

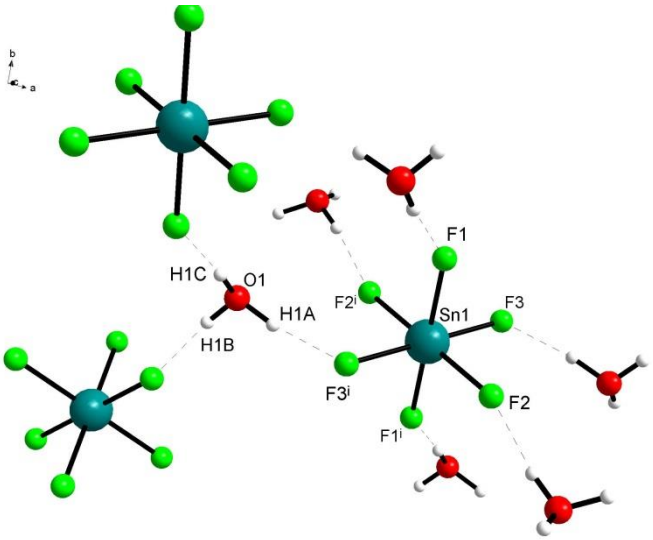


Figure 4.59: Coordination environment of H_3O^+ and SnF_6^- ions in $[H_3O]_2[SnF_6]$. Through strong hydrogen bonds, each H_3O^+ cation is coordinated by three adjacent anions and each SnF_6-unit is connected to six H_3O^+ cations. Symmetry code: (i) −*x*+1, −*y*+1, −*z*+1.

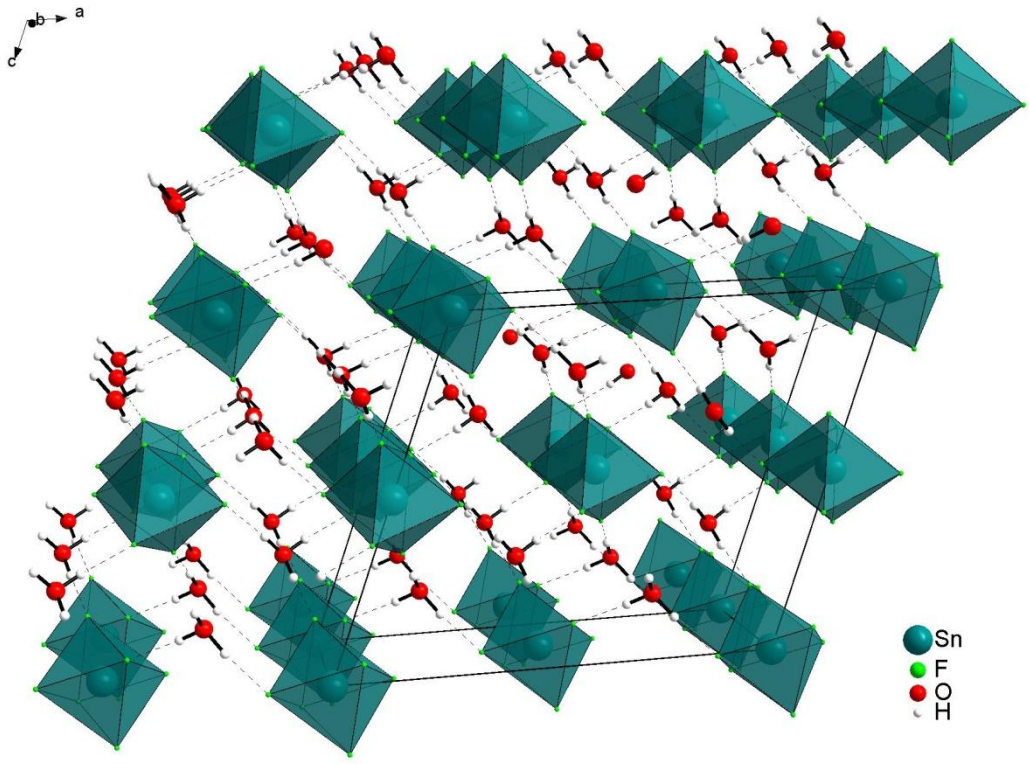


Figure 4.60: Unit cell, hydrogen bonding and packing arrangement of cations and anions in compound $[H_3O]_2[SnF_6]$.

Table 4.20: Geometric parameters associated with hydrogen bonding in $[H_3O]_2[SnF_6]$.

D—H···*A*	*D*—H (Å)	H···*A* (Å)	*D*···*A* (Å)	*D*—H···*A* (°)
O1—H1C···F1^{ii}	0.82 (3)	1.68 (3)	2.495 (2)	175 (3)
O1—H1B···F2^{iii}	0.82 (3)	1.66 (3)	2.477 (2)	171 (3)
O1—H1A···F3^{i}	0.91 (3)	1.62 (3)	2.524 (2)	170 (3)

Symmetry codes: (i) −*x*+1, −*y*+1, −*z*+1; (ii) −*x*+1/2, −*y*+3/2, −*z*+1; (iii) *x*−1/2, −*y*+1/2, *z*−1/2.

The Raman spectrum of $[H_3O]_2[SnF_6]$ recorded on a bulk sample is given in Figure 4.61. The vibrational bands arising from the $[SnF_6]^{2-}$ anion (O_h) are well known[198] and can be tentatively assigned also in this case (596 cm^{-1}, $\nu_1(A_{1g})$; 470 cm^{-1}, $\nu_2(E_g)$; 305 cm^{-1}, $\nu_4(F_{1u})$; 232 cm^{-1},$\nu_5(F_{2g})$).

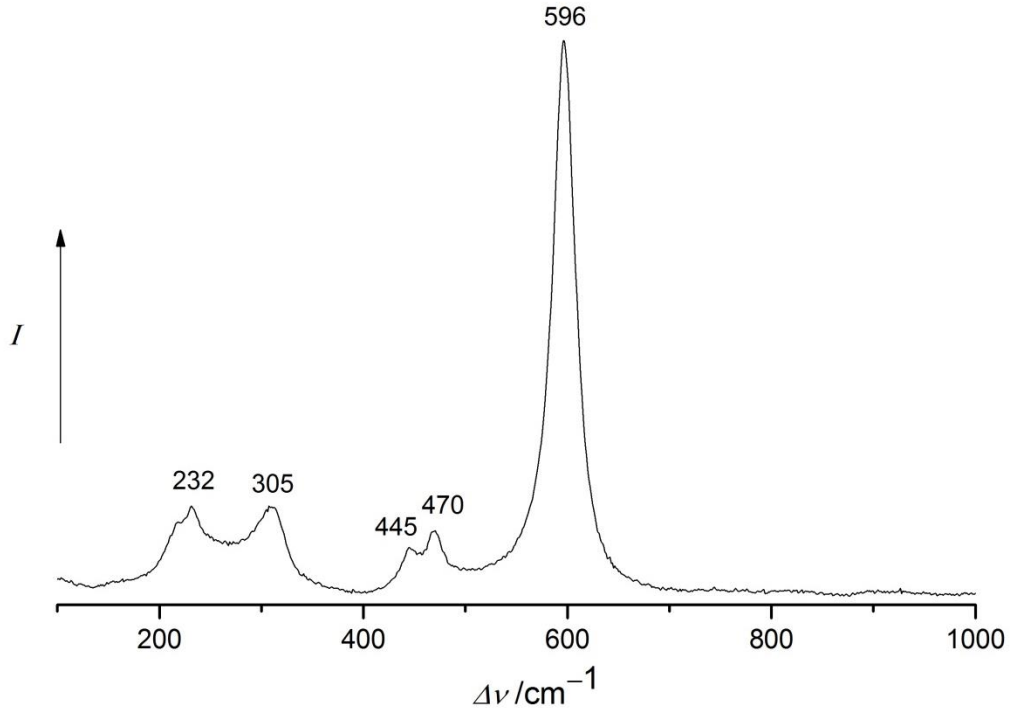


Figure 4.61: Raman spectrum of $[H_3O]_2[SnF_6]$ recorded on a bulk sample is consistent with spectra obtained on randomly oriented single crystals with verified unit cell parameters.

4.2.4.2 $[H_3O][SnF_5]$

A few crystals of the title compound were found in the product mixture after a 3 month crystallization attempt (ordinary T-shaped FEP reactor) of $XeF_2 \cdot 2SnF_4$. Later, the compound has been synthesized with an equimolar reaction of H_2O (18 mg, 1 mmol) and SnF_4 (195 mg, 1 mmol) in aHF (1,2 mL). After two-week crystallization by slow solvent evaporation, the compound was isolated in the glove-box and a suitable single crystal was mounted on the diffractometer. The details on the crystal structure analysis are given in Table 4.21.

Table 4.21: Crystal structure determination and refinement details for compound $[H_3O][SnF_5]$.

Crystal data	*Data collection*	*Refinement*
SnF_5OH_3	Rigaku AFC7 diffractometer	$R_1[F^2 > 2\sigma(F^2)] = 0.040$
$M_r = 232.73$	Mercury CCD detector	$wR_2\ (F^2) = 0.091$
Crystal system: monoclinic	λ = 0.71069 Å (Mo K_α)	1041 reflections
Space group: *C*2/*c*	1939 measured reflections	73 parameters
a = 14.887(4) Å	1041 independent reflections	GOF = 1.186
b = 4.9549(11) Å	948 observed reflections	$\Delta\rho_{max} = 2.35$ e/Å^3

	(I > 2 σ (I))	
c = 13.951(3) Å	R_{int} = 0.032	$\Delta\rho_{min}$ = −1.23 e/Å^3
β = 115.908(9)°	θ_{max} = 29.1°, θ_{min} = 3.3°	
V = 925.7(4) Å^3	$-19 \leq h \leq 10$	
Z = 8	$-6 \leq k \leq 4$	
ρ_{calc} = 3.34 g/cm^3	$-13 \leq l \leq 17$	
$4.4° \leq \theta \leq 27.6°$		
Cell parameters from 272 reflections		
μ = 5.53 mm^{-1}		
T = 200 K		
F(000) = 848		
Size: 0.1×0.1×0.07 mm		
Appearance: Colorless prism		

Similarly to $[H_3O]_2[SnF_6]$, the compound was refined in a monoclinic C2/c lattice. Eight formula units fulfill the unit cell and ten atoms lying on general positions (Wyckoff 8f) form the asymmetric unit (Table C. 5 in Appendix C.4).

Thus far, the structural knowledge of fluoridostannates(IV) has been limited only to isolated octahedral $[SnF_6]^{2-}$ anions (see Section 1.4.2). The XRD analysis on a single crystal of $[H_3O][SnF_5]$ reveals the structural nature of $[SnF_5]^-$ for the first time, for which it was previously correctly predicted to adopt a polymeric structure consisting of *cis*-fluorine-bridged SnF_6 octahedra[194].

Figure 4.62 depicts the chain-like 1-D structure of $[SnF_5]^-$ found in $[H_3O][SnF_5]$, which resembles the structural arrangement in analogous afore-discussed $[TiF_5]^-$ compounds (Section 4.1.2). A complete list of bond lengths and angles is given in

Table 4.22. The adjacent octahedra sharing F4 apexes (Sn1-F4-Sn1 bond angle: 145.6(2)°) are significantly twisted with a torsion angle of ~ 40°. Each octahedron has two *cis*-bridging and four terminal fluorine atoms, of which three are strongly hydrogen bonded (Figure 4.63, *left*). Following the expectations, the terminal Sn-F1 bonds have the shortest lengths (1.907(4) Å), the hydrogen bonded Sn-F(2, 3, 5) lengths are intermediate (1.922(4)-1.934(4) Å), while the bridging Sn-F4 are the longest (2.046(4)-2.059(4) Å) Sn-F bonds observed in $[H_3O][SnF_5]$. All hydrogens of the tetrahedral oxonium cations form hydrogen bonds (Table 4.23), so that each H_3O^+ unit connects three separate $[SnF_5]$-chains (Figure 4.63 *right*, and Figure 4.64).

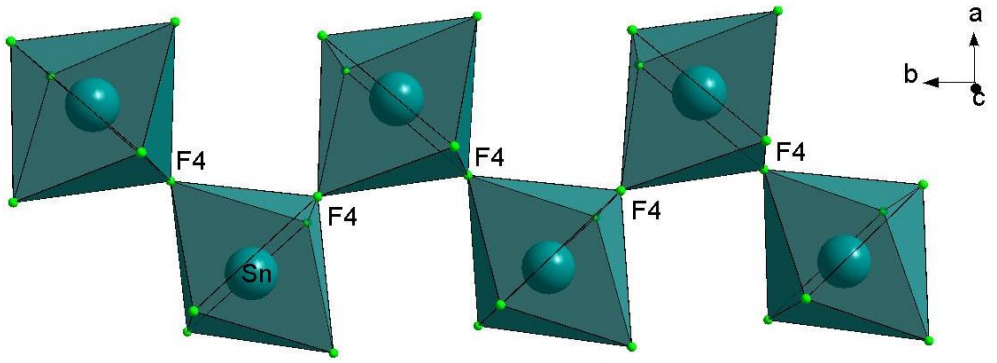
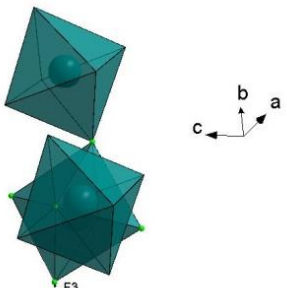


Figure 4.62: The polymeric $[SnF_5]^-$ anion determined in the crystal structure of $[H_3O][SnF_5]$ consists of *cis*-μ-F bridged SnF_6-octahedra.



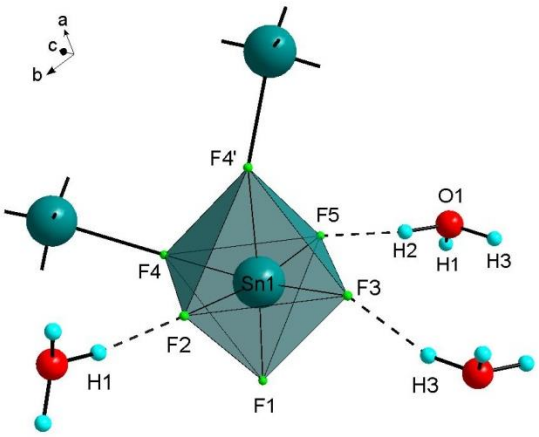


Figure 4.63: Coordination environment of SnF_6-octahedra (*left*) and oxonium cations (*right*) found in the crystal structure of $[H_3O][SnF_5]$.

Table 4.22: Selected geometric parameters for the compound $[H_3O][SnF_5]$.

Bond Lengths (Å)			
Sn1—F1	1.907 (4)	Sn1—F4	2.059 (4)
Sn1—F3	1.922 (4)	F4—Sn1^{ii}	2.046 (4)
Sn1—F5	1.934 (4)	O1—H1	0.955 (18)
Sn1—F2	1.934 (4)	O1—H2	0.947 (18)
Sn1—F4^{i}	2.046 (4)	O1—H3	0.947 (18)
Bond Angles (°)			
F1—Sn1—F3	98.79 (18)	F1—Sn1—F4	173.80 (16)
F1—Sn1—F5	92.55 (17)	F3—Sn1—F4	87.03 (16)
F3—Sn1—F5	94.70 (17)	F5—Sn1—F4	84.82 (16)
F1—Sn1—F2	94.81 (18)	F2—Sn1—F4	87.35 (17)
F3—Sn1—F2	89.31 (18)	F4^{i}—Sn1—F4	84.29 (7)
F5—Sn1—F2	171.00 (16)	Sn1^{ii}—F4—Sn1	145.6 (2)
F1—Sn1—F4^{i}	90.04 (16)	H1—O1—H2	113 (3)
F3—Sn1—F4^{i}	170.52 (16)	H1—O1—H3	113 (3)
F5—Sn1—F4^{i}	88.30 (16)	H2—O1—H3	114 (3)
F2—Sn1—F4^{i}	86.51 (16)		

Symmetry codes: (i) $-x+1/2, y+1/2, -z+3/2$; (ii) $-x+1/2, y-1/2, -z+3/2$.

Table 4.23: Geometric parameters associated with hydrogen bonding in $[H_3O][SnF_5]$.

D—H···*A*	*D*—H (Å)	H···*A* (Å)	*D*···*A* (Å)	*D*—H···*A* (°)
O1—H1···F2	0.96 (2)	1.59 (5)	2.501 (6)	157 (4)
O1—H2···F5^{i}	0.95 (2)	1.60 (4)	2.543 (6)	168 (4)
O1—H3···F3	0.95 (2)	1.65 (4)	2.521 (5)	151 (5)

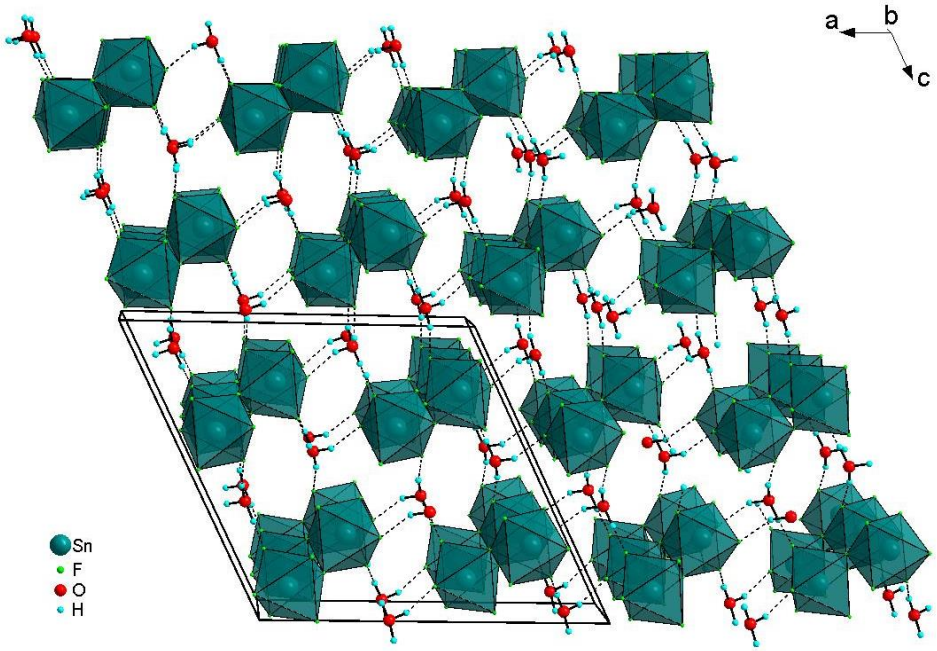


Figure 4.64: Packing diagram showing the unit cell and hydrogen interactions between the $[SnF_5]^-$ chains and H_3O^+ cations.

The Raman spectrum of $[H_3O][SnF_5]$ recorded on a randomly oriented single crystal is given in Figure 4.65. Due to the lack of spectroscopically characterized $[SnF_5]^-$ compounds (reliable vibrational data are limited to compounds $[NF_4][SnF_5]$[194] and $[N_5][SnF_5]$[202]) and without a significant computational support, it is very difficult to assign the observed frequencies. However, based on comparisons with the lines found in the aforementioned NF_4^+ and N_5^+ salts, at least the bands at 638 cm^{-1}, 604 cm^{-1}, 536 cm^{-1} and 451 cm^{-1} might be attributed to the $[SnF_5]^-$ anion.

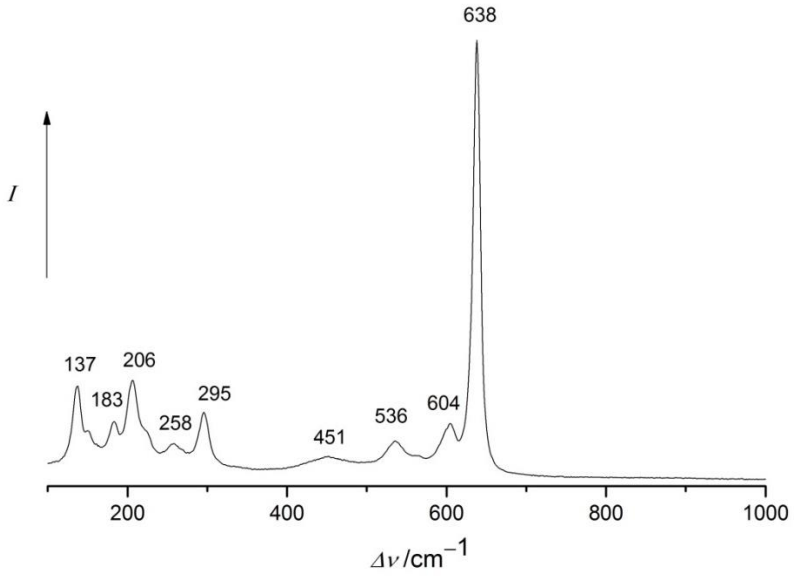


Figure 4.65: Raman spectrum of $[H_3O][SnF_5]$ obtained on a randomly oriented crystal.

4.2.4.3 Na[SnF5]

Colorless crystals of the compound $Na[SnF_5]$ were grown from an aHF (1,1 mL) solution containing equimolar quantities of NaF (4 mg, 0.095 mmol) and SnF_4 (19 mg, 0.097 mmol). The product was isolated and structurally characterized as described before. Detailed crystallographic information is given in Table 4.24.

Table 4.24: Crystal structure determination and refinement details for compound $Na[SnF_5]$.

Crystal data	*Data collection*	*Refinement*
$NaSnF_5$	Agilent Gemini diffractometer	$R_1[F^2 > 2\sigma(F^2)] = 0.023$
$M_r = 236.69$	Atlas CCD detector	$wR_2\ (F^2) = 0.063$
Crystal system: orthorhombic	λ = 1.54184 Å (Cu K_α)	396 reflections
Space group: *Pnna*	4308 measured reflections	33 parameters
a = 5.5843(4) Å	396 independent reflections	GOF = 1.017
b = 4.8945(4) Å	345 observed reflections (I > 2 σ (I))	$\Delta\rho_{max}$ = 1.97 e/Å^3
c = 14.4256(7) Å	R_{int} = 0.083	$\Delta\rho_{min}$ = −0.72 e/Å^3
V = 394.28(4) Å^3	θ_{max} = 73.1°, θ_{min} = 6.1°	
Z = 4	$-6 \leq h \leq 6$	
ρ_{calc} = 3.987 g/cm^3	$-6 \leq k \leq 5$	
$6.1° \leq \theta \leq 72.8°$	$-17 \leq l \leq 17$	
Cell parameters from 1711 reflections		
μ = 53 mm^{-1}		
T = 150 K		
F(000) = 424		
Size: 0.003×0.002×0.002 mm		

Appearance: Colorless block

After the oxonium salt $[H_3O][SnF_5]$ described in the previous section, $Na[SnF_5]$ represents the second example of a structurally determined compound with the $[SnF_5]^-$ anion. The substitution of larger tetrahedral H_3O^+ cations with smaller spherical Na^+ cations and the absence of hydrogen bonding resulted in the crystallization of this salt in a different crystal lattice. The compound was refined in the orthorhombic *Pnna* space group with four formula units per unit cell. The asymmetric unit (atom positions are given in Appendix C.5, Table C. 6) is defined by five crystallographically independent atoms (Sn1, Na1 (Wyckoff 4c) and F3 (Wyckoff 4d) residing on 2-fold rotational axes, and F1 and F2 on general (Wyckoff 8e) positions).

The $[SnF_5]^-$ anion (Figure 4.66) in $Na[SnF_5]$ retained the zig-zag chain structure as found in the $[H_3O][SnF_5]$. The octahedra are connected via μ-F3 bridges with an average torsion angle between twisted neighboring SnF_6-units of $\sim 47°$.

Each SnF_6-octahedron has 2 *cis*-bridging (Sn-F_b: 2.0529(9) Å; symmetric bridge with Sn1-F3-Sn1' bond angle of 141.06(14)°) and four terminal Sn-F bonds (Sn-F_t: 1.913(2)-1.947(2) Å), where all terminal fluorine atoms are additionally interacting with sodium cations (Figure 4.67, *left*). In this way, each sodium cation has a distorted octahedral environment of six fluorine ligands, sharing two octahedral edges with adjacent Na^+ centers (Figure 4.67, *right*). The Na···F contacts range from 2.213(2) to 2.341(2) Å, giving the sum of bond valences for Na^+ in $Na[SnF_5]$ a value of 1.143 (considering *BV* parameters R_0 = 1.677 and b = 0.37)[315]. Other associated bond lengths and angles are summarized in Table 4.25.

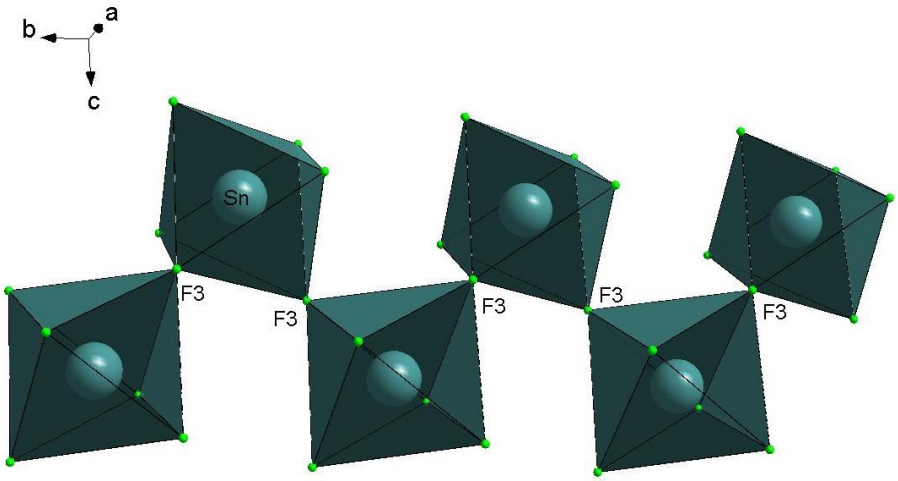


Figure 4.66: Linkage of SnF_6-octahedra in the polymeric $[SnF_5]^-$ anion found in the structure of $Na[SnF_5]$.

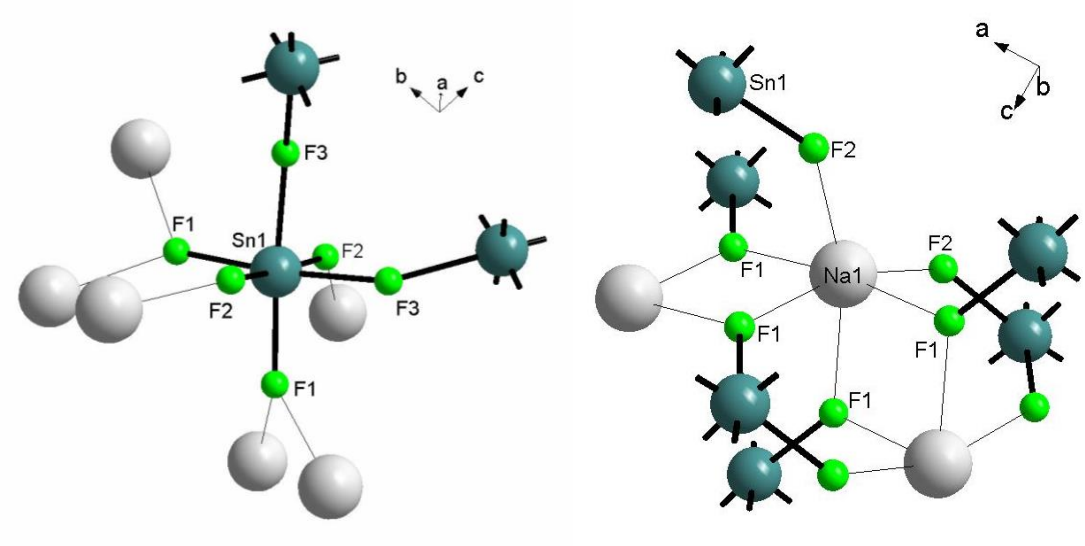


Figure 4.67: Coordination environment of Sn (left) and Na (right) atoms in $Na[SnF_5]$.

Table 4.25: Selected geometric parameters for the compound $Na[SnF_5]$.

Bond Lengths (Å)			
Sn1—F1^{i}	1.9474 (19)	Na1—Na1^{iv}	3.425 (3)
Sn1—F1	1.9474 (19)	Na1—F1^{iv}	2.341 (2)
Sn1—F2	1.913 (2)	Na1—F1^{v}	2.341 (2)
Sn1—F2^{i}	1.913 (2)	Na1—F1^{vi}	2.332 (3)
Sn1—F3^{i}	2.0529 (9)	Na1—F1	2.332 (3)
Sn1—F3^{ii}	2.0529 (9)	Na1—F2^{vii}	2.213 (2)
Na1—Na1^{iii}	3.425 (3)	Na1—F2^{iii}	2.213 (2)
Bond Angles (°)			
F1^{i}—Sn1—F1	97.36 (12)	F1^{vi}—Na1—F1^{iv}	87.75 (8)
F2^{i}—Sn1—F1^{i}	92.89 (9)	F1^{vi}—Na1—F1	77.94 (12)
F2^{i}—Sn1—F1	91.04 (8)	F1^{v}—Na1—F1^{iv}	171.62 (16)
F2—Sn1—F1	92.89 (9)	F1^{v}—Na1—F1	87.75 (8)
F2—Sn1—F1^{i}	91.04 (8)	F2^{vii}—Na1—Na1^{iv}	83.41 (6)
F2^{i}—Sn1—F2	174.05 (11)	F2^{iii}—Na1—Na1^{iv}	138.61 (6)
F3^{i}—Sn1—F1	173.65 (8)	F2^{vii}—Na1—F1^{v}	98.75 (8)
F3^{i}—Sn1—F1^{i}	88.33 (7)	F2^{vii}—Na1—F1^{iv}	85.88 (8)
F3^{ii}—Sn1—F1^{i}	173.65 (8)	F2^{vii}—Na1—F1	84.47 (7)
F3^{ii}—Sn1—F1	88.33 (7)	F2^{vii}—Na1—F1^{vi}	161.68 (12)
F3^{i}—Sn1—F2	89.83 (9)	F2^{iii}—Na1—F1^{v}	85.88 (8)

$F3^{i}$—Sn1—$F2^{i}$	85.82 (9)	$F2^{iii}$—Na1—$F1^{iv}$	98.75 (8)
$F3^{ii}$—Sn1—$F2^{i}$	89.83 (9)	$F2^{iii}$—Na1—F1	161.68 (12)
$F3^{ii}$—Sn1—F2	85.82 (9)	$F2^{iii}$—Na1—$F1^{vi}$	84.47 (7)
$F3^{i}$—Sn1—$F3^{ii}$	86.15 (5)	$F2^{vii}$—Na1—$F2^{iii}$	113.47 (15)
$F1^{vi}$—Na1—$Na1^{iv}$	80.27 (10)	Na1—F1—Sn1	134.46 (11)
F1—Na1—$Na1^{iv}$	42.97 (7)	$Na1^{iv}$—F1—Sn1	129.12 (11)
$F1^{iv}$—Na1—$Na1^{iv}$	42.76 (5)	$Na1^{iii}$—F2—Sn1	139.78 (11)
$F1^{v}$—Na1—$Na1^{iv}$	130.51 (11)	Sn1—F3—$Sn1^{ii}$	141.06 (14)

Symmetry codes: (i) $-x+3/2, -y+1, z$; (ii) $x, -y+3/2, -z+3/2$; (iii) $-x+1, -y+2, -z+1$; (iv) $-x+2, -y+2, -z+1$; (v) $x-1/2, y, -z+1$; (vi) $-x+3/2, -y+2, z$; (vii) $x+1/2, y, -z+1$.

The Raman spectra of $Na[SnF_5]$ (Figure 4.68) were obtained on several randomly oriented single crystals, whose identities were additionally confirmed with lattice parameters measurements by XRD. The observed bands are in good agreement with previously obtained lines, which were assigned to Sn-F stretching frequencies of the $[SnF_5]^-$ anions found in $[NF_4][SnF_5]$[194] (622(9.2) cm^{-1}, 574(0.5) cm^{-1}, 558(2.0) cm^{-1}, 490(0+) cm^{-1}) and $[N_5][SnF_5]$[202] (624(3.8) cm^{-1}, 475(0.5) cm^{-1}).

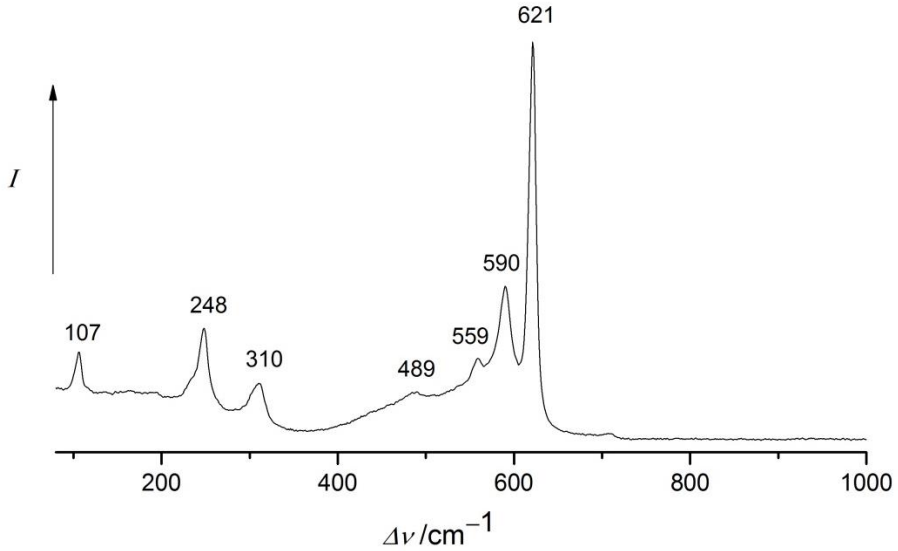


Figure 4.68: Raman spectrum of compound $Na[SnF_5]$ obtained on a randomly oriented single crystal with certified unit cell parameters.

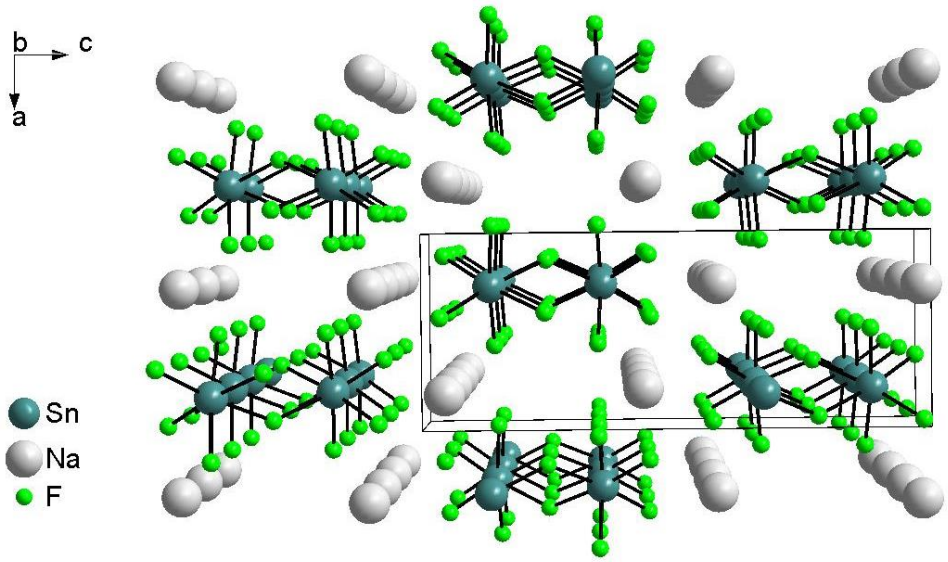


Figure 4.69: Packing diagram of compound $Na[SnF_5]$. View along the *b*-axis.

4.2.4.4 $Na[H_3O][SnF_5]_2$

The title compound was obtained as a side-product during the re-crystallization attempt of $Na[SnF_5]$. Due to the long period (26 days) of the process, eventually enough H_2O diffused through the FEP walls forming colorless crystals of $Na[H_3O][SnF_5]_2$. Details on the XRD analysis are given in Table 4.26.

Table 4.26: Crystal structure determination and refinement details for compound $Na[H_3O][SnF_5]_2$.

Crystal data	*Data collection*	*Refinement*
$F_{10}Sn_2 \cdot H_3O \cdot Na$	Agilent Gemini diffractometer	$R_1[F^2 > 2\sigma(F^2)] = 0.029$
$M_r = 469.39$	Atlas CCD detector	$wR_2\ (F^2) = 0.055$
Crystal system: monoclinic	λ = 0.71073 Å (Mo K_α)	2057 reflections
Space group: *C*2/*c*	4360 measured reflections	136 parameters
a = 22.9481(19) Å	2057 independent reflections	GOF = 0.966
b = 4.9194(4) Å	1274 observed reflections (I > 2 σ (I))	$\Delta\rho_{max}$ = 1.01 e/Å^3
c = 15.5065(13) Å	R_{int} = 0.032	$\Delta\rho_{min}$ = −0.93 e/Å^3
β = 101.750(7)°	θ_{max} = 29.7°, θ_{min} = 3.5°	
V = 1713.9(2) Å^3	$-30 \leq h \leq 31$	
Z = 8	$-6 \leq k \leq 5$	
ρ_{calc} = 3.638 g/cm^3	$-14 \leq l \leq 20$	
$3.5° \leq \theta \leq 29.6°$		
Cell parameters from 1313 reflections		
μ = 6.02 mm^{-1}		
T = 150 K		
F(000) = 1696		
Size: 0.12×0.08×0.02 mm		
Appearance: Colorless plate		

In the mixed-cation salt $Na[H_3O][SnF_5]_2$, the presence of two monovalent cations different in size and shape resulted in a polymeric $[SnF_5]^-$ anion generated by two crystallographically independent, $Sn(1)F_6$ and $Sn(2)F_6$ units, which alternate their positions in an infinite zig-zag array along the *b*-axis (Figure 4.70). The octahedra are *cis*-connected through F5 and F6 vertices, forming Sn(2)-F5-Sn(1) (Sn(2)-F5, 2.056(3) Å; F5-Sn(1), 2.052(3) Å; Sn(2)-F5-Sn(1): 140.6(2)°) and symmetrical Sn(1)-F6-Sn(2) (Sn(1,2)-F6, 2.047(3) Å; Sn(1)-F6-Sn(2): 145.0(2)°) bridges. Terminal Sn(1, 2)-Ft bond lengths are expectedly shorter (1.903(3)-1.935(3) Å) and apparently not significantly affected by the nature of further interactions (e.g. Sn1-F2(Na), 1.925(3) Å, Sn1-F3(H1), 1.925(3) Å). Contacts between the $[SnF_5]^-$ anion and the cations in $Na[H_3O][SnF_5]_2$ are depicted in Figure 4.71. Each $Sn(1)F_6$-octahedron is coordinated by two adjacent $Sn(2)F_6$-units, three Na^+ and one H_3O^+ cations, while each $Sn(2)F_6$-octahedron further interacts with two $Sn(1)F_6$-units, two Na^+ and two H_3O^+ cations. In this way, each Na^+ cation is octahedrally coordinated with six fluorine ligands (Figure 4.72, *left*) belonging to four $Sn(1)F_6$-units and two $Sn(2)F_6$-units with Na···F distances ranging from 2.225(4) to 2.350(4) Å (ΣBV = 1.175 for Na^+ in $Na[H_3O][SnF_5]_2$, considering *BV* parameters R_0 = 1.677 and b = 0.37)[315]. In the crystal structure of $Na[H_3O][SnF_5]_2$, the sodium cations are located between $[SnF_5]^-$ chains in pairs (Figure 4.73) by sharing their octahedral F4–F4 edge (Figure 4.72, *left*).

The structure is additionally stabilized with hydrogen bonding. Each tetrahedral H_3O^+ cation connects three different $[SnF_5]$-chains (Figure 4.72, *right*) through moderate-strong hydrogen bonds (table), forming a complex 3-D network (Figure 4.73).

Table 4.27: Selected geometric parameters for the compound $Na[H_3O][SnF_5]_2$.

Bond Lengths (Å)			
Sn1—F1	1.903 (3)	Na1—F8^{iii}	2.275 (4)
Sn1—F3	1.925 (3)	Na1—F2^{iv}	2.294 (3)
Sn1—F2	1.925 (3)	Na1—F4^{v}	2.325 (4)
Sn1—F4	1.930 (3)	Na1—F4	2.350 (4)
Sn1—F6	2.047 (3)	Na1—Na1^{v}	3.430 (4)
Sn1—F5	2.052 (3)	F1—Na1^{vi}	2.230 (3)
Sn2—F7	1.906 (3)	F2—Na1^{iv}	2.294 (3)
Sn2—F8	1.919 (3)	F4—Na1^{v}	2.325 (4)
Sn2—F9	1.924 (3)	F5—Sn2^{vi}	2.056 (3)
Sn2—F10	1.935 (3)	F7—Na1^{iii}	2.225 (4)
Sn2—F6	2.047 (3)	F8—Na1^{ii}	2.275 (4)
Sn2—F5^{i}	2.056 (3)	O1—H1	0.928 (17)
Na1—F7^{ii}	2.225 (4)	O1—H2	0.894 (17)
Na1—F1^{i}	2.230 (3)	O1—H3	0.908 (17)
Bond Angles (°)			
F1—Sn1—F3	172.34 (12)	F1^{i}—Na1—F8^{iii}	95.06 (14)
F1—Sn1—F2	93.67 (12)	F7^{ii}—Na1—F2^{iv}	88.15 (13)
F3—Sn1—F2	90.47 (12)	F1^{i}—Na1—F2^{iv}	161.45 (15)

F1—Sn1—F4	91.60 (12)	F8^{iii}—Na1—F2^{iv}	89.99 (11)
F3—Sn1—F4	94.16 (12)	F7^{ii}—Na1—F4^{v}	167.16 (14)
F2—Sn1—F4	98.52 (12)	F1^{i}—Na1—F4^{v}	83.19 (13)
F1—Sn1—F6	90.67 (12)	F8^{iii}—Na1—F4^{v}	88.54 (13)
F3—Sn1—F6	84.58 (12)	F2^{iv}—Na1—F4^{v}	79.11 (12)
F2—Sn1—F6	172.66 (11)	F7^{ii}—Na1—F4	95.77 (13)
F4—Sn1—F6	87.26 (12)	F1^{i}—Na1—F4	84.64 (12)
F1—Sn1—F5	85.84 (12)	F8^{iii}—Na1—F4	174.12 (14)
F3—Sn1—F5	87.76 (12)	F2^{iv}—Na1—F4	88.52 (13)
F2—Sn1—F5	89.43 (12)	F4^{v}—Na1—F4	85.59 (12)
F4—Sn1—F5	171.80 (12)	F7^{ii}—Na1—Na1^{v}	136.87 (16)
F6—Sn1—F5	84.99 (12)	F1^{i}—Na1—Na1^{v}	81.69 (11)
F7—Sn2—F8	93.37 (13)	F8^{iii}—Na1—Na1^{v}	131.62 (14)
F7—Sn2—F9	172.68 (13)	F2^{iv}—Na1—Na1^{v}	81.62 (11)
F8—Sn2—F9	93.47 (13)	F4^{v}—Na1—Na1^{v}	43.08 (8)
F7—Sn2—F10	92.85 (12)	F4—Na1—Na1^{v}	42.52 (9)
F8—Sn2—F10	96.88 (13)	Sn1—F1—Na1^{vi}	140.67 (17)
F9—Sn2—F10	88.91 (13)	Sn1—F2—Na1^{iv}	134.53 (15)
F7—Sn2—F6	91.07 (12)	Sn1—F4—Na1^{v}	134.32 (16)
F8—Sn2—F6	88.93 (12)	Sn1—F4—Na1	130.04 (16)
F9—Sn2—F6	86.46 (12)	Na1^{v}—F4—Na1	94.41 (12)
F10—Sn2—F6	172.79 (12)	Sn1—F5—Sn2^{vi}	140.61 (15)
F7—Sn2—F5^{i}	86.06 (12)	Sn2—F6—Sn1	145.00 (15)
F8—Sn2—F5^{i}	175.04 (12)	Sn2—F7—Na1^{iii}	132.03 (15)
F9—Sn2—F5^{i}	86.90 (12)	Sn2—F8—Na1^{ii}	131.38 (15)
F10—Sn2—F5^{i}	88.07 (12)	H1—O1—H2	115 (3)
F6—Sn2—F5^{i}	86.16 (12)	H1—O1—H3	114 (2)
F7^{ii}—Na1—F1^{i}	109.65 (12)	H2—O1—H3	118 (3)
F7^{ii}—Na1—F8^{iii}	89.86 (12)		

Symmetry codes: (i) *x*, *y*−1, *z*; (ii) −*x*+1/2, *y*+1/2, −*z*+1/2; (iii) −*x*+1/2, *y*−1/2, −*z*+1/2; (iv) −*x*+1/2, −*y*+3/2, −*z*; (v) −*x*+1/2, −*y*+1/2, −*z*; (vi) *x*, *y*+1, *z*.

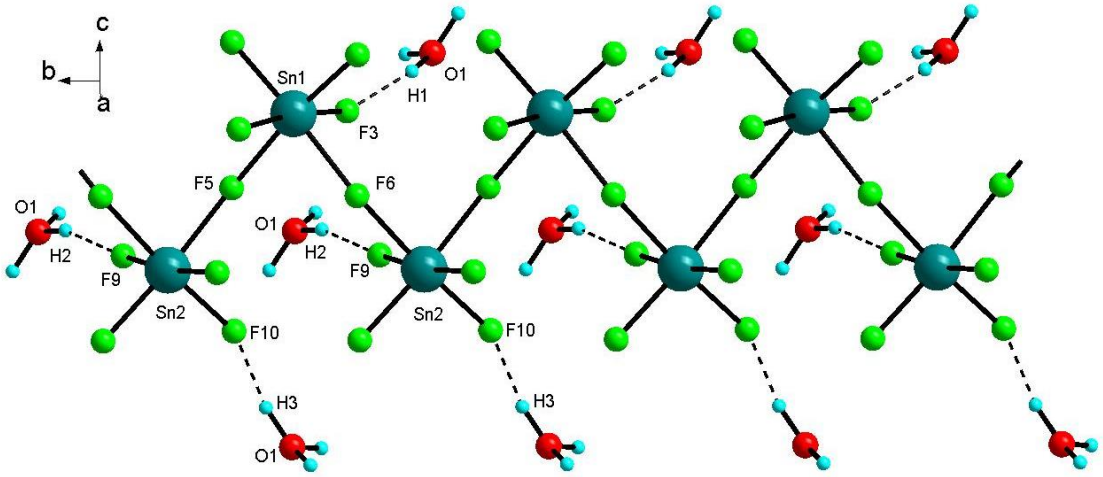


Figure 4.70: Chain-like structure of the polymeric $[SnF_5]$ anion and hydrogen bonding found in the double-salt $Na[H_3O][SnF_5]_2$.

Table 4.28: Geometric parameters associated with hydrogen bonding in $Na[H_3O][SnF_5]_2$.

D—H···*A*	*D*—H (Å)	H···*A* (Å)	*D*···*A* (Å)	*D*—H···*A* (°)
O1—H1···F3	0.93(2)	1.67(3)	2.544(4)	153(3)
O1—H2···F9	0.89(2)	1.66(4)	2.517(5)	159(3)
O1—H3···F10	0.91(2)	1.60(4)	2.498(5)	169(3)

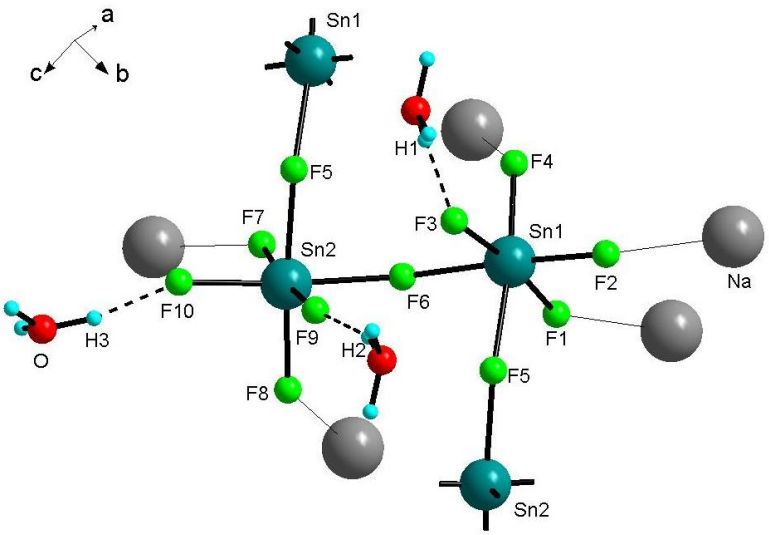
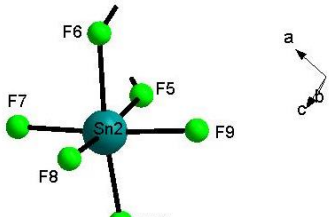


Figure 4.71: Coordination environment of $Sn(1)F_6$ and $Sn(2)F_6$ octahedra in $Na[H_3O][SnF_5]_2$.



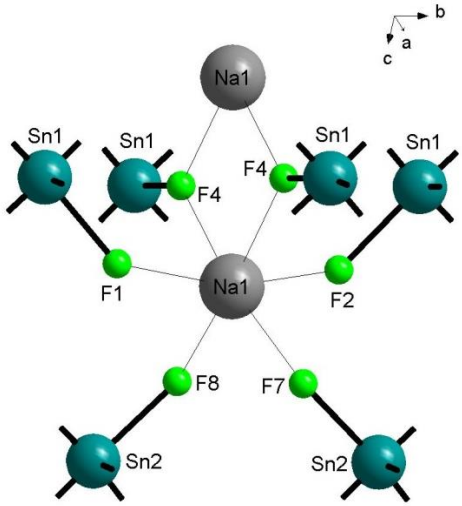


Figure 4.72: Coordination environment of Na^+ (*left*) and H_3O^+ (*right*) cations in $Na[H_3O][SnF_5]_2$.

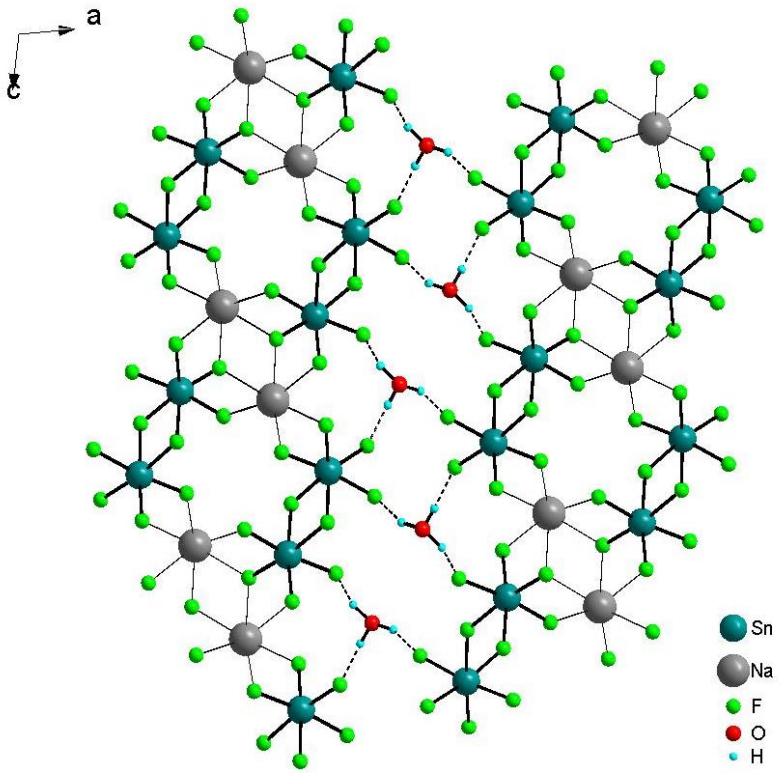


Figure 4.73: Packing of Na^+, $[H_3O]^+$ and $[SnF_5]^-$ ions in the crystal structure of $Na[H_3O][SnF_5]_2$.

4.2.4.5 $Na[Sn_2F_9]\cdot HF$

Crystals of $Na[Sn_2F_9]\cdot HF$ were firstly identified and structurally characterized (Table 4.29) in the product mixture upon a failed re-crystallization attempt of $XeF_2\cdot 2SnF_4$ from a diluted aHF

solution, where most probably a NaF impurity reacted either with $XeF_2 \cdot 2SnF_4$ or SnF_4 (present in chemical equilibrium). Later, the compound was synthetized from NaF (11 mg, 0.26 mmol) and SnF_4 (96 mg, 0.49 mmol) in aHF (1.1 mL) and characterized by single-crystal X-ray diffraction and Raman spectroscopy. Interestingly, a five-fold molar excess of SnF_4 over NaF produced only crystals of $Na[SnF_5]$ instead forming the SnF_4-richer $[Sn_2F_9]^-$ anion. One possible explanation is that the overabundance of SnF_4 might prevent the co-crystallization of HF molecules into the crystal lattice of $Na[Sn_2F_9] \cdot HF$, leading to its destabilization following by the preferential formation of $Na[SnF_5]$.

Table 4.29: Crystal structure determination and refinement details for $Na[Sn_2F_9] \cdot HF$.

Crystal data	*Data collection*	*Refinement*
$NaHSn_2F_{10}$	Rigaku AFC7 diffractometer	$R_1[F^2 > 2\sigma(F^2)] = 0.048$
$M_r = 451.38$	Mercury CCD area detector	$wR_2\ (F^2) = 0.153$
Crystal system: orthorhombic	λ = 0.71069 Å (Mo K_α)	1025 reflections
Space group: *Pnma*	3283 measured reflections	80 parameters
a = 14.6705(12) Å	1025 independent reflections	GOF = 1.103
b = 4.0359(4) Å	831 observed reflections (I > 2 σ (I))	$\Delta\rho_{max}$ = 2.78 e/Å^3
c = 12.8304(9) Å	R_{int} = 0.056	$\Delta\rho_{min}$ = −3.01 e/Å^3
V = 759.67(11) Å^3	θ_{max} = 29.1°, θ_{min} = 2.8°	
Z = 4	$-18 \leq h \leq 19$	
ρ_{calc} = 3.947 g/cm^3	$-5 \leq k \leq 5$	
$2.1° \leq \theta \leq 29.0°$	$-8 \leq l \leq 16$	
Cell parameters from 1613 reflections		
μ = 6.77 mm^{-1}		
T = 200 K		
F(000) = 808		
Size: 0.1×0.08×0.06 mm		
Appearance: Colorless chunk		

The title compound was refined in the orthorhombic *Pnma* space group. The asymmetric unit contains 14 crystallographically independent atoms (2 Sn, 10 F, 1 Na and 1 H atom, all atoms reside on mirror planes, Wyckoff 4c; fractional atomic coordinates are given in Appendix C.7, Table C. 8), which build two crystallographically unique SnF_6-units, a Na^+ cation and a HF molecule.

Although the $[Sn_2F_9]^-$ anion has been known to exist (the synthesis and characterization of $[N_2F][Sn_2F_9]$ has been reported[203] within the studies of dinitrogen difluoride chemistry), thus far its structure has not been published. The structural characterization of $Na[Sn_2F_9] \cdot HF$ reveals the assembly of the $[Sn_2F_9]^-$ anion for the first time. Similarly to the $[Ti_2F_9]^-$ structure, it consists of infinite double *trans*-chains of SnF_6-octahedra, transversally linked via μ-F11 bridges along the *b*-axis, forming a ladder-like structure (Figure 4.74). Thus, each SnF_6 octahedron shares fluorine atoms at *mer*-position with three neighbouring octahedra, forming $([Sn_2F_9]^-)_\infty$ double chains in an infinite array. Important bond lengths and bond angles are listed in Table 4.30. The Sn-F_b-Sn angles of symmetrical *trans*-bridges within each individual single chain are almost linear, ranging from 169.9(4)° to 172.0(4)°, while the angle of transversal Sn(1)-F(11)-Sn(2) bridge between the two chains equals 159.6(4)° (Figure 4.74). Octahedra of the two neighbouring chains are in eclipsed conformation. The bridging (2.0229(6)-2.043(7) Å) and terminal (1.883(7)-1.917(7) Å) bond lengths are consistent with the corresponding values of the previously discussed $([SnF_5]^-)_\infty$ anions.

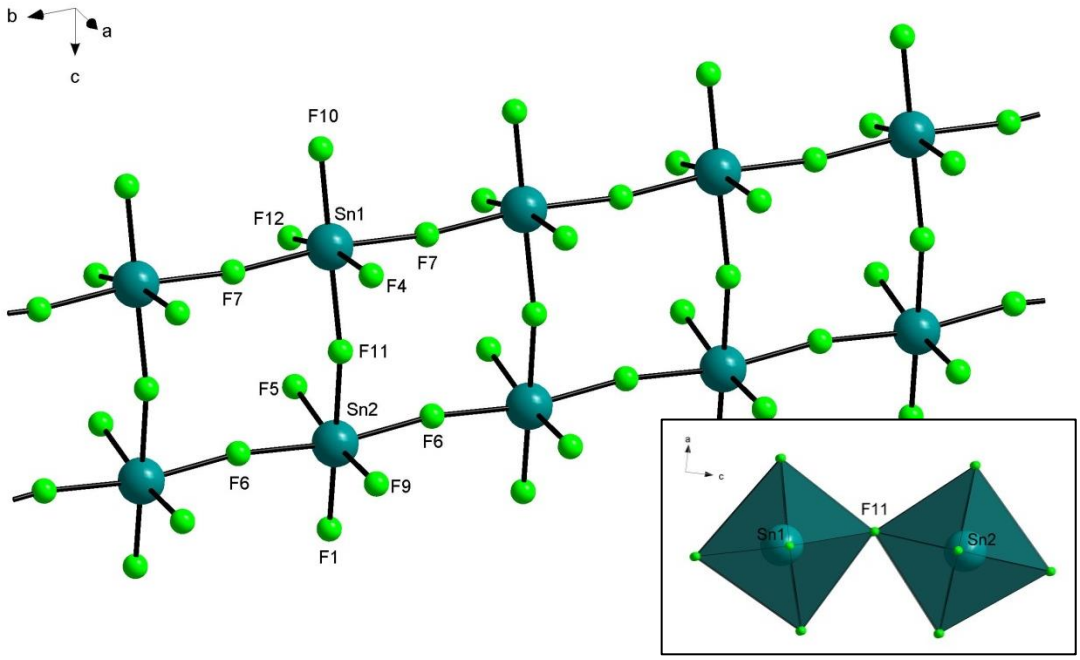


Figure 4.74: Ladder-like structure of the $([Sn_2F_9]^-)_\infty$ anion determined in the compound $Na[Sn_2F_9]\cdot HF$. Broken-off bonds denote further connections.

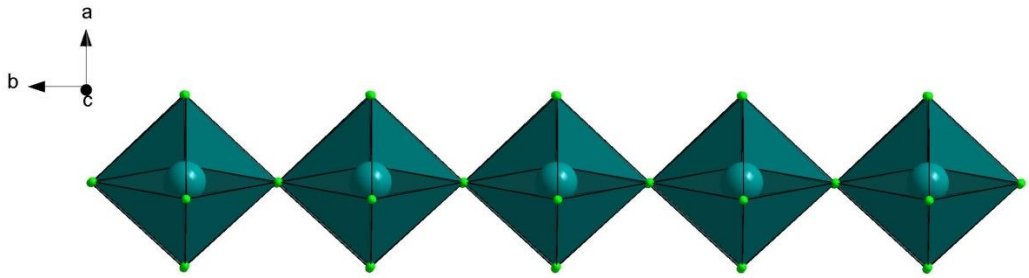


Figure 4.75: The $([Sn_2F_9]^-)_\infty$ anion found in $Na[Sn_2F_9]\cdot HF$ viewed along the crystallographic *c*-axis. The SnF_6 octahedra belonging to separate chains are in eclipsed conformation.

Table 4.30: Selected geometric parameters for the compound $Na[Sn_2F_9]\cdot HF$.

Bond Lengths (Å)			
Sn1—F4	1.899 (7)	Na1—F2	2.430 (5)
Sn1—F10	1.914 (7)	Na1—F2^{i}	2.430 (5)
Sn1—F12	1.915 (7)	Na1—F1^{iii}	2.483 (5)
Sn1—F7	2.0229 (6)	Na1—F1^{iv}	2.483 (5)
Sn1—F7^{i}	2.0229 (6)	Na1—Na1^{i}	4.0359 (4)
Sn1—F11	2.040 (6)	Na1—Na1^{v}	4.0359 (4)

Sn2—F9	1.883 (7)	F1—Na1^{vi}	2.483 (5)
Sn2—F5	1.890 (7)	F1—Na1^{vii}	2.483 (5)
Sn2—F1	1.917 (7)	F2—Na1^{v}	2.430 (5)
Sn2—F6^{i}	2.0258 (7)	F2—H1	0.951 (8)
Sn2—F6	2.0258 (7)	F5—Na1^{viii}	2.360 (9)
Sn2—F11	2.043 (7)	F6—Sn2^{v}	2.0258 (7)
Na1—F12^{ii}	2.315 (8)	F7—Sn1^{v}	2.0229 (6)
Na1—F4	2.330 (8)	F12—Na1^{viii}	2.315 (8)
Na1—F5^{ii}	2.360 (9)		

Bond Angles (°)

F4—Sn1—F10	96.6 (3)	F2—Na1—F2^{i}	112.3 (4)
F4—Sn1—F12	168.2 (3)	F12^{ii}—Na1—F1^{iii}	115.6 (2)
F10—Sn1—F12	95.2 (3)	F4—Na1—F1^{iii}	71.4 (2)
F4—Sn1—F7	90.7 (2)	F5^{ii}—Na1—F1^{iii}	71.6 (2)
F10—Sn1—F7	93.8 (2)	F2—Na1—F1^{iii}	166.7 (3)
F12—Sn1—F7	88.5 (2)	F2^{i}—Na1—F1^{iii}	67.9 (2)
F4—Sn1—F7^{i}	90.7 (2)	F12^{ii}—Na1—F1^{iv}	115.6 (2)
F10—Sn1—F7^{i}	93.8 (2)	F4—Na1—F1^{iv}	71.4 (2)
F12—Sn1—F7^{i}	88.5 (2)	F5^{ii}—Na1—F1^{iv}	71.6 (2)
F7—Sn1—F7^{i}	172.0 (4)	F2—Na1—F1^{iv}	67.9 (2)
F4—Sn1—F11	82.4 (3)	F2^{i}—Na1—F1^{iv}	166.7 (3)
F10—Sn1—F11	179.0 (3)	F1^{iii}—Na1—F1^{iv}	108.7 (3)
F12—Sn1—F11	85.8 (3)	F12^{ii}—Na1—Na1^{i}	90
F7—Sn1—F11	86.2 (2)	F4—Na1—Na1^{i}	90
F7^{i}—Sn1—F11	86.2 (2)	F5^{ii}—Na1—Na1^{i}	90
F9—Sn2—F5	168.9 (3)	F2—Na1—Na1^{i}	146.16 (19)
F9—Sn2—F1	96.7 (3)	F2^{i}—Na1—Na1^{i}	33.84 (19)
F5—Sn2—F1	94.3 (3)	F1^{iii}—Na1—Na1^{i}	35.63 (16)
F9—Sn2—F6^{i}	90.40 (19)	F1^{iv}—Na1—Na1^{i}	144.37 (16)
F5—Sn2—F6^{i}	88.64 (19)	F12^{ii}—Na1—Na1^{v}	90

F1—Sn2—F6^{i}	95.0 (2)	F4—Na1—Na1^{v}	90
F9—Sn2—F6	90.40 (19)	F5^{ii}—Na1—Na1^{v}	90
F5—Sn2—F6	88.64 (19)	F2—Na1—Na1^{v}	33.84 (19)
F1—Sn2—F6	95.0 (2)	F2^{i}—Na1—Na1^{v}	146.15 (19)
F6^{i}—Sn2—F6	169.9 (4)	F1^{iii}—Na1—Na1^{v}	144.37 (16)
F9—Sn2—F11	84.6 (3)	F1^{iv}—Na1—Na1^{v}	35.63 (16)
F5—Sn2—F11	84.4 (3)	Na1^{i}—Na1—Na1^{v}	180.0 (3)
F1—Sn2—F11	178.7 (3)	Sn2—F1—Na1^{vi}	125.53 (16)
F6^{i}—Sn2—F11	85.0 (2)	Sn2—F1—Na1^{vii}	125.53 (16)
F6—Sn2—F11	85.0 (2)	Na1^{vi}—F1—Na1^{vii}	108.7 (3)
F12^{ii}—Na1—F4	165.4 (4)	Na1—F2—Na1^{v}	112.3 (4)
F12^{ii}—Na1—F5^{ii}	80.6 (3)	Na1—F2—H1	123.84 (19)
F4—Na1—F5^{ii}	114.0 (3)	Na1^{v}—F2—H1	123.84 (19)
F12^{ii}—Na1—F2	76.5 (2)	Sn1—F4—Na1	142.2 (4)
F4—Na1—F2	95.6 (3)	Sn2—F5—Na1^{viii}	155.6 (4)
F5^{ii}—Na1—F2	117.5 (2)	Sn2^{v}—F6—Sn2	169.9 (4)
F12^{ii}—Na1—F2^{i}	76.5 (2)	Sn1—F7—Sn1^{v}	172.0 (4)
F4—Na1—F2^{i}	95.6 (3)	Sn1—F11—Sn2	159.6 (4)
F5^{ii}—Na1—F2^{i}	117.5 (2)	Sn1—F12—Na1^{viii}	154.1 (4)

Symmetry codes: (i) *x*, *y*+1, *z*; (ii) *x*−1/2, −*y*+1/2, −*z*+1/2; (iii) −*x*+1/2, *y*+1/2, *z*+1/2; (iv) −*x*+1/2, *y*−1/2, *z*+1/2; (v) *x*, *y*−1, *z*; (vi) −*x*+1/2, *y*−1/2, *z*−1/2; (vii) −*x*+1/2, *y*+1/2, *z*−1/2; (viii) *x*+1/2, −*y*+1/2, −*z*+1/2.

The compound also represents a rare example of HF acting as a bridging ligand between cations and fluoridometalate anions (Figure 4.76). Each Sn(1)F_6 octahedron is coordinated by three adjacent SnF_6-units, two Na^+ cations and a HF molecule (F2···F10, 2.54(1) Å; F2···H1···F10, 118.0(5)°), while each Sn(2)F_6 octahedron interacts with three octahedral SnF_6-units and three Na^+ cations as shown in Figure 4.77. Only the terminal F9 atom does not exhibit further contacts, which reflects in the shortest Sn-F length (1.883(7) Å).

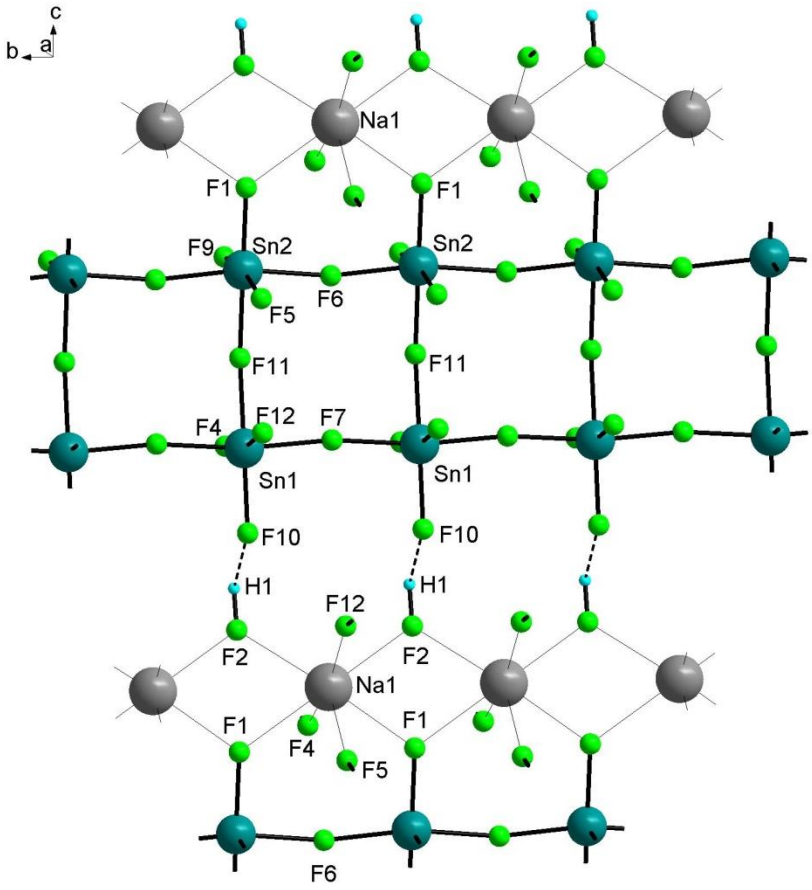


Figure 4.76: Interactions between Na^+ cations, HF molecules and $([Sn_2F_9]^-)_\infty$ anions in the crystal structure of $Na[Sn_2F_9]\cdot HF$.

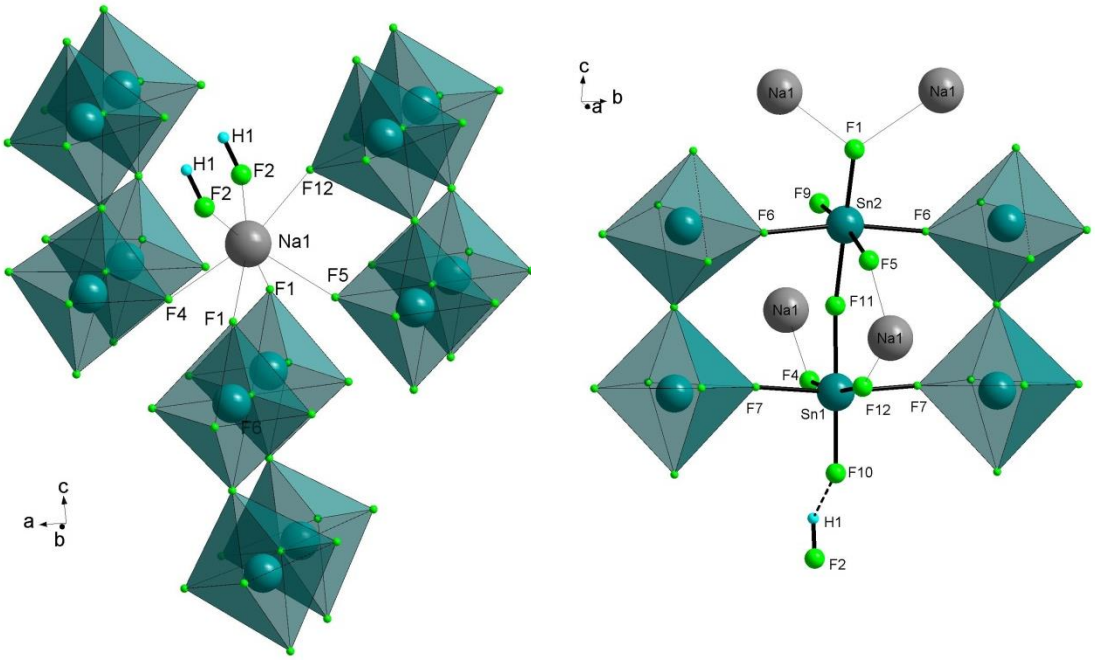


Figure 4.77: Selected structural features of compound $Na[Sn_2F_9]\cdot HF$. *Left* – coordination environment of sodium cations. *Right* – $Sn(1)F_6$ and $Sn(2)F_6$ environment.

The Raman spectra of the reaction bulk sample and randomly oriented (opaque) crystals correspond with the one obtained on $Na[SnF_5]$, which might be due to the partial decomposition on the sample surface. The measurement should be repeated with a freshly synthetized product, possibly wetted with the mother liquor in order to prevent the weakly associated HF molecules from leaving the crystal lattice.

Chapter 5

Conclusions

Thus far, most of the products which resulted from interactions between XeF_2 and strong Lewis acids (e.g. AsF_5, SbF_5, etc.) have been synthetized by reacting pre-calculated amounts of XeF_2 with the corresponding fluoride ion acceptor. After decades of research in the exciting field of noble gas chemistry, the solvent of choice remains anhydrous hydrofluoric acid, aHF. However, at the very beginning of the experimental work on the system XeF_2 – TiF_4, it became obvious that a simple stoichiometric mixing of the reactants may fail to deliver the desired product. Instead, the complex process determining the preferential formation of one among many possible $a XeF_2 \cdot b MF_4$ phases is governed by a subtle interplay of stability of intermediates and products, chemical equilibrium and solubility in the given solvent.

The polymeric nature of TiF_4 and SnF_4 in the solid-state accounts for their low solubility in aHF and considerably hinders their intrinsic fluoride ion accepting affinity. With the addition of strong fluoride ion donors (e.g. NaF, XeF_6, etc.), these compounds dissolve readily in aHF forming monomeric, oligomeric and/or polymeric anions built by vertex-sharing MF_6 octahedra. On the other hand, the fluoride ion transfer from weaker (moderate strong) F^- donors like XeF_2 does not result necessarily in the formation of separate ions or tight ion-pairs. This is well demonstrated by the synthesis and structural determination of $(XeF_2 \cdot TiF_4)_2 \cdot XeF_2$, (and other previously reported compounds $XeF_2 \cdot CrF_4$, $XeF_2 \cdot 2CrF_4$, $(XeF_2 \cdot MnF_4)_2 \cdot XeF_2$ and $XeF_2 \cdot MnF_4$) from TiF_4 and excess of XeF_2 in aHF. The adduct formulation is justified based on the variations in the Xe–F_b bridge bond lengths that can be used to assess the relative fluoride ion acceptor strength of the parent Lewis acid employed. Moreover, the formation of the isostructural compounds $(XeF_2 \cdot MF_4)_2 \cdot XeF_2$, (M = Mn, Ti) indicates a close relationship between the colorless TiF_4 and the colorful MnF_4 chemistry, which might help in predicting their reactivity towards XeF_2 in further studies. Similar complexes are also expected to be formed in the systems KrF_2 – MF_4. (M = Mn, Ti).

The formation of the $(XeF_2 \cdot TiF_4)_2 \cdot XeF_2$ adduct is consistent with the relatively lower Lewis acidity of TiF_4, which is not supposed to give XeF^+ or $Xe_2F_3^+$ salts upon reaction with XeF_2. Surprisingly, thermal reactions between XeF_2 and TiF_4 yielded crystals of the compounds $[Xe_2F_3][Ti_8F_{33}]$ and $[XeF]_2[Ti_9F_{38}]$, which differ from the only known Xe(II) salts containing discrete fluoridoanions with pentavalent metalloid/metal centers and represent the first examples of thermodynamically very stable XeF^+ and $Xe_2F_3^+$ salts with anions of higher dimensionality. The structural determination of these products revealed a novel structural type of the layered $^2_\infty[Ti_8F_{33}]^-$ polyanion and the new columnar $^1_\infty[(Ti_9F_{38})^{2-}]$ anion. $[XeF]_2[Ti_9F_{38}]$ also represents the first example with two efficiently ionized XeF^+ cations, which means that two fluoride ions had to be abstracted from two XeF_2 molecules. Moreover, the $[Xe_2F_3][Ti_8F_{33}]$ salt was prepared with an excess of Lewis acid (TiF_4) over XeF_2, which is in marked contrast to that observed in previous experimental studies.

A large excess of XeF_2 was also used for the synthesis of $[Xe_2F_3][Sn_4F_{17}] \cdot XeF_2 \cdot HF$, part of which co-crystallized in the crystal lattice as in the case of $(XeF_2 \cdot TiF_4)_2 \cdot XeF_2$, thus facilitating the dissolution and subsequent crystallization from the mother liquor. Its crystal structure determination discovered a novel layered wave-like $^2_\infty[Sn_4F_{17}]^-$ anion. The negative charge is balanced by $Xe_2F_3^+$ cations, which are forced to interact with XeF_2 molecules trapped in channels formed between layers. Once more, the association of SnF_6 and SnF_7 units (CN 7 firstly observed for Sn(IV) in a fluorine environment) into larger assemblies provided sufficient charge distribution to stabilize and maintain the $Xe_2F_3^+$ cation. In case of XeF_2 – SnF_4, the association did

not occur during solventless thermal reactions (in contrast to TiF_4, the vapor pressure of SnF_4 is negligible within the acceptable temperature range), but in aHF at low temperatures. Ironically, it seems that the most challenging experimental step is creating the right conditions to overcome the association energies that prevent the dissolution or sublimation of the starting MF_4, only to associate its building blocks again in a rich XeF_2 environment. The discovered ability of novel polymeric anions derived from weaker F^- acceptors to retain highly ionized species of XeF_2 can be understood as a small contribution to Xe(II) chemistry and an opportunity to expand the range of possible architectures which can be provided by the $XeF_2 – MF_4$ systems. However, a much wider impact can be foreseen in the light of the knowledge gained during this research and might be applied to other situations that for various reasons require an un-conventional approach in a one-step synthesis/crystallization. Moreover, the development of a preparative synthetic technique for XeF_2-rich compounds can provide further access to the variety of reported XeF_2-poor complexes, since the majority of these products were obtained by the thermal degradation or solvolysis of the parent XeF_2-rich compounds. Another powerful method worth trying in order to circumvent poor F^- affinity and low solubility problems (as in case of PbF_4) is metathesis, which might deliver the desired anions by simple displacement reactions. Probably the most interesting are phases of different stoichiometry previously detected in the $XeF_2 – PdF_4$ and $XeF_2 – PtF_4$ systems, which remain structurally undefined. Of special interest among these compounds is the product "$XePtF_6$", not only due to its historical role but also because of the experimental challenge that lies behind its elusiveness.

In addition, the by-products structurally characterized within the present work significantly expand the available structural information on fluoridostanates(IV), which have been thus far confined to the $[SnF_6]^{2-}$ anion. The single-chained anion $[SnF_5]^-$ was determined in three compounds - $[H_3O][SnF_5]$, $Na[SnF_5]$, $Na[H_3O][SnF_5]_2$, while the double-chained $[Sn_2F_9]^-$ was found in $Na[Sn_2F_9]\cdot HF$.

Raman spectroscopy proved to be a very powerful tool in an early identification of various fluoridotitanate(IV) anions and the obtained results within this work are in accordance with the reported influence of the TiF_4 content in the polyanion on the Raman shift. However, no such correlation was observed in case of the here described fluoridostannates(IV).

Appendix A

Xenon(II) Fluoridometalates(IV) – General Supporting Information

A.1 $XeF_2 \cdot 2CrF_4$

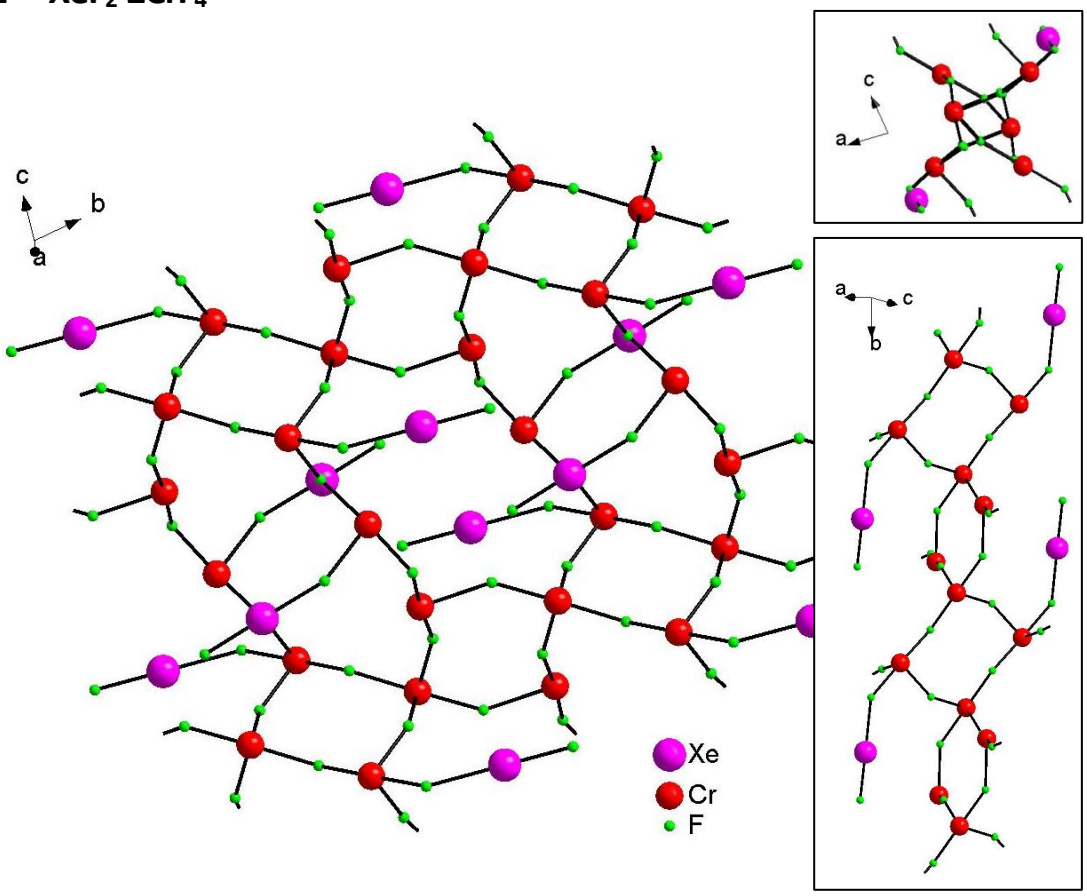


Figure A. 1: Extended structure of the adduct $XeF_2 \cdot 2CrF_4$. The terminal fluorine atoms of CrF_6 units are omitted for clarity; further connections to neighboring units are depicted as broken-off bonds. The exposed (*framed*) parts of the 3-D network show the XeF_2-carrying centrosymmetric rings perpendicularly alternating their positions with XeF_2-free tetrameric rings.

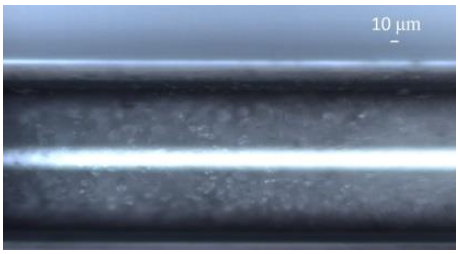
Appendix B

XeF_2 – TiF_4 System

B.1 $(XeF_2 \cdot TiF_4)_2 \cdot XeF_2$

Table B. 1: Fractional atomic coordinates and isotropic/equivalent isotropic displacement parameters (Å^2) for the compound $(XeF_2 \cdot TiF_4)_2 \cdot XeF_2$.

Atom	*x*	*Y*	*z*	U_{iso}*/U_{eq}
Xe1	1	0	1	0.0289 (2)
Xe2	0.91137 (4)	0.47962 (8)	0.67607 (3)	0.0259 (2)
Ti3	1.2060 (1)	0.0615 (2)	0.63593 (8)	0.0210 (3)
F4	1.2863 (3)	0.2803 (7)	0.7591 (2)	0.0289 (8)
F5	1.1144 (4)	−0.1350 (8)	0.5419 (3)	0.0388 (9)
F6	1.1873 (4)	0.3575 (8)	0.5619 (3)	0.0375 (9)
F7	1.3635 (4)	−0.0152 (7)	0.6071 (3)	0.0359 (9)
F8	1.0411 (3)	0.1545 (7)	0.6978 (3)	0.0311 (8)
F9	0.8825 (4)	−0.1875 (10)	0.8895 (4)	0.057 (1)
F10	0.7941 (4)	0.7722 (9)	0.6592 (3)	0.048 (1)



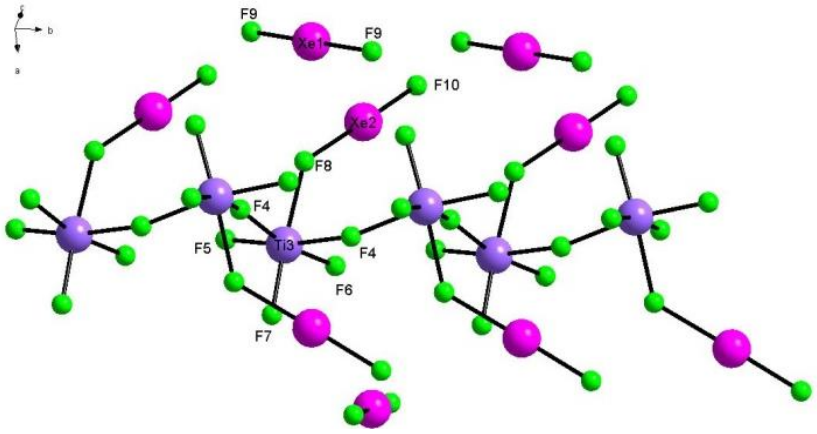


Figure B. 1: Crystal structure (*left*) and tiny crystals of $(XeF_2 \cdot TiF_4)_2 \cdot XeF_2$ (*right*) produced with a high-yield preparative method.

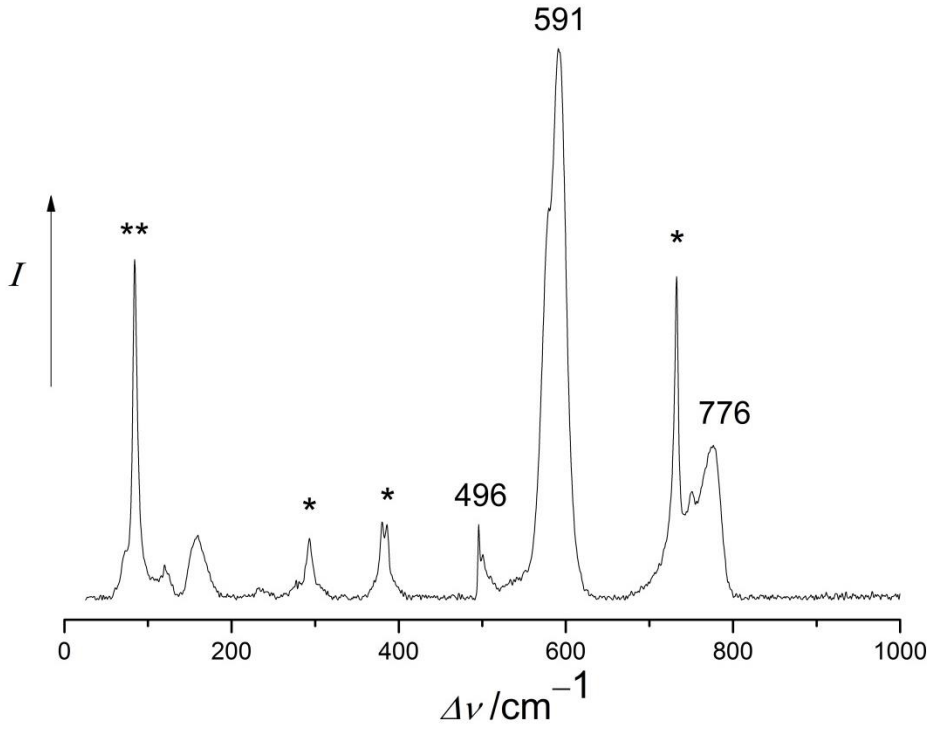


Figure B. 2: Low temperature (−150 °C) Raman spectrum (with applied baseline correction) of the viscous compound of unknown composition in aHF preceding the formation of $(XeF_2 \cdot TiF_4)_2 \cdot XeF_2$. Upon concentration or addition of significant amounts of XeF_2, this substance dissolves and crystals of $(XeF_2 \cdot TiF_4)_2 \cdot XeF_2$ form by slow solvent evaporation or by lowering the reaction temperature. Unreacted XeF_2 is present in the bulk sample (496 cm^{-1}). Symbols denote FEP tube lines (*) and instrumental artifact (**).

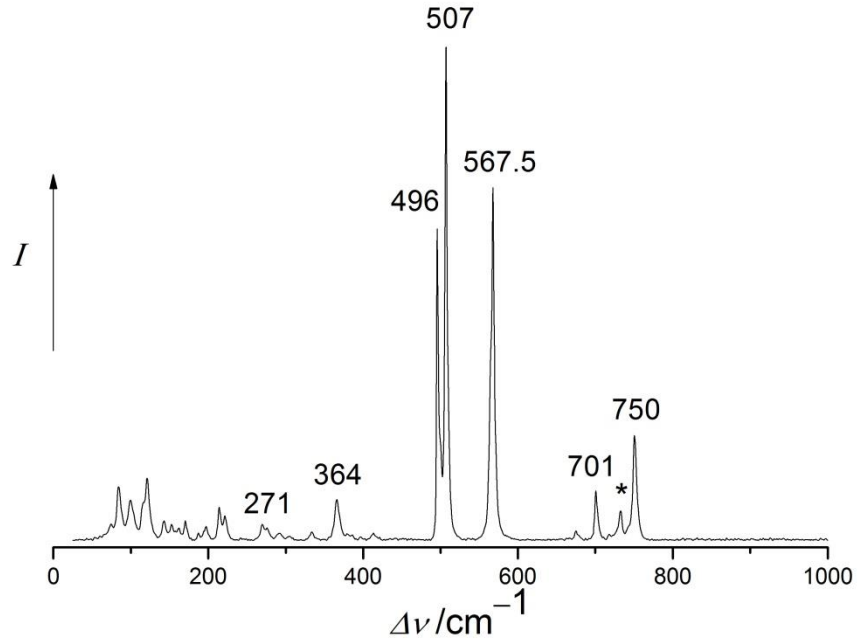


Figure B. 3: Low temperature (−150 °C) Raman spectrum (with applied baseline correction) of $(XeF_2 \cdot TiF_4)_2 \cdot XeF_2$ (bulk). The spectrum corresponds with that obtained on randomly oriented single crystals at room temperature. Since a noticeable amount of XeF_2 is still present (496 cm^{-1}), the existence of an even XeF_2-richer compound is questionable. FEP tube lines are marked with (*) symbol.

B.2 $[Xe_2F_3][Ti_8F_{33}]$

Table B. 2: Fractional atomic coordinates and isotropic/equivalent isotropic displacement parameters ($Å^2$) for the compound $[Xe_2F_3][Ti_8F_{33}]$.

Atom	*x*	*y*	*z*	U_{iso}*/U_{eq}
Xe1	0.27361 (2)	0.51302 (5)	0.281487 (18)	0.03537 (14)
Xe2	0.21268 (3)	0.03225 (5)	0.22218 (2)	0.03883 (14)
Ti1	0.32386 (5)	0.39848 (11)	−0.06040 (4)	0.0194 (2)
Ti2	0.38606 (5)	0.80142 (11)	0.01742 (4)	0.0198 (2)

Ti3	0.51108 (5)	0.60628 (11)	0.17236 (4)	0.0217 (2)
Ti4	0.45142 (5)	0.20645 (11)	0.09378 (4)	0.0199 (2)
Ti5	0.48586 (5)	0.10787 (11)	0.32816 (4)	0.0231 (2)
Ti6	0.32594 (5)	0.10228 (11)	0.44016 (4)	0.0209 (2)
Ti7	0.45148 (5)	0.29889 (11)	0.59387 (4)	0.0208 (2)
Ti8	0.61471 (5)	0.30128 (11)	0.47835 (4)	0.0215 (2)
F1	0.2277 (3)	0.2819 (5)	0.2451 (2)	0.0580 (11)
F2	0.1982 (3)	−0.1878 (5)	0.2018 (2)	0.0611 (12)
F3	0.3118 (3)	0.7162 (5)	0.3106 (2)	0.0571 (11)
F4	0.25	0.4535 (5)	0	0.0251 (9)
F5	0.2763 (2)	0.5180 (4)	−0.12408 (17)	0.0366 (8)
F6	0.27758 (19)	0.2200 (4)	−0.08295 (17)	0.0352 (8)
F7	0.37947 (17)	0.2996 (4)	0.01959 (15)	0.0293 (7)
F8	0.37753 (18)	0.5937 (4)	−0.02079 (16)	0.0302 (7)
F9	0.30687 (17)	0.7771 (4)	0.06031 (17)	0.0319 (7)
F10	0.34413 (19)	0.8953 (4)	−0.05568 (16)	0.0362 (8)
F11	0.4111 (2)	1.0040 (4)	0.05996 (18)	0.0324 (7)
F12	0.45114 (17)	0.7124 (4)	0.09480 (15)	0.0290 (7)
F13	0.59284 (17)	0.6374 (4)	0.10738 (15)	0.0281 (7)
F14	0.5410 (2)	0.7866 (4)	0.21073 (17)	0.0362 (8)
F15	0.42742 (19)	0.5673 (4)	0.20780 (16)	0.0351 (8)
F16	0.5763 (2)	0.4823 (4)	0.22137 (18)	0.0383 (8)
F17	0.48901 (19)	0.4133 (4)	0.10925 (16)	0.0334 (7)
F18	0.38263 (19)	0.2224 (4)	0.14907 (16)	0.0340 (7)
F19	0.5239 (2)	0.1175 (5)	0.14753 (18)	0.0406 (9)
F20	0.51468 (17)	0.1896 (4)	0.01885 (15)	0.0271 (6)
F21	0.4366 (2)	0.2846 (5)	0.3083 (2)	0.0465 (9)
F22	0.5677 (2)	0.1326 (4)	0.28852 (18)	0.0385 (8)
F23	0.4300 (2)	−0.0137 (5)	0.2703 (2)	0.0440 (9)
F24	0.5334 (2)	−0.0925 (4)	0.37395 (18)	0.0365 (8)

F25	0.5368 (2)	0.2034 (4)	0.41317 (16)	0.0374 (8)
F26	0.4089 (2)	0.0524 (4)	0.39560 (17)	0.0356 (8)
F27	0.2608 (2)	−0.0101 (5)	0.3869 (2)	0.0508 (11)
F28	0.3506 (2)	−0.0938 (4)	0.49653 (18)	0.0387 (8)
F29	0.25	0.1385 (6)	0.5	0.0309 (10)
F30	0.39407 (19)	0.2021 (5)	0.51213 (17)	0.0392 (8)
F31	0.3086 (2)	0.2830 (5)	0.3995 (2)	0.0472 (10)
F32	0.3661 (2)	0.3241 (4)	0.62773 (19)	0.0410 (9)
F33	0.5136 (2)	0.3846 (5)	0.65755 (18)	0.0444 (9)
F34	0.4369 (2)	0.4994 (4)	0.54529 (19)	0.0359 (8)
F35	0.53606 (16)	0.2693 (4)	0.53932 (15)	0.0282 (7)
F36	0.6729 (2)	0.3908 (5)	0.5433 (2)	0.0485 (10)
F37	0.6721 (2)	0.3219 (4)	0.4143 (2)	0.0435 (9)

B.3 $[XeF]_2[Ti_9F_{38}]$

Table B. 3: Fractional atomic coordinates and isotropic/equivalent isotropic displacement parameters (Å^2) for the compound $[XeF]_2[Ti_9F_{38}]$.

Atom	*x*	*y*	*z*	U_{iso}*/U_{eq}
Xe1	0.60550 (2)	1.06521 (3)	0.94942 (3)	0.02249 (10)
Xe2	0.03915 (2)	1.06795 (3)	0.38264 (3)	0.02189 (10)
Ti1	0.50379 (7)	0.85868 (8)	1.02118 (10)	0.0167 (2)
Ti2	0.28014 (6)	0.85815 (8)	0.99818 (10)	0.0142 (2)
Ti3	0.39442 (7)	0.64083 (8)	1.01560 (10)	0.0170 (2)
Ti4	0.42686 (7)	0.86620 (7)	0.67620 (10)	0.0133 (2)
Ti5	0.20487 (7)	0.85326 (8)	0.66019 (10)	0.0143 (2)
Ti6	0.32602 (8)	0.64074 (6)	0.67017 (13)	0.01458 (18)
Ti7	0.35040 (7)	0.86692 (8)	0.33683 (10)	0.0135 (2)

Ti8	0.12880 (6)	0.83945 (8)	0.31554 (9)	0.0163 (2)
Ti9	0.26030 (7)	0.63677 (8)	0.32506 (10)	0.0161 (2)
F1	0.5181 (2)	0.9807 (2)	1.0013 (3)	0.0238 (8)
F2	0.6735 (3)	1.1387 (3)	0.8971 (5)	0.0417 (12)
F3	0.1029 (2)	0.9576 (3)	0.3325 (4)	0.0253 (8)
F4	−0.0078 (3)	1.1669 (3)	0.4263 (4)	0.0454 (13)
F5	0.5955 (2)	0.8370 (3)	1.0002 (3)	0.0252 (8)
F6	0.5350 (3)	0.8631 (3)	1.1732 (4)	0.0270 (9)
F7	0.4688 (2)	0.7430 (2)	1.0081 (3)	0.0195 (8)
F8	0.4541 (2)	0.8587 (3)	0.8405 (3)	0.0206 (8)
F9	0.2567 (2)	0.9679 (3)	0.9951 (4)	0.0274 (9)
F10	0.1862 (2)	0.8166 (3)	0.9906 (4)	0.0274 (9)
F11	0.2559 (2)	0.8543 (3)	0.8316 (4)	0.0240 (9)
F12	0.3920 (2)	0.8860 (2)	1.0107 (3)	0.0166 (7)
F13	0.3194 (2)	0.7401 (2)	0.9980 (4)	0.0196 (8)
F14	0.4245 (3)	0.6561 (3)	1.1695 (4)	0.0275 (9)
F15	0.4733 (3)	0.5723 (3)	1.0103 (4)	0.0300 (11)
F16	0.3201 (3)	0.5635 (3)	1.0023 (5)	0.0294 (10)
F17	0.3937 (2)	0.7438 (2)	0.6664 (3)	0.0170 (7)
F18	0.3607 (3)	0.6545 (3)	0.8381 (4)	0.0222 (9)
F19	0.4059 (3)	0.5720 (2)	0.6761 (4)	0.0244 (10)
F20	0.2529 (3)	0.5633 (3)	0.6678 (5)	0.0264 (10)
F21	0.2908 (3)	0.6498 (3)	0.5036 (4)	0.0233 (9)
F22	0.2483 (2)	0.7350 (2)	0.6699 (3)	0.0182 (8)
F23	0.1174 (2)	0.8123 (3)	0.6804 (4)	0.0284 (9)
F24	0.1748 (2)	0.8438 (3)	0.4972 (3)	0.0216 (8)
F25	0.1793 (2)	0.9626 (3)	0.6594 (4)	0.0243 (8)
F26	0.3140 (2)	0.88427 (19)	0.6645 (4)	0.0171 (6)
F27	0.5193 (2)	0.8370 (3)	0.6619 (4)	0.0242 (9)
F28	0.4417 (2)	0.9787 (2)	0.6800 (3)	0.0228 (8)

F29	0.3799 (3)	0.8663 (3)	0.5045 (4)	0.0229 (8)
F30	0.3558 (2)	0.9799 (2)	0.3312 (3)	0.0228 (8)
F31	0.3132 (3)	0.8540 (2)	0.1683 (4)	0.0244 (8)
F32	0.2377 (2)	0.8798 (3)	0.3300 (4)	0.0204 (8)
F33	0.3256 (2)	0.7439 (2)	0.3449 (4)	0.0188 (8)
F34	0.3436 (3)	0.5713 (2)	0.3410 (4)	0.0254 (9)
F35	0.1891 (3)	0.5578 (3)	0.3291 (5)	0.0270 (10)
F36	0.1763 (2)	0.7287 (3)	0.3320 (3)	0.0191 (8)
F37	0.2309 (3)	0.6520 (3)	0.1726 (4)	0.0292 (10)
F38	0.4475 (2)	0.8412 (3)	0.3396 (4)	0.0264 (9)
F39	0.0397 (2)	0.8040 (3)	0.3355 (4)	0.0263 (9)
F40	0.1005 (3)	0.8440 (3)	0.1634 (4)	0.0290 (9)

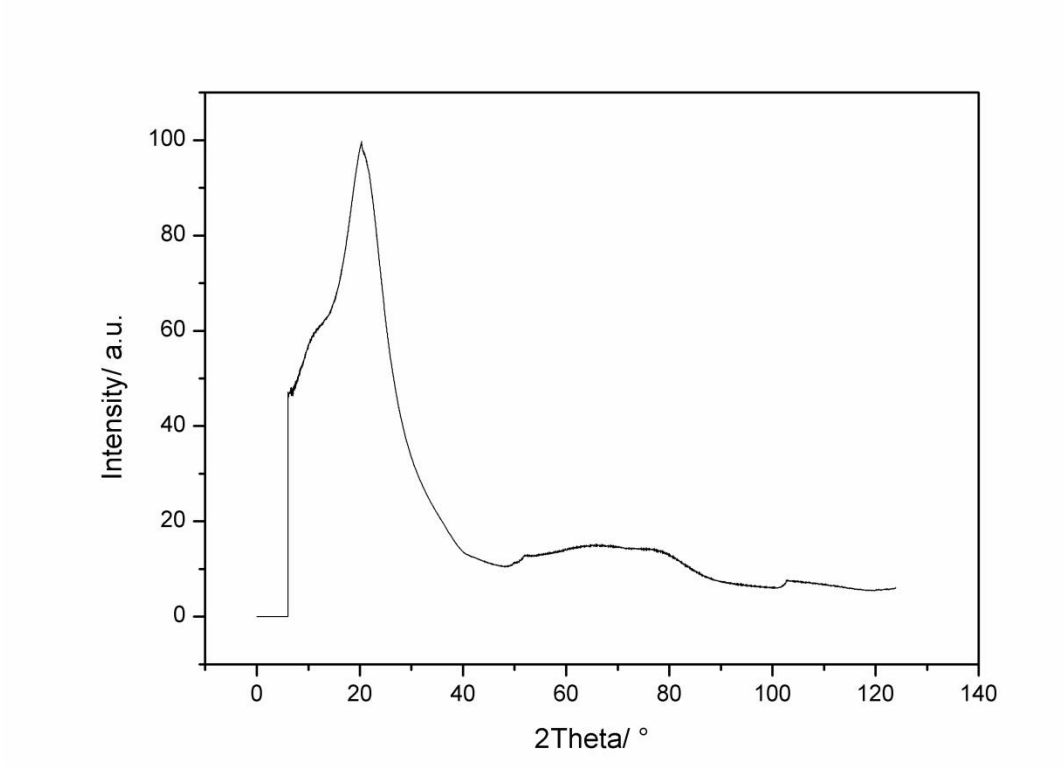


Figure B. 4: X-ray diffraction pattern of a powdered sample of the glassy material found in thermal reactions between XeF_2 and TiF_4.

B.4 β-$[H_3O][Ti_2F_9]$

Table B. 4: Fractional atomic coordinates and isotropic/equivalent isotropic displacement parameters (Å^2) for the compound β -$[H_3O][Ti_2F_9]$.

Atom	*x*	*y*	*z*	U_{iso}*/U_{eq}
Ti1	0.75114 (15)	0.95912 (5)	0.75833 (9)	0.0300 (3)
Ti2	0.74616 (15)	0.87767 (5)	0.34673 (9)	0.0314 (3)
F1	0.7907 (5)	0.91426 (16)	0.5551 (3)	0.0391 (7)
F2	0.4859 (5)	0.89595 (16)	0.7852 (3)	0.0460 (8)
F3	0.9617 (5)	0.88099 (16)	0.8322 (3)	0.0411 (7)
F4	0.4576 (5)	0.95662 (16)	0.3459 (3)	0.0342 (7)
F5	0.6776 (6)	0.86128 (18)	0.1516 (3)	0.0476 (8)
F6	0.7382 (5)	1.02038 (17)	0.9226 (3)	0.0440 (8)
F7	0.5365 (6)	0.79813 (17)	0.4109 (4)	0.0539 (8)
F8	1.0158 (5)	0.81354 (16)	0.3573 (3)	0.0427 (7)
F9	1.0473 (5)	1.02763 (15)	0.6989 (3)	0.0380 (7)
O1	0.2506 (6)	0.8102 (2)	0.0245 (4)	0.0425 (9)
H1	0.1264	0.8420	−0.0200	0.051*
H2	0.2420	0.7560	−0.0150	0.051*
H3	0.4090	0.8350	0.0226	0.051*

Appendix C

XeF_2 – SnF_4 System

C.1 $[Xe_2F_3][Sn_4F_{17}]\cdot XeF_2\cdot HF$

C.1.1 Supplementary Data

Table C. 1: Fractional atomic coordinates and isotropic/equivalent isotropic displacement parameters (Å^2) for the compound $[Xe_2F_3][Sn_4F_{17}]\cdot XeF_2\cdot HF$.

Atom	*x*	*y*	*z*	U_{iso}*/U_{eq}
Xe1	0.663973 (19)	0.347667 (8)	0.508676 (17)	0.01832 (5)
Xe2	0.46877 (3)	0.498684 (11)	0.750000	0.01585 (6)
Sn1	0.25915 (3)	0.233797 (11)	0.250000	0.00837 (6)
Sn2	0.00815 (3)	0.482632 (11)	0.750000	0.00959 (6)
Sn3	0.179045 (18)	0.385155 (7)	0.451576 (16)	0.00795 (5)
F1	0.6118 (4)	0.250000	0.500000	0.0437 (8)
F2	0.6939 (2)	0.43623 (8)	0.51358 (19)	0.0347 (5)
F3	0.4387 (3)	0.59092 (10)	0.750000	0.0236 (5)
F4	0.4992 (3)	0.40633 (10)	0.750000	0.0261 (6)
F5	0.2099 (4)	0.25460 (18)	0.250000	0.0661 (11)
H5	0.109 (2)	0.252 (4)	0.250000	0.16 (4)*
F6	0.4583 (2)	0.22809 (10)	0.250000	0.0190 (5)
F7	0.0582 (2)	0.24244 (11)	0.250000	0.0231 (5)
F8	0.24062 (17)	0.16728 (7)	0.38484 (14)	0.0160 (3)
F9	0.26890 (16)	0.29953 (6)	0.38909 (14)	0.0143 (3)
F10	0.1434 (2)	0.54755 (10)	0.750000	0.0204 (5)
F11	−0.1295 (3)	0.41860 (11)	0.750000	0.0233 (5)
F12	0.12320 (17)	0.43626 (7)	0.61720 (14)	0.0178 (3)
F13	−0.09802 (17)	0.52789 (6)	0.89103 (14)	0.0153 (3)

F14	−0.00149 (17)	0.34838 (8)	0.45358 (16)	0.0207 (4)
F15	0.36027 (16)	0.42136 (7)	0.45957 (15)	0.0156 (3)
F16	0.1818 (3)	0.38611 (9)	0.250000	0.0173 (5)

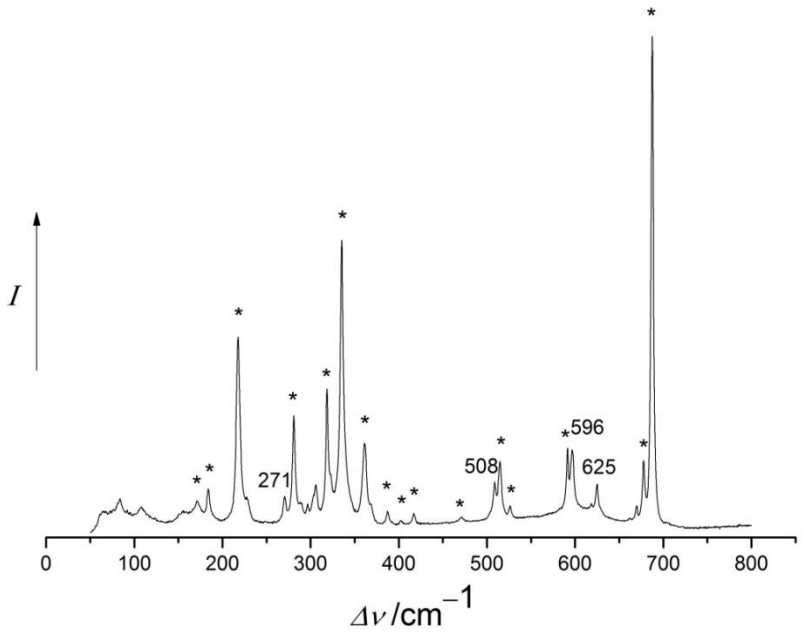


Figure C. 1: Raman spectrum recorded on a single-crystal of $[Xe_2F_3][Sn_4F_{17}]\cdot XeF_2\cdot HF$. The background is dominated by peaks (*) arising from a protective layer of perfluorinated oil (perfluordecalin).

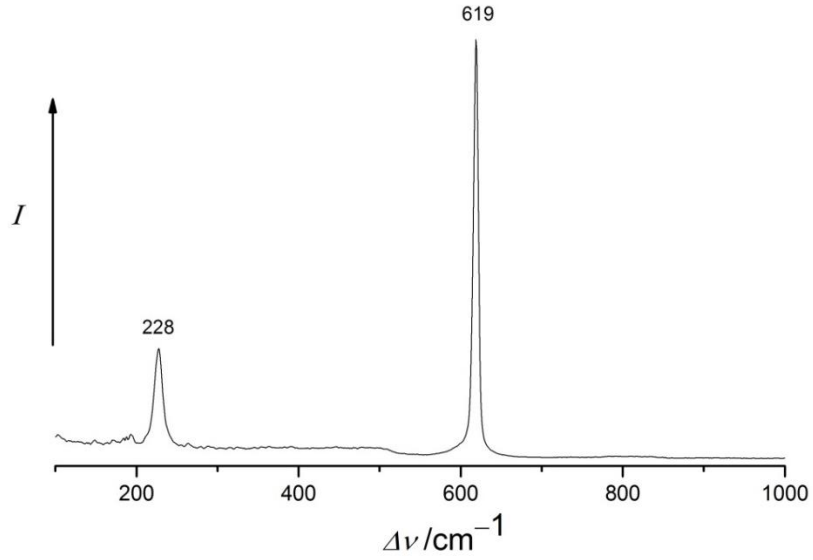


Figure C. 2: Raman spectrum of SnF_4 recorded on a powdered sample.

C.1.2 Anionic $[Sn_4F_{17}]^-$ Layers – Sinusoidal Approximation

A sine wave mathematical curve, usually represented as a periodic function of time, describes a regular repetitive oscillation:

$$y(t) = A\,sin(\omega t + \varphi) \quad \text{(A.1)}$$

where *A* is the amplitude, ω the angular frequency and φ the phase shift. The main concept was to transform the basic form by substituting the function values and time dependency with fractional atomic coordinates of interest, in our case:

$$x(y) = A\,sin(By) \quad \text{(A.2)}$$

where x and y (but not z) variables were used, as the sinusoid propagation can only be observed along the *ab* plane.

Details on the sine-wave calculation and data fitting are given below.

Calculation. The least square method (LS) was used for regression analysis. This approach finds the optimum model function to fit the given data set (**Error! Reference source not found.**) by adjusting the parameters (constants A and B in Eq. (A.2)) in order to minimize the sum of squared residuals ($S = \sum(x\text{-}x')^2$).

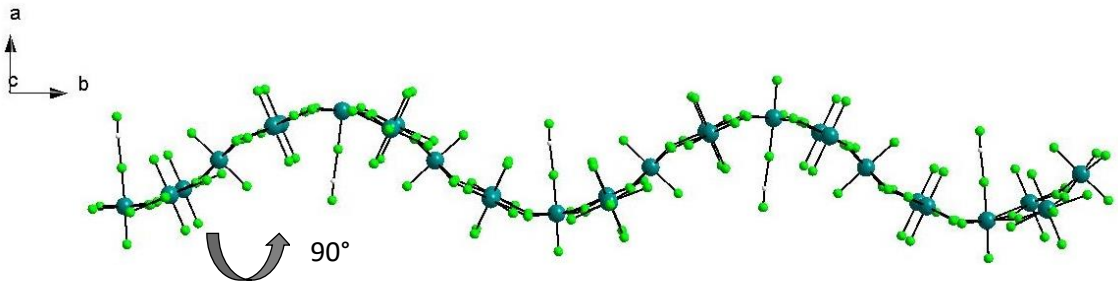
Table C. 2: Answer report[316] and details on the fitting process. The starting values of the constants A and B (educated guess, A = amplitude; B = π/0.48) were optimized to the objective minimum.

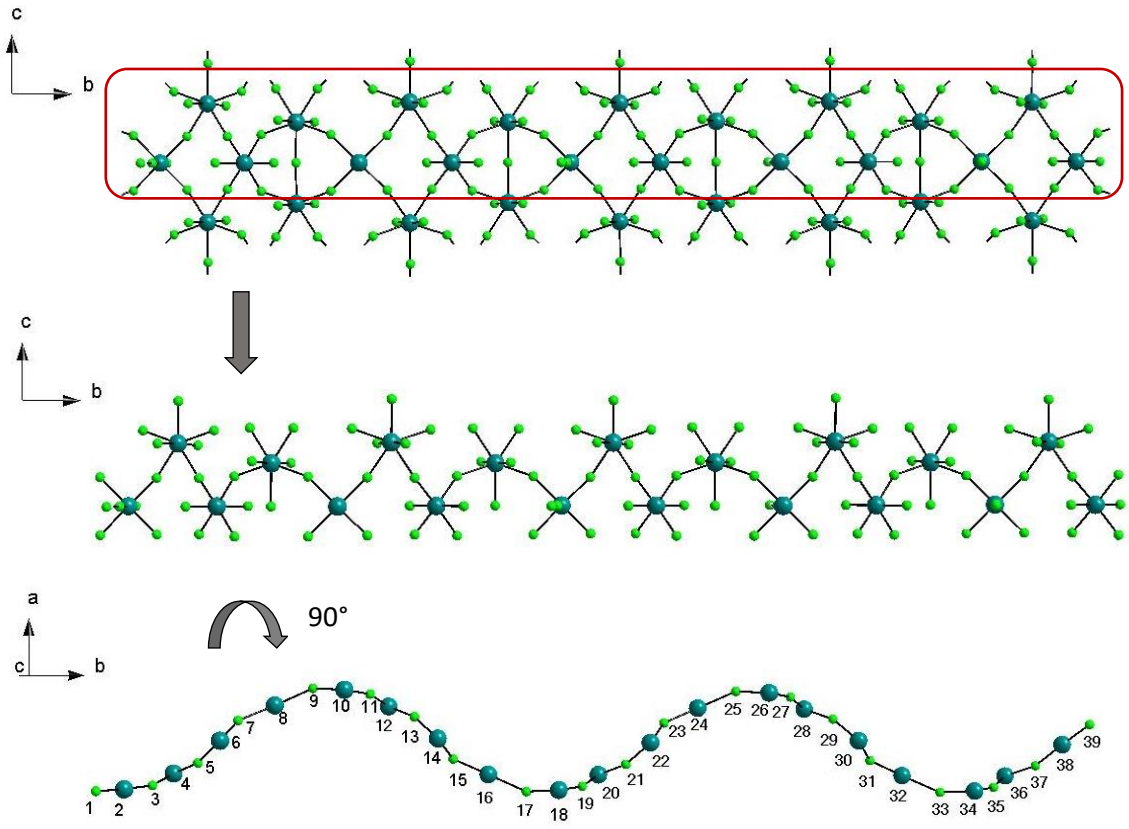
Engine	GRG Nonlinear	
Solution Time	0.016 seconds	
Iterations	5	
Variables	Original value	Final value
A	0.268	0.27598
B	6.541	6.28505
Objective $S = \sum(x\text{-}x')^2$	0.06707	0.01754

Table C. 3: Selected atoms used for regression analysis, their corresponding symmetry operations, fractional atomic coordinates, computed values (x') and squared residuals.

No.	Atom	Symmetry	x	y	z	x'	$(x\text{-}x')^2$
1	F9	-x, -1-y, 1-z	-0.2689	-1.29953	0.61091	-0.26252	4.07E-05
2	Sn1	-x, -1-y, 0.5+z	-0.25915	-1.2338	0.75	-0.27462	0.000239
3	F8	-x, -1-y, 0.5+z	-0.24062	-1.16728	0.88484	-0.23983	6.19E-07
4	Sn3	-x, -1.5+y, 1.5-z	-0.17905	-1.11485	1.04842	-0.18274	1.36E-05
5	F12	-x, -1.5+y, 1.5-z	-0.1232	-1.06374	0.8828	-0.1081	0.000228

6	Sn2	-x, -1.5+y, 1.5-z	-0.00815	-1.01737	0.75	-0.03058	0.000503
7	F13	-x, -1.5+y, z	0.09802	-0.97211	0.89103	0.047623	0.00254
8	Sn3	x, -0.5-y, 0.5+z	0.17905	-0.88515	0.95158	0.181971	8.53E-06
9	F9	x, -0.5-y, 0.5+z	0.2689	-0.79953	0.88909	0.262597	3.97E-05
10	Sn1	x, -0.5-y, 1-z	0.25915	-0.7338	0.75	0.274589	0.000238
11	F8	x, -0.5-y, 0.5+z	0.24062	-0.66728	0.88484	0.239706	8.36E-07
12	Sn3	x, -1+y, 1.5-z	0.17905	-0.61485	1.04842	0.182551	1.23E-05
13	F12	x, -1+y, 1.5-z	0.1232	-0.56374	0.8828	0.107863	0.000235
14	Sn2	x, -1+y, z	0.00815	-0.51737	0.75	0.030325	0.000492
15	F13	x, -1+y, z	-0.09802	-0.47211	0.89103	-0.04788	0.002514
16	Sn3	-x, -y, 0.5+z	-0.17905	-0.38516	0.95158	-0.18215	9.62E-06
17	F9	-x, -y, 0.5+z	-0.2689	-0.29953	0.88909	-0.26268	3.87E-05
18	Sn1	-x, -y, 0.5+z	-0.25915	-0.2338	0.75	-0.27456	0.000238
19	F8	-x, -y, 0.5+z	-0.24062	-0.16728	0.88484	-0.23958	1.09E-06
20	Sn3	-x, -0.5+y, 1.5-z	-0.17905	-0.11485	1.04842	-0.18236	1.09E-05
21	F12	-x, -0.5+y, 1.5-z	-0.1232	-0.06374	0.8828	-0.10763	0.000243
22	Sn2	-x, -0.5+y, 1.5-z	-0.00815	-0.01737	0.75	-0.03007	0.00048
23	F13	-x, -0.5+y, z	0.09802	0.02789	0.89103	0.048129	0.002489
24	Sn3	x, 0.5-y, 0.5+z	0.17905	0.11485	0.95158	0.182358	1.09E-05
25	F9	x, 0.5-y, 0.5+z	0.2689	0.20047	0.88909	0.262755	3.78E-05
26	Sn1	x, 0.5-y, 1-z	0.25915	0.2662	0.75	0.274537	0.000237
27	F8	x, 0.5-y, 0.5+z	0.24062	0.33272	0.88484	0.23945	1.37E-06
28	Sn3	x, y, 1.5-z	0.17905	0.38516	1.04842	0.182152	9.62E-06
29	F12	x, y, 1.5-z	0.1232	0.43626	0.8828	0.107389	0.00025
30	Sn2	x, y, z	0.00815	0.48263	0.75	0.029814	0.000469
31	F13	x, y, z	-0.09802	0.52789	0.89103	-0.04838	0.002464
32	Sn3	-x, 1-y, 0.5+z	-0.17905	0.61485	0.95158	-0.18255	1.23E-05
33	F9	-x, 1-y, 0.5+z	-0.2689	0.70047	0.88909	-0.26283	3.68E-05
34	Sn1	-x, 1-y, 0.5+z	-0.25915	0.7662	0.75	-0.27451	0.000236
35	F8	-x, 1-y, 0.5+z	-0.24062	0.83272	0.88484	-0.23932	1.68E-06
36	Sn3	-x, 0.5+y, 1.5-z	-0.17905	0.88515	1.04842	-0.18197	8.53E-06
37	F12	-x, 0.5+y, 1.5-z	-0.1232	0.93626	0.8828	-0.10715	0.000258
38	Sn2	-x, 0.5+y, 1.5-z	-0.00815	0.98263	0.75	-0.02956	0.000458
39	F13	-x, 0.5+y, 1.5-z	0.09802	1.02789	0.60897	0.048636	0.002439





$x(v) = 0.27598\,sin(6.28505v)$

S = 0.01754

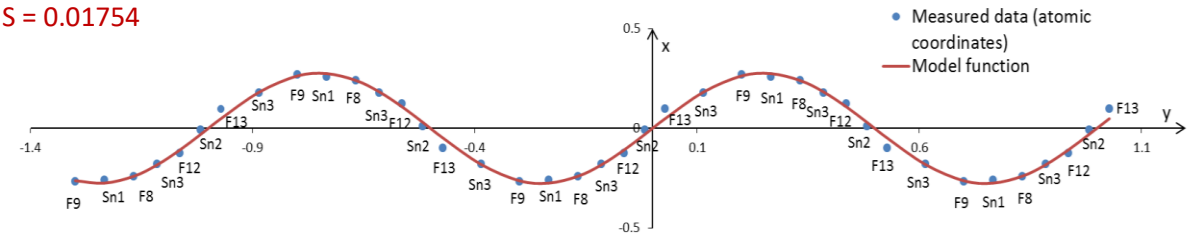


Figure C. 3: A wave-like ribbon was selected from the anionic layer found in the structure of $[Xe_2F_3][Sn_4F_{17}]\cdot XeF_2\cdot HF$ and rotated for 90°. A group of 39 atoms bound in an alternating sequence [-F-Sn-F-] was chosen from the upper part (chain) of the ribbon as shown above. Although the model sinusoid fitted better with tin parameters, an excellent match was achieved taking into account both fluorine and tin atoms. The equation is also simplified due to the favorable crystallographic selection of the origin of the coordinate system.

C.2 Experiments in Liquid Xenon

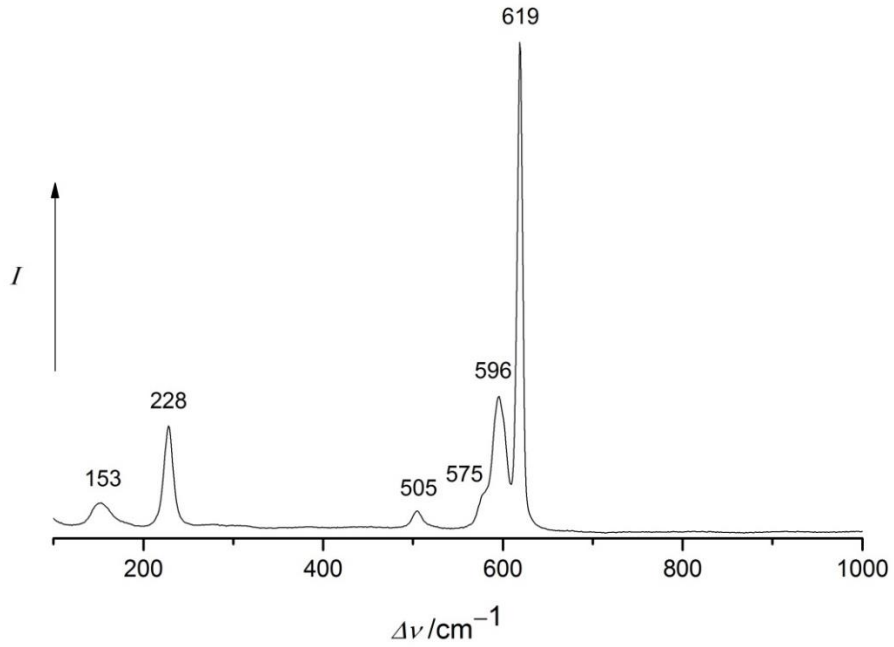


Figure C. 4: Raman spectrum of a sample at RT obtained after aHF-solvolysis of the product formed in a reaction of XeF_2 and SnF_4 in liquid xenon.

C.3 $[H_3O]_2[SnF_6]$

Table C. 4: Fractional atomic coordinates and isotropic/equivalent isotropic displacement parameters (Å²) for the compound $[H_3O]_2[SnF_6]$.

Atom	*x*	*y*	*z*	U_{iso}*/U_{eq}
Sn1	0.5000	0.5000	0.5000	0.0175 (5)
F1	0.6469 (2)	0.6502 (6)	0.5153 (3)	0.0339 (9)
F2	0.5339 (3)	0.2071 (7)	0.4071 (3)	0.0393 (10)
F3	0.5749 (3)	0.3278 (7)	0.6661 (3)	0.0389 (9)
O1	0.1736 (7)	0.5227 (9)	0.3153 (9)	0.0277 (15)
H1	0.1460	0.3820	0.2560	0.033*
H2	0.1239	0.5600	0.3626	0.033*
H3	0.2478	0.4849	0.3710	0.033*

C.4 $[H_3O][SnF_5]$

Table C. 5: Fractional atomic coordinates and isotropic/equivalent isotropic displacement parameters (Å^2) for the compound $[H_3O][SnF_5]$.

Atom	*x*	*y*	*z*	U_{iso}*/U_{eq}
Sn1	0.36132 (3)	0.50729 (7)	0.82319 (3)	0.01318 (17)
F1	0.4498 (3)	0.7423 (8)	0.9315 (3)	0.0268 (9)
F2	0.3796 (3)	0.6814 (8)	0.7088 (3)	0.0268 (9)
F3	0.4558 (3)	0.2352 (8)	0.8297 (3)	0.0274 (9)
F4	0.2534 (3)	0.2731 (8)	0.7086 (3)	0.0222 (8)
F5	0.3216 (3)	0.3247 (8)	0.9211 (3)	0.0238 (8)
O1	0.3756 (3)	1.0153 (8)	0.5726 (3)	0.0176 (9)
H1	0.377 (5)	0.927 (11)	0.634 (3)	0.021*
H2	0.363 (5)	0.895 (9)	0.515 (3)	0.021*
H3	0.431 (3)	1.131 (11)	0.589 (4)	0.021*

C.5 $Na[SnF_5]$

Table C. 6: Fractional atomic coordinates and isotropic/equivalent isotropic displacement parameters (Å^2) for the compound $[Na][SnF_5]$.

Atom	*x*	*y*	*z*	U_{iso}*/U_{eq}
Sn1	0.750000	0.500000	0.64605 (2)	0.0078 (2)
Na1	0.750000	1.000000	0.43123 (17)	0.0119 (5)
F1	0.8941 (4)	0.7495 (4)	0.55691 (14)	0.0131 (4)
F2	0.4603 (4)	0.7078 (4)	0.65293 (13)	0.0145 (5)
F3	0.8725 (5)	0.750000	0.750000	0.0113 (6)

C.6 $Na[H_3O][SnF_5]_2$

Table C. 7: Fractional atomic coordinates and isotropic/equivalent isotropic displacement parameters (Å^2) for the compound $Na[H_3O][SnF_5]_2$.

Atom	*x*	*y*	*z*	U_{iso}*/U_{eq}
Sn1	0.159787 (13)	0.75157 (10)	0.06629 (2)	0.00774 (9)
Sn2	0.115480 (13)	0.24573 (9)	0.23601 (2)	0.00811 (9)

Na1	0.29382 (7)	0.2533 (5)	0.10375 (12)	0.0113 (4)
F1	0.22579 (12)	0.9549 (6)	0.1281 (2)	0.0126 (7)
F2	0.14602 (12)	0.9930 (6)	−0.0335 (2)	0.0130 (7)
F3	0.08836 (12)	0.5534 (6)	0.0173 (2)	0.0133 (7)
F4	0.21172 (12)	0.4955 (6)	0.0251 (2)	0.0116 (6)
F5	0.10860 (12)	0.9989 (6)	0.12744 (19)	0.0113 (7)
F6	0.16322 (12)	0.5027 (6)	0.17299 (19)	0.0115 (7)
F7	0.18547 (12)	0.0439 (6)	0.2842 (2)	0.0138 (7)
F8	0.12659 (13)	0.4952 (6)	0.3331 (2)	0.0146 (7)
F9	0.04567 (13)	0.4300 (6)	0.1731 (2)	0.0162 (7)
F10	0.06426 (13)	−0.0064 (6)	0.2811 (2)	0.0157 (7)
O1	0.02839 (14)	0.2293 (9)	−0.0946 (2)	0.0132 (8)
H1	0.0586 (13)	0.305 (8)	−0.052 (2)	0.016*
H2	−0.0029 (13)	0.339 (8)	−0.113 (3)	0.016*
H3	0.0417 (17)	0.128 (9)	−0.136 (2)	0.016*

C.7 $Na[Sn_2F_9]\cdot HF$

Table C. 8: Fractional atomic coordinates and isotropic/equivalent isotropic displacement parameters (Å^2) for the compound $Na[Sn_2F_9]\cdot HF$.

Atom	*x*	*y*	*z*	U_{iso}*/U_{eq}
Sn1	0.38375 (5)	0.25	0.37492 (6)	0.0140 (3)
Sn2	0.36118 (5)	0.25	0.06281 (6)	0.0142 (3)
Na1	0.1185 (3)	0.25	0.3019 (4)	0.0234 (11)
F1	0.3767 (4)	0.25	−0.0856 (6)	0.0216 (17)
F2	0.1506 (6)	−0.25	0.2030 (6)	0.0294 (18)
F4	0.2554 (5)	0.25	0.3939 (6)	0.0194 (15)
F5	0.4876 (5)	0.25	0.0912 (6)	0.0238 (15)
F6	0.3621 (5)	−0.25	0.0767 (6)	0.0214 (17)
F7	0.3841 (5)	−0.25	0.3639 (6)	0.0226 (18)
F9	0.2328 (5)	0.25	0.0626 (5)	0.0207 (16)
F10	0.4152 (5)	0.25	0.5197 (5)	0.0201 (15)

F11	0.3479 (5)	0.25	0.2213 (5)	0.0210 (16)
F12	0.5071 (5)	0.25	0.3259 (5)	0.0238 (16)
H1	0.1732	−0.25	0.1335	0.029*

Bibliography

Publications Related to the Thesis

Journal Articles

K. Radan, E. A. Goreshnik and B. Žemva, "Xenon(II) Polyfluoridotitanates(IV): Synthesis and Structural Characterization of $[Xe_2F_3]^+$ and $[XeF]^+$ Salts," *Angewandte Chemie International Edition,* vol. 53, pp. 13715-13719, 2014.

Conference Paper

K. Radan and B. Žemva, "Solvent capabilities of liquid and supercritical xenon", in *Proceedings of the 4th Jožef Stefan International Postgraduate School Students Conference*, Ljubljana, Slovenia: Jožef Stefan International Postgraduate School, 2012.

K. Radan, E. A. Goreshnik and B. Žemva, "Structures from the systems XeF_2/MF_4", in *Proceedings of the 7th Young researchers' day*, Ljubljana, Slovenia: Jožef Stefan Institute, 2013.

K. Radan, E. A. Goreshnik and B. Žemva, "XeF_2 rich" and "XeF_2 poor" compounds in the system XeF_2 – TiF_4", in *Final program and book of abstracts of the 17th European Symposium on Fluorine Chemistry*, Paris, France, 2012.

K. Radan, E. A. Goreshnik and B. Žemva, "Oksonijeve soli nekaterih perfluorostanatov(IV) in perfluorotitanatov(IV) ter kristalna struktura $Na(Sn_2F_9)\cdot HF$", in *Proceedings of the Slovenian chemical days 2013*, Maribor, Slovenia: Faculty of Chemistry and Chemical Technology, University of Maribor, Slovenian Chemical Society, 2013.

K. Radan, M. Lozinšek and B. Žemva, "Inonization pathway of XeF_2 from neutral molecules to XeF^+ salts", in *Proceedings of the 248th ACS National Meeting & Exposition*, San Francisco, USA: American Chemical Society, 2014.

K. Radan and B. Žemva, "Novosti na področju ksenonovih spojin s polimernimi fluoridoanioni", in *Proceedings of the Slovenian chemical days 2016*, Portorož, Slovenia: Slovenian Chemical Society, 2016.

Other Publications

Journal Articles

K. Radan, M. Lozinšek, E. A. Goreshnik and B. Žemva, "Syntheses, structures and Raman spectra of $Cd(BF_4)(AF_6)$ (A = Ta, Bi) compounds," *Journal of Fluorine Chemistry,* vol. 132, pp. 767-771, 2011.

Conference Paper

T. Ogrin, K. Radan, A. Štefančič and M. Lozinšek, "Nevarni" eksperimenti v in ob šoli", in *Proceedings of the Slovenian chemical days 2006*, Maribor, Slovenia: Faculty of Chemistry and Chemical Technology, University of Maribor, 2006.

K. Radan, M. Lozinšek, E. A. Goreshnik, M. Tramšek and B. Žemva, "Synthesis of $Sr(BF_4)(AF_6)$(A = P, As, Sb, Bi, V, Nb, Ta, Ru) compounds : characterization and structural similarities with their barium analogues", in *Book of abstracts of the 16th European Symposium on Fluorine Chemistry - ESFC*, Ljubljana, Slovenia: Jožef Stefan Institute, 2010.

M. Lozinšek, K. Radan, E. A. Goreshnik and B. Žemva, "Metal oxotetrafluorovanadates(V) and related chemistry", in *Chemistry of air, space & water : 242nd ACS National Meeting & Exposition,* Denver, USA: American Chemical Society, 2011.

M. Lozinšek, K. Radan, E. A. Goreshnik, M. Tramšek and B. Žemva, "Structural behaviour of a new series of salts containing divalent cations and two different fluoro anions", in *Chemistry of air, space & water : 242nd ACS National Meeting & Exposition,* Denver, USA: American Chemical Society, 2011.

K. Radan, E. A. Goreshnik, M. Lozinšek, M. Tramšek and B. Žemva, "Sinteza in karakterizacija nekaterih spojin kalcija in kadmija z dvojnimi perfluoro anioni", in *Proceedings of the 5th Young researchers' day*, Ljubljana, Slovenia: Jožef Stefan Institute, 2011.

K. Radan, M. Lozinšek, E. A. Goreshnik and B. Žemva, "Sinteza in karakterizacija spojin $Cd(BF_4)(AF_6)$ (A=Ta, Bi)" in *Proceedings of the Slovenian chemical days 2011*, Portorož, Slovenia: Faculty of Chemistry and Chemical Technology, University of Maribor, 2011.

M. Lozinšek, K. Radan, E. A. Goreshnik and B. Žemva, "VOF_3 in anioni, ki jih le-ta tvori v brezvodnem HF", in *Proceedings of the Slovenian chemical days 2011*, Portorož, Slovenia: Faculty of Chemistry and Chemical Technology, University of Maribor, 2011.

M. Lozinšek, K. Radan, E. A. Goreshnik and B. Žemva, "New series of compounds with fluoridooxidovanadate(V) anions", in *Abstracts of The 8th Japanese-French joint Seminar on Fluorine Chemistry*, Kyoto, Japan: Japan Society for the Promotion of Science, 2012.

T. Ogrin, A. Bačnik, M. Tramšek, K. Radan, "Ali kisik gori?", in *Proceedings of the Slovenian chemical days 2014*, Maribor, Slovenia: Faculty of Chemistry and Chemical Technology, University of Maribor, 2014.

Biography

Kristian Radan was born in Ljubljana, Slovenia, in 1983. His interest in Natural Sciences led him to enroll in the Chemistry program at the Faculty of Chemistry and Chemical Technology of the University of Ljubljana. During his student years he was actively involved in science education and promotion projects, which were ran by the Department of Inorganic Chemistry and Technology at the Jožef Stefan Institute (JSI) in Ljubljana. There he was eventually introduced to the exciting field of inorganic fluorine chemistry and with a JSI company scholarship support, he began his training in unconventional experimental techniques and handling of highly reactive materials. After completing his B.Sc. degree in 2010 under the supervision of Professor Boris Žemva, he joined the Jožef Stefan International Postgraduate School as a young researcher to pursue his Ph.D. in Nanoscience and Nanotechnology, again under the supervision of Professor Žemva. His research interests are in the area of synthetic and structural inorganic fluorine chemistry, with a special emphasis on noble-gas chemistry.

References

[1] B. A. Averill and P. Eldredge, "The Elements of Group 18 (The Noble Gases)," in *Principles of General Chemistry v.1.0.,* Creative Commons by-nc-sa 3.0 license, 2718-2731, 2012.

[2] G. Oddo, "Sul potere di combinarsi del cripton e dello xenon: due lettere inedite del prof. W. Ramsay", *Gazzetta Chimica Italiana*, vol. 62, pp. 380-395, 1932.

[3] L. Pauling, "The Formulas of Antimonic Acid and the Antimonates," *Journal of the American Chemical Society,* vol. 55, pp. 1895-1900, 1933.

[4] D. M. Yost and A. L. Kaye, "An attempt to prepare a chloride or fluoride of xenon," *Journal of the American Chemical Society,* vol. 55, pp. 3890-3892, 1933.

[5] P. Laszlo and G. J. Schrobilgen, "One or Several Pioneers? The Discovery of Noble-Gas Compounds," *Angewandte Chemie International Edition in English,* vol. 27, pp. 479-489, 1988.

[6] L. V. Streng and A. G. Streng, "Formation of Xenon Difluoride from Xenon and Oxygen Difluoride or Fluorine in Pyrex Glass at Room Temperature," *Inorganic chemistry,* vol. 4, pp. 1370-1371, 1965.

[7]J. H. Holloway, "The photochemical reaction of xenon with fluorine at room temperature: A demonstration of the reactivity of xenon," *Journal of Chemical Education,* vol. 43, p. 202, 1966.

[8]A. von Antropoff, K. Weil, and H. Frauenhof, "Die Gewinnung von Halogenverbindungen der Edelgase," *Naturwissenschaften,* vol. 20, pp. 688-689, 1932.

[9] A. von Antropoff, H. Frauenhof, and K. H. Krüger, "Nachtrag zur vorläufigen Mitteilung über „Die Gewinnung von Halogenverbindungen der Edelgase“," *Naturwissenschaften,* vol. 21, pp. 315-315, 1933.

[10] O. Ruff and W. Menzel, "Das Verhalten von Fluor gegen Argon und Krypton unter dem Einfluß elektrischer Entladungen," *Zeitschrift für anorganische und allgemeine Chemie,* vol. 213, pp. 206-207, 1933.

[11] K. A. Udachin, H. Lu, G. D. Enright, C. I. Ratcliffe, J. A. Ripmeester, N. R. Chapman, M. Riedel and G. Spence, "Single Crystals of Naturally Occurring Gas Hydrates: The Structures of Methane and Mixed Hydrocarbon Hydrates," *Angewandte Chemie International Edition,* vol. 46, pp. 8220-8222, 2007.

[12] M. Choukroun, S. W. Kieffer, X. Lu and G. Tobie, "Clathrate Hydrates: Implications for Exchange Processes in the Outer Solar System," in *The Science of Solar System Ices*, M. S. Gudipati and J. Castillo-Rogez, Eds., ed New York, NY: Springer New York, 2013, pp. 409-454.

[13] V. I. Artyukhov, A. Y. Pulver, A. Peregudov, and I. Artyuhov, "Can xenon in water inhibit ice growth? Molecular dynamics of phase transitions in water–Xe system," *The Journal of Chemical Physics,* vol. 141, p. 034503, 2014.

[14] L. Chen, P. S. Reiss, S. Y. Chong, D. Holden, K. E. Jelfs, T. Hasell, M. A. Little, A. Kewley, M. E. Briggs, A. Stephenson, K. M. Thomas, J. A. Armstrong, J. Bell, J. Busto, R. Noel, J. Liu, D. M. Strachan, P. K. Thallapally and A. I. Cooper, "Separation of rare gases and chiral molecules by selective binding in porous organic cages," *Nature Materials,* vol. 13, pp. 954-960, 2014.

[15] L. Yang, C. A. Tulk, D. D. Klug, I. L. Moudrakovski, C. I. Ratcliffe, J. A. Ripmeester, B. C. Chakoumakos, L. Ehm, C. D. Martin and J. B. Parise, "Synthesis and characterization of a new structure of gas hydrate," *Proceedings of the National Academy of Sciences,* vol. 106, pp. 6060-6064, 2009.

[16] N. Bartlett and D. H. Lohmann, "Dioxygenyl Hexafluoroplatinate(V) $O_2^+[PtF_6]^-$," *Proceedings of the Chemical Society,* vol. 3*,* pp. 115-116, 1962.

[17] I. Hargittai, "Who did not win," in *The Road to Stockholm, Nobel Prizes, Science, and Scientists,* Oxford University press, 2002.

[18] K. O. Christe, "Obituary: Neil Bartlett (1932-2008)," *Nature,* vol. 455, pp. 182-182, 2008.

[19] Although the ionization potentials are indeed comparable, different values can be found in the literature. Professor Bartlett used the following reference, which provides values of 12.2 eV and 12.1 eV for O_2 and Xe, respectively: R. D. Levin and S. G. Lias, "Ionization and Appearance Potential Measurements," 1971-1981, *NSRDS-NBS 71*, U.S. Department of Commerce, N.B.S., Washington DC 20234, 1982.
In more recent publications on the topic, the values cited (O_2: 12.075 eV, Xe: 12.129 eV) can be found in the following references: a) J. G. Dillard, K. Draxl, J. L. Franklin, F. H. Field, J. T. Herron, and H. H. Rosenstock, "Appendix - Ionization Potentials, Appearance Potentials, and Heats of Formation of Gaseous Positive Ions," in *Pure and Applied Physics*, vol. 1, F. F.H and F. J.L, Eds., ed: Elsevier, 1957, pp. 239-531. b) *Handbook of Chemistry and Physics,* 70th ed., R. C. West and D. R. Lide, Ed., CRC Press: Boca Raton, FL, 1989. c) A. J. C. Nicholson, "Photo-Ionization Efficiency Curves. Measurement of Ionization Potentials and Interpretation of Fine Structure," *The Journal of Chemical Physics,* vol. 39, pp. 954-961, 1963.

[20] N. Bartlett "Xenon Hexafluoroplatinate(V) $Xe^+[PtF_6]^-$," *Proceedings of the Chemical Society,* vol. 6*,* pp. 218-219, 1962.

[21] N. Bartlett, N. K. Jha, *Noble gas Compounds* (Ed. H. H. Hyman), University of Chicago Press, Chicago and London, pp. 23-30, 1963.

[22] P. Ball, "Not so Noble," in *Elegant Solutions: Ten Beautiful Experiments in Chemistry*, ed: The Royal Society of Chemistry, pp. 139-150, 2005.

[23] M. Freemantle, "Chemistry at its most beautiful," *Chemical & Engineering News Archive,* vol. 81, pp. 27-30, 2003.

[24] H. H. Claassen, H. Selig and J. G. Malm, "Xenon Tetrafluoride," *Journal of the American Chemical Society,* vol. 84, pp. 3593-3593, 1962.

[25] R. Hoppe, W. Dähne, H. Mattauch and K. M. Rödder, "Fluorierung von Xenon," *Angewandte Chemie,* vol. 74, pp. 903, 1962.

[26] J. Slivnik, B.S. Brčić, B. Volavšek, J. Marsel, V. Vrščaj, A. Šmalc, B. Frlec and A. Zemljič, *Croatica Chemica Acta*, vol. 34, pp. 253, 1962.

[27] K. O. Christe, "A Renaissance in Noble Gas Chemistry," *Angewandte Chemie International Edition,* vol. 40, pp. 1419-1421, 2001.

[28] G. A. Olah, G. K. Surya Prakash, Á. Molnár and J. Sommer, "Superacid Systems," in *Superacid Chemistry*, ed: John Wiley & Sons, Inc., 2008, pp. 35-82.

[29] S. Ahrland, J. Chatt and N. R. Davies, "The relative affinities of ligand atoms for acceptor molecules and ions," *Quarterly Reviews, Chemical Society,* vol. 12, pp. 265-276, 1958.

[30] B. D. Rowsell, R. J. Gillespie and G. L. Heard, "Ligand Close-Packing and the Lewis Acidity of BF_3 and BCl_3," *Inorganic chemistry,* vol. 38, pp. 4659-4662, 1999.

[31] Pearson RG. Acids and Bases. *Science.*1966;151(3707):172-177.

[32] Pearson RG. Hard and Soft Acids and Bases. *Journal of the American Chemical Society.* 1963/11/01 1963;85(22):3533-3539.

[33] Ho T-L. Hard soft acids bases (HSAB) principle and organic chemistry. *Chemical Reviews.* 1975/02/01 1975;75(1):1-20.

[34] Lozinšek M. *Sinteza in karakterizacija novih spojin šibko koordinirajočih fluoridoanionov* [doctoral thesis]. Ljubljana, Slovenia: Fakulteta za kemijo in kemijsko tehnologijo, Univerza v Ljubljani; 2013

[35] Olah GA, Chapter 5. In: *Friedel-Crafts Chemistry*. New York, Wiley; 1973.

[36] Laszlo P, Teston M. Determination of the acidity of Lewis acids. *Journal of the American Chemical Society.* 1990/11/01 1990;112(24):8750-8754.

[37] Koppel IA, Burk P, Koppel I, Leito I, Sonoda T, Mishima M. Gas-Phase Acidities of Some Neutral Brønsted Superacids: A DFT and ab Initio Study. *Journal of the American Chemical Society.* 2000/05/01 2000;122(21):5114-5124.

[38] Koppel IA, Burk P, Koppel I, Leito I. Generalized Principle of Designing Neutral Superstrong Brønsted Acids. *Journal of the American Chemical Society.* 2002/05/01 2002;124(19):5594-5600.

[39] Christe KO, Dixon DA, McLemore D, Wilson WW, Sheehy JA, Boatz JA. On a quantitative scale for Lewis acidity and recent progress in polynitrogen chemistry. *Journal of Fluorine Chemistry.* 2000;101(2):151-153.

[40] Larson JW, McMahon TB. Trends in gas-phase fluoride ion affinities of main-group oxyfluorides and fluoride sulfides. Generation and characterization of the fluoride adducts of FAsO, FPO, FPO_2, F_2SiO, F_4SO, FBO, F_2SiS, FPS, FAsS, F_2S_2, and S_2O by ion cyclotron resonance addition-elimination reactions. *Inorganic chemistry.* 1987/12/01 1987;26(24):4018-4023.

[41] Gillespie RJ, Schrobilgen GJ. Fluorokrypton(1+) and .mu.-fluorodifluorodikrypton(1+) cations. Preparation of $KrF^+MF_6^-$, $KrF^+Sb_2F_{11}^-$, $Kr_2F_3^+MF_6^-$, and $Kr_2F_3^+ \cdot xKrF_2.MF_6^-$ salts and their characterization by fluorine-19 nuclear magnetic resonance and Raman spectroscopy. *Inorganic chemistry.* 1976;15(1):22-31.

[42] Gillespie RJ, Martin D, Schrobilgen GJ. A Raman spectroscopic study of noble-gas fluoride adduct formation with bismuth pentafluoride. *Journal of the Chemical Society, Dalton Transactions.* 1980(10):1898-1903.

[43] Žemva B, Jesih A, Templeton DH, Zalkin A, Cheetham AK, Bartlett N. Phases in the System XeF_2/XeF_5AsF_6 and Structural and Vibrational Evidence for the Following Ionization Pathway: XeF_2 --> $XeF^+ + F^-$. *Journal of the American Chemical Society.* 1987;109:7420-7427.

[44] Christe KO, Dixon DA. 16th Winter Fluorine Conference. St. Petersburg,Fl. Jan. 12 – 17, 2003.

[45] Hwang I-C, Seppelt K. Gold Pentafluoride: Structure and Fluoride Ion Affinity. *Angewandte Chemie International Edition.* 2001;40(19):3690-3693.

[46] Christe, K. O.; Dixon, D. A. Recent Progress on the Christe/Dixon Quantitative Scale of Lewis Acidity. Presented at the 92nd Canadian Society for Chemistry Conference, Hamilton, ON, May-June 2009.

[47] Riedel S. 2.08 - High-Valent Fluorides and Fluoro-Oxidizers. In: Poeppelmeier JR, ed. *Comprehensive Inorganic Chemistry II (Second Edition)*. Amsterdam: Elsevier; 2013:187-221.

[48] Christe KO. Bartlett's discovery of noble gas fluorides, a milestone in chemical history. *Chem. Comm.* 2013;49(41):4588-4590.

[49] Malm JG, Selig H, Jortner J, Rice SA. The Chemistry of Xenon. *Chemical Reviews.* 1965;65(2):199-236.

[50] Bartlett N, Sladky F0, In *Comprehensive Inorganic Chemistry,* Bailer, 1. C. Jr.; Emeleus, H. *I.;* Nyholm, S. R; Trotman-Dickenson A F., eds.; Pergamon Press: New York, 1973, *Vol.* 1, p. 213 - 330.

[51] Hawkins, D. T; Falconer, W. E.; Bartlett, N., In *Noble Gas Compounds: A Bibliography,* Plenum Press Inc.: New York, 1978, p. 1962 - 1976.

[52] H. Selig and J. H. Holloway, "Cationic and anionic complexes of the noble gases," in *Inorganic chemistry*, Topics in Current Chemistry, vol. 124, ed Berlin, Heidelberg: Springer Berlin Heidelberg, 1984, pp. 33-90.

[53] B. Žemva, "Binary Fluorides of Noble-Gases and Their Compounds," *Croatica Chemica Acta*, vol. 61, pp. 163-187, 1988.

[54] Schrobilgen GJ, Brock DS, Mercier HPA. Noble-Gas Compounds. In: *Kirk-Othmer Encyclopedia of Chemical Technology*: John Wiley & Sons, Inc.; 2012:1-21.

[55] Brock DS, Schrobilgen GJ, Žemva B. 1.25 - Noble-Gas Chemistry. In: Poeppelmeier JR, ed. *Comprehensive Inorganic Chemistry II (Second Edition)*. Amsterdam: Elsevier; 2013:755-822.

[56] C. L. Chernick, H. H. Claassen, P. R. Fields, H. H. Hyman, J. G. Malm, W. M. Manning, M. S. Matheson, L. A. Quarterman, F. Schreiner, H. H. Selig, I. Sheft, S. Siegel, E. N. Sloth, L. Stein, M. H. Studier, J. L. Weeks, M. H. Zirin, *Science* 1962, *138,* 136-138.

[57] J. L. Weeks, C. L. Chernick, M. S. Matheson, *J. Am. Chem. Soc.*, 1962, *84*, 4612

[58] R. Hoppe, H. Mattauch, K. M. Rödder, W. Dähne, *Z. Anorg. Chem.*, 1963, *324*, 214

[59] D. F. Smith, *J. Chem. Phys.*, 1963, *38*, 270

[60] W. E. Falconer, W. A. Sunder, *J. Inorg. Nucl. Chem.*, 1967, *29*, 1380

[61] B. Žemva, J. Slivnik, *J. Inorg. Nucl. Chem. Suppl.,* 1976, 173-178

[62] A. Šmalc, K. Lutar, in R. N. Grimes, Inorganic Syntheses, John Wiley, New York, 1992, Vol. 29, pp. 1-4

[63] N. Bartlett, F. O. Sladky, in J. C. Bailar, A. F. Trotman-Dickenson (Ed.): The Chemistry of Krypton, Xenon and Radon in »Comprehensive Inorganic Chemistry«, Pergamon Press, Oxford and New York, 1973, Vol. 1, pp. 213-330.

[64] Dukat WW, Holloway JH, Hope EG, Townson PJ, Powell RL. The reactions of xenon difluoride with 'inert' solvents. *Journal of Fluorine Chemistry.* 1993;62(2–3):293-296.

[65] S. Reichman, F. Schreiner, *J. Chem. Phys.* 1969, *51*, 2355-2358

[66] R.J. Gillespie, I. Hargittai in *The VSEPR Model of Molecular Geometry*, Allyn and Bacon, Boston, 1991

[67] Gillespie RJ. The VSEPR model revisited. *Chemical Society reviews.* 1992;21(1):59-69.

[68] Treichel PM. The VSEPR model of molecular geometry (Gillespie, Ronald J.; Hargittai, Istvan). *Journal of Chemical Education.* 1993/08/01 1993;70(8):A223.

[69] Gillespie RJ, Robinson EA. Elektronendomänen und das VSEPR-Modell der Molekülgeometrie. *Angewandte Chemie.* 1996;108(5):539-560. Electron Domains and the VSEPR Model of Molecular Geometry. *Angewandte Chemie International Edition in English.* 1996;35(5):495-514.

[70] J. Jortner, E. G. Wilson, S. A. Rice, *J. Am. Chem. Soc*., 1963, *85*, 814-815

[71] Tramšek M, Žemva B. Synthesis, Properties and Chemistry of Xenon(II) Fluoride. *Acta Chim. Slov.* 2006;53:105-116.

[72] Agron PA, Begun GM, Levy HA, Mason AA, Jones CG, Smith DF. Xenon Difluoride and the Nature of the Xenon-Fluorine Bond. *Science.* 1963;139(3557):842-844.

[73] Siegel, S.; Gebert, E. Chem. Commun. 1963, 85, 240.

[74] Elliott HS, Lehmann JF, Mercier HP, Jenkins HD, Schrobilgen GJ. X-ray crystal structures of [XeF][MF_6] (M = As, Sb, Bi), [XeF][M_2F_{11}] (M = Sb, Bi) and estimated thermochemical data and predicted stabilities for noble-gas fluorocation salts using volume-based thermodynamics. *Inorganic chemistry.* Sep 20 2010;49(18):8504-8523.

[75] Brassington, N. J.; Edwards, H. G. M.; Long, D. A. J. Chem. Soc.,Faraday Trans. 2 1978, 74, 1208–1213.

[76] Bürger, H.; Kuna, R.; Ma, S.; Breidung, J.; Thiel, W. J. Chem. Phys.1994, 101, 1–14.

[77] A. J. Bondi, *J. Phys. Chem*. **1964**, *68*, 441 – 451.

[78] N. Bartlett, F. O. Sladky, *Chem. Comm.,* **1968**, 1046-1047

[79] N. I. Denisenko, S. I. Troyanov, A. A. Popov, I. V. Kuvychko, B. Žemva, E. Kemnitz, S. H. Strauss, O. V. Boltalina, *J. Am. Chem. Soc.,* **2004**, *126*, 1618-1619

[80] Stine R, Lee W-K, Whitener KE, Robinson JT, Sheehan PE. Chemical Stability of Graphene Fluoride Produced by Exposure to XeF2. *Nano Letters.* 2013;13(9):4311-4316.

[81] Poleschner H, Seppelt K. XeF_2/fluoride acceptors as versatile one-electron oxidants. *Angew Chem Int Ed Engl.* Dec 2 2013;52(49):12838-12842.

[82] Tavčar G, Tramšek M. XeF_2 as a ligand to a metal center, an interesting field of noble gas chemistry. *Journal of Fluorine Chemistry.* 2014: *article in Press*.

[83] R. Hagiwara, F. Hollander, C. Maines, N. Bartlett, J. Eur, Solid State Inorg. Chem. 28 (1991) 855–866.

[84] Tavčar G, Žemva B. [Li(XeF2)n](AF6) (A = P, As, Ru, Ir), the First Xenon(II) Compounds of Lithium. Synthesis, Raman Spectrum, and Crystal Structure of [Li(XeF2)3](AsF6). *Inorganic chemistry.* 2013/04/15 2013;52(8):4319-4323.

[85] Matsumoto K, Hagiwara R, Ito Y, Tamada O. Synthetic, structural and thermal studies of Ag(I)–XeF2 complex salts. *Solid State Sci.* 2002;4(11–12):1465-1469.

[86] Tavcar G, Zemva B. XeF4 as a ligand for a metal ion. *Angew Chem Int Ed Engl.* 2009;48(8):1432-1434.

[87] Tramsek M, Benkic P, Zemva B. Mg(XeF2)(n) (AsF6)(2) (n=4, 2): First compounds of magnesium with XeF2. *Inorganic chemistry.* Jan 2004;43(2):699-703.

[88] Turičnik A. *XeF2 kot ligand v koordinacijskih spojinah z nekaterimi kovinskimi fluoroantimonati(V) in fluorobizmutati(V)* [doctoral thesis]. Ljubljana, Slovenia: Fakulteta za kemijo in kemijsko tehnologijo, Univerza v Ljubljani; 2003.

[89] XeF2 in polihidrogenfluoridni anioni kot ligandi v spojinah nekaterih kovinskih(II) heksafluorometalatov in heksafluorosfatov[doctoral thesis]. Ljubljana, Slovenia: Fakulteta za kemijo in kemijsko tehnologijo, Univerza v Ljubljani; 2008.

[90] Bunic T, Tavcar G, Tramsek M, Zemva B. Coordination of XeF2 to calcium and cadmium hexafluorophosphates(V). *Inorganic chemistry.* Feb 2006;45(3):1038-1042.

[91] Benkic P, Tramsek M, Zemva B. Ca(XeF2)n (AsF6)': (n=4, 2.5): the first coordination compounds of Ca2+ with XeF2 ligand. *Solid State Sci.* Nov-Dec 2002;4(11-12):1425-1434.

[92] Tramšek M, Benkič P, Žemva B. *Angew. Chem., Int. Ed.* 2004;43:3456.

[93] Tramsek M, Benkic P, Zemva B. M(XeF2)(3) (AsF6)(2) (M = Pb, Sr): the first coordination compounds of M2+ with XeF2 ligand. *Solid State Sci.* Jan 2002;4(1):9-14.

[94] Bunic T, Tramsek M, Goreshnik E, Tavcar G, Zemva B. Metal(II) Hexafluorophosphates(V) (M = Sr, Pb) containing XeF2-Coordinated metal ions M(XeF2)(3) (PF6)(2), Pb-3(XeF2)(11) (PF6)(6), and Sr-3(XeF2)(10) (PF6)(6). *Inorganic chemistry.* Jun 2007;46(13):5276-5282.

[95] Bunic T, Tramsek M, Goreshnik E, Zemva B. Synthesis, Raman spectrum and crystal structure of Ba(XeF(2))(4) (PF(6))(2). *Solid State Sci.* Nov 2008;10(11):1511-1516.

[96] Gerken M, Hazendonk P, Iuga A, et al. Solid-state NMR spectroscopic study of coordination compounds of XeF2 with metal cations and the crystal structure of Ba(XeF2)(5) AsF6 (2). *Inorganic chemistry.* Jul 2007;46(15):6069-6077.

[97] Turičnik A, Benkič P, Žemva B. Ba(SbF6)2·5XeF2: First Xenon(II) Compound with Barium. Synthesis, Vibrational Spectra, and Crystal Structure. *Inorganic chemistry.* 2002/10/01 2002;41(21):5521-5524.

[98] Bunic T, Tramsek M, Goreshnik E, Zemva B. Ba(XeF2)5](AF6)2, A = Ru, Nb - Synthesis, Crystal Structure and Raman Spectra. *Collect. Czech. Chem. Commun.* **2008**, *73*, 1645-1654.

[99] Mazej Z, Goreshnik E. Synthesis, Raman Spectra and Crystal Structures of [Cu(XeF2)n](SbF6)2 (n = 2, 4). *Inorganic chemistry.* 2008/05/01 2008;47(10):4209-4214.

[100] Tavčar G, Goreshnik E, Mazej Z. Homoleptic [M(XeF2)6]2+ cations of copper(II) and zinc(II)—Syntheses and crystal structures of [M(XeF2)6](SbF6)2 (M=Cu, Zn). *Journal of Fluorine Chemistry.* 2006;127(10):1368-1373.

[101] Tavčar G. Binarni fluoridi kot ligandi v spojinah s šibko koordiniranimi anioni [doctoral thesis]. Ljubljana, Slovenia: Fakulteta za kemijo in kemijsko tehnologijo, Univerza v Ljubljani; 2005.

[102] Tavčar G, Žemva B. XeF2 as a Ligand in a Coordination Compound with the BF4- Anion. *Inorganic chemistry.* 2005/03/01 2005;44(5):1525-1529.

[103] Tavčar G, Benkič P, Žemva B. New Coordination Compounds of Cd(AsF6)2 with HF and XeF2. *Inorganic chemistry.* 2004/02/01 2004;43(4):1452-1457.

[104] Tavčar G, Goreshnik E, Žemva B. Koordinacijska kemija 12. Skupine periodnega sistema s fluoridnimi ligandi, Slovenski kemijski dnevi 2011, portorož, 14-16 september 2011, FKKT Maribor, 2011.

[105] Tavcar G, Tramsek M, Bunic T, Benkic P, Zemva B. New class of coordination compounds with noble gas fluorides as ligands to metal ions. *Journal of Fluorine Chemistry.* Nov 2004;125(11):1579-1584.

[106] DeBackere JR, Mercier HPA, Schrobilgen GJ. Noble-Gas Difluoride Complexes of Mercury(II): The Syntheses and Structures of Hg(OTeF5)2·1.5NgF2 (Ng = Xe, Kr) and Hg(OTeF5)2. *Journal of the American Chemical Society.* 2014/03/12 2014;136(10):3888-3903.

[107] Lutar K, Borrmann H, Mazej Z, Tramsek M, Benkic P, Zemva B. Novel lanthanoid fluoroarsenates. *Journal of Fluorine Chemistry.* Feb 2000;101(2):155-160.

[108] Tramsek M, Lork E, Mews R, Zemva B. Synthesis and raman spectra of Nd (XeF2)(n) (AsF6)(3) (n=3, 2.5) and crystal structure of Nd (XeF2)(2.5) (AsF6)(3). *Journal of Solid State Chemistry.* Dec 2001;162(2):243-249.

[109] Lozinšek M, Mercier HPA, Brock DS, Žemva B, Schrobilgen GJ. Coordination of KrF2 to a Naked Metal Cation, Mg2+. *Angewandte Chemie International Edition.* 2017:n/a-n/a. Lozinšek M, Mercier HPA, Brock DS, Žemva B, Schrobilgen GJ. Coordination of KrF2 to a Naked Metal Cation, Mg2+. *Angewandte Chemie.* 2017:n/a-n/a.

[110] Keller N, Schrobilgen GJ. Preparation of the XeOTeF5+, FXeFXeOTeF5+, XeF2.cntdot.BrOF2+, and XeOSO2F+ cations and their study by xenon-129, tellurium-125, and fluorine-19 pulse Fourier transform NMR and Raman spectroscopy. *Inorganic chemistry.* 1981/07/01 1981;20(7):2118-2129.

[111] Brock DS, Casalis de Pury JJ, Mercier HPA, Schrobilgen GJ, Silvi B. XeF2 Coordination to a Halogen Center; Raman Spectra (n = 1, 2) and X-ray Crystal Structures (n = 2) of [BrOF2][AsF6]·nXeF2 and [XOF2][AsF6] (X = Cl, Br). *Inorganic chemistry.* 2010/07/19 2010;49(14):6673-6689.

[112] Sladky FO, Bulliner PA, Bartlett N. Xenon Difluoride as a Fluoride Ion Donor. Evidence for the Salts $[Xe_2F_3]^+[MF_6]^-$, $[XeF]^+[MF_6]^-$ and $[XeF]^+[M_2F_{11}]^-$. *J. Chem. Soc. (A).* 1969:2179-2188.

[113] A. Zalkin, D. L. Ward, R. N. Biagioni, D. H. Templeton, N. Bartlett, *Inorg. Chem.* 1978, *17*, 1318 – 1322.

[114] F. Tamadon, S. Seidel, K. Seppelt, *Acta Chim. Slov.* 2013, *60*, 491 – 494.

[115] Žemva B, Slivnik J. Xenon difluoride-vanadium pentafluoride compound. *Journal of Inorganic and Nuclear Chemistry.* 1971;33(11):3952-3953.

[116] Turičnik A. *Reakcije ksenonovega difluorida v brezvodnem vodikovem fluoridu* [master thesis]. Ljubljana, Slovenia: Fakulteta za kemijo in kemijsko tehnologijo, Univerza v Ljubljani; 2000.

[117] N. Bartlett, M. Gennis, D. D. Gibler, B. K. Morrell, A. Zalkin, *Inorg. Chem.* **1973**, *12*, 1717 – 1721.

[118] V. M. McRae, R. D. Peacock, D. R. Russell, *Chem. Commun*. **1969**, 62 – 63.

[119] Burgess J, Fraser CJW, McRae VM, Peacock RD, Russell DR. The adduct $XeF_2 \cdot 2SbF_5$: Its crystal structure and thermochemistry. *Journal of Inorganic and Nuclear Chemistry.* 1976;28, Supplement 1:183-188.

[120] F. O. Sladkey, P. A. Bulliner, N. Bartlett, B. G. DeBoer and A. Zalkin, "Xenon difluoride as a fluoride ion donor and the crystal structure of $[Xe_2F_3][AsF_6]$," *Chemical Communications (London),* pp. 1048-1049, 1968.

[121] N. Bartlett, B. G. DeBoer, F. J. Hollander, F. O. Sladky, D. H. Templeton and A. Zalkin, "Crystal structures of $[Xe_2F_3^+][AsF_6^-]$ and $[XeF_5^+][AsF_6^-]$," *Inorganic chemistry,* vol. 13, pp. 780-785, 1974.

[122] B. A. Fir, M. Gerken, B. E. Pointner, H. P. A. Mercier, D. A. Dixon and G. J. Schrobilgen, "An X-ray crystallographic study of $[Xe_2F_3][SbF_6]$ and dimorphism in $[Xe_2F_3][AsF_6]$; and a density functional theory study of the $Xe_2F_3^+$ cation," *Journal of Fluorine Chemistry,* vol. 105, pp. 159-167, 2000.

[123] M. Tramšek, E. Goreshnik, and G. Tavčar, "Oxidation of ruthenium and iridium metal by XeF_2 and crystal structure determination of $[Xe_2F_3][RuF_6] \cdot XeF_2$ and $[Xe_2F_3][MF_6]$ (M = Ru, Ir)," *Acta Chimica Slovenica,* vol. 63, no. 2, pp. 369-375, 2016.

[124] Holloway JH, Schrobilgen GJ, Taylor P. The preparation and characterisation of XeF2.WOF4 and XeF2.2WOF4 by 19F nuclear magnetic resonance and Raman spectroscopy. Examples of non-labile xenon-fluorine-metal bridges. *Journal of the Chemical Society, Chemical Communications.* 1975(2):40-41.

[125] Holloway JH, Schrobilgen GJ. Fluorine-19 and xenon-129 NMR studies of the XeF2.nWOF4 and XeF2..nMoOF4 (n = 1-4) adducts: examples of nonlabile xenon-fluorine-metal bridges in solution. *Inorganic chemistry.* 1980/09/01 1980;19(9):2632-2640.

[126] Holloway JH, Schrobilgen GJ. The preparation and study by Raman spectroscopy of KrF2.MOF4, XeF2.MOF4, and XeF2.2MOF4 (M = molybdenum, tungsten) and a solution fluorine-19 NMR study of KrF2.nMoOF4 (n = 1-3) and KrF2.WOF4. *Inorganic chemistry.* 1981/10/01 1981;20(10):3363-3368.

[127] Breddemann U. Neue Edelgas-Sauerstoff Kationen, Diplomarbeit II, Universitat Duisburg-Essen (McMaster University), Hamilton; 2011.

[128] Tucker PA, Taylor PA, Holloway JH, Russell DR.The Adduct $XeF_2 \cdot WOF_4$. *Acta Crystallogr.* 1975;B31:906-908.

[129] Jones GR, Burbank RD, Bartlett N. Crystal structure of the 1:1 molecular addition compound xenon difluoride-iodine pentafluoride, XeF2.IF5. *Inorganic chemistry.* 1970/10/01 1970;9(10):2264-2268.

[130] Bartlett N, Wechsberg M. The Xenon Difluoride Complexes XeF2 · XeOF4; XeF2 · XeF6 · AsF5 and XeF2 · 2 XeF6 · 2 AsF5 and Their Relevance to Bond Polarity and Fluoride Ion Donor Ability of XeF2 and XeF6. *Zeitschrift für anorganische und allgemeine Chemie.* 1971;385(1-2):5-17.

[131] Hughes MJ, Brock DS, Mercier HPA, Schrobilgen GJ. A Raman spectroscopic study of the XeOF4/XeF2 system and the X-ray crystal structure of α-XeOF4·XeF2. *Journal of Fluorine Chemistry.* 2011;132(10):660-668.

[132] Burns JH, Ellison RD, Levy HA. The crystal structure of the molecular addition compound xenon difluoride–xenon tetrafluoride. *Acta Crystallographica.* 1965;18(1):11-16.

[133] Massa W, Babel D. Crystal structure and bonding in transition-metal fluoro compounds. *Chemical Reviews.* 1988/01/01 1988;88(1):275-296.

[134] Wells, A. F. (1984), *Structural Inorganic Chemistry* (5th ed.), Oxford: Clarendon Press

[135] Laval J-P. Crystal chemistry of anion-excess ReO3-related phases. III. [gamma]-ZrF4, a high-pressure form of zirconium tetrafluoride, and a comparison of MX4 structure typesFor Parts I and II, see Laval & Abaouz (1992a) and Laval & Abaouz (1992b), respectively. *Acta Crystallographica Section C.* 2014;70(8):742-748.

[136] H. Bialowons, M. Müller, B. G. Müller, *Z. Anorg. Allg. Chem*. 1995, *621*, 1227 – 1231.

[137] Kraemer, O. & Mueller, B. G. (1995). Z. Anorg. Allg. Chem. 621, 1969–1972.

[138] Benkič P, Mazej Z, Žemva B. A New Crystal Modification of Chromium Tetrafluoride: β-CrF4. *Angewandte Chemie.* 2002;114(8):1456-1457.

[139] Becker S, Müller BG. Vanadium Tetrafluoride. *Angewandte Chemie International Edition in English.* 1990;29(4):406-407.

[140] Mueller, B. G. & Serafin, M. (1987). Z. Naturforsch. Teil B, 42, 1102–1106.

[141] Casteel WJ, Wilkinson AP, Borrmann H, Serfass RE, Bartlett N. Preparation and structure of ruthenium tetrafluoride and a structural comparison with ruthenium trifluoride and ruthenium pentafluoride. *Inorganic chemistry.* 1992/07/01 1992;31(14):3124-3131.

[142] Hoppe, R.; Daehne, W. Die Kristallstruktur von SnF4 und PbF4. Naturwissenschaften (1962) 49, p254-p255

[143] Bartlett, M. & Tressaud, A. (1974).Sur un nouveau type structural de tetrafluorures d'elements: sythese, etude cristalographique et magnetique de IrF4. C. R. Acad. Sci. Ser. C, 278, 1501–1504.

[144] Rao PR, Tressaud A, Bartlett N. The tetrafluorides of iridium, rhodium and palladium. *Journal of Inorganic and Nuclear Chemistry.* 1976;28, Supplement 1:23-28.

[145] Mueller, B. G. & Serafin, M. (1992). Eur. J. Solid State Inorg. Chem. 29, 625–633.

[146] Zalkin, A., Forrester, J. D. & Templeton, D. H. (1964). Inorg. Chem. 3, 639–644.

[147] Mooney, R. C. L. (1949). Acta Cryst. 2, 189–191.

[148] Papiernik, R., Mercurio, D. & Frit, B. (1982). Acta Cryst. B38, 2347–2353.

[149] Taoudi, A., Mikou, A. & Laval, J. P. (1996). Eur. J. Solid State Inorg. Chem.33, 1051–1062.

[150] C. E. Housecroft, A. G. Sharpe, *Inorganic Chemistry*, *3th ed*., Pearson, Essex, **2008**, p. 544.

[151] Benjamin SL, Levason W, Reid G. Medium and high oxidation state metal/non-metal fluoride and oxide-fluoride complexes with neutral donor ligands. *Chemical Society reviews.* 2013;42(4):1460-1499.

[152] Nikiforov GB, Roesky HW, Koley D. A survey of titanium fluoride complexes, their preparation, reactivity, and applications. *Coordination Chemistry Reviews.* 2014;258–259:16-57.

[153] Leblanc M, Maisonneuve V, Tressaud A. Crystal Chemistry and Selected Physical Properties of Inorganic Fluorides and Oxide-Fluorides. *Chemical Reviews.* 2015/01/28 2015;115(2):1191-1254.

[154] Davidovich RL, Marinin DV, Stavila V, Whitmire KH. Structural chemistry of fluoride and oxofluoride complexes of titanium(IV). *Coordination Chemistry Reviews.* In Press.

[155] I.M. Shlyapnikov, *PhD Thesis*, Ljubljana, 2016.

[156] I.M. Shlyapnikov, H.P.A. Mercier, E.A. Goreshnik, G.J. Schrobilgen, Z. Mazej, Inorg. Chem. 52 (2013) 8315-8326.

[157] L.-Q. Tang, M.S. Dadachov, X.-D. Zou, Z. Kristallogr. NCS 216 (2001) 387-388.

[158] R.L. Davidovich, V.V. Tkachev, V.B. Logvinova, V.I. Kostin, V. Stavila, Zh. Strukt. Khim. 55 (2014) 969-972 (J. Struct. Chem. 55 (2014) 000-000).

[159] Mazej Z, Goreshnik E. Synthesis and Characterisation of [XeF5]3[Ti4F19] Containing a Discrete [Ti4F19]3-Anion. *European Journal of Inorganic Chemistry.* 2009;2009(29-30):4503-4506.

[160] Jura M, Levason W, Petts E, Reid G, Webster M, Zhang W. Taking TiF_4 complexes to extremes – the first examples with phosphine co-ligands. *Dalton Trans*. 2010;39:10264–10271.

[161] Mazej Z, Goreshnik E. Poly[perfluorotitanate(IV)] salts of [H3O]+, Cs+, [Me4N]+, and [Ph4P]+ and about the existence of an isolated [Ti2F9]- anion in the solid state. *Inorganic chemistry.* Jul 20 2009;48(14):6918-6923.

[162] Decken A, Jenkins HDB, Knapp C, Nikiforov GB, Passmore J, Rautiainen JM. The Autoionization of [TiF4] by Cation Complexation with [15]Crown-5 To Give [TiF2([15]crown-5)][Ti4F18] Containing the Tetrahedral [Ti4F18]2− Ion. *Angewandte Chemie International Edition.* 2005;44(48):7958-7961.

[163] Shlyapnikov IM, Goreshnik EA, Mazej Z. The cubic [Ti8F36]4- anion found in the crystal structures of K4Ti8F36[middle dot]8HF and Rb4Ti8F36[middle dot]6HF. *Chemical Communications.* 2013;49(26):2703-2705.

[164] Mazej Z, Goreshnik EA. Largest perfluorometallate [Ti10F45]5- oligomer and polymeric ([Ti3F13]-)[infinity] and ([TiF5]-)[infinity] anions prepared as [XeF5]+ salts. *New Journal of Chemistry.* 2016;40(9):7320-7325.

[165] Cohen S, Selig H, Gut R. The structure of $H_3O^+TiF_5^-$. *J Fluor Chem.* 1982;20:349–356.

[166] Kavun VYa, Bukvetskii BV, Laptash NM, Maslennikova IG, Sergienko SS. Structure and Internal Mobility of Complex Ions in Ammonium Pentafluorotitanate According to XRD and NMR Data. *J Struct Chem.* 2001;42:771–776.

[167] B.G. Müller, J. Fluor. Chem. 17 (1981) 489-499.

[168] H. Bialowons, B.G. Müller, Z. Anorg. Allg. Chem. 621 (1995) 1223-1226.

[169] Housecroft CE, Constable EC. *Chemistry: An Introduction to Organic, Inorganic and Physical Chemistry*: Prentice Hall; 2010: 769.

[170] Davis MF, Levason W, Reid G, Webster M. Synthesis and characterisation of tin(IV) fluoride complexes of phosphine and arsine oxide ligands. *Polyhedron.* 2006;25(4):930-936.

[171] D. Tudela and F. Rey, Z. Anorg. Allg. Chem., 1989, 575, 202.

[172] D. Tudela and J. A. Patron, Inorg. Synth., 1997, 31, 92.

[173] Sanhoury MA, Ben Dhia MT, Khaddar MR. Synthesis and characterization of tin tetrafluoride adducts with fluoroalkyl phosphoryl ligands. *Journal of Fluorine Chemistry.* 2013;146(0):15-18.

[174] Marseglia EA, Brown ID. Lithium hexafluorotitanate dihydrate and lithium hexafluorostannate dihydrate. *Acta Crystallographica Section B.* 1973;29(6):1352-1354.

[175] Hebecker C, von Schnering HG, Hoppe R. Zur Kristallstruktur von Na2SnF6. *Naturwissenschaften.* 1966// 1966;53(6):154-154.

[176] Benner G, Hoppe R. Zur struktur von Na2SnF6 [1]. *Journal of Fluorine Chemistry.* 1990;48(2):219-227.

[177] Weiss, R.; Chevrier, B.; Fischer, J. Structure cristalline du fluorostannate acide de potassium (K2 Sn F6) (K H F2). Comptes Rendus Hebdomadaires des Seances de l'Academie des Sciences (1884 - 1965) (1965) 260, p3664-p3665.

[178] a)Baidina, I.A.; Bakakin, V.V.; Borisov, S.V.; Podberezskaya, N.V. Kristallicheskaya struktura monohidrata heksaflorstannatakaliya K2 Sn F6 (H2 O). Zhurnal Strukturnoi Khimii (1976) 17, 505-509. b) Kavun, V.Ya.; Gabuda, S.P.; Gerasimenko, A.V.; Trofimov, G.L.; Tkachenko, I.A. Crystal structure refinement of K2 Sn F6 * (H2 O) using single crystal (1)H NMR data. Zhurnal Strukturnoi Khimii; (2002) 43, (2) p382-p386.

[179] Babel D. Structural chemistry of octahedral fluorocomplexes of the transition elements. In: Jørgensen CK, Neilands JB, Nyholm RS, Reinen D, Williams RJP, eds. *Structure and Bonding*. Berlin, Heidelberg: Springer Berlin Heidelberg; 1967:1-87.

[180] Lari-Lavassani A., Jourdan G., Avinens C., CotL. Etude cristallographique d'hexafluorostannates cubiques et hexagonaux M2SnF6. C.R. Acad. Sc. Paris. Ser. C. 1974. T.279. P. 193-195.

[181] M. René Sabatier, Mlle Anne-Marie Hébrard et M. Jean-Claude Cousseins, présentée par M. Georges Champetier. CHIMIE MINÉRALE. - Contribution à l'étude des systèmes MF-SnF_4 (M = Li, Na, K). C.R. Acad. Sc. Paris. Ser. C. 1975. T.281. P. 873-876.

[182] Durand J., Galigne J.L., Larilavassani A. Etude Structurale de Cs2SnF6 // Journal of Solid State Chemistry. 1976. V. 16. P. 157-160.

[183] Chang JH, Köhler J. Preparation and Rietveld refinements of the structures Tl2SnF6 and Tl2TiF6. *Materials Research Bulletin.* 2000;35(1):25-32.

[184] Mayer HW, Reinen D, Heger G. Struktur und Bindung in Übergangsmetall-Fluoriden MIIMeIVF6: Neutronenbeugungs-Strukturuntersuchungen an CaSnF6, FeZrF6, und CrZrF6. *Journal of Solid State Chemistry.* 1983;50(2):213-224.

[185] Hoppe R, Wilhelm V, Müller B. Zur Kenntnis der Verbindungen MIISnF6 mit MII = Mn, Fe, Zn, Hg, Pb) bzw. Co, Ni, Cu, Cd). *Zeitschrift für anorganische und allgemeine Chemie.* 1972;392(1):1-9.

[186] Becker S, Benner G, Hoppe R. Zur Kenntnis des K[OsF6]-Typs: Über die Konstitution von BaSnF6 und BaTiF6. *Zeitschrift für anorganische und allgemeine Chemie.* 1990;591(1):7-16.

[187] Müller BG, Schrötter F. Zur Kristallstruktur ternärer Cu(II)-Fluoride CuMIVF6 (MIV = Sn, Pb, Ti, Mn, Pd). *Zeitschrift für Kristallographie - Crystalline Materials.* Vol 1961991:261.

[188] Fischer R, Müller BG. Synthese und Kristallstruktur von Silber(II)-Fluoriden AgMIVF6 (MIV = Sn, Ti, Pb, Pd, Pt, Rh). *Zeitschrift für anorganische und allgemeine Chemie.* 2001;627(3):445-452.

[189] Gerasimenko, A.V.; Ivanov, S.B.; Antokhina, T.F.; Sergienko, V.I. Crystal structure of NaKSnF6. Koordinatsionnaya Khimiya (1992) 18, p129-p132

[190] Gerasimenko, A.V.; Ivanov, S.B.; Antokhina, T.F.; Sergienko, V.I. Crystal structures of Na Rb Sn F6 and Na Cs Sn F6. Koordinatsionnaya Khimiya (1992) 18, p1139-p1143

[191] Meyer, G.; Boehmer, N. Refinement of the crystal structure of diammonium hexafluorostannate(IV), (NH4)2SnFi. *Zeitschrift für Kristallographie - New Crystal Structures.* Vol 216, 2001:20.

[192] Plitzko C, Meyer G. Kristallstruktur von (NH4)3SnF7: Ein Doppelsalz gemäß (NH4)3[SnF6]F und kein (NH4)4SnF8. *Zeitschrift für anorganische und allgemeine Chemie.* 1997;623(9):1347-1348.

[193] Pugh W. 397. Hydrazine. Part III. The hydrazinium salts of complex fluoro-acids of tin, antimony, and bismuth. *Journal of the Chemical Society (Resumed).* 1953(0):1934-1936.

[194] Christe KO, Schack CJ, Wilson RD. Synthesis and characterization of bis(tetrafluoroammonium) hexafluorostannate and tetrafluoroammonium pentafluorostannate. *Inorganic chemistry.* 1977/04/01 1977;16(4):849-854.

[195] Rahten R, Gantar D, Leban I. Preparation and characterization of hydrazinium(1+) and (2+) hexafluorostannate(IV) and hydrazinium(2+) hexafluorostannate(IV) difluoride. *Journal of Fluorine Chemistry.* 1990;46(3):521-528.

[196] Garcia C, Barbusse D, Fourcade R, Ducourant B. Synthese et etude structurale de l'octafluorostannate (IV) de dihydrazinium: (N2H6)2SnF6F2. *Journal of Fluorine Chemistry.* 1991/02/01 1991;51(2):245-256.

[197] Varnek VA, Varnek AA. Quantum chemical analysis of the effect of the outer-spheric cation on the electronic state of the tin atom and isomer shift in hexafluorostannates. *Zhurnal Strukturnoi Khimii*, 1998;39(1):154–157 and *Journal of Structural Chemistry.* 1998;39(1):125-127.

[198] Carter HA, Qureshi AM, Sams JR, Aubke F. Vibrational and Mössbauer spectra of some hexachloro- and hexafluorostannate complexes. *Canadian Journal of Chemistry.* 1970/09/15 1970;48(18):2853-2859.

[199] Varnek V. A., Tychinskaya I. I., Yudanov N. F., Mazalov L. N. The Mössbauer effect in hexafluorostannates. Zhurnal Strukturnoi Khimii; (1976) 17, (4) p579-p587 and Journal of Structural Chemistry, 1977, vol. 17, p. 507-514.

[200] Gabuda SP, Kavun VY, Kozlova SG, Tverskikh VV. Structure of Hexafluorostannate Ion [SnF6]2–: the 119Sn and 19F NMR MAS-Spectroscopic Studies and Ab Initio Calculations. *Russian Journal of Coordination Chemistry.* 2003// 2003;29(1):1-5.

[201] Christe KO, Schack CJ. Chemistry and structure of N2F3+ salts. *Inorganic chemistry.* 1978/10/01 1978;17(10):2749-2754.

[202] Wilson WW, Vij A, Vij V, Bernhardt E, Christe KO. Polynitrogen Chemistry: Preparation and Characterization of (N5)2SnF6, N5SnF5, and N5B(CF3)4. *Chemistry - A European Journal.* 2003;9(12):2840-2844.

[203] Christe KO, Dixon DA, Grant DJ, et al. Dinitrogen difluoride chemistry. improved syntheses of cis- and trans-N2F2, synthesis and characterization of N2F(+)Sn2F9(-), ordered crystal structure of N2F(+)Sb2F11(-), high-level electronic structure calculations of cis-N2F2, trans-N2F2, F2N=N, and N2F(+), and Mechanism of the trans-cis isomerization of N2F2. *Inorganic chemistry.* Aug 2 2010;49(15):6823-6833.

[204] Dean PAW. A 19F Nuclear Magnetic Resonance Study of Polymeric Fluoroanions of Tin(IV) and Titanium(IV). *Canadian Journal of Chemistry.* 1973/12/15 1973;51(24):4024-4030.

[205] Graham L, Graudejus O, Jha NK, Bartlett N. Concerning the nature of XePtF6. *Coordination Chemistry Reviews.* 2000;197(1):321-334.

[206] N. Bartlett, D. H. Lohmann, *J. Chem. Soc.*, 1964, 619

[207] N. Bartlett, B. Žemva, L. Graham, *J. Fluor. Chem.*, 1976, *7*, 301

[208] J. Slivnik, B. Žemva, *Z. Anorg. Allg. Chem.*, 1971, *385*, 137

[209] B. Žemva, J. Zupan, J. Slivnik, *J. Inorg. Nucl. Chem.*, 1973, *35*, 3941

[210] K. Lutar, I. Leban, T. Ogrin, B. Žemva, $XeF_2 \cdot CrF_4$ and $(XeF_5^+CrF_4^-) \cdot XeF_4$: Syntheses, crystal structures and some properties, *Eur. J. Solid State Inorg. Chem.*, 1992, *29*, 713–727.

[211] Lutar K, Borrmann H, Žemva B. XeF2·2CrF4 and XeF5+CrF5-: Syntheses, Crystal Structures, and Some Properties. *Inorganic chemistry.* 1998/06/01 1998;37(12):3002-3006.

[212] Žemva B, Slivnik J. On the xenon-fluorine reactions. *J Inorg Nucl Chem.* 1976; 28:173-178.

[213] B. Žemva, J. Zupan, J. Slivnik, *Fluorine Chemistry Symp.*, Milwaukee (Wisc., U.S.A), June **1970** IJS Report R-585; B. Žemva, J. Zupan, J. Slivnik, *J. Nucl. Chem.*, **1971**, *33*, 3953-3955.

[214] M. Bohinc, J. Grannec, J. Slivnik, B. Žemva, *J.inorg. nucl. chem.*, **1976**, *38*, 75–76.

[215] M. Lozinšek, *Bachelor Thesis*, Ljubljana, **2008**.

[216] V. A. Legasov and A. S. Marinin, *Zhurnal Neorganicheskoi Khimii,* vol. 17, p. 2408, 1972.

[217] B. Žemva, S. Milićev, J. Slivnik, *J. Fluorine Chem.*, **1978**, *11*, 545

[218] Pullen KE, Cady GH. Systems xenon hexafluoride-germanium tetrafluoride and xenon hexafluoride-silicon tetrafluoride. *Inorganic chemistry.* 1967;6(7):1300-1302.

[219] Žemva B, Jesih A. On the syntheses of xenon(VI) fluoroplumbates(IV) and fluorostannates(IV). *Journal of Fluorine Chemistry.* 1984;24(3):281-289.

[220] Atwood DA. Noble Gases: Inorganic Chemistry. *Encyclopedia of Inorganic Chemistry*: John Wiley & Sons, Ltd; 2006.

[221] MAZEJ, Zoran, GORESHNIK, Evgeny A. Photochemical synthesis and crystal structures of xenon(VI) fluoride manganates(IV). V: *248th ACS National Meeting & Exposition : August 10-14, 2014, San Francisco, CA*. [S. l.]: American Chemical Society, 2014.

[222] MAZEJ, Zoran, GORESHNIK, Evgeny A. Structural studies of [XeF[sub]5][sup]+ / [Xe[sub]2F[sub](11)][sup]+ salts of [MF[sub]6][sup](2-) and fluoro-bridged oligomeric and polymeric anions of Ti[sup](4+), Mn[sup](4+) and Pb[sup](4+). V: *IISFC 2014*, 2nd Indian International Symposium on Fluorine Chemistry, 3rd to 7th November, Hyderabad, India. Hyderabad: Indian Institute of Chemical Technology, 2014, str. 32.

[223] Mazej Z, Shlyapnikov IM, Goreshnik E. From simple $[TiF_6]^{2-}$ octahedra to the largest known oligomeric fluoride-metalate anion $[Ti_{10}F_{45}]^{5-}$. *The First South African Fluorine Symposium*. Cape Town, South Africa: 14–18 Februar 2016.

[224] MAZEJ, Zoran, GORESHNIK, Evgeny A. Crystal structures of the $XeF_6 \cdot nMF_4$ (M = Mn, Ti, Sn), more than simple formulas. V: *[Book of abstracts]*, 18th European Symposium on Fluorine Chemistry, 7-12 August 2016, Kyiv, Ukraine. Kyiv: Private Enterprise Afonin A, 2016, str. 69.

[225] Leary K, Templeton DH, Zalkin A, Bartlett N. Crystal structure of $[XeF_5^+]_2[PdF_6^{2-}]$. *Inorganic chemistry.* 1973;12(8):1726-1730.

[226] Jesih A, Lutar K, Leban I, Zemva B. Synthesis and crystal structure of bis[undecafluorodixenon(1+)] hexafluoronickelate(2-). *Inorganic chemistry.* 1989/07/01 1989;28(15):2911-2914.

[227] Lehmann JF, Mercier HPA, Schrobilgen GJ. The chemistry of krypton. *Coordination Chemistry Reviews.* 2002;233–234(0):1-39.

[228] Šmalc A, Lutar K, Kinkead SA. Xenon Difluoride (Modification). *Inorganic Syntheses*: John Wiley & Sons, Inc.; 2007:1-4.

[229] Crystal Clear, Rigaku Corp., Woodland, Texas, 1999.

[230] A. Altomare, M. Cascarano, C. Giacovazzo, A. Guagliardi, *J. Appl. Cryst*. 1993, *26*, 343–350.

[231] teXan for Windows, version 1.06 ed., Molecular Structure Corporation, Woodland, Texas, 1999

[232] G. M. Sheldrick, *Acta Cryst.* 2008, *A64*, 112–122.

[233] L. J. Farrugia, *J. Appl. Cryst.* 1999, *32*, 837–838.

[234] CrysAlisPro, Agilent Technologies, Version 1.171.37.31 (release 14-01-2014 CrysAlis171 .NET).

[235] L. Palatinus, G. Chapuis,: SUPERFLIP - a computer program for the solution of crystal structures by charge flipping in arbitrary dimensions. J. Appl. Cryst. 2007, 40, 786–790.

[236] O. V. Dolomanov, L. J. Bourhis, R. J. Gildea, J. A. K. Howard and H. Puschmann, OLEX2: a complete structure solution, refinement and analysis program, J. Appl. Cryst. 2009, 42, 339–341.

[237] G.M. Sheldrick. Acta Cryst. 2015, C71, 3−8.

[238] L.J. Farrugia. J. App. Cryst. 2012, 45, 849–854.

[239] Crystal Impact GbR, Bonn, Germany (2004-2005) DIAMOND v3.1.

[240] Westrip S. publCIF: software for editing, validating and formatting crystallographic information files. *Journal of Applied Crystallography.* 2010;43(4):920-925.

[241] S. Rüdiger, H. Meinert, *Z. Chem. 9*, 1969, 434

[242] Žemva B, Slivnik J, Bohinc M. On the syntheses of xenon fluorotitanates(IV). *J Inorg Nucl Chem.*1976;38(1):73-74.

[243] Slivnik J, Družina B, Žemva B. Reactions of Some Ammonium Fluorometalates with XeF_2. *Zeitschrift für Naturforschung B.* Vol 361981:1457.

[244] McKee DE, Zalkin A, Bartlett N. Crystal structure of [XeF3+] [Sb2F11-]. *Inorganic chemistry.* 1973/08/01 1973;12(8):1713-1717.

[245] Hughes MJ, Mercier HPA, Schrobilgen GJ. Fluoride Ion Donor Properties of cis-OsO2F4: Synthesis, Raman Spectroscopic Study, and X-ray Crystal Structure of [OsO2F3][Sb2F11]. *Inorganic chemistry.* 2010/01/04 2010;49(1):271-284.

[246] Mazej Z, Goreshnik E. Alkali Metal (Li+–Cs+) Salts with Hexafluorochromate(V), Hexafluorochromate(IV), Pentafluorochromate(IV), and Undecafluorodichromate(IV) Anions. *European Journal of Inorganic Chemistry.* 2008;2008(11):1795-1812.

[247] Bondi A. van der Waals Volumes and Radii. *The Journal of Physical Chemistry.* 1964/03/01 1964;68(3):441-451.

[248] F. Schreiner, G. N. McDonald, C. L. Chernick, *J. Phys. Chem.* **1968**, *72*, 1162 – 1166.

[249] Radan K, Goreshnik E, Žemva B. Xenon(II) Polyfluoridotitanates(IV): Synthesis and Structural Characterization of [Xe2F3]+ and [XeF]+ Salts. *Angewandte Chemie International Edition.* 2014;53(50):13715-13719.

[250] de Petris G, Ricci A. Experimental evidence for an asymmetric Xe2F3+ ion in the gas-phase. *Chemical Physics Letters.* 2000;332(3–4):290-294.

[251] Dixon DA, Arduengo AJ, Farnham WB. Electronic structures of trifluorodixenon(+) and xenon iodide trifluoride. Examples of 5c,6e hypervalent bonding. *Inorganic chemistry.* 1989/12/01 1989;28(26):4589-4593.

[252] Blatov VA, O'Keeffe M, Proserpio DM. Vertex-, face-, point-, Schlafli-, and Delaney-symbols in nets, polyhedra and tilings: recommended terminology. *CrystEngComm.* 2010;12(1):44-48.

[253] O'Keeffe M, Hyde BG. Plane Nets in Crystal Chemistry. *Philosophical Transactions of the Royal Society of London. Series A, Mathematical and Physical Sciences.* 1980;295(1417):553-618.

[254] Cundy, H. and Rollett, A., *Mathematical Models* (1952), (3rd edition, 1989, Stradbroke, England: Tarquin Pub.), 3.7 *The Archimedean Polyhedra*, pp. 101–115. P.118-119 Table I, Nets of Archimedean Duals, V.*a*.*b*.*c*... as *vertically-regular* symbols.

[255] IUCr checkCIF, a crystallographic tool used to check the integrity and consistency of crystal structure encodings in CIF format, International Union of Crystallography; http://checkcif.iucr.org/ (24.12.2016).

[256] Jenkins HDB, Krossing I, Passmore J, Raabe I. A computational study of Sb_nF_{5n} (n = 1–4): Implications for the fluoride ion affinity of $n$$SbF_5$. *Journal of Fluorine Chemistry.* 2004;125(11):1585-1592.

[257] Christe KO, Schack CJ. Synthesis and Characterization of $(NF_4)_2TiF_6$ and of Higher NF_4^+ and Cs^+ Poly(perfluorotitanate(IV)) Salts. *Inorg Chem.* 1977;16:353–359.

[258] Von der Ohe W. Raman spectrum of $(NH_4)_2TiF_6$ and trigonal Cs_2TiF_6. *J Chem Phys.* 1976;65:3575–3585.

[259] Burgess J, Frlec B, Holloway JH. Enthalpies of formation of 1 : 1,1 : 2, and 2 : 1 adducts of xenon difluoride with antimony, niobium, and tantalum pentafluorides. *Journal of the Chemical Society, Dalton Transactions.* 1974(16):1740-1742.

[260] Burgess J, Fawcett J, Peacock RD, Lutar K, Ẑemva B. Enthalpies of hydrolysis of the xenon complexes XeF2·VF5, XeF2·CrF4, XeF2·MnF4 and XeF6·CrF4. *Journal of Fluorine Chemistry.* 1992;58(1):53-58.

[261] Frlec B, Holloway JH. New krypton difluoride adducts. *Journal of the Chemical Society, Chemical Communications.* 1973(11):370-371.

[262] R. J. Gillespie, B. Landa and G. J. Schrobilgen, "Fluorine Bridging in the Xenon Fluoride Cations and Their Salts: The Base Strengths of XeF_2, XeF_4 and XeF_6; in Journal of Inorganic and Nuclear

Chemistry, Herbert H. Hyman Memorial Volume, Supplement to Journal of Inorganic and Nuclear Chemistry, J. J. Katz and I. Sheft, eds., Oxford: Pergamon Press, **1976**, 179-182.

[263] Lutar K, Jesih A, Žemva B. KrF2/MnF4 adducts from KrF_2/MnF_2 interaction in HF as a route to high purity MnF_4. *Polyhedron.* 1988;7(13):1217-1219.

[264] Žemva B, Slivnik J. Some reactions with krypton difluoride and xenon fluorides. *Journal of Fluorine Chemistry.* 1980;16(6):583.

[265] Christe KO, Wilson WW, Wilson RD. Coordinatively saturated fluoro cations. Oxidative fluorination reactions with fluorokrypton(1+) salts and platinum hexafluoride (PtF6). *Inorganic chemistry.* 1984;23(14):2058-2063.

[266] Lehmann JF, Dixon DA, Schrobilgen GJ. X-ray Crystal Structures of α-KrF2, [KrF][MF6] (M = As, Sb, Bi), [Kr2F3][SbF6]·KrF2, [Kr2F3]2[SbF6]2·KrF2, and [Kr2F3][AsF6]·[KrF][AsF6]; Synthesis and Characterization of [Kr2F3][PF6]·nKrF2; and Theoretical Studies of KrF2, KrF+, Kr2F3+, and the [KrF][MF6] (M = P, As, Sb, Bi) Ion Pairs. *Inorganic chemistry.* 2001/06/01 2001;40(13):3002-3017.

[267] Radan K, Goreshnik E, Žemva B. Oksonijeve soli nekaterih perfluoridostanatov(IV) in perfluoridotitanatov(IV) ter kristalna struktura $Na(HF)[Sn_2F_9]$. *Slovenski kemijski dnevi.* Maribor, Slovenia: 10–12 September 2013.

[268] Steiner T. The Hydrogen Bond in the Solid State. *Angew Chem Int Ed.* 2002;41:48–76.

[269] Dannenberg JJ. An Introduction to Hydrogen Bonding By George A. Jeffrey (University of Pittsburgh). Oxford University Press: New York and Oxford. 1997. ix + 303 pp. $60.00. ISBN 0-19-509549-9. *Journal of the American Chemical Society.* 1998/06/01 1998;120(22):5604-5604.

[270] B. Družina and B. Žemva, "On the synthesis of xenon(II) fluorostannates(IV)," *Journal of Fluorine Chemistry,* vol. 34, pp. 233-239, 1986.

[271] For a Review, see Y. I. Baukov, S. N. Tandura in The Chemistry of Organic Germanium, Tin and Lead Compounds, Vol. 2, Part 1 (Ed.: Z. Rappoport), Wiley, Chichester, UK, 2002, pp. 963 – 1239.

[272] **a)** Akiba K-y, Yamashita M, Yamamoto Y, Nagase S. Synthesis and Isolation of Stable Hypervalent Carbon Compound (10-C-5) Bearing a 1,8-Dimethoxyanthracene Ligand. *Journal of the American Chemical Society.* 1999;121(45):10644-10645. b) Yamashita M, Yamamoto Y, Akiba K-y, et al. Syntheses and Structures of Hypervalent Pentacoordinate Carbon and Boron Compounds Bearing an Anthracene Skeleton − Elucidation of Hypervalent Interaction Based on X-ray Analysis and DFT Calculation. *Journal of the American Chemical Society.* 2005;127(12):4354-4371. c) Akiba K-y, Moriyama Y, Mizozoe M, et al. Synthesis and Characterization of Stable Hypervalent Carbon Compounds (10-C-5) Bearing a 2,6-Bis(p-substituted phenyloxymethyl)benzene Ligand. *Journal of the American Chemical Society.* 2005/04/01 2005;127(16):5893-5901.

[273] Garner CD, Sutton D, Wallwork SC. The crystal structures of anhydrous nitrates and their complexes. Part IV. Tin(IV) nitrate. *Journal of the Chemical Society A: Inorganic, Physical, Theoretical.* 1967(0):1949-1954.

[274] Smith PJ. *Chemistry of Tin*: Springer Netherlands; 2012:29.

[275] Flerov IN, Molokeev MS, Laptash NM, et al. Structural transformation between two cubic phases of (NH4)3SnF7. *Journal of Fluorine Chemistry.* 2015;178:86-92.

[276] Benner, G., Hoppe, R. Two new compounds of the $SmZrF_7$-type: $EuSnF_7$ and $YSnF_7$. European Journal of Solid State and Inorganic Chemistry. 1992;29(4-5), 659-677.

[277] Graudejus O, Müller BG. Neue Fluoride $M^{III}M^{IV}F_7$ mit M^{III} = SE, Tl und M^{IV} = Sn, Pb, Pt. *Zeitschrift für anorganische und allgemeine Chemie.* 1996;622(9):1601-1608.

[278] a) Jones D. The chemist's open window. *New Scientist.* 1984;104(1434):16-19. b) Emsley J. Xenon chemistry comes out of the cold. *New Scientist.* 1989;124(1695):20.

[279] van Aalst RM, van der Elsken J. The far-infrared spectrum of hydrogen chloride in liquid xenon. *Chemical Physics Letters.* 1973/11/15 1973;23(2):198-199.

[280] Calado JCG, Kozdon AF, Morris PJ, Da Ponte MN, Staveley LAK, Woolf LA. Thermodynamics of liquid mixtures of xenon and hydrogen chloride. *Journal of the Chemical Society, Faraday Transactions 1: Physical Chemistry in Condensed Phases.* 1975;71(0):1372-1378.

[281] Rentzepis PM, Douglass DC. Xenon as a solvent. *Nature.* 1981;293(5828):165-166.

[282] G. W. Castellan. *Physical Chemistry, 2nd Edition.* Addison-Wesley, Reading MA, 1971

[283] Andréa RR, Luyten H, Vuurman MA, Stufkens DJ, Oskam A. A Cryogenic Cell for Liquid Noble Gases. Vibrational Spectroscopy and Photochemistry of Transition Metal Carbonyls in Liquid Xenon. *Appl. Spectrosc.* 1986/11/01 1986;40(8):1184-1190.

[284] Marshall DB, Strohbusch F, Eyring EM. Solubility of organic substances in liquid xenon. *Journal of Chemical & Engineering Data.* 1981/07/01 1981;26(3):333-334.

[285] Krukonis VJ, McHugh MA, Seckner AJ. Xenon as a supercritical solvent. *The Journal of Physical Chemistry.* 1984/06/01 1984;88(13):2687-2689.

[286] Upmacis RK, Poliakoff M, Turner JJ. Structure and thermal reactions of dihydrogen complexes: the IR characterization of M(CO)5(H2) (M = chromium, molybdenum, and tungsten) and cis-Cr(CO)4(H2)2 in liquid xenon solution and the formation of HD during exchange of hydrogen and deuterium. *Journal of the American Chemical Society.* 1986/06/01 1986;108(13):3645-3651.

[287] Sponsler MB, Weiller BH, Stoutland PO, Bergman RG. Liquid xenon: an effective inert solvent for carbon-hydrogen oxidative addition reactions. *Journal of the American Chemical Society.* 1989/08/01 1989;111(17):6841-6843.

[288] Hamley PA, Kazarian SG, Poliakoff M. Hydrogen-Bonding and Photochemistry of Organometallics in Liquid Xenon Solution in the Presence of Proton Donors: A Low Temperature Infrared Study of the Interaction of (CF3)3COH with (C5Me5)M(CO)2L (M = Mn and Re; L = CO, N2, and H2) and with (C5Me5)V(CO)4. *Organometallics.* 1994/05/01 1994;13(5):1767-1774.

[289] Bengali AA, Arndtsen BA, Burger PM, et al. Activation of carbon-hydrogen bonds in alkanes and other organic molecules by Ir(I), Rh(I) and Ir(III) complexes. *Pure and Applied Chemistry.* Vol 671995:281.

[290] Sun X-Z, George MW, Kazarian SG, Nikiforov SM, Poliakoff M. Can Organometallic Noble Gas Compounds Be Observed in Solution at Room Temperature? A Time-Resolved Infrared (TRIR) and UV Spectroscopic Study of the Photochemistry of M(CO)6 (M = Cr, Mo, and W) in Supercritical Noble Gas and CO2 Solution. *Journal of the American Chemical Society.* 1996/01/01 1996;118(43):10525-10532.

[291] Nabiev SS, Klimov VD, Khodjiev BS. IR-Cryospectroscopy as a method for trace analysis of molecular impurities in inorganic fluorides. *Journal of Fluorine Chemistry.* 1992;58(2–3):293.

[292] Goetschel CT, Loos KR. Reaction of xenon with dioxygenyl tetrafluoroborate. Preparation of FXe-BF2. *Journal of the American Chemical Society.* 1972/05/01 1972;94(9):3018-3021.

[293] Drews T, Seppelt K. The Xe 2+ Ion—Preparation and Structure. *Angewandte Chemie International Edition in English.* 1997;36(3):273-274.

[294] Seidel S, Seppelt K, van Wüllen C, Sun XY. The Blue Xe4+ Cation: Experimental Detection and Theoretical Characterization. *Angewandte Chemie International Edition.* 2007;46(35):6717-6720.

[295] Yoo, J. Solid Xenon Project at Fermilab. Xenon Based detector Workshop, Lawrence Berkeley National Laboratory (LBNL), November 18, 2009.

[296] Närger U, Balzarini DA. Coexistence-curve diameter and critical density of xenon. *Physical Review B.* 1990;42(10):6651-6657.

[297] Hwang IC, Seidel S, Seppelt K. Gold(I) and mercury(II) xenon complexes. *Angew Chem Int Ed Engl.* Sep 22 2003;42(36):4392-4395.

[298] Reichardt C, Welton T. Solvent Effects on the Position of Homogeneous Chemical Equilibria. *Solvents and Solvent Effects in Organic Chemistry*: Wiley-VCH Verlag GmbH & Co. KGaA; 2010:107-163.

[299] Dybowski C, Bansal N, Duncan TM. NMR Spectroscopy of Xenon in Confined Spaces: Clathrates, Intercalates, and Zeolites. *Annual Review of Physical Chemistry.* 1991;42(1):433-464.

[300] Lutar, K.; Zemva, B.; Borrmann, H. Novel type of oxonium salts H3OM(AsF6)3 (M = Co, Ni): syntheses, structures and some properties *European Journal of Solid State and Inorganic Chemistry*, 1996, *33*, 957-969

[301] Mazej Z, Benkič P, Lutar K, Žemva B. Novel oxonium compounds of lanthanoids: synthesis of (H3O)3La2F(AsF6)8, and syntheses and crystal structures of (H3O)8La2F(AsF6)13 and (H3O)4La2F(AsF3)2(AsF6)9. *Journal of Fluorine Chemistry.* 2001;112(2):173-183.

[302] Mazej Z, Goreshnik E. Syntheses and characterization of ANi(AsF6)3 (A = H3O+, O2+, NO+, NH4+, K+, Rb+, and Cs+) compounds. *Journal of Fluorine Chemistry.* 2009;130(4):399-405.

[303] Tavčar G, Mazej Z. Crystal structures of mixed oxonium–cadmium(II) salts with [SbF6]−/[Sb2F11]− anions: From complex chains to layers and three-dimensional frameworks. *Inorganica Chimica Acta.* 2011;377(1):69-76.

[304] Mazej Z, Goreshnik E, Jagličić Z. Syntheses and Crystal Structures of [H3O]+/M2+ (M = Fe, Zn, Cu, Hg) Salts with [AsF6]–. *European Journal of Inorganic Chemistry.* 2012;2012(11):1734-1741.

[305] Mazej Z, Goreshnik E. Crystal structures of phases observed in [H3O]+/M2+/[SbF6]− system (M = Mg, Cr, Mn, Fe, Co, Ni, Cu, Zn, Pd, Cd). *Journal of Fluorine Chemistry.* 2017;193:82-88.

[306] Mootz D, Oellers EJ, Wiebcke M. Hexafluorotitan(IV)-Säure: Untersuchungen zur Bildung und Struktur kristalliner Hydrate. *Zeitschrift für anorganische und allgemeine Chemie.* 1988;564(1):17-25.

[307] Christe KO, Charpin P, Soulie E, Bougon R, Fawcett J, Russell DR. Structure and vibrational spectra of oxonium hexafluoroarsenates(V) and -antimonates(V). *Inorganic chemistry.* 1984/11/01 1984;23(23):3756-3766.

[308] Zhang D, Rettig SJ, Trotter J, Aubke F. Superacid Anions: Crystal and Molecular Structures of Oxonium Undecafluorodiantimonate(V), [H3O][Sb2F11], Cesium Fluorosulfate, CsSO3F, Cesium Hydrogen Bis(fluorosulfate), Cs[H(SO3F)2], Cesium Tetrakis(fluorosulfato)aurate(III), Cs[Au(SO3F)4], Cesium Hexakis(fluorosulfato)platinate(IV), Cs2[Pt(SO3F)6], and Cesium Hexakis(fluorosulfato)antimonate(V), Cs[Sb(SO3F)6]. *Inorganic chemistry.* 1996/01/01 1996;35(21):6113-6130.

[309] Mootz D, Steffen M. Kristallstrukturen von Säurehydraten und Oxoniumsalzen. XX. Die Oxoniumtetrafluoroborate H3OBF4, [H5O2]BF4 und [H(CH3OH)2]BF4. *Zeitschrift für anorganische und allgemeine Chemie.* 1981;482(11):193-200.

[310] Masson JP, Desmoulin JP, Charpin P, Bougon R. Synthesis and characterization of a new uranium(V) compound: oxonium hexafluorouranate(V). *Inorganic chemistry.* 1976/10/01 1976;15(10):2529-2532.

[311] Christe KO, Wilson WW, Schack CJ. On the syntheses and properties of some hexafluorobismuthate (V) salts and their in the metathetical synthesis of NF+4 salts. *Journal of Fluorine Chemistry.* 1978;11(1):71-85.

[312] Selig H, Sunder WA, Disalvo FA, Falconer WE. Hydrolysis reactions of transition metal hexafluorides in liquid hydrogen fluoride: oxonium salts with Pt, Ir and Ru. *Journal of Fluorine Chemistry.* 1978;11(1):39-50.

[313] Selig H, Sunder WA, Schilling FC, Falconer WE. Hydrolysis reactions of transition metal fluorides in liquid hydrogen fluoride: Oxonium salts with Nb, Ta and W. *Journal of Fluorine Chemistry.* 1978;11(6):629-635.

[314] Dupont™ Teflon® Industrial Coatings Brochure (GB). Typical properties 2005:12

[315] Brown ID, Altermatt D. Bond-valence parameters obtained from a systematic analysis of the Inorganic Crystal Structure Database. *Acta Cryst*. 1985;B41:244−247.

[316] Solver Add-in, Tool for optimization and equation solving, Microsoft Excel Ver.14.0.7166.5000, Microsoft Office Professional Plus 2010.